The University Of Sheffield.

University of Sheffield

M.L. Perciato

Investigating the role of ADAM17 in the crosstalk between cancer associated fibroblasts and cancer cells

A thesis submitted in partial fulfilment of the requirements for the degree of

Doctor of Philosophy

2022

The University Of Sheffield.

Investigating the role of ADAM17 in the crosstalk between cancer associated fibroblasts and cancer cells

Maria Luna Perciato

A thesis submitted in partial fulfilment of the requirements for the degree of Doctor of Philosophy

The University of Sheffield

Faculty of Medicine, Dentistry and Health

School of Clinical Dentistry

June 2022

Acknowledgments

First of all, I would like to thank my supervisors Prof. Daniel Lambert and Prof. Simon Whawell for giving me the opportunity of working on this project, which I profoundly loved and which helped me to become both a better scientist and individual. I also want to thank them for believing in me since the very beginning, and for genuinely and constantly supporting me at each stage of my PhD journey.

I would like to thank Brenka McCabe, Jason Heath and Kirsty Franklin for their precious technical support and for bearing with my never-ending questions and requests and, more importantly, for their cheerful attitude and pleasant chats. A big Thank also to Matthew Worsely for being kind, impeccable and committed, a pillar in the laboratory.

A big thank to all the research students and postdocs at the Dental School, who made this journey sparkling and gratifying, especially in the darkest moment, such those amid the COVID19 restrictions.

Thank you to the University of Sheffield for finding my PhD.

Finally, I would like to express my utmost gratitude to my parents and sister. Whatever I have become and I have achieved I owe to my loving parents, who believed in me and motivated me also when, before starting my PhD, things were not working as expected, bearing with the distance and the years away from them. Thanks to my father Vincenzo who patiently helped me starting my long international journey moving from a country to another. Thank you, Viviana, I am lucky to have you as a sister and thank you for being there for me whenever I need.

A special thanks to my mother Vita, whose immense sacrifices, perseverance, strength, positive and cheerful attitude are to me a key motivation to keep going with determination and optimism. I could not have asked for a better mother and inspiration.

A warm thanks to my grandmother Maria, a strong, relentless and committed woman, who would have been happy to celebrate another achievement with all of us.

A big thank to my best friends Nazarena and Federica, no matter how distant we are, you never let me feel alone. Thank you both for your support and precious and great moments we spend together.

To conclude, a special thanks to Dr. Ajinkya Revandkar. You have been, and still, you are, a pillar and example to me, as a scientist and as individual. I will never thank you enough. You helped me becoming the better version of myself so far, regardless my ups and downs. You believed in and motivated me since my firsts steps as a researcher. Your passion for and devotion to science inspired me, as well as your profound and genuine kindness and love for life. I could not have asked for a better mentor and friend.

Abstract

Background: Cancer associated fibroblasts (CAFs) promote cancer progression. Moreover, upregulation of a disintegrin and metalloproteinases (ADAMs) can foster cancer growth and invasion in diverse malignancies. ADAM17, which modulates over 80 substrates including many involved in tumour progression, can be upregulated in CAFs. Hence, a better understanding of the role of ADAM17 in CAFs may help identify novel mechanisms driving CAF-mediated cancer progression and new therapeutic targets.

Aims: This project aimed to assess the role of ADAM17 in interactions between CAFs and cancer cells. It was investigated whether cancer cells programme CAFs to release pro-migratory factors through the activation of the CAF-associated ADAM17.

Approach: Normal Oral Fibroblasts (NOFs) and CAFs were stimulated with the conditioned medium (C.M.) derived from oral squamous cell carcinoma (OSCC) cell lines and ADAM17 expression was determined. Next, ADAM17 was genetically silenced in NOFs and CAFs gene expression changes identified using proteomics. Thereafter, cancer cells were cultured with the C.M. derived from ADAM17-deficient CAFs to determine their impact on cancer cell migration.

To confirm the CAF-specific role of ADAM17, ADAM17 was also silenced in OSCC cell lines and their migration assessed.

Results: OSCC cell-derived C.M. induced upregulation of ADAM17 in NOFs and CAFs. Furthermore, silencing of ADAM17 in NOFs and CAFs downregulated CAF markers and reprogrammed their secretome. C.M. from ADAM17-deficient NOFs or CAFs reduced cancer cell migration and N-cadherin levels. This observation was mirrored by chemically inhibiting N-cadherin in cancer cells. Moreover, ADAM17-deficient CAFs displayed lower levels of the fibroblast growth factor 2 (FGF2), a regulator of cancer cell migration. Chemical targeting of the FGF receptor recapitulated the anti-migratory phenotype of cancer cells and N-cadherin reduction.

Conclusions: This project showed that cancer cells upregulate ADAM17 in fibroblasts which, in turn, shed pro-migratory factors, and induce N-cadherin expression in cancer cells. Targeting CAF-associated ADAM17 reversed this phenotype by reducing CAF-derived FGF2. Similarly, inhibiting cancer cell-associated N-cadherin restricted cancer cell migration. Collectively, this study identifies a novel ADAM17-N-cadherin axis contributing to CAF-induced cancer cell migration.

Table of Contents

List of Figures

List of Tables

Abbreviations

α-SMA	Alpha smooth muscle actin
ADAM	A disintegrin and metalloproteinase
ADAMTS	A disintegrin and metalloproteinase with thrombospondin motif
ANOVA	Analysis of variance
ATG(3/5)	Autophagy-related gene (3/5)
BSA	Bovine serum albumine

CAF	Cancer associated fibroblast
CANDIS	Conserved ADAM17 dynamic interaction sequence
CCL5	C-C motif chemokine ligand 5
cDNA	Complementary deoxyribonucleic acid
cGAS	cyclic GMP-AMP synthase
CXCL12	C-X-C motif chemokine ligand 12
DAPI	4', 6-diamidino-2-phenylindole
DDR	DNA damage response
DMEM	Dulbecco's modified eagle's medium
DMSO	Dimethyl sulfoxyde
DNA	Deoxyribonucleic acid
ECM	Extra cellular matrix
EdU	5-ethynyl-2′-deoxyuridine
EGF	Epidermal growth factor
EGFR	Epidermal growth factor receptor
ELISA	Enzyme-linked immunosorbent assay
EMP	Epithelial-mesenchymal plasticity
EMT	Epithelial to mesenchymal transition
EV	Extracellular vesicle
F-Actin	Fibrous actin

FAP	Fibroblast activation protein
FC	Fold change
FDR	False discovery rate
FGF2	Fibroblast growth factor 2
FGFR	Fibroblast growth factor receptor
GAPDH	Glyceraldehyde-3-phosphate dehydrogenase
HB-EGF	Heparin-binding EGF-like growth factor
HGF	Hepatocyte growth factor
HNSCC	Head and neck squamous cell carcinoma
HRP	Horseradish peroxidase
ICR	Intracellular region
IFIT1	Interferon induced protein with tetratricopeptide repeats 1
IFNB	Interferon beta
IL	Interleukin
IRF(1/9)	Interferon regulatory factor (1/9)
LC3B	Light chain 3 B
LFQ	Label-free quantification
KD	Knock-down
Mass-spec	Mass spectrometry
MDSC	Myeloid-derived suppressor cell

MMP	Matrix metalloproteinase
MPD	Membrane-proximal domain
MSC	Mesenchymal stem cell
MX1	MX Dynamin Like GTPase 1
NFκB	Nuclear factor kappa beta
NK	Natural killer
NOF	Normal oral fibroblast
OAS2	2'-5'-Oligoadenylate Synthetase 2
OSCC	Oral squamous cell carcinoma
PBS	Phosphate buffered saline
PCA	Principal component analysis
PDGFRA	Platelet-derived growth factor alpha
PDI	Protein disulfide isomerase
PMA	phorbol-12-myristate-13-acetate
PPI	Protein-protein interaction
qPCR	Quantitative polymerase chain reaction
RHDBF2	Rhomboid 5 Homolog 2
RNA	Ribonucleic acid
siRNA	Small interfering RNA
SMAD3	Suppressor of mothers against decapentaplegic 3

STAT(1/2/3)	Signal transducer and activator of transcription (1/2/3)
TACE	Tumour necrosis factor alpha converting enzyme
TAM	Tumour associated macrophage
TAP1	Transporter associated with antigen processing 1
TBS	Tris-buffered saline
TGF-β1	Transforming growth factor beta
TIMP	Tissue inhibitor of metalloproteinase
TME	Tumour micro-environment
TNF-α	Tumour necrosis factor alpha

Chapter 1

Introduction and Literature Review

1.1 Introduction

Cancer is a leading cause of death worldwide and significantly on the rise, with a mortality rate higher than HIV/AIDS, malaria, and tuberculosis combined (World Health Organization, 2020). In 2020, cancer-related deaths were estimated to be 9.6 million worldwide, predicted to reach 16.2 million by 2040 (GCO, 2021). This calls for more urgent research to reduce cancer progression that leads to mortality and improve the overall quality of life of those affected by it.

While cancer initiation and progression was initially thought to arise in a cell-autonomous manner, several studies have demonstrated the existence of non-cell autonomous-mediated mechanisms (Maman and Witz, 2018; Anderson and Simon, 2020; Hanahan, 2022). These include the active involvement of the cells from the tumour-associated stromal microenvironment, such as immune cells and cancer-associated fibroblasts (CAFs) (Maman and Witz, 2018; Sahai *et al.*, 2020; Chen, McAndrews and Kalluri, 2021; Hanahan, 2022). This cooperation promotes tumour development and progression that eventually leads to fatal outcomes. A common feature of the tumour microenvironment (TME) involves the transition of fibroblasts to cancer-associated fibroblast (CAF)-like features (Sahai *et al.*, 2020; Chen, McAndrews and Kalluri, 2021). In addition to CAFs, the recruitment of blood vessels and endothelial cells, neurons, and pro-inflammatory or tumour-promoting immune cells also remain instrumental (Hanahan and Weinberg, 2011; De Palma, Biziato and Petrova, 2017; Zahalka and Frenette, 2020; Hanahan, 2022).

While a substantial body of research has determined an active role of tumour cells in orchestrating the stromal microenvironmental changes that in turn affect tumour growth, recent studies have highlighted novel roles of CAF and infiltrating immune cells in driving tumour progression (Quail and Joyce, 2013; Sahai *et al.*, 2020; Chen, McAndrews and Kalluri, 2021; Hanahan, 2022). Tumour cells secrete a myriad of cytokines, chemokines, metabolites, extracellular matrix proteins, extracellular vesicles, and other factors that activate and recruit cellular components of the TME (Hanahan and Weinberg, 2011; Anderson and Simon, 2020; Hanahan, 2022). Subsequently, these TME cells drive tumour progression by secreting factors that allow neoplastic cells to acquire invasive and migratory potential (Hanahan and Weinberg, 2011; Anderson and Simon, 2020; Hanahan, 2022). However, whether the interaction between activated CAFs and recruited immune cells could alter the tumour progression independently of additional acquired mutations in tumour cells remains unclear. This information would provide insights on how CAFs

and immune cells sustain tumour progression and promote therapy-resistance (one of the major challenges of cancer research) in a tumour-independent manner.

Thanks to the advanced computational and experimental technologies, it has been possible to identify specific traits, referred to as hallmarks of cancer, that are generally shared by the variety of cancers, thus helping to better understand the core mechanisms of cancer for a more effective clinical translation. Therefore, the hallmarks that rationalise the complexity of this disease development and progression are as follows: sustained proliferative signalling, genome instability and somatic mutation, resistance to cell death, enabled replicative immortality, evasion of growth suppression, escape from immune surveillance, tumour-promoting inflammation, metabolic switch, induction of angiogenesis, evading growth suppression, acquisition of the invasive and metastatic potential, epigenetic reprogramming, unlocking phenotypic plasticity, cellular senescence and polymorphic microbiomes (Figure 1.1).

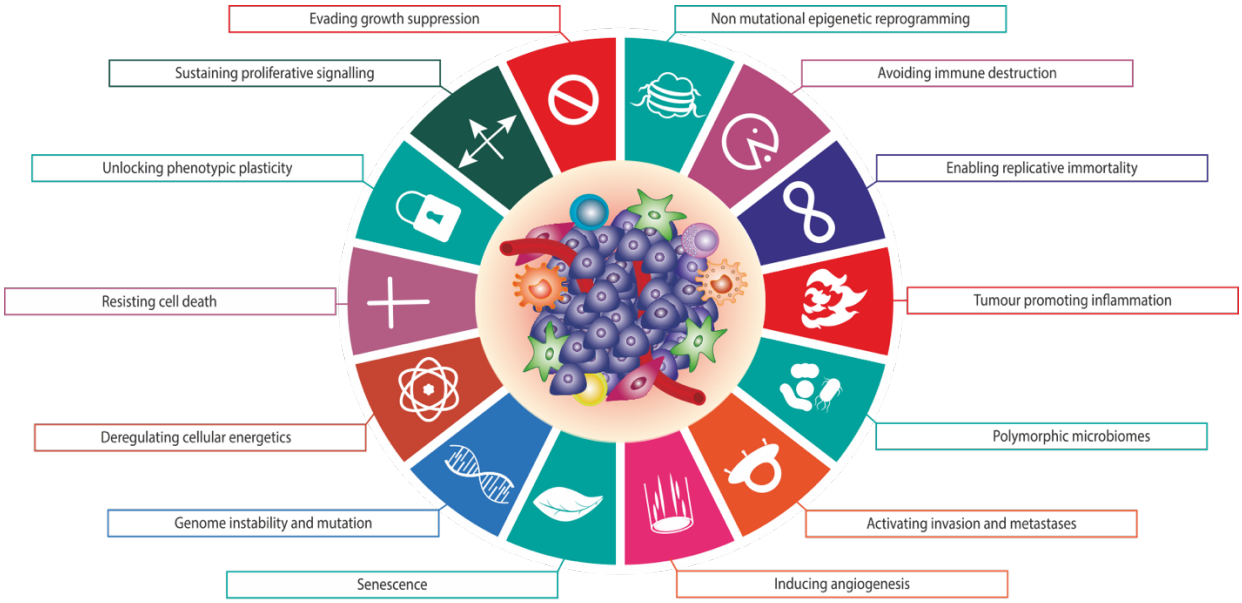

Figure 1.1 The Hallmarks of Cancer.

The illustration represents the updated version of the hallmarks of cancer adopted by incipient cancers to overcome restricting responses and evolve into malignancy. (Illustration generated using Adobe Illustrator software).

The TME, by providing aberrant physical and paracrine stimuli, represents a key player in the acquisition of the hallmarks and the engagement of developmental regulatory program, such as

the epithelial to mesenchymal transition (EMT), by cancer cells even in the absence of a mutational reprogramming (Olumi et al., 1999; Hanahan and Coussens, 2012; Hanahan, 2022). This leads to the acquisition of a migratory potential by cancer cells which then constitute metastases, the terminal stage of tumour progression responsible for most cancer-related deaths.

1.2 Cancer metastases: an unsolved enigma

Cancer metastasis accounts for most cancer-related deaths worldwide, with limited effective clinical management of the disease (Lambert, Pattabiraman and Weinberg, 2017; Esposito, Ganesan and Kang, 2021). The main reason behind this outcome is intrinsic to the nature of cancer, which is a dynamic and plastic biological system constantly adapting to its challenging environment to survive and spread (Stuelten, Parent and Montell, 2018; Weiss, Lauffenburger and Friedl, 2022). Migrating cells respond to the mechanical cues deriving from the surrounding ECM. For instance, migration through confined spaces (e.g. pores and gaps), which can induce nuclear deformation, undermines nuclear integrity thus triggering potential genomic rearrangements (Denais *et al.*, 2016). The biochemical properties of the ECM, dictated by its composition (e.g. hyaluronan content, collagen types, intra-fibrillar cross-links, fibre patterns etc.) determines either the reinforcement of focal adhesions, cellular elongation and spreading, commonly supported by proteolytic ECM digestion (events triggered in the context of stiff ECM) (Paszek *et al.*, 2005) or, conversely, reduction of adhesion forces followed by cellular rounding in the absence of proteolytic ECM breakdown (processes elicited in soft ECM) (Wolf *et al.*, 2003; Ulrich, De Juan Pardo and Kumar, 2009). As a result, this adaptive behaviour leads to metastasis formation and therapy resistance.

Metastasis is a complex multistep process governed at each stage by the intricated crosstalk engaged with the peritumoral stroma (Shintani *et al.*, 2016; Pistore *et al.*, 2017; Liu *et al.*, 2019; Weiss, Lauffenburger and Friedl, 2022). While a few milestones have emerged (determination of the events leading to metastasis, molecular patterns activated, types of cell migration), the key mechanisms underlying metastasis origin and progression remain still far from being completely deciphered (Lambert, Pattabiraman and Weinberg, 2017; Gui and Bivona, 2022). Further complications arise from decades of large-scale genomic sequencing which did not identify new mutations, beyond those acquired in primary tumours, as potential drivers of metastases spawning (Finnegan *et al.*, 1989; Garraway and Lander, 2013; Vogelstein *et al.*, 2013; Gui and Bivona, 2022). These findings imply the crucial role of the peritumoral microenvironment in contributing

to metastasis formation and disease outcome (Hanahan and Coussens, 2012; Quail and Joyce, 2013; Wan, Pantel and Kang, 2013; Shintani *et al.*, 2016; Hanahan, 2022).

1.2.1 The invasion and metastasis cascade

Metastasis represents the final stage of a sequential multistep process initiated within primary tumours. Carcinoma cells acquire specific traits which allow them to detach from and leave the primary site and penetrate the surrounding stroma into the normal tissue parenchyma (a process termed invasion) (Lambert, Pattabiraman and Weinberg, 2017; Dongre and Weinberg, 2018). Next, these motile cells penetrate the peritumoral bloodstream (intravasation) and, after surviving in the circulatory system, they reach distant tissues, arrest and pass through the local blood vessels (extravasation) to eventually attach and colonise the new parenchyma (metastases formation) (Figure 1.2). This complex process is at the same time extremely and fortunately inefficient, wherein the final stage of colonisation accounts of a small percentage of success due to the stringency of the adaptation programme in a new and relatively biologically different tissue (Luzzi *et al.*, 1998; Chambers, Groom and MacDonald, 2002; Wan, Pantel and Kang, 2013). Of note, there are currently two models proposed to explain cancer metastasis spawning, the "linear progression" and the "parallel progression" (Wan, Pantel and Kang, 2013; Turajlic and Swanton, 2016). The former, and more corroborated, model implies that ancestral clones bestowed with pro-metastatic capabilities occur during the late stages of malignancies, in line with the evidence of small genetic divergency between primary tumour-derived cells and metastatic cells (W. Liu *et al.*, 2009; Campbell *et al.*, 2010; Yachida *et al.*, 2010; Wu *et al.*, 2012; Turajlic and Swanton, 2016). The latter, on the contrary, assumes that metastasic dissemination occurs at early stages of tumorigenesis, stemming from cells which underwent an intermediate transformation which allowed them to spread and adapt to the new environment as the result of selecting further genetic mutations (Kuukasjärvi *et al.*, 1997; Stoecklein and Klein, 2010; Wan, Pantel and Kang, 2013; Turajlic and Swanton, 2016).

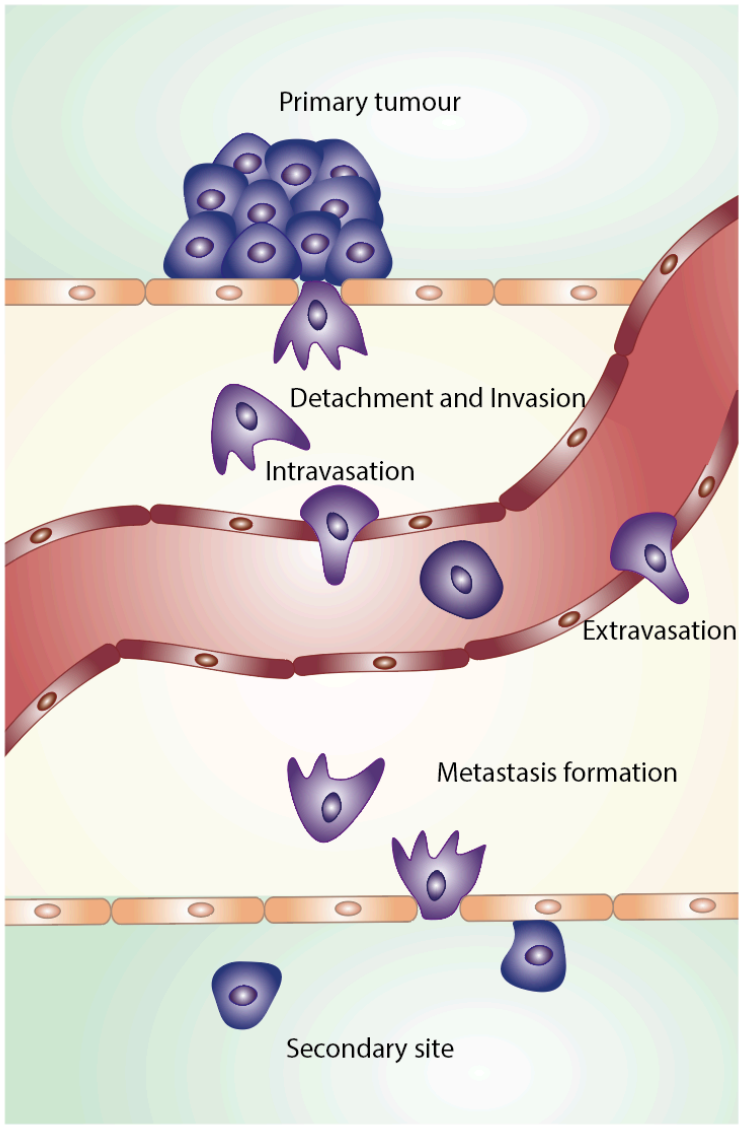

Figure 1.2 The invasion and metastasis cascade.

The illustration represents the classical multi-step process associated to neoplastic cells invasion and metastases. Once cancer cells detach from the primary site, they can invade the surrounding parenchyma and intravasate. The cells which survive in the circulatory system can arrest and extravasate in order to colonise a new tissue (secondary site) forming metastases. (Illustration generated using Adobe Illustrator software).

1.2.2 The Epithelial to Mesenchymal Transition (EMT) in cancer

EMT is a highly conserved and pleiotropic programme involved in a variety of biological processes such as embryogenesis and wound healing, although, it is mostly associated with cancer (Thiery *et al.*, 2009; Pastushenko and Blanpain, 2019). The switch from the epithelial to the mesenchymal phenotype, which renders the cells more motile and invasive, is exploited by cancer

cells to sustain their progression and eventually disseminate to distant organs, and occurs through distinct transition events which are the loss of epithelial polarity, disruption of the cell-cell junctions, erosion of the underlying basement membrane and re-organisation of the ECM (Nieto *et al.*, 2016; Pastushenko and Blanpain, 2019). The EMT programme is a highly dynamic and plastic multistep process whose orchestration depends on the expression of a panel of transcription factors which in turn are tightly context dependent (e.g., tissue type, grade of the malignancy, type of TME) (Dongre and Weinberg, 2018). Amongst the master regulators of EMT the most investigated, referred to as core EMT transcription factors, are Snail (Snail Family Transcriptional Repressor 1, SNAI1), Slug (Snail Family Transcriptional Repressor 2, SNAI2), Zeb1(Zinc Finger E-Box Binding Homeobox 1) and Twist (Twist Family Basic Helix-Loop-Helix Transcription Factor 1) (Peinado, Olmeda and Cano, 2007; Yang and Weinberg, 2008; Yang *et al.*, 2020). These factors are not involved only in EMT but they have been shown to regulate other cellular programmes, such as drug resistance, cell stemness, resistance to apoptosis and metabolic rewiring, known to also constitute typical traits displayed by cells which have undergone EMT (Vega *et al.*, 2004; Guo *et al.*, 2012; Dong *et al.*, 2013; Lim *et al.*, 2013).

In addition, these EMT transcriptional factors have been shown to regulate the expression of the cell-cell adhesion molecules known as cadherins which are involved in adherens junctions, cellular polarity and tissue integrity (Huang *et al.*, 2019). During EMT, Snail, Slug, Zeb1 and Twist foster a cadherin switch by repressing the expression of the epithelial cadherin (E-cadherin) and by upregulating the mesenchymal neural cadherin (N-cadherin) (Lamouille, Xu and Derynck, 2014). This process results in the disruption of the association with the neighbouring epithelial cells, in favour of a higher affinity for those which are mesenchymal, and the acquisition of an invasive and migratory potential (Yilmaz and Christofori, 2009).

EMT is often depicted as the major cause of metastasis, despite a lack of definitive evidence (Lambert, Pattabiraman and Weinberg, 2017; Dongre and Weinberg, 2018). Moreover, recent studies reported the formation of metastases from malignant cells which never underwent EMT, suggesting that EMT contribution to metastasis could be dispensable (Fischer *et al.*, 2015; Zheng *et al.*, 2015).

The complexity of EMT lies also on its plasticity and context dependent nature which renders EMT a non-binary process, implying the coexistence, within a neoplastic lesion, of malignant cells harbouring mixed epithelial/mesenchymal phenotypes (Jolly *et al.*, 2015; Derynck and Weinberg, 2019).

Another layer of complexity derives from the presence of malignant cells displaying mixed epithelial/mesenchymal traits which renders an unambiguous distinction between the epithelial and mesenchymal state impossible. Thus, to overcome this paradox, it has been recently recommended the use of the term "Epithelial-Mesenchymal Plasticity" (EMP) to describe these hybrid EMT contexts (Yang *et al.*, 2020).

1.2.3 Collective migration

Another crucial aspect, which partially contributed to undermining the role of EMT in metastasis formation, is the collective migration of primary tumour cells (Lambert, Pattabiraman and Weinberg, 2017). Unlike the migration associated with EMT, the cells involved in the collective migration keep their adherens junctions and migrate as a cohesive and coordinated aggregate of cells within the adjacent parenchyma (Cheung and Ewald, 2016; Lambert, Pattabiraman and Weinberg, 2017; Vilchez Mercedes *et al.*, 2021). Moreover, this strategy has been shown to be more successful and to lead to a higher and more efficient rate of colony formation both *in vitro* and *in vivo*, thus representing a pivotal mechanism in cancer progression (Cheung and Ewald, 2016; Vilchez Mercedes *et al.*, 2021). Collective migration is typical of solid tumours, commonly observed at the invasive borders and characterised by a heterogenous population which might explain the heterogeneity within the metastatic colonies at distant sites (Cheung and Ewald, 2016; Lambert, Pattabiraman and Weinberg, 2017; Vilchez Mercedes *et al.*, 2021). Similarly to carcinoma cells that undergo EMT, the cells at the invasive front of these migrating clusters, referred to as "leader" cells, display more aggressive features such as a re-organised cytoskeleton (enriched in protruding actin fibres) and ECM-remodelling functions, and integrate and respond to the stimuli generated within the TME to better coordinate the invasive phalanx across the tissue (Stuelten, Parent and Montell, 2018; Vilchez Mercedes *et al.*, 2021).

1.2.4 Targeting metastases in cancer

Despite the ever growing efforts and advances in cancer therapy, metastases remain the major cause of death from cancer and represent the terminal stage of this disease (Steeg, 2016; Lambert, Pattabiraman and Weinberg, 2017; Anderson *et al.*, 2018; Esposito, Ganesan and Kang, 2021). This outcome could be partially ascribed to the longstanding tradition in cancer research of targeting the pathways underpinning tumorigenesis, thus overlooking the pivotal role of those promoting resistance to the conventional therapies and the formation or acceleration of cancer metastases (Steeg, 2016; Anderson *et al.*, 2018). To add more complexity to this scenario, the current therapies targeting metastases under development are mainly cytostatic and not cytotoxic,

which complicate their validation fuelling the scepticism around the topic (Steeg, 2016). To date, the available therapeutic approaches (tyrosine kinase inhibitors, antibody-drug conjugates etc.) have shown a very limited impact on keeping the progression of metastases at bay, nevertheless, the latest immunotherapeutic strategies have shown promising results by extending the survival rate of metastatic patients (Steeg, 2016; Anderson *et al.*, 2018; Esposito, Ganesan and Kang, 2021). Another aspect contributing to this mild though promising survival extension derives from the advances in the adjuvant treatments which help with the clearance of the disseminated malignant cells, thus delaying or preventing the occurrence of relapse (Anderson *et al.*, 2018; Esposito, Ganesan and Kang, 2021). Nevertheless, the multidisciplinary approach characterising the latest cancer research has allowed the identification of new potential candidates to overcome therapy resistance and metastases. Indeed, the awareness of a pivotal role played by the TME in determining the outcome of malignancies, especially of solid tumours, has led to investigating the bidirectional interactions engaged by cancer cells with stromal cells to identify the Achilles's heel in this detrimental liaison and eventually target it in better designed preclinical and clinical trials (Steeg, 2016; Anderson *et al.*, 2018; Ganesh and Massagué, 2021).

Table 1.1: Preclinical data for potential anti-metastatic therapy (Anderson et al., 2018)

Agent	Target	Preclinical data	References
Antibodies	CCL2	Prevention of colorectal cancer liver metastases	(Zhao *et al.*, 2013)
	BMP6	Reduction of prostate cancer bone metastases	(Dai *et al.*, 2005)
	PTHrP	Reduction of melanoma liver and bone metastases	(Huang *et al.*, 2014)
	N-cadherin	Reduction of prostate cancer growth, metastases and castration resistanceReduction of	(Tanaka *et al.*, no date)

	CD24	bladder cancer lung metastases	(Overdevest *et al.*, 2011)
	CDCP1	Prevention of lung metastases	
	TSPAN8	Reduction of ovarian cancer metastases	(Casar *et al.*, 2011)
			(Park *et al.*, 2016)
Small-molecule inhibitors			
BL3923	CCR1	Suppression of colon cancer liver metastases	(Kitamura *et al.*, 2010)
SD208	TFGβ-receptor	Reduction of melanoma and prostate cancer bone metastases	(Mohammad *et al.*, 2011; Sato *et al.*, 2015)
CCT129254	Multiple kinases	Inhibition of melanoma lung metastases	(Sadok *et al.*, 2015)
CA-074	Cathepsin B	Reduction of breast cancer bone metastases	(Withana *et al.*, 2012)
Peptides			
T22	CXCR4	Synergic with anti-CTLA-4 therapy in shrinking melanoma metastases	(Lee *et al.*, 2006)
Ac-PhScN-NH_2	α5β1 integrin	Inhibition of breast cancer bone	(Yao, Veine and Livant, 2016)

		metastases and lung colonisation	
Immunotherapies			
***MTDH* DNA vaccine**	MTDH	Prevention of breast cancer lung metastases	(Qian *et al.*, 2011)
***LMP1* DNA vaccine**	LMP1 viral antigen	Inhibition of lung metastases	(Lin *et al.*, 2017)
Others			
Retinoic acid	Retinoic acid receptor	Inhibition of melanoma lung metastases	(Edward, Gold and Mackie, 1992)
IGF trap	IGF receptor	Reduction of colon and lung cancer liver metastases	(N. Wang *et al.*, 2015)
***N*-acetylcysteine**	Reactive oxygen species	Inhibition of pancreatic cancer liver metastases	(Shimojo *et al.*, 2013)

1.3 The role of the tumour microenvironment in malignant progression

For a long time, cancer was believed to originate due to genetic alterations making it a cell-autonomous process; however, recent studies have recognised tumours as heterogeneous systems dynamically influenced by its micro-environment (Maman and Witz, 2018). These stromal components comprise CAFs, immune cells, and various others, such as endothelial cells and neurons (Jin and Jin, 2020). Together, these cellular components within the tumour constitute the TME (see Figure 1.3). TME is highly dynamic and plastic and its components engaged in a persistent bidirectional interaction with cancer cells. Indeed, the latter educate the TME to better co-opt it and exploit it for developing the hallmarks needed to survive and thrive (Jin and Jin, 2020; Hanahan, 2022). In this scenario, the cellular components governing the TME, which eventually influence the tumour growth, communicate with each other by producing and secreting factors such as cytokines, chemokines, metabolites, neurotransmitters, proteases and a

characteristic extracellular matrix (ECM) (Whiteside, 2008; Cole *et al.*, 2015; Wu and Dai, 2017; Maman and Witz, 2018; Jin and Jin, 2020). Altogether, this complex network is an ultimate orchestrator of tumour initiation, progression, and propagation (Jin and Jin, 2020; Hanahan, 2022). An outstanding role is played by CAFs which are not simply the most represented cell type within the TME but, thanks to their versatility and broad range of functions, they contribute to most of the hallmarks of cancer (Sahai *et al.*, 2020).

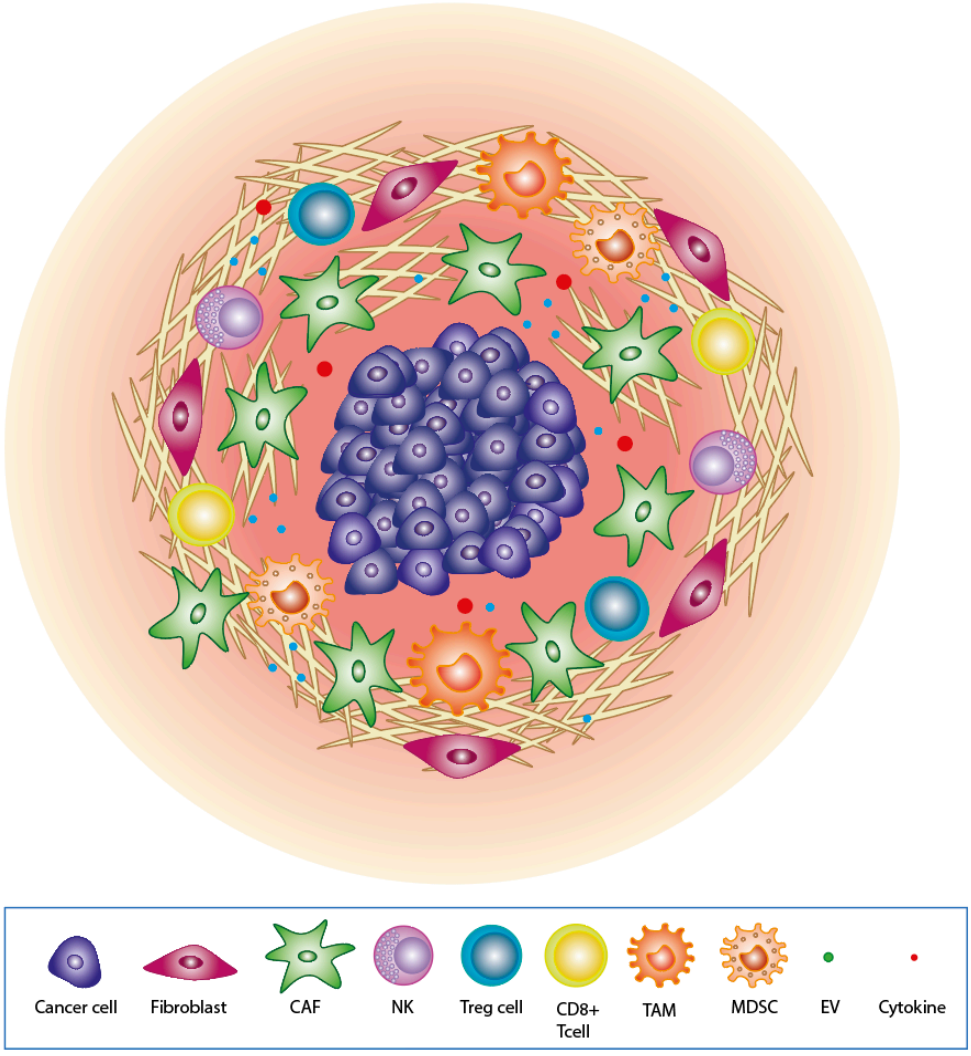

Figure 1.3: Tumour microenvironment components.

The tumour microenvironment is a highly dynamic system wherein a variety of cells cross-talk with cancer cells. These cells include stromal, immune and endothelial cells which are embedded in the fibrillary extracellular matrix (ECM) (Illustration generated using Adobe Illustrator software).

1.3.1 Cancer-Associated Fibroblasts

Cancer-associated fibroblasts (CAFs), also referred to as tumour-associated fibroblasts (TAFs), myofibroblasts, reactive stromal fibroblasts, or activated fibroblasts, form the predominant cell population within the tumour stroma (Chen and Song, 2019; Sahai *et al.*, 2020; Chen, McAndrews and Kalluri, 2021). CAFs derive from the activation of a variety of mesenchymal-like cell subpopulations of mesodermal origin. These include resident quiescent fibroblasts, bone-marrow-derived fibrocytes, mesenchymal stem cells (MSCs), endothelial cells, epithelial cells, pericytes, smooth muscle cells, and adipocytes (LeBleu and Kalluri, 2018; Chen and Song, 2019; Sahai *et al.*, 2020; Chen, McAndrews and Kalluri, 2021).

In normal tissue, during homeostasis, the resident fibroblasts represent a discrete population of resting cells embedded within the fibrillary ECM, which is activated in response to context-dependent stimuli, such as wound healing, tissue inflammation, organ fibrosis, and neoplastic lesions (Sahai *et al.*, 2020; Chen, McAndrews and Kalluri, 2021). Upon activation, fibroblasts transdifferentiate into "activated fibroblasts" and, eventually, can differentiate in further subtypes in a context-dependent fashion (Kalluri, 2016; Sahai *et al.*, 2020). This results in the acquisition of proliferative and migratory properties, exerting a variety of functions including ECM remodelling, immune cell recruitment, altered cytokine and chemokines production and induction of angiogenesis (Kalluri, 2016; LeBleu and Kalluri, 2018; Chen and Song, 2019; Sahai *et al.*, 2020). However, detection of CAF *in vivo* poses challenges. Existing markers of CAF are not specific nor exclusive since other cell types also express some of these markers. In this regard, considering multiple markers in parallel is highly recommended to help distinguish a specific subset (Kalluri, 2016; Chen and Song, 2019; Sahai *et al.*, 2020; Chen, McAndrews and Kalluri, 2021). Some of the markers of CAFs are summarised in Table 2.

Table 1.2 Cancer-associated fibroblast markers

Marker	Example	References
Extracellular matrix	Tenascin C	(Ni *et al.*, 2017)
	Collagen I and II	(LeBleu and Kalluri, 2018)
	Fibronectin	(Clarke *et al.*, 2016)
Growth factors and cytokines	TGF-β	(LeBleu and Kalluri, 2018)
	HGF	(Grugan *et al.*, 2010)
	bFGF	(LeBleu and Kalluri, 2018)
	Il-6	(Abulaiti *et al.*, 2013)
Growth factor receptors	TGFβRI and II	(LeBleu and Kalluri, 2018)
	EGFRs	(Mink *et al.*, 2010)
Integral membrane proteins	VCAM1	(LeBleu and Kalluri, 2018)
	FAP	(Yang *et al.*, 2016)
Cytoskeleleton and cytoplasmic components	α-SMA	(LeBleu and Kalluri, 2018)
	Vimentin	(LeBleu and Kalluri, 2018)

Tumours shape the tumour stroma by reprogramming the indolent quiescent fibroblasts into CAFs to generate a tumour-supportive microenvironment. This conversion is achieved through the production of cancer-derived factors in combination with specific TME stimuli, such as TGFβ, pro-inflammatory cytokines, hypoxia, oxidative stress and exosomes (carrying growth factors, functional DNA fragments and coding/non-coding RNAs) (Kalluri, 2016; Sahai *et al.*, 2020). In addition, this process leads to a metabolic shift towards aerobic glycolysis, to fulfil, in a paracrine manner, the biosynthetic and energetic demands of cancer and stromal cells (Kalluri, 2016; Sahai *et al.*, 2020). Altogether, this metamorphosis lays the foundation for a symbiotic relationship between malignant cells and CAF, which is responsible for their co-evolution and mutual adaptation and influence. Despite the widely recognised functional significance of CAFs in tumorigenesis and tumour progression, the mechanisms underpinning their bimodal influence, both pro- and anti-tumorigenic, remain poorly understood (Kalluri, 2016; LeBleu and Kalluri, 2018; Maman and Witz, 2018; Chen and Song, 2019). Thus, determining how CAFs are differentiated and how they influence tumours, other cells of the TME and induce metabolic changes may be instrumental in designing new targeted therapies for treating cancer.

1.3.1.1 CAF heterogeneity

The heterogenous nature of CAFs is not surprising considering the variety of cells they originate from. To date, from different neoplastic lesions it has been possible to isolate at least two "distinct" subsets of CAFs with specific functions consistently with the tumour landscape features (Chen, McAndrews and Kalluri, 2021) (Table 3). Those frequently identified are referred to as myofibroblastic CAFs (myCAFs) and inflammatory CAFs (iCAFs). Intuitively, the former exhibit a contractile and ECM-remodelling phenotype, expressing high levels of α-SMA, whereas the latter is characterised by an immunomodulating phenotype through a pro-inflammatory secretome, and expressing lower α-SMA but higher IL-6 levels (Öhlund *et al.*, 2017). Furthermore, although recently single-cell RNA sequencing along with functional assays shed light on the potential subdivisions of CAFs in specialised populations, whether a single type of CAFs or whether subsets of specialised CAFs are responsible of multiple simultaneous functions remains unclear (Sahai *et al.*, 2020). This confusion might arise from the co-expression of biomarkers shared by the different subsets of CAFs or by the loss of biomarkers as consequence of the protocols used to isolate and culture CAFs *ex vivo* (Puram *et al.*, 2017; Kieffer *et al.*, 2020).

Table 1.3 CAF subpopulations identified in indicated cancer types (Chen, McAndrews and Kalluri, 2021)

Tumour type	CAF subpopulation	Biomarkers
Breast cancer and ovarian cancer (Costa *et al.*, 2018; Givel *et al.*, 2018; Kieffer *et al.*, 2020; Pelon *et al.*, 2020)	CAF-S1 CAF-S2CAF-S3 CAF-S4	α-SMA^{high}, FAP^{high} Low expression of most detected markers α-SMA^{low}, FSP1^{+} and PDGFRβ^{+} α-SMA^{high}, CD29^{high}, FAP^{low},
Colorectal cancer (Li *et al.*, 2017; Zhang *et al.*, 2020)	CAF-A CAF-B	FAP^{+}, MMP2^{+}, DCN^{+} α-SMA^{+}, TAGLN^{+}, PDGFA^{+}
Head and Neck Cancer	Myofibroblasts	α-SMA^{+}, MYLK^{+}, MYL9^{+}

(Puram *et al.*, 2017)	CAF1	FAP^+, $PDPN^+$, $COL1A2^+$, $THY1^+$, VIM^+, $CAV1^+$, $MMP11^+$
	CAF2	FAP^+, $PDPN^+$, FOS^+, JUN^+, $FGF7^+$, $TGFB2^+$
Melanoma	S1	Immune CAFs, $CD34^+$
(Davidson *et al.*, 2020)	S2	Desmoplastic CAFs, TNC^+
	S3	Contractile CAFs, α-SMA^+
Pancreatic cancer	Myofibroblastic CAFs	αSMA^+, $THY1^+$, $TAGLN^+$,
(Öhlund *et al.*, 2017; Bernard *et al.*, 2019; Elyada *et al.*, 2019; Hosein *et al.*, 2019; Y. Chen *et al.*, 2021)	(myCAFs)	$CTGF^+$, $IGFBP3^+$, $COL12A1^+$, $THBS2^+$, $LRRC15^+$
	Inflammatory CAFs (iCAFs)	$CLEC3B^+$, $COL14A1^+$, $LY6C^+$
	Antigen-presenting CAFs	$CD74^+$, $SLPI^+$, $SAA3^+$, $MHCII^+$, $FSP1^+$
Prostate cancer	CAF-S1	αSMA^+, $PDGFR\beta^+$
(S. Chen *et al.*, 2021)	CAF-S2	$PDGFR\alpha^+$, $CREB3L1^+$, $PLAGL1^+$
	CAF-S3	αSMA^+, $HOXB2^+$, $MAFB^+$

1.3.1.2 The tumour-promoting role of CAFs

The majority of CAFs' activities centre on their versatile secretome, which functions in both an autocrine and paracrine (and potentially endocrine) manner (Chen and Song, 2019). A well-characterised property of CAFs is the ability to remodel the extracellular matrix (ECM). The ECM is a complex network comprised of cell-secreted proteins and polysaccharides, which provides biochemical, structural and adhesive support within tissues and organs (Erez *et al.*, 2010; Frantz, Stewart and Weaver, 2010). In contrast to normal fibroblasts, CAFs increase the production of ECM components, such as fibronectin (and its variant ED-A), hyaluronan and type I and IV collagens (Kalluri and Zeisberg, 2006; Chen *et al.*, 2010; Kobayashi *et al.*, 2010; Zhang *et al.*, 2016; Chen, McAndrews and Kalluri, 2021). These molecules exacerbate ECM stiffening, cell

adhesion and migration and immune suppressive cell recruitment, respectively (Ohno *et al.*, 2002; Kalluri and Zeisberg, 2006; Cirri and Chiarugi, 2012; Cox *et al.*, 2013; Pickup, Mouw and Weaver, 2014; Gascard and Tlsty, 2016). On the other hand, CAFs exert an ECM degradation function by producing and releasing proteases such as the metalloproteinases (MMPs) and plasminogen activators, which promote tumour cell migration and epithelial to mesenchymal transition (EMT) (Jedeszko *et al.*, 2009; Vosseler *et al.*, 2009; Kessenbrock, Plaks and Werb, 2010; Shieh *et al.*, 2011; Cirri and Chiarugi, 2012; De Palma, Biziato and Petrova, 2017). These enzymes can cleave adhesion molecules like cadherins, enhancing tumour growth by cleaving membrane-bound growth factors or cytokines, including their receptors, and trigger invasiveness and angiogenesis (Murphy, 2008; Kessenbrock, Plaks and Werb, 2010; Cirri and Chiarugi, 2012; De Palma, Biziato and Petrova, 2017). Tumour growth and migration is promoted by the production of several growth factors including transforming growth factor β (TGF-β), epidermal growth factor (EGF), hepatocyte growth factor (HGF) and basic fibroblast growth factor (bFGF) (Cowden Dahl *et al.*, 2008; Duffy *et al.*, 2009; Kessenbrock, Plaks and Werb, 2010; Bonnans, Chou and Werb, 2014; De Palma, Biziato and Petrova, 2017). The tumour immunity and vascular network programmes are regulated by the secretion of cytokines and growth factors such as stromal derived growth factor 1 (SDF1, also known as C-X-C motif chemokine 12 or CXCL12), interleukin 6 (IL-6), interleukin β (IL-β) through nuclear factor-kB (NF-kB) signalling, vascular endothelial growth factor (VEGF), platelet-derived growth factor C (PDGFC) and osteopontin. In turn, cancer cells secrete soluble factors that enhance the CAF pro-tumorigenic secretome (Kessenbrock, Plaks and Werb, 2010; Cirri and Chiarugi, 2012; De Palma, Biziato and Petrova, 2017; Chen and Song, 2019).

As consequence of both the intra-tumoral hypoxia and the high demand of metabolic substrates to sustain cancer cell proliferation, CAF shift towards aerobic glycolysis, supported by the stabilisation of the hypoxia-inducible factor 1α (HIF1α), reactive oxygen species (ROS) and growth factors including TGF-β and PDGF (Pietras *et al.*, 2008; Toullec *et al.*, 2010; Martinez-Outschoorn *et al.*, 2011; Cirri and Chiarugi, 2012; Ghesquière *et al.*, 2014; Gascard and Tlsty, 2016; Chen and Song, 2019). More importantly, in addition to the direct contribution to cancer progression by fuelling metabolic pathways like the TCA cycle, the metabolic shift in CAFs may indirectly modulate the immune response by regulating the availability of metabolites that are essential for immune cells (e.g. increased arginase levels can deplete arginine that is essential for T effector cell activation) (Cirri and Chiarugi, 2012; Fiaschi *et al.*, 2012; Ino *et al.*, 2013; Kalluri, 2016; Chen and Song, 2019).

Altogether, the above-mentioned functions can lay the foundation of drug-resistance, by fostering an immune suppressive environment, by increasing the intra-tumoral interstitial pressure that leads to reduced access of chemotherapeutics, by inducing a dormancy phenotype through modulation of cell adhesion and by boosting pro-survival signalling cascades (Hazlehurst *et al.*, 2000; Heldin *et al.*, 2004; White, Rayment and Muller, 2006; Meads, Gatenby and Dalton, 2009; Kalluri, 2016; Chen and Song, 2019; Chen, McAndrews and Kalluri, 2021).

1.3.2.3 The tumour-restraining role of CAFs

Accumulating evidence showed that some subsets of CAFs display anti-tumorigenic properties and that identification of specific markers might contribute to design therapeutic strategies which might help to discriminate and preserve them from indiscriminate targeting (Kalluri, 2016; Chen and Song, 2019; Chen, McAndrews and Kalluri, 2021). For example, it has been shown that in pancreatic ductal adenocarcinoma (PDAC), the depletion of a specific subpopulation of CAFs correlated with a more aggressive phenotype and poor survival in mice (Özdemir *et al.*, 2014). Moreover, in oestrogen receptor positive (ER^+) breast cancer, the $CD146^+$ CAF population sustains oestrogen-dependent proliferation and sensitivity to tamoxifen in luminal breast cancer cells (Brechbuhl *et al.*, 2017). The mechanisms underpinning the negative regulation of cancer in these studies rely on the modulation of the immunosuppressive response and on angiogenesis, respectively (Özdemir *et al.*, 2014; Brechbuhl *et al.*, 2017). However, a comprehensive characterisation of the CAF subsets is still required and, in this regard, it is important to take into account the nature of the tissue/organ harbouring the malignancy, which might allow stratification of patients based on more reliable markers, avoiding deleterious therapeutic side effects.

Beside this CAF-intrinsic negative regulatory role, a considerable number of studies suggest the possibility of directly modulating the CAF secretome by enhancing its anti-tumorigenic immunomodulatory repertoire (Öhlund, Elyada and Tuveson, 2014; Kalluri, 2016; LeBleu and Kalluri, 2018; Chen, McAndrews and Kalluri, 2021). This may allow re-programming of CAF from a pro-tumorigenic to an anti-tumorigenic role without eliminating them, which may shift the physiological balance within the tissue.

1.3.2.4 Targeting CAFs

In light of the dichotomous nature of CAFs and thanks to an increased understanding of their biological function in cancer, many preclinical studies have been carried out. The most challenging obstacle to overcome remains the identification of reliable and specific markers to ensure precise targeting therapies (Valkenburg, De Groot and Pienta, 2018; Chen and Song, 2019; Chen, McAndrews and Kalluri, 2021). Nevertheless, the strategies currently adopted are summarised in Table 4.

Table 1.4: CAF-targeting therapeutic strategies

Strategy	Outcome	References
CAF depletion	CAFs are cleared by targeting their marker, either pharmacologically or via immunotherapeutics	(Scott *et al.*, 2003; Feig *et al.*, 2013)
Normalisation	CAFs are reversed into an inactive state or diverted towards an anti-tumorigenic phenotype	(Froeling *et al.*, 2011; Sherman *et al.*, 2014)
Targeting activation signalling and down-stream effectors	Targeting either the molecules inducing CAF formation or/and the pro-tumorigenic cytokines and chemokines released by CAFs	(Pietras *et al.*, 2008)

Targeting CAF-derived proteins	Inhibition of the signalling pathways responsible of the production of ECM components; Enhancement of ECM degradation	(Sato *et al.*, 2016)
Therapeutics delivery via CAFs	Induction of CAF uptake of nanoparticles containing anti-cancer agents: CAFs metabolise and release the content within the stroma	(Guo, 2013; Miao *et al.*, 2017)

Despite the advances in developing CAF-targeting therapies, it remains still challenging designing therapies applicable to all the forms of malignant tumours due to the extremely heterogeneous nature of CAFs and their context-dependent functions (Chen and Song, 2019; Chen, McAndrews and Kalluri, 2021).

In this regard, characterising the processes underpinning CAF initiation and CAF-mediated TME remodelling is crucial. Of note, one of the major mechanisms that determines CAF initiation is driven by tumour cells in a paracrine manner through the secretion of growth factors, such as TGF-β, in the stromal microenvironment, which results in conversion of fibroblasts into myofibroblasts (Sahai *et al.*, 2020). In turn, myofibroblasts sustain tumour progression and dissemination both directly and indirectly by influencing cancer cells via secretion of growth factor and by releasing ECM-degrading proteases respectively (Sahai *et al.*, 2020; Chen, McAndrews and Kalluri, 2021).

1.4 The ADAMs family of proteases

ADAMs (a disintegrin and metalloproteinases) are transmembrane and secreted metalloproteinases pertaining to the metzincin -superfamily of zinc-dependent metalloproteinases, constituting the astacins and matrix metalloproteinases (MMPs) (Seals and Courtneidge, 2003; Murphy, 2008). Along with snake venom metalloproteinases (SVMP) and the ADAMs containing thrombospondin motifs (ADAMTS), ADAMs comprise the adamalysin subfamily (Seals and Courtneidge, 2003; Murphy, 2008). At present, 21 functional ADAMs have been identified and characterised in 40 different organisms, including humans. Interestingly, only 13 human ADAMs display intact metalloproteinase domains exerting proteolytic activity (Edwards, Handsley and Pennington, 2009; Reiss and Saftig, 2009).

ADAMs exist as a distinct multi-domain structure (see Figure 1.4) comprise of an N-terminal signal peptide, a pro-domain, a furin-recognition site, a Zn^{2+}-dependent metalloproteinase catalytic domain, a disintegrin domain, a cysteine-rich domain, an epidermal growth factor (EGF)-like domain, a transmembrane domain and a cytoplasmic domain. The pro-domain is involved in the initial protein folding and in modulation of the metalloproteinase domain by keeping it inactive during the intracellular trafficking (Murphy, 2008). The furin-recognition site mediates the maturation process of some ADAMs such as ADAM10, ADAM12 and ADAM17. The disintegrin domain is responsible for cell–cell adhesion processes, including the disruption of integrin binding, and jointly with the cysteine-rich domain, negatively regulates access to the catalytic domain (Reiss, Ludwig and Saftig, 2006; Murphy, 2008; Rocks *et al.*, 2008; Edwards, Handsley and Pennington, 2009; Reiss and Saftig, 2009; Lambrecht, Vanderkerken and Hammad, 2018).

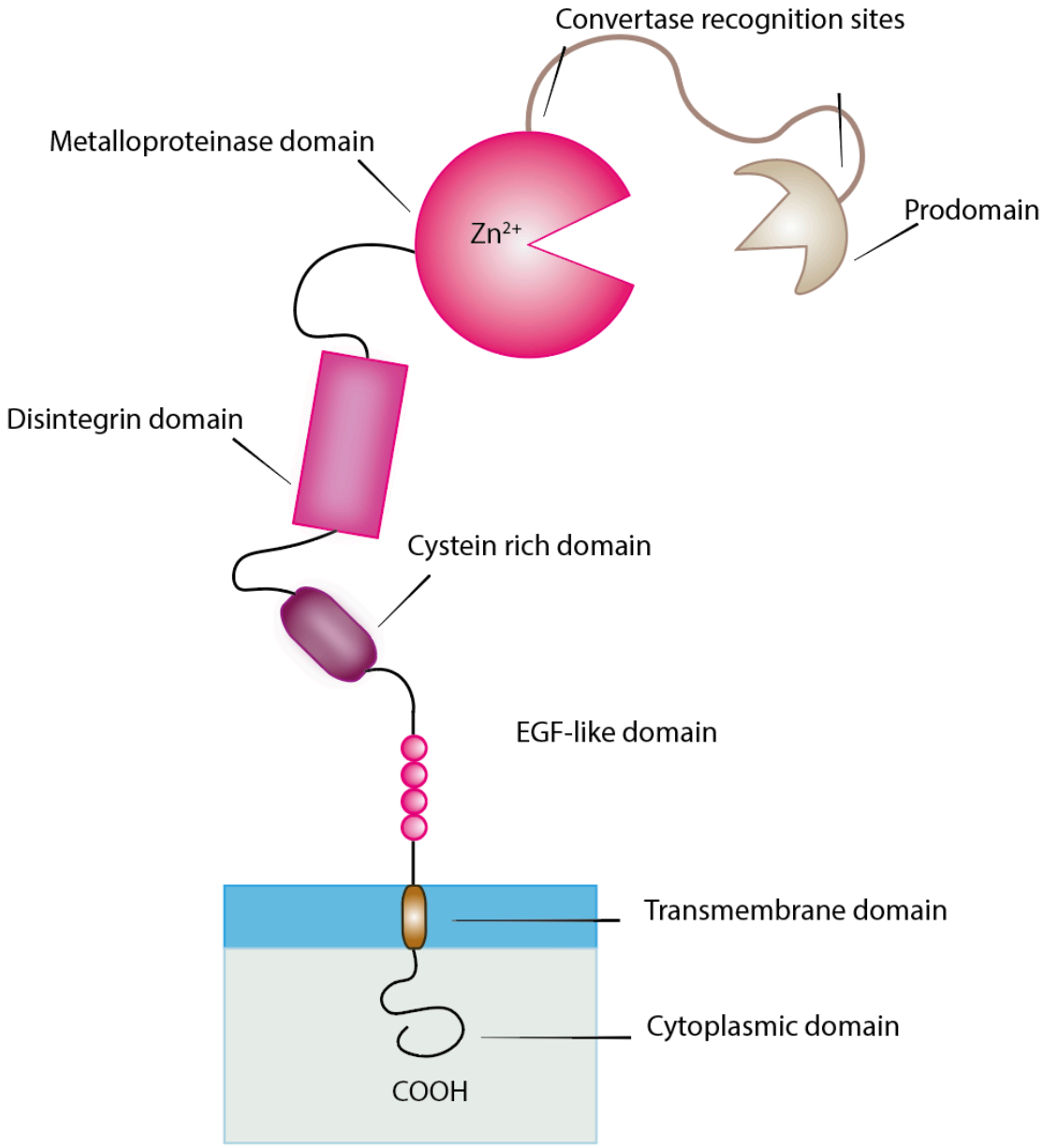

Figure 1.4: General ADAM structure (Illustration generated using Adobe Illustrator software).

Once synthesised within the rough endoplasmic reticulum (ER), ADAMs are translocated to the Golgi apparatus wherein, via either a furin- or a pro-protein convertase 7 mediated removal of the pro-domain, they are converted into their mature form (Reiss and Saftig, 2009). Although ADAMs are primarily located either in the Golgi or on the cell membrane, some of them have been described as soluble forms (e.g. ADAM12 and ADAM33) (Duffy *et al.*, 2011). Almost half of the family is proteolytically active (including ADAM10 and ADAM17), and shown to be implicated in both physiological and pathological processes, including cancer development and progression (Murphy, 2008). In this respect, high expression levels or upregulated proteolytic activity of some ADAMs members along with their detection predominantly at the invasive front of the neoplastic lesions have been demonstrated to correlate with aggressiveness, poor response to therapy and shorter overall survival (Sieuwerts *et al.*, 2005; McGowan *et al.*, 2008; Murphy, 2008; Duffy *et al.*, 2011; Dong *et al.*, 2015; Xiang *et al.*, 2020).

Additionally, ADAMs play an important role in the modulation of the regulated intra-membrane proteolysis (RIPping), a shedding process that results in the release of the intact cytoplasmic domain of a transmembrane protein within the cell, either for lysosome-mediated degradation or for translocation to other compartments (Blobel, 2005; Murphy, 2008).

1.4.1 ADAMs in cancer

The mechanisms through which ADAMs exert their pro-tumorigenic function are summarised in Table 4.

Table 1.5: ADAMs pro-tumorigenic functions

Function	Example	References
Activation of tumour-promoting signalling pathways	Cleavage and release of growth factors (e.g. HB-EGF) and growth factor receptors (e.g. CSF1R)	(Duffy *et al.*, 2009; Ebi *et al.*, 2010; Qing *et al.*, 2016)

Inactivation of growth inhibitory pathways	Prevention of the binding between inhibitory factors (e.g. TGF-β1) and their receptor (e.g. TGFBR1)	(C. Liu *et al.*, 2009; Duffy *et al.*, 2011)
Regulation of angiogenesis	Alteration of cell-cell interactions between neighbouring cells through the shedding of adhesion molecules Activation of angiogenic growth factors and cytokines	(Horiuchi *et al.*, 2003; Guaiquil *et al.*, 2009; Donners *et al.*, 2010)
Invasion and migration modulation	Through ECM remodelling and shedding of adhesion molecules (e.g. E-cadherin)	(Najy, Day and Day, 2008; Micocci *et al.*, 2013)
Immune response modulation	By cleaving and releasing cytokines and chemokines (e.g. TNF-α)	(Duffy *et al.*, 2011; Saad, Rose-John and Jenkins, 2019)
EMT regulation	Through alteration of cell-cell interactions and activation of EMT-promoting signalling pathways	(Duffy *et al.*, 2009; Ruff *et al.*, 2015; Jin *et al.*, 2020)

Due to their contribution in establishing some of the hallmarks of cancer (e.g. inactivating growth inhibitory pathways), ADAMs are potential candidates for targeted therapies, despite the challenges of validation and translation into clinics (Duffy *et al.*, 2011). In addition, the increasing body of evidence reporting the frequent association of specific ADAMs with certain malignancies and disease outcomes lays the foundation for the use of ADAMs as potential biomarkers (Duffy *et al.*, 2011). In this regard, ADAMs have been proposed as candidate markers for diverse purposes as described in Table 5.

Table 1.6: ADAMs as biomarkers

Clinical utility	Example	References
Diagnosis	ADAM12 in bladder cancer	(Fröhlich *et al.*, 2006)
Prognosis	ADAM17 in breast cancer	(McGowan *et al.*, 2008)
Response to therapy	ADAM9 and ADAM11 in breast cancer	(Sieuwerts *et al.*, 2005)

To date, the approaches adopted to tackle ADAMs pro-tumorigenic properties include low molecular weight synthetic inhibitors, purified or synthetic forms of ADAM pro-domains, engineered tissue inhibitors of metalloproteinases (TIMPs) and monoclonal antibodies (Duffy *et al.*, 2011). Nevertheless, most of these strategies have been limited to phase I and phase II trials due to inefficacy and significant hepatotoxicity (Murphy, 2008; Duffy *et al.*, 2011).

From a TME perspective, recent studies conducted on stromal fibroblast, especially on CAFs, demonstrated, for the first time, an important role of ADAMs in fostering CAFs traits and, mainly, their pro-tumorigenic functions. For example, CAFs isolated from colorectal cancer patients were shown to express higher levels of ADAM9 and ADAM17 as compared to the donor-matched normal fibroblasts (Mochizuki *et al.*, 2019), whereas high levels of ADAM12 were detected in αSMA^{+} stromal fibroblasts adjacent to neoplastic cells in murine models of prostate and breast cancer (Peduto *et al.*, 2006). In addition, CAFs isolated from breast cancer patients displayed higher levels of ADAM17 compared with donor-matched normal fibroblasts and that it enhanced cancer cell proliferation by cleaving TGF-α (Gao *et al.*, 2013) whereas CAFs derived from gastric cancer patients expressed high levels of iRhom2, encoded by the gene RHDBF2 (rhomboid 5

homolog 2), which triggered an ADAM17-mediated cleavage of the TGFBR1 thus rendering CAFs more invasive and more capable of favouring the invasion of cancer cells through the ECM (Ishimoto *et al.*, 2017). Moreover, using an indirect approach, another study reported the acquisition of CAF-like features by normal fibroblasts isolated from a mouse model deficient for all four tissue inhibitor of metalloproteinases (TIMPs) and that they exerted oncogenic functions via exosomes enriched with ADAM10, indicating a crucial role played by metalloproteinases in determining fibroblasts activation (Shimoda *et al.*, 2014).

1.4.2 ADAM17

ADAM17, discovered in 1997, was originally named TACE (TNF-α-converting enzyme) due to its role as a sheddase of the pro-inflammatory cytokine TNF-α. Currently, the spectrum of ADAM17 substrates numbers encompasses more than 90, including cytokines, chemokines adhesion molecules and several EGFR ligands (Zunke and Rose-John, 2017). ADAM17 is a protein of 824 amino acids encoded by a gene located at the chromosomal locus 2p25. Although belonging to the ADAMs family, ADAM17 shares very little sequence similarities with the other adamalysins including ADAM-10, which is the closest despite their protein sequence homology being less than 30% (Gooz, 2010; Zunke and Rose-John, 2017; Düsterhöft *et al.*, 2019). Distinct from the other adamalysins, wherein the cysteine-rich domain and the EGF-like domain are located between the disintegrin-like domain and the short stalk region, in ADAM17 a single domain, referred to as membrane-proximal domain (MPD), replaces both the cysteine-rich and the EGF-like domains (Düsterhöft *et al.*, 2019), see figure 1.5. Moreover, its stalk region contains a crucial motif referred to as CANDIS motif (Conserved Adam seventeeN Dynamic Interaction Sequence), which regulates the substrate recognition of some of the type-I transmembrane substrates, such as IL-6 receptor, but it is not involved in the type-II transmembrane substrate TNF-α recognition (Gooz, 2010; Zunke and Rose-John, 2017; Düsterhöft *et al.*, 2019). The N-terminal pro-domain of ADAM17 has chaperone-like functions, can inhibit the catalytic activity and is excised by the pro-protein convertase furin within the Golgi apparatus.

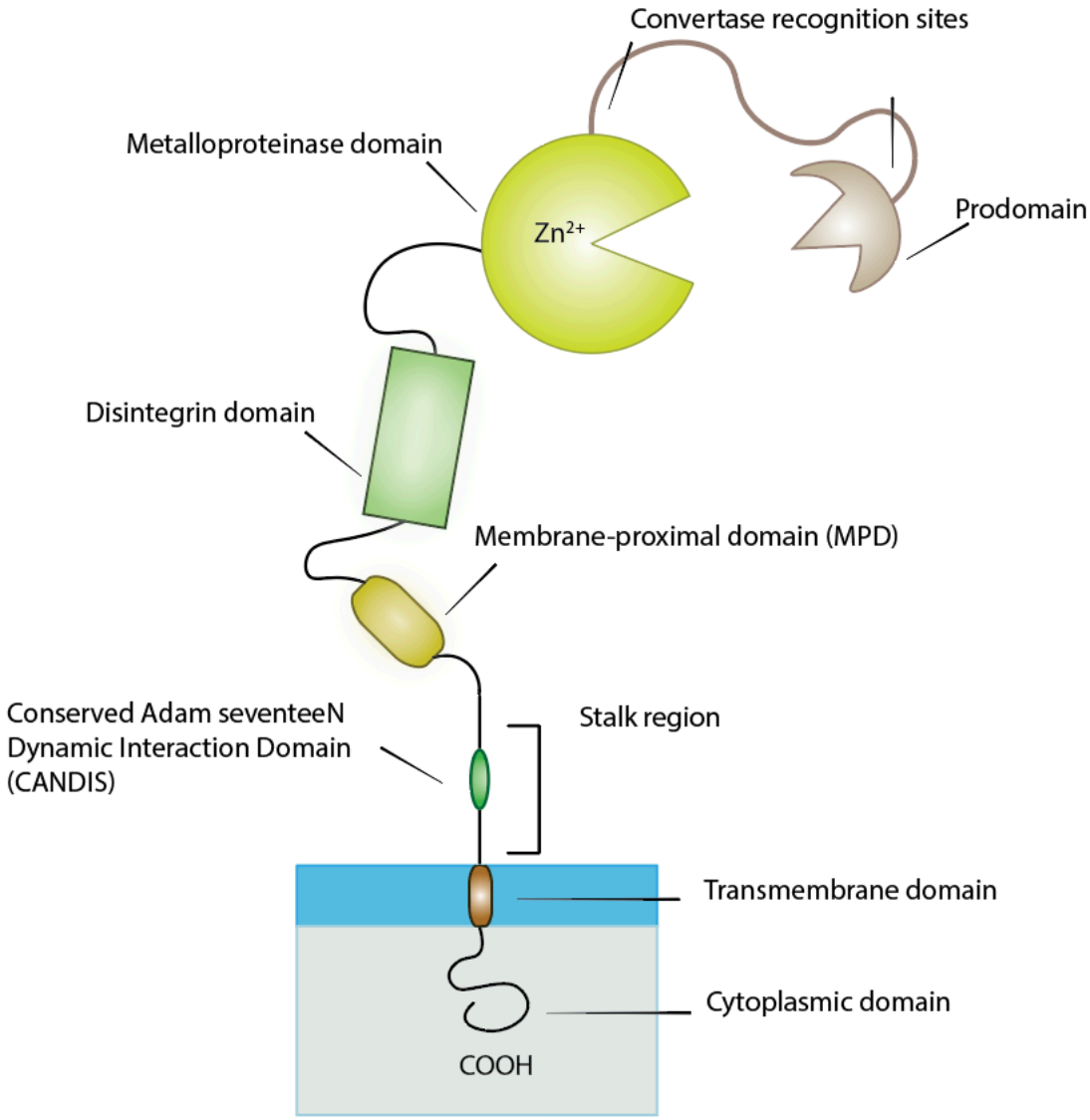

Figure 1.5: ADAM17 structure (Illustration generated using Adobe Illustrator software).

Furin-deficient cells, however, preserve their ability to activate ADAM17, suggesting an alternative and furin-independent proteolytic activation (Srour *et al.*, 2003; Gooz, 2010; Zunke and Rose-John, 2017). In addition, although the ADAM17 intracellular region (ICR) contains phosphorylation sites implicated in regulation of the proteolytic activity of the enzyme, mainly through p38 MAPK and extracellular signal–regulated kinases (ERKs), it has been reported that ADAM17 is functional in the absence of the ICR (Stefan Düsterhöft, Juliane Lokau, 2019).

ADAM17 is regulated at the post-translational level. In addition to its inhibitory effect exerted by its pro-domain, extracellular protein disulphide isomerases (PDI) have been shown to alter the conformation of and inhibit ADAM17 by converting the MPD from a flexible into an inflexible

structure (Düsterhöft *et al.*, 2013, 2019). Moreover, further widely recognised negative regulators of ADAM17 sheddase activity include interactions with integrins, annexins, the tetraspanin CD9 and secreted frizzled-related protein 3 (sFRP3). Endogenously, the tissue inhibitor of metalloproteinase 3 (TIMP3) represents the only TIMP member able to inhibit ADAM17 by binding to the catalytic domain of the dimerised form of ADAM17 (Amour *et al.*, 1998; Le Gall *et al.*, 2010). In addition, ADAM17 can be regulated through two members of the rhomboid-like superfamily of intramembrane serine proteases called iRhom1 and iRhom2, which mediate its maturation and trafficking (Christova *et al.*, 2013; Düsterhöft *et al.*, 2019).

1.4.3 ADAM17 in physiology

ADAM17 is ubiquitously expressed in a variety of organs including the brain, the heart, kidney, and skeletal muscle and its expression changes in a spatiotemporal regulated manner. It plays a crucial role during development, as confirmed by several *in vivo* studies wherein *Adam17*-deficient mouse models or transgenic mice lacking the Zn^{2+}-binding site of the catalytic domain showed perinatal lethality, epithelial development dysregulation, pulmonary hypoplasia, myocardial dysmorphism, bone development impairment and metabolic alterations (Peschon *et al.*, 1998; Shi *et al.*, 2003; Horiuchi *et al.*, 2007, 2009; Gelling *et al.*, 2008; Gooz, 2010). For example, in a mouse model of conditional inactivation of *ADAM-17* using the Cre-loxP system, wherein the expression of the inducible Cre recombinase is under the control of the promoter of the *Sox9* transcription factor, implicated in skeletal development, the littermates showed shortened bones along with an osteoporosis-like phenotype, bone marrow hypercellularity and extramedullary haematopoiesis in both the liver and spleen (Horiuchi *et al.*, 2009; Gooz, 2010).

ADAM17 also regulates crucial biological programmes including the immune and the nervous systems (Scheller *et al.*, 2011; Palazuelos *et al.*, 2014). Of note, its neural regulatory functions have been shown to be performed both directly, by acting as a α-secretase and shedding the amyloid-beta precursor protein (APP) (Rogers, Krieger and Vogt, 2001; Sastre, Walter and Gentleman, 2008) and indirectly through the release of pro-inflammatory molecules, thus acting as a neuro-inflammatory modulator (Romera *et al.*, 2004; Qian, Shen and Wang, 2016).

1.4.4 ADAM17 in cancer

ADAM17 has been widely investigated owing toits role in several diseases, including diverse types of cancer. However, the majority of the findings come from breast cancer studies, which showed

an ADAM17 contribution to breast cancer development and metastasis as well as an association with shorter overall survival (Gooz, 2010; Simabuco *et al.*, 2014; Shen *et al.*, 2016; Fang *et al.*, 2017; Schmidt *et al.*, 2018; Saad *et al.*, 2019).

The role of ADAM-17 in carcinogenesis is thought to be dependent on its sheddase activity, which fosters a pro-inflammatory response and sheds growth factors necessary for tumour progression and neovascularisation (Gooz, 2010; Moss and Minond, 2017a) (Table 6). In this regard, an increase of ADAM17–mediated shedding of epidermal growth factor ligands was reported to promote the development of malignancies (Zheng *et al.*, 2009; Rios-Doria *et al.*, 2015; J. Sun *et al.*, 2017; Schmidt *et al.*, 2018). Amongst the myriad of ADAM17 substrates, those proven to be involved in carcinogenesis are TNF-α, L-selectin, ALCAM, transforming growth factor (TGF)-α and TGFB1R (Kornfeld *et al.*, 2011).

In OSCC, ADAM17 plays a critical role in tumour invasion and metastasis through positive-feedback loop whereby TNFα mediates NFκB activation, leading to ADAM-17 maturation and cancer cell migration (Takamune *et al.*, 2008; Gooz, 2010). ADAM17 has been reported to contribute to anoikis (a type of programmed cell death elicited in anchorage-dependent cells upon detachment from the ECM) resistance and acquisition of stemness features in HNSCC. This event is underpinned by ADAM17-mediated cleavage of the multifunctional surface glycoprotein CD44, disrupting the cell-ECM interactions in favour of those between cells (Takamune *et al.*, 2008; Kamarajan *et al.*, 2013). A first attempt to use ADAM17 as a biomarker for the stratification of patients with OSCC showed that ADAM17 sheddase activity is strongly increased in neoplastic lesions compared to normal tissues and that the detection of this increased activity within primary tumours correlates with a significantly increased risk of cancer recurrence (Ge *et al.*, 2009).

Table 1.7: Some of the ADAM17 Substrates with a role in cancer.

Substrate	Role in cancer
Jagged 1 (JAG1) (Li *et al.*, 2014)	Notch-mediated regulation of tumour development and progression in colon, breast, cervical, ovarian, and hematological cancers

Glypican-1 (GLP1) (Aikawa *et al.*, 2008)	Its downregulation in pancreatic cancer cells resulted in attenuated tumour growth, angiogenesis, and metastasis *in vivo*.
Neuregulin 1 (NRG1) (Alava *et al.*, 2006)	Expressed in a subset breast cancer patients, it correlates with clinical response to antitumoral treatments such as trastuzumab
C-MET receptor (Mo and Liu, 2017)	CMET and its receptor C-MET are involved in proliferation, motility, migration, and invasion of diverse cancers
Vasorin (Liang *et al.*, 2019)	It stimulates malignant progression and angiogenesis
IL-6R (Goumas *et al.*, 2015; Yousefi *et al.*, 2019)	Thorough its binding to IL-6 promote pancreatic ductal adenocarcinoma (PDAC) cells growth and chemoresistance in ovarian cancer cells

1.4.5 Targeting ADAM17

As a consequence of the importance of ADAM17 in a broad range of malignancies many attempts have been carried out to either pharmaceutically or genetically target it (Yang *et al.*, 2021). In the last decades the advances in developing ADAM17 targeted therapies led to creation of neutralising antibodies which successfully inhibited ADAM17 activity (Trad *et al.*, 2013; Saha *et al.*, 2022), nevertheless, developing agents that selectively inhibit ADAM17 pro-tumorigenic functions, sparing other members of the family implicated in physiological processes, remains a challenge (Zunke and Rose-John, 2017; Düsterhöft, Lokau and Garbers, 2019). Furthermore, recent studies reported ADAM17 to be involved in a form of cell cycle arrest induced upon oncogene activation, known as oncogene-induced senescence or OIS. Interestingly, during OIS, senescent cells can exert their functions through their secretome, wherein some of the pro-tumorigenic components include ectodomains derived from transmembrane proteins are targets of ADAM17 (Effenberger *et al.*, 2014; Morancho *et al.*, 2015). In addition, in a *Pten*-deficient prostate conditional mouse

model, the loss of *Pten* triggered a strong upregulation of ADAM17 which, in turn, activated the Notch1 signalling pathway and resulted in by-passing anti-tumorigenic p27-driven senescence, leading to tumour progression and metastasis (Revandkar *et al.*, 2016).

1.5 Summary

Cancer therapeutics have often fallen short of the expectation of long-term eradication of the malignancies. The explanation to these disappointing results could be partially ascribed to the initial short-sighted approach to cancer research which was mainly cancer-centric, thus ignoring the potential contribution of the surrounding environment (Maman and Witz, 2018; Jin and Jin, 2020). Recently, the awareness of the tumour microenvironment as a fundamental orchestrator of tumour biology has led to it becoming a novel target for next generation therapies. Moreover, the latest data extrapolated from the large-scale sequencing of metastatic tumours revealed the absence of newly acquired mutations as source of spawning of metastases, suggesting, amongst the diverse theories, the TME as pivotal mediator (Lambert, Pattabiraman and Weinberg, 2017; Hanahan, 2022). However, the therapeutic strategies effectively targeting the TME remain insufficient (Jin and Jin, 2020). In this scenario, CAFs play a central role due to their abundance and involvement in tumour progression and therapy response. Nevertheless, a clear dissection of the sequence of events and mechanisms underpinning the functional contribution of CAFs in tumour progression remains elusive.

Noteworthy, many CAF functions within the TME are ascribed to their secretome, which can regulate the activation of crucial signalling pathways, remodel the ECM and mediate intercellular communications (Mueller and Fusenig, 2004; Kalluri and Zeisberg, 2006; Cirri and Chiarugi, 2012; Chen and Song, 2019).

Metalloproteinases, including ADAMs, have been reported to be up- regulated in tumours and ADAMs expression in the stromal compartment can promote malignancies by modulating the cell secretome (Blanchot-Jossic *et al.*, 2005; Mazzocca *et al.*, 2005; Kalluri and Zeisberg, 2006; Peduto *et al.*, 2006; Kessenbrock, Plaks and Werb, 2010; Shimoda *et al.*, 2014; Kalluri, 2016). For example, ADAM17 is pleiotropically implicated in cancer promotion and drug resistance (Kyula *et al.*, 2010; VanSchaeybroeck *et al.*, 2014; Zunke and Rose-John, 2017; Li *et al.*, 2018; Stefan Düsterhöft, Juliane Lokau, 2019). Indeed, ADAM17 has been reported to be up-regulated in different stromal cells and to shed a large repertoire of factors (more than 80 substrates), most of

which involved in promoting malignancies (Bohrer *et al.*, 2016; Mochizuki *et al.*, 2019; Sun *et al.*, 2020). Nonetheless, its role within CAFs remains poorly understood. Thus, a deeper characterisation of ADAM17, and eventually of the other members of the ADAMs family, in malignancies would shed light on the mechanisms involved in both cancer progression and cancer-mediated reprogramming of the microenvironment. More importantly, dissecting its role within the bi-directional interaction between cancer cells and CAFs and determining the exact sequence of events underlying this interaction could lead to the identification of better therapeutic strategies. As such, targeting ADAM17 could be combined with already existing cancer therapies, helping to overcome the current limitations reported with drug resistance and tumour recurrence.

1.6 Project hypothesis, aims and objectives

1.6.1 Project hypothesis

ADAM17 regulates the CAF phenotype and thereby modifies the interactions between CAF and malignant cells within the TME, influencing cancer cell behaviour.

1.6.2 Aims

The overall aim of this study is to investigate whether A Disintegrin and Metalloproteinases 17 (ADAM17) in CAF can influence their biology and functions and whether and how this could play a role in modulating cancer progression and migration. This overall aim will be addressed through the following:

1. Investigation of the bi-directional crosstalk between cancer cells and stromal fibroblasts.
2. Investigation of the impact of depleting ADAM17 in fibroblasts and how it affects their interaction with cancer cells.
3. Investigation of the pro-migratory mechanisms triggered in cancer cells by the CAF-associated ADAM17.
4. Determination of the CAF-associated molecular factors underlying the ADAM17-mediated paracrine regulation of cancer cell migration.
5. Investigation of the role of ADAM17 in experimentally induced CAF (eCAF).

1.6.3 Objectives

1. **To determine whether the crosstalk between cancer cells and fibroblasts could lead to any change in fibroblasts features and functions, including ADAM17 expression, and whether this could determine the stromal fibroblasts' paracrine-mediated influence on cancer cells.** Indirect co-culture of cancer cells and stromal fibroblasts will be used and the above-mentioned parameters will be assessed by western blot, qPCR, proliferation and migration assays.
2. **To determine the impact of depleting Adam17 in stromal fibroblasts on fibroblasts and cancer cell migration.** Firstly, ADAM17 will be depleted in both NOF and CAF using a small interfering RNA (siRNA) and CAF markers will be assessed by qPCR, western blot, immunofluorescence, proliferation and ELISA assays. Secondly, to evaluate the effect of C.M. derived from NOF and CAF depleted of Adam17 on cancer cell (H357 and H376) migratory and invasive potential migration, invasion and proliferation assays will be performed.
3. **To determine the molecular mechanisms elicited in cancer cells in response to the CAF-associated ADAM17 input.** A panel of markers associated with cancer cell migration will be assessed by western blot and qPCR assays. Next, the molecular factors identified as potentially involved in the observed phenotype will be pharmacologically targeted. Lastly, ADAM17-paracrine effect will be evaluated also in OSCC cells through depletion of ADAM17 by siRNA.
4. **To identify the changes determined by genetically inhibiting ADAM17 in CAF and whether these could be associated to the role of ADAM17 in mediating cancer cell migration.** Proteomics analysis will be performed via Label-Free Mass Spectrometry (LFMS) to identify the differentially expressed proteins between control CAF and ADAM17-depleted CAF. To allow statistical comparisons, three biological replicates will be prepared for each group. Next, the signalling pathways identified will be genetically targeted to assess whether involved in the phenotype observed upon depletion of ADAM17 and the relative markers will be associated by western blot and qPCR assays. Moreover, the C.M. derived from each condition will be used in indirect coculture experiments to evaluate the impact on cancer cell migration through wound healing assays.
5. **To determine whether eCAF could recapitulate the phenotype observed upon stimulation of NOF and CAF with the C.M. derived from cancer cell.** NOF will be initially treated with recombinant TGF-β1 and ADAM17 levels will be assessed by western

blot, qPCR and ELISA assays. CAF markers will be evaluated by western blot and qPCR assays along with immunofluorescence staining. Next, ADAM17 will be depleted by siRNA, CAF markers evaluated as above-mentioned and the C.M. will be tested on cancer cells to determine its impact on their migration through wound healing assays.

Chapter 2

Materials and methods

2.1 Cell growth and propagation

2.1.1 Cell lines and culture conditions

2.1.1.1 Normal oral fibroblasts

Primary normal oral fibroblasts (NOF) were isolated from human gingival or buccal tissue, as previously described (Hearnden *et al.*, 2009) (Sheffield Research Ethics Committee reference number 09/H1308/66). NOFs were used at passage 3-11.

2.1.1.2 Cancer-associated fibroblasts

Primary human cancer associated fibroblasts were isolated from OSCC resection specimens (Elmusrati et al., 2017) from Sheffield Teaching Hospitals NHS Foundation Trust (Sheffield Research Ethics Committee reference number 13/NS/0120, STH17021). CAFs were used at passage 3-11.

2.1.1.3 H357

The human oral squamous cell carcinoma (OSCC)-derived cell line H357 was retrieved from the department bio-repository. This cell line was established from a SCC of the tongue excised from a 74 year-old Caucasian male patient (Prime *et al.*, 1990). Cells were authenticated by NorthGene by the Short Tandem Repeat (STR) DNA profiling analysis based on the Deutsche Sammlung von Mikroorganismen und Zellkulturen (DSMZ) database (matching percentage of 97%).

2.1.1.4 H376

The human oral squamous cell carcinoma (OSCC)-derived cell line H376 was retrieved from the department bio-repository. This cell line was established from a SCC of the floor of the mouth excised from a 40 year-old patient (Prime *et al.*, 1990). Cells were authenticated by NorthGene by the Short Tandem Repeat (STR) DNA profiling analysis based on the Deutsche Sammlung von Mikroorganismen und Zellkulturen (DSMZ) database (matching percentage of 93%).

2.1.2 Cell subculture and propagation

Cells were grown until sub-confluent (70-80% confluence) in DMEM (catalogue number D6546-500ML, Sigma-Aldrich) supplemented with 10% fetal bovine serum (FBS) (catalogue number 10270-106, Gibco by Life Technologies), 2 mM L-glutamine (catalogue number G7513-100ML, Sigma-Aldrich) and penicillin and streptomycin (100 i.u.ml and 100 µg/ml, respectively) (catalogue number P0781-100ML, Sigma-Aldrich). Cell propagation was performed by discarding spent cell culture media from the T175 cm^2 cell culture flask and rinsing 2-3 times the flask using 5 ml of sterile calcium- and magnesium-free phosphate buffered saline (PBS) (P4417-100TAB, Sigma-Aldrich). Afterwards, cells were incubated with 3 ml of Trypsin-EDTA solution (catalogue number T3924, Sigma-Aldrich) at 37°C for 5 minutes to allow their detachment from the flask. Trypsin was neutralised with fresh cell culture media, in a ratio of at least 1:1. Cells were re-suspended and centrifuged (centrifuge Sigma 3-18KS) at 192 x g for 5 minutes, supernatant was carefully discarded and the cellular pellet homogenously re-suspended in 1 ml of cell culture media by gently pipetting up and down. Cells were diluted in fresh cell culture media, the volume varied accordingly both the number of cells required and the flask of destination. Cells were incubated at 37°C in a humidified atmosphere with 5% CO_2.

2.1.3 Cell cryopreservation

Cell pellets were obtained as described in section 2.1.2. Supernatant was discarded and pellet was gently re-suspended in freezing down media containing FBS supplemented with 10% dimethyl sulfoxide (DMSO) (catalogue number D2650-100ML, Sigma Aldrich). 1 ml of suspension was transferred to cryo-vials and placed in a Nalgene freezing container (ThermoFisher, UK), filled with isopropanol to allow slow freezing of the cells, at the rate of -1ºC per minute, in a -80 ºC freezer for 24 h. Afterwards, cryo-vials were moved to liquid nitrogen for long-term storage.
To recover the cells, cryo-vials were thawed quickly in a water-bath at 37°C (ThermoFisher, UK), centrifuged at 192 x g for 5 min, to ensure complete removal of the DMSO, and re-suspended in fresh cell culture media. Cells were seeded in T25/T75 flasks, based on the number of cells required.

2.2 TGF-β1-induced myofibroblasts differentiation

NOFs were cultured in T175 flasks until sub-confluent. Cells were harvested as previously mentioned (see section 2.1.2). Once the cell pellet was homogenously re-suspended in 1ml of

culture medium, it was further diluted to facilitate the cell counting. Afterwards, 10 µl of cell suspension was mixed with an equal volume of Trypan blue 0.4 % solution (catalogue number T10282, Life Technologies). Trypan blue stains only dead cells and it is used to estimate the proportion of viable cells within a cell population (Strober, 2015). Cells were quantified using a haemocytometer (Mishra, Chandrasekar and Mishra, 2014), and the volume of cells needed for the experiment was determined accordingly the number of cells required.

For western blot (WB) (see section 2.8) analysis and quantitative real-time polymerase chain reaction (qPCR) (see section 2.7) 250,000 cells were seeded in 6 well plates and incubated overnight, to allow cell attachment. The same number of cells were seeded on sterile coverslips (VWR) (2 ml / well) in a 6 well plate for immunofluorescence (see Figure 2.1).

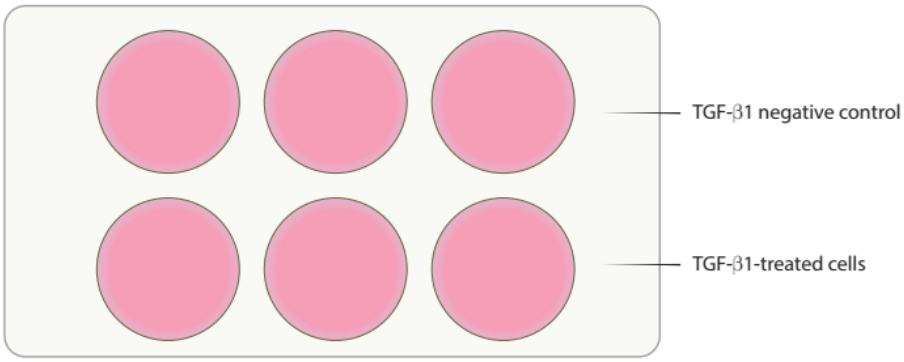

Figure 2.1 Schematic representation of TGF-β1 treatment.

NOFs or H357 cells both treated and untreated with TGF-β1. NOFs were seeded on coverslips in 6-well cell culture plates and treated with recombinant human TGF-β1 (2.5ng/ml) or kept in serum-free media as negative control.

On the following day, spent media was discarded and plates rinsed 2-3 times with PBS, to ensure complete removal of FBS. Afterwards, cells were serum-starved in serum-free media (2 ml/ well) for 24 h (Kabir *et al.*, 2016; Elmusrati *et al.*, 2017). The absence of serum is fundamental to rule out its involvement during TGF-β signalling pathway stimulation (Danielpour *et al.*, 1989; Midgley *et al.*, 2013). At the end of the incubation, serum-free media was discarded and replaced with serum-free supplemented with 2.5 ng/ml recombinant human TGF-β1 (R&DSystems, UK) for 48h at 37^{o} C. Both TGF-β1 concentration and 48h for the incubation were determined upon evaluation of TGF-β1 downstream targets via a TGF-β1 dose response assay and time course experiment, respectively. As a negative control, some wells were not treated with TGF-β1.

2.3 Small interfering RNA (siRNA)-mediated knock-down (KD)

Cells were seeded onto 6, 12 or 24 well plates, the number of cells and volume of both reagents and cell culture media was scaled down according to the plate type.

Cells were transiently transfected with the siRNA targeting the desired gene and negative control siRNA (see Table 2.1) using an oligofectamine lipid-based protocol (catalogue number 12252011, Invitrogen). Afterwards, 50 nM of siRNA was mixed with 5 µl of oligofectamine in a final volume of 200 µl of serum-free and antibiotic-free DMEM per well. After 5-6 h of incubation at 37° C the transfection mix was discarded and replaced with fresh culture media (complete media or serum-free, depending on the experiment).

Table 2.1: List of siRNA

siRNA target	Catalogue number
ADAM17	4390824, s13718, ThermoFisher Scientific 4390824, s13720 ThermoFisher Scientific L-003453-00-0005, Horizon Perkin Elmer
STAT2	L-012064-00-0005, Horizon Perkin Elmer
STAT3	L-003544-00-0005, Horizon Perkin Elmer
cGAS	L-015607-02-0005, Horizon Perkin Elmer
AKT1	L-003000-00-0005, Horizon Perkin Elmer
Negative control #1 (scramble)	AM4611, ThermoFisher Scientific
Non-targeting control pool	D-001810-10-05, Horizon Perkin Elmer

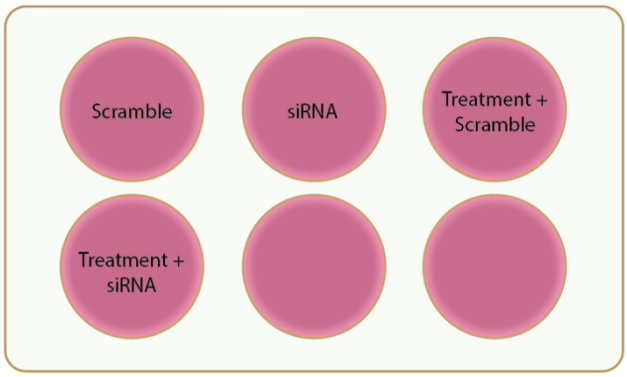

Figure 2.2 Schematic representation of gene downregulation mediated by siRNA.

NOFs, CAFs and OSCC cell lines were seeded in 6-well cell culture plates (or other plate format) and depleted of the desired target gene using 50 nM of siRNA or negative control (scramble) for 24/48 hours. The siRNA treatment could be performed prior or post a specific treatment (conditioned medium, drugs etc.).

2.6 RNA isolation and cDNA preparation

2.6.1 RNA extraction, purification and quantification

Prior to RNA isolation using the Monarch Total RNA Miniprep Kit (catalogue number T2010S, New England BioLabs), cell culture media was discarded and cells were rinsed 2-3 times with ice-cold PBS to prevent sample degradation. PBS was completely removed and 300 µl of RNA lysis buffer were added to each well. Using cell scrapers, lysate was harvested and promptly loaded into genomic DNA (gDNA) removal columns fitted with a collection tube and centrifuged for 30 seconds at 16,000 x g. After discarding the gDNA columns, an equal volume of ethanol (≥95%) was added to each flow-through and mixed by pipetting, the mix was transferred to RNA purification columns fitted with a collection tube and centrifuged for 30 seconds at 16,000 x g. After discarding the flow-through, each column was loaded with 500 µl of wash buffer and spun for 30 seconds at 16,000 x g. Afterwards, each column was loaded with 80 µl of a DNase I mixture to ensure complete removal of genomic DNA and incubated at room temperature (RT) for 15 minutes. The DNase I mixture was prepared by combining 5 µl of DNase I with 75 µl of DNase I reaction buffer per column.

At the end of the incubation, each column was loaded with 500 µl of RNA priming buffer and centrifuged for 30 seconds at 16,000 x g. The flow-through was discarded and 500 µl of RNA wash buffer added and columns centrifuged twice at 16,000 x g, first for 30 seconds and then for 2 minutes. The collection tubes were discarded and the columns were fitted with sterile and RNase free Eppendorf tubes. Each column was loaded with 50 µl of nuclease free water, incubated at RT for at least 1 min and spun at 16,000 x g for 1 min. Columns were discarded and the flow-through containing the RNA was placed either on ice, when used for following steps, or at -20 ^{o}C for short-term storage. mRNA was quantified using a Nanodrop 1000 spectrophotometer (Thermo Scientific).

2.6.2 Reverse Transcription (RT) of mRNA to cDNA

RNA (250 µg) was reverse transcribed using the High Capacity cDNA Reverse Transcription Kit (Applied Biosystems, USA), accordingly the manufacturer's instructions. Per sample, the reverse transcription master mix reaction was prepared as shown in Table 2.2.

Table 2.2: Reverse Transcription (RT) master mix components

Master mix reagents	Volume per sample
Nuclease free water	4.2 µl
Deoxynucleotides (dNTPs)	0.8 µl
Random primers	2 µl
Reverse transcriptase buffer	2 µl
Reverse Transcriptase (Multiscribe)	1 µl
Total volume	10 µl

Each PCR tube (VWR International, USA) was loaded with 10 µl of diluted mRNA and 10 µl of the previously prepared master mix. Samples were centrifuged for 15 sec at 10,000 rpm and placed in a thermo-cycler (2720 Thermal Cycler, Applied Biosystems), set as shown in Table 2.3.

Table 2.3: RT-PCR thermal profileT-PCR thermal profile

Step	Temperature	Time
	25 °C	10 min
DNase inactivation	37 °C	2 h
Annealing	85 °C	5 min
Preservation	4 °C	forever

Once cDNA was synthesised, it was either immediately used or stored at -80°C for long-term storage.

2.7 Quantitative Real-Time Polymerase Chain Reaction (qPCR)

To evaluate the levels of expression of the genes of interest, real time qPCR was performed using the previously obtained cDNAs and primers purchased from Sigma Aldrich (Table 2.4) and ThermoFisher Scientific (Table 2.5). Per sample, the master mix relative to each target gene was prepared as shown in Table 2.6 and Table 2.7.

Table 2.4: Sybr green primers

Primer	Forward	Reverse
AKT	TACGAGAAGAAGCTCAGCCC	TCCACACACTCCATGCTGTC
cGAS	GCCTGCGCATTCAAAACTGG	TAGCCGCCATGTTTCTTCTTGG
IRF1	GCCAAGAGGAAGTCATGTGG	TGTTGTAGCTGGAGTCAGGG
IRF9	TCTCCTCCAGCCAAGACAATG	AAAGGCCTGCTCCATCTTCAC
MX1	CTGGGAGGGTGGCTGTTAAG	GCCACAGAATTCCAAAGCCC
OAS2	CAGGGAGTGGCCATAGGTGG	CGAGGATGTCACGTTGGCT
STAT2	AGACCAGAACTGGCAGGAAG	GATCCTGAATGTCCCGGCAG
STAT3	GAGCTGCACCTGATCACCTT	TCCAATTGGGGGCTTGGTAA

Table 2.5 TaqMan primers

Primer	Assay ID and catalogue number
ADAM17	Hs01041915_m1, 4331182
Collagen I	Hs00164004_m1, 4331182
αSMA	Hs05005339_m1, 4351372
Vimentin	Hs00958111_m1, 4331182
Snail	Hs00195591_m1, 4331182
Twist	Hs04989912_s1, 4331182
Slug	Hs00161904_m1, 4331182
N-cadherin	Hs00983056_m1, 4331182
Il-6	Hs00174131_m1, 4331182
IFNB	Hs01077958_s1, 4331182

CCL5	Hs00982282_m1, 4331182
Il-1β	Hs01555410_m1, 4331182
CXCL12	Hs02829207_m1, 4331182
FGF2	Hs00266645_m1, 4331182

Table 2.6: Real time qPCR Sybr green master mix components

Master mix reagents	Volume per sample
Nuclease free water	3.5 µl
Forward primer (10 µM)	0.5 µl
Reverse primer (10 µM)	0.5 µl
Sybr green (catalogue number PB20.15-05, qPCRBIO)	5 µl
Total volume	9.5 µl

Table 2.7: Real time qPCR Taqman master mix components

Master mix reagents	Volume per sample
Nuclease free water	3.5 µl
Taqman primer	0.5 µl
B2M endogenous control (catalogue number 4326319E, ThermoFisher Scientific)	0.5 µl
qPCRBIO Probe Blue Mix Lo-ROX (catalogue number PB20.25-05, qPCRBIO)	5 µl
Total volume	9.5 µl

0.5 µl of each sample was loaded into PCR tubes (catalogue number 14230225, Fisherbrand) in triplicates along with 9.5 µl of master-mix, to a final volume of 10 µl. The tubes were placed in the Rotor-Gene Q PCR system (Qiagen, Germany) and a two-step program was set as follows (Table 2.8):

Table 2.8: qPCR settings

Step	Temperature	Time	N° Cycles
Denaturation	95°C	10 min	1
	95°C	10 sec	40
Amplification	60°C	45 sec	40

Gene expression of each sample was analysed according to the comparative threshold cycle (C_T) method, also referred to as the $2^{-\Delta\Delta CT}$ method (Schmittgen and Livak, 2008).

2.8 Protein isolation and western blot (WB) samples preparation

2.8.1 Protein extraction

Prior to protein isolation, the plates were kept on ice, cell culture media was discarded and cells were rinsed 2-3 times with ice-cold PBS to prevent sample degradation. PBS was completely removed and 50 µl of RIPA lysis buffer (catalogue number sc-24948A ChemCruz, Santa Cruz Biotechnology) supplemented with both protease and phosphatase inhibitors (catalogue number 04693159001, Roche) were added to each well. Using cell scrapers, lysates were harvested and transferred to sterile Eppendorf tubes. After incubation on ice for 10 min, the samples were centrifuged at maximum speed for 15 min at 4°C. The supernatants were harvested and transferred to new sterile Eppendorf tubes and kept on ice for following steps or stored at -80°C for long-term storage.

2.8.2 Protein quantification

The protein concentration of each sample was assessed using the Pierce bicinchoninic protein assay (BCA) kit (catalogue number 23225, Thermo Scientific). In a 96 well plate, a volume of 2-10 µl of lysate and 190 µl of the mixed BCA reagents were pipetted per well. In parallel, in the same plate 10 µl of bovine serum albumin (BSA) standards and 190 µl of the mixed BCA reagents were loaded. The protein concentration of the standards ranged from 0 mg/ml to 2 mg/ml. The mix was prepared by mixing the BCA reagents A and B in a 50:1 ratio.
The plate was incubated at 37°C for 10-15 minutes, to allow the colorimetric reaction to develop and eventually the protein concentration was estimated using a plate reader (Infinite M200,

TECAN) at a wavelength of 562nm. The values of the absorbance were analysed in Excel by interpolation, comparing the absorbance of each sample to those of the standards which were plotted in a standard curve.

2.8.3 Western blot samples preparation

Protein samples for western blot analysis were prepared by mixing a volume of lysates calculated according to the desired amount of the protein samples (e.g. 30 µg) with distilled water and 5X SDS loading dye buffer. The final volume varied based on the capacity of the wells of the gel used for the electrophoresis (e.g. 30 µl for a 10 wells gel, 15-20 µl for a 15 wells gel). The mixed samples were vortexed and spun for 10 seconds and placed into a thermo-block (JENCONS-PLUS) set at 95°C for 10 minutes. Afterwards, the samples were centrifuged and either stored at 4°C for short-term or at -20°C for long-term storage.

2.8.4 Western blot procedure

The protein samples were loaded onto 6-12% SDS-polyacrylamide gels along with 5µl of the protein ladder (catalogue number 773302, BioLegend). Afterwards, proteins were resolved electrophoresis in SDS-Tris-glycine buffer, at 80-100V.

Eventually, proteins were transferred onto a nitrocellulose blotting membrane (catalogue number 10600003, GE Healthcare Life Science) by wet transfer using the XCell II Blot Module (Invitrogen) at 25V for 1-2 h. Once the transfer was complete, its efficiency was assessed by incubating the membrane with Ponceau S solution (catalogue number 27195, Sigma Aldrich) for 30 seconds to 1 minute and then washing with distilled water.

The membrane was incubated with either 5% bovine serum albumin (BSA)(catalogue number A4503-100G, Sigma Aldrich) or 5% skimmed milk (catalogue number 84615.0500, VWR Prolabo Chemicals) in Tris- or phosphate- buffered saline with 0.05% Tween 20 (TBS-T and PBS-T respectively) for 1h at RT on a shaker. This step is necessary to prevent antibody non-specific binding. Next step was removal of the blocking buffer and incubation with a primary antibody (see Table 2.9) diluted in fresh blocking solution either for 1h at RT or at 4°C overnight.

Table 2.9: List of primary antibodies

Target	Dilution	Host-species	Details
ADAM17	1:1000 1:1000	Rabbit Mouse	ab2051, Abcam ab57484, Abcam
β-Actin	1:10000	Mouse	A1978-200UL, Sigma
Collagen I	1:1000	Rabbit	39952S, Cell Signaling Technology
GAPDH	1:5000	Mouse	60004-1-Ig, Proteintech
α-SMA	1:1000	Mouse	ab7817, Abcam
Phospho-SMAD3	1:2000	Rabbit	ab52903, Abcam
SMAD3	1:1000	Rabbit	ab40854, Abcam
Vinculin	1:1000	Rabbit	13901S, Cell Signaling Technology
FAP	1:1000	Rabbit	66562S, Cell Signaling Technology
N-cadherin	1:1000	Mouse	14215S, Cell Signaling Technology
Phospho-STAT3	1:1000	Rabbit	9145S, Cell Signaling Technology
STAT3	1:1000	Rabbit	12640S, Cell Signaling Technology

Phospho-AKT	1:1000	Rabbit	9271S, Signaling Technology	Cell
AKT	1:1000	Rabbit	9272S, Signaling Technology	Cell
Phospho-EGFR	1:1000	Rabbit	3777S, Signaling Technology	Cell
EGFR	1:1000	Rabbit	4276S, Signaling Technology	Cell
Phospho-STAT1	1:1000	Rabbit	9167S, Signaling Technology	Cell
STAT1	1:1000	Rabbit	9172S, Signaling Technology	Cell
Phospho-STAT2	1:1000	Rabbit	88410S, Signaling Technology	Cell
STAT2	1:1000	Rabbit	4594S, Signaling Technology	Cell
cGAS	1:1000	Rabbit	15102S, Signaling Technology	Cell
MX1	1:1000	Rabbit	37849S, Signaling Technology	Cell
Phospho-IRF3	1:1000	Rabbit	4947S, Signaling Technology	Cell

IRF3	1:1000	Rabbit	4302S, Cell Signaling Technology
LC3B	1:1000	Rabbit	2775S, Cell Signaling Technology
FGF2	1:1000	Rabbit	ab208687, Abcam
Phospho-FGFR	1:1000	Rabbit	3471S, Cell Signaling Technology
ATG5	1:1000	Rabbit	12994S, Cell Signaling Technology
ATG3	1:1000	Rabbit	3415S, Cell Signaling Technology

Afterwards, the membrane was washed 3 times for 5 minutes with TBS-T or PBS-T and subsequently incubated with a horseradish peroxidase- conjugated (HRP) secondary antibody (Table 2.10), diluted 1:5000 in fresh blocking solution, for 1h at RT.

Table 2.10: List of secondary antibodies

Secondary antibody	Dilution	Details
Anti-Rabbit HRP	1:3000	7074S, Cell Signaling Technology
Anti-Mouse HRP	1:5000	GTX213112-01, Gene Tex

The membrane was then washed 3 times with either TBS-T or PBS-T and incubated with enhanced chemo-luminescent (ECL) Clarity Western ECL substrates (catalogue number 1705060, BioRad) for 1-2 minutes at RT. This substrate is activated by the HRP bound to the secondary antibody.

The membrane was subsequently developed either using a digital developer (C-Digit, LI-COR) or by exposing it to an x-ray film (Thermo Scientific) in the dark and developing using a Compact X4 Developer (Xograph Imaging Systems). Nitrocellulose membranes were reused for detection of further protein. When protein molecular weights overlapped, the membranes were stripped of the previous antibodies by incubating in 50 ml of Restore Western Blot stripping buffer (catalogue number 21059, Thermo Scientific) for 5-15 minutes at RT. Finally, the membranes were washed 3 times with TBS-T or PBS-T, blocked for 60 minutes and incubated with a new antibody as previously described. The results were analysed using the Java-based image processing program FIJI. The blot was converted to an 8- bit image and boxes were drawn, keeping the size constant, around each band. The area of each lane was measured and normalised to the loading controls.

2.9 Immunofluorescence staining

As previously described, cells were plated onto coverslips placed into 6-12 well plates. The cell culture media was removed and plates rinsed 2-3 times with ice-cold PBS. After complete removal of PBS, cells were fixed with 4% paraformaldehyde (PFA) in 1X PBS for 10 minutes at RT. To allow intracellular targets to be accessible to antibodies, cells were permeabilised by incubation with a permeabilising solution (0.1-0.3 % Triton X-100 in PBS) for 10 minutes at RT. Afterwards, the coverslips were washed 3 times for 5 minutes with PBS and incubated with blocking solution (5% goat serum and 0.3% Triton X-100 in PBS) for 30 minutes at RT. Then, coverslips were washed 3 times for 5 minutes with ice-cold PBS and incubated with the primary antibody (see Table 2.11) diluted in 1% BSA PBS-T for 1h at RT or overnight at 4°C.

Table 2.11: Primary antibodies

Target	Dilution	Host-species	Details
F-Actin (Rhodamine Phalloidin)	1:500	NA	R415
α-SMA	1:500	Mouse	ab7817, Abcam
Ki67	1:500	Rabbit	9129S, Cell Signaling Technology

After washing 3 times for 5 minutes with ice-cold PBS, coverslips were incubated with secondary antibodies (see Table 2.12), conjugated with a fluorescent probe, diluted in 1% BSA PBS-T for 1h at RT in the dark.

Table 2.12: Secondary antibodies list

Secondary antibody	Dilution	Details
Alexa Fluor 568 anti-mouse	1:500/1000	A11004, Life Technologies
Alexa Fluor 488 anti-rabbit	1:500/1000	A11008, Life Technologies
Alexa Fluor 594 anti-rabbit	1:500/1000	A11037, Life Technologies

At the end of the incubation, coverslips were mounted with Prolong Gold Antifade Mountant with DAPI (catalogue number P36931, Life Technologies). The slides were viewed using a Zeiss Axioplan 2 fluorescence light microscope at 20-40x, and imaged using Proplus 7.0.1 image software. The images were then analysed with Fiji. After subtracting the background, the intensity of the pixels was measured and normalised to the cell number.

2.10 Cell proliferation evaluation by EdU proliferation assay

To assess the DNA synthesis in live cells, the 5-ethynyl-2'-deoxyuridine (EdU) incorporation assay was performed using the EdU proliferation assay Kit (iFluor 488) (catalogue number ab219801, Abcam).

On the very last day of the experiment, cells seeded onto coverslips were incubated with EdU by replacing 100 µl of cell culture media with an equal volume of 1X EdU solution, at 37°C for 2-4 h. Afterwards, media was removed and cells were fixed with 200 µl of 1X Fixative solution for 15 minutes at RT. Cells were washed twice with 200 µl of Wash Buffer and permeabilised with 200 µl of Permeabilisation Buffer for 20 minutes at RT. Then, cells were washed twice with 200 µl of Wash Buffer and incubated with 100 µl of Reaction mix (see Table 2.13) for 30 minutes at RT protected from light. Afterwards, cells were washed twice with Wash Buffer and once with 200 µl of PBS. At this step, cells could be processed for immunofluorescence as described in the previous

section. The coverslips were mounted onto microscope slides using the Prolong Gold Antifade Mountant with DAPI and viewed using a Zeiss Axioplan 2 fluorescence light microscope, at 20-40x, setting the filter for Excitement/Emission between 491 and 520nm. Images were acquired using Proplus 7.0.1 image software.

Table2.13: Reaction mix components

Component	Mix for 5 tests	Mix for 50 tests	Mix for 250 tests
TBS	430 µl	4.3 ml	21.4 ml
$CuSO_4$	20 µl	200 µl	1 ml
iFluor 488 azide	1.2 µl	12.5 µl	0.062 µl
EdU additive solution	50 µl	500 µl	2.5 ml
Total volume	500 µl	5 ml	25 ml

2.11 Harvesting conditioned media

Cell culture medium was harvested from all the plates and centrifuged at 1000 x g for 10 minutes. Then, the supernatant was gently transferred to a new sterile falcon tube and aliquoted into small volumes. The resulting aliquots were stored at -20°C.

2.12 Wound-healing assay

H357 and H376 cells were seeded into 6-well plates and cultured until 80/90% of confluence. The following day, the culture medium was discarded and replaced with the desired conditioned medium or treatment. Cells were incubated for 48 h and then, using a 200 µl pipette tip inclined at around 30 degrees, a straight scratch was made per well. The cell culture media was disposed and cells were rinsed twice to ensure complete removal of cellular debris and detached cells. Afterwards, cells were incubated with the fresh culture medium and a first image was acquired, using the Olympus CKX41 inverted microscope, and labelled as time 0. Further images were acquired after 6 and 24 h and analysed by Fiji using the MRI Wound Healing Tool plugin.

2.13 Transwell migration and invasion assay

Prior to the transwell migration or invasion assays, OSCC cell lines were seeded into 6 well plates and incubated with conditioned medium derived from NOFs/CAFs or with fresh DMEM as control. After 48 hours, when the cells reached a confluency between 70/90 %, cells were trypsinised and counted for the assay. In a 24 well plate, 1 ml of complete DMEM was added per well and a transwell insert (catalogue number 662638 Greiner BIO-ONE) or a Matrigel coated transwell insert (catalogue number 354480 Corning) was placed into each well. Next, 25 x 10^3 cells/200 µl/insert were seeded in serum-free DMEM. The cells were then incubated for 24-48 hours at 37 °C in humidified atmosphere with 5 % CO_2. At the end of the incubation, the medium from each insert was discarded and the inserts were washed quickly in PBS 1X by immersion. Next, each transwell was fixed in pure methanol for 2 minutes at room temperature. The cells adhering to the insert from the side facing the lid of the plate were gently removed using a cotton swab. Afterwards, the inserts were stained by incubation with 1% crystal violet in 0.1% acetic acid for 20 minutes at room temperature. Next, the crystal violet was removed and the inserts were washed 3 times in tap water and let dry at room temperature. The next day, each insert was incubated with 1% acetic acid for 20 minutes at room temperature on a shaker. Then the optical density was measure via TECAN and the migration rate quantified by normalising the absorbance to the control.

2.14 Enzyme-Linked Immunosorbent Assay (ELISA)

In order to perform the sandwich ELISA for the detection and quantification of each target, CAFs were treated accordingly the experiment requirements (i.e., incubation with OSCC cells-derived conditioned medium and ADAM 17 knock-down as described in Methods see) and the resulting condition medium was harvested and filtered using 0.22 µm filters. The sandwich ELISA assays performed were against HB-EGF, IL-6 and IL-8 (catalogue number DY259B, DY206 and DY208 respectively from R&D SYSTEMS) and all the reagents used throughout the assays were prepared according to the manufacturer's recommendations (Table 2.14).

Table 2.14: List of reagents required for the ELISA

Solutions	Components
PBS	137 mM NaCl, 2.7 mM KCl, 8.1 mM Na_2HPO_4
Wash buffer	0.05 % Tween 20 in PBS
Reagent Diluent	1 % BSA in PBS
Stop Solution	2 N H_2SO_4

Prior to performing the assay, a 96-well plate (catalogue number 655061 Greiner BIO-ONE) was coated using 100 µl of capture antibody diluted in PBS at 2 µg/ml (HB-EGF and IL-8) and 4 µg/ml (IL-6) as indicated by the manufacturer (Table 2.15). The plate was then sealed and incubated overnight at room temperature.

Table 2.15: List of Capture antibody

Capture Antibody	Working concentration
Human HB-EGF	2 µg/ml
Human IL-6	4 µg/ml
Human IL-8	2 µg/ml

The following day, the capture antibody was discarded and the plate washed three times with wash buffer by using a squeeze bottle. Complete and excess of buffer was ensured by blotting the plate against clean paper towel. Afterwards, the plate was blocked by adding 300 µl of reagent diluent to each well and incubating at room temperature for a minimum of 1 hour. At the end of the incubation the blocking solution was removed and the plate washed three times as described above. Standards were prepared as indicated as indicated by the manufacturer (Table 2.16) and 100 µl of standards and samples were added to each well. The plate was then sealed and incubated for 2 hours at room temperature.

Table 2.16: List of Standards

Standards	Working concentration
Human HB-EGF	7.81-500 pg/ml (2-fold serial dilution)
Human IL-6	9.38-600 pg/ml (2-fold serial dilution)
Human IL-8	31.3-2000 pg/ml (2-fold serial dilution)

After 2 hours, the standards and samples were discarded and the plate was washed three times as previously described. The plate was incubated with 100 µl of detection antibody diluted in reagent diluent, at the working concentration as indicated by the manufacturer (see Table 2.17), at room temperature for 2 hours.

Table 2.17: List of Detection antibodies

Detection antibody	Working concentration
Human HB-EGF	50 ng/ml
Human IL-6	50 ng/ml
Human IL-8	20 ng/ml

After removing the detection antibody and washing the plate, the plate was incubated with 100 µl of streptavidin (diluted 40 times in reagent diluent) at room temperature for 20 minutes avoiding exposure to direct light. After washing, the plate was incubated with 100 µl of substrate solution (catalogue number 421501 Biolegend) at room temperature for 20 minutes avoiding exposure to direct light. The reaction was stopped adding 50 µl of stop solution to each well when the solution started to turn to blue. The optical density was immediately measured using a plate reader set at 450 nm and the wavelength correction was obtained by subtracting the readings at 570 nm. The readings were plotted in Prism GraphPad and the concentration of each sample was determined in function of the standard curve obtained with the serial dilution of the standards. Data was expressed as mean ± standard deviation. A one-way ANOVA test was used to determine the statistical significance of results where appropriate. A p-value ≤ 0.05 was considered as significant.

2.15 N-cadherin inhibition in OSCC cell lines via ADH-1

H357 and H376 cells were seeded in 6 well plates as previously described. When cells reached 80 % of confluency, cells were treated either with 0.1 % DMSO (as control) or 0.2 mg/ml of ADH-1 (catalogue number HY-13541 Generon) for 24 hours (see Figure 2.3). If cells were to be used for a scratch assay, the scratch would have been performed as previously described and the same treatment applied for those cells. The cells were kept at 37° C in humidified atmosphere with 5% CO_2 .

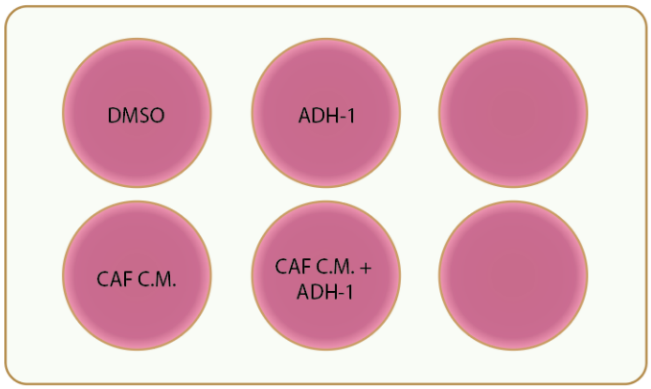

Figure 2.3 Schematic representation of the N-cadherin inhibition in OSCC cell lines via ADH-1.

OSCC cells were treated with 0.2 mg/ml of ADH-1 in the presence or not of CAF-derived conditioned medium.

2.16 EGFR signalling pathway inhibition via Gefitinib in OSCC cell lines

H357 and H376 cell lines were seeded in 6 well plates as previously described. When cells reached 70% confluency, cells were treated either with 100% DMSO (as control) or with 1mg/ml of Human Recombinant EGF (catalogue number SRP3027 Merck) or with 5/10 μM of Gefitinib (catalogue number SML1657 Sigma-Aldrich) or with the combination of both EGF and Gefitinib as shown in the diagram below (see Figure 2.4). Of note, cells were first treated with Gefitinib for 4 hours before stimulating them with EGF for 1 hour. The whole procedure was performed by incubating the cells at 37° C in humidified atmosphere with 5% CO_2 .

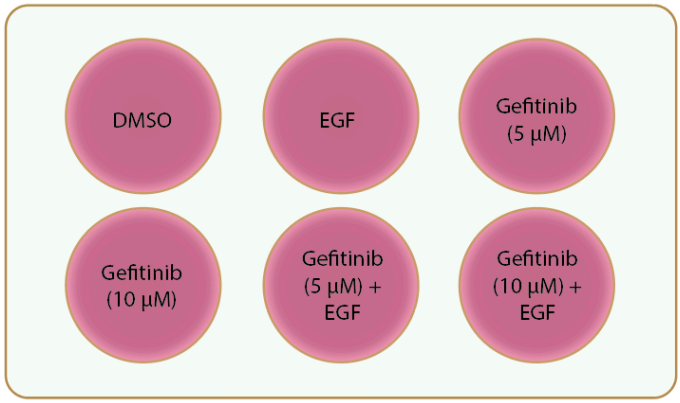

Figure 2.4 Schematic representation of EGFR signalling pathway stimulation and inhibition using EGF and Gefitinib respectively.

2.17 FGFR signalling pathway inhibition via SSR128129E in OSCC cell lines

H357 and H376 cell lines were seeded in 6 well plates as previously described. Some cells were treated either with distilled water (as control) or with 20 ng/ml of Human Recombinant FGF2 (catalogue number PHG0026 Thermo Fisher Scientific) for 48 h. After 48 h, when cells were 90% confluent, they were treated with 100% DMSO (as control) or with or with the FGFR inhibitor SSR128129E at three different concentrations (2.5, 5 and 10 µg/ml) (catalogue number 5334340001 Sigma-Aldrich) for 24 h (Figure 2.5). The whole procedure was performed by incubating the cells at 37° C in humidified atmosphere with 5% CO_2 .

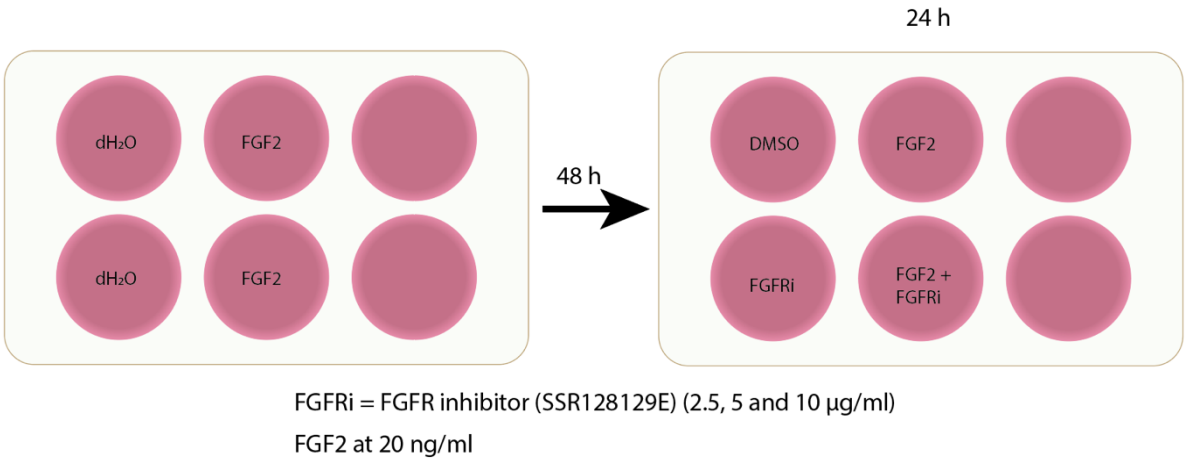

Figure 2.5 Schematic representation of FGFR signalling pathway stimulation and inhibition using FGF2 and SSR128129E respectively.

2.18 Lysosome inhibition via chloroquine

NOFs and CAFs were seeded in 6 well plates for the desired treatments (stimulation with OSCC cell-derived condition medium and ADAM 17 downregulation via siRNA) as previously described. The day before the end of the experiment, cells were treated with either nuclease-free water (as control) or with 100 µM of Chloroquine (catalogue number C6628-50G Sigma Aldrich) for 24 hours (Figure 2.6). Cells were kept at 37° C in humidified atmosphere with 5% CO_2.

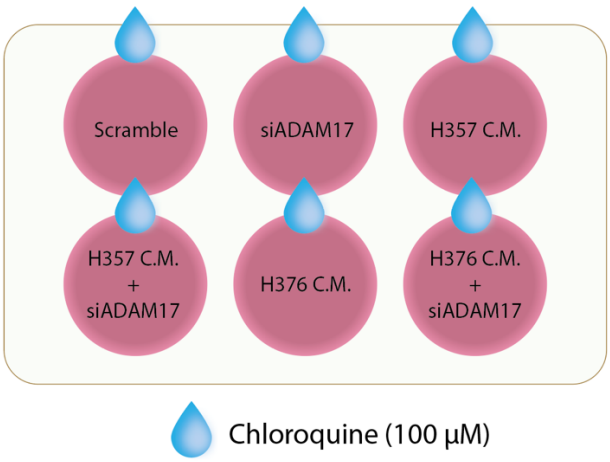

Figure 2.6 Schematic representation of the lysosome inhibition via chloroquine.

The diagram shows the experimental set up for the chloroquine-mediated lysosomal inhibition in NOFs and CAFs depleted or not of ADAM17 and incubated or not with the C.M. derived from cancer cells. Under these conditions, both NOFs and CAFs were treated with either water, as negative control, or with chloroquine.

2.19 Mass Spectrometry sample preparation and data analysis

2.19.1 Sample preparation

CAFs at low passage (between 5 and 7) were seeded in 6 well plates accordingly to the planned treatments (stimulation with OSCC cell-derived condition medium and ADAM 17 downregulation via siRNA) as previously described. For each cell type, there were 3 biological replicates (Figure 2.7). The day of sample harvesting, cells were scraped in 1 ml of culture medium (the presence of serum in the medium aids cell pellet formation when centrifuging), transferred to 1.5 microfuge tubes and spun down. The culture medium was then discarded, without perturbing the cell pellet, and the pellet was washed 3 times in 500 µl of ice-cold PBS by pipetting and spinning down. Once

the final washing was completed, the PBS was discarded and the labelled tubes stored at -80° C until sample submission to the Mass-Spectrometry Facility for a Label-Free Quantification (LFQ) Mass-Spec analysis. Each sample was processed by the collaborator via the Q-Exactive HF mass spectrometer (Thermo Scientific), using buffers prepared accordingly the protocols provided by the facility, and were injected into the mass spectrometer as technical replicates.

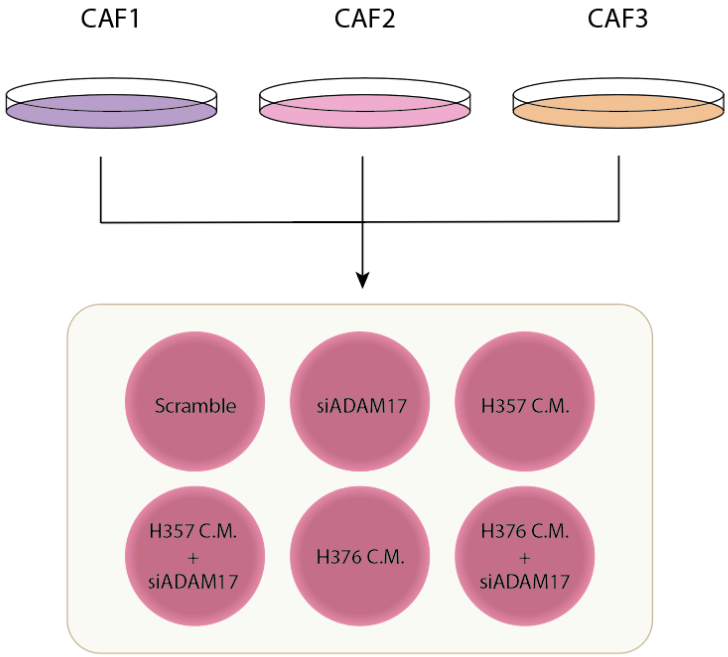

Figure 2.7 Schematic representation of sample preparation for mass-spectrometry analysis.

CAFs generated from three different patients were initially stimulated or not with OSCC cell-derived conditioned medium for 48h. Then they were seeded in 6 well plates and depleted of Adam17 for 48 hours.

2.19.2 Data analysis

The raw data were then processed using the MaxQuant quantitative proteomics software package (Cox *et al.*, 2014) which is a free platform designed for the analysis of large mass-spectrometric data sets. The settings used are described in Foers et al paper (Foers *et al.*, 2020). The resulting text file (renamed protein_groups.txt), containing information about the protein identification and intensities, was used as one of the two input files (the second file was a text file containing the experimental set up and was renamed experimental.txt) required for the statistical analysis performed via LFQ Analyst, a web-based and free platform designed for the analysis of label-free quantitative experiments processed with MaxQuant (Shah *et al.*, 2019)(see Figure 2.8). The

settings used for the statistical analysis were adjusted to a p-value cut-off equal to 0.05, Log2 fold change cut-off equal to 0.5, Imputation type bpca, Type of FDR correction Benjamini Hochberg.

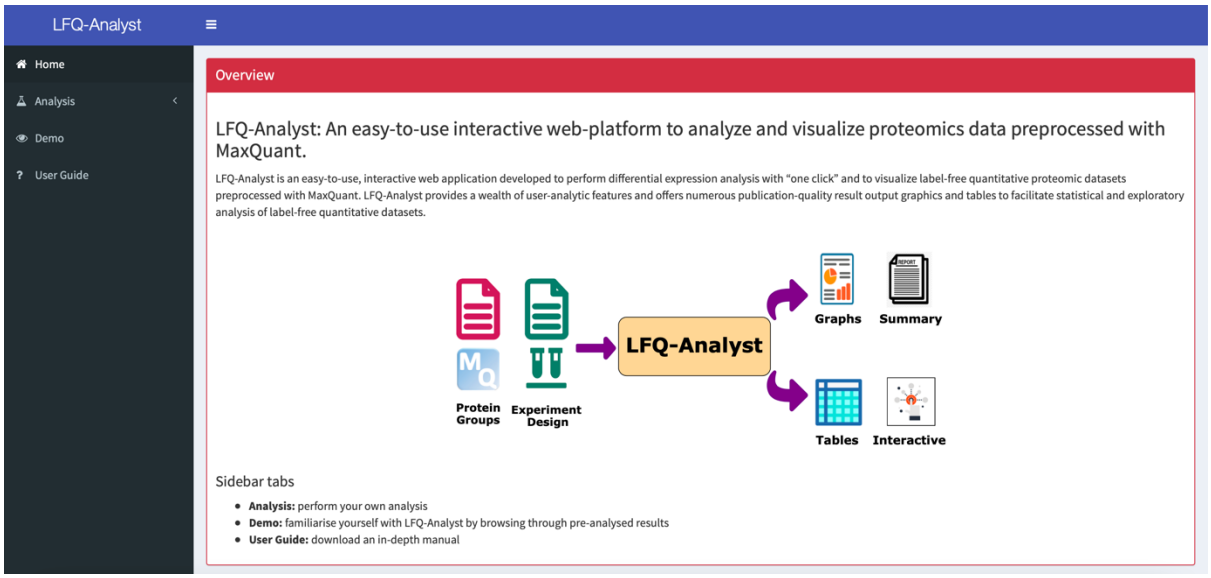

Figure 2.8 Snapshot of the LFQ-Analyst platform interface.

2.21 Statistical analysis

Data were reported as a mean and standard deviation. When more than two groups were compared and only one factor was considered, the One-Way Analysis Of Variance (one-way ANOVA) was applied. Student's t-test was used to test differences between two means. A P-value of less than 0.05 was considered significant. Data were analysed using GraphPad Prism 9 software.

Chapter 3: Investigation of the role of ADAM17 within the bidirectional interaction between cancer cells and stromal fibroblasts

3.1 Aims and objectives

After many years of tumour-centric dominated cancer research, which largely overlooked the role played by tumour-surrounding cells (stromal cells) in malignancy progression, it is now understood that cancer cells and stromal cells engage with a complex bidirectional communication which defines malignancy development, progression and outcome (Hanahan and Coussens, 2012; Maman and Witz, 2018; Laplane *et al.*, 2019a). In this scenario, CAFs, the most abundant and versatile cells within the TME, represent one of the most relevant and investigated cell type. CAF formation results from the activation of either indolent resident fibroblasts or from the transdifferentiation of recruited stromal cells (e.g. endothelial cells, adipocytes etc.) upon stimulation by neoplastic cells (either through direct contact or indirectly by releasing cytokines, growth factors and nucleic acids such as miRNA) and/or by pro-inflammatory immune cells (through the release of pro-inflammatory cytokines) (Löhr *et al.*, 2001; Giannoni *et al.*, 2010; Elkabets *et al.*, 2011; Calvo *et al.*, 2013; Fang *et al.*, 2018; Sahai *et al.*, 2020). Unlike indolent fibroblasts, the activated fibroblasts and CAFs assume a peculiar large spindle-like shape after undergoing a profound cytoskeletal rearrangement, and acquire a more contractile phenotype by overexpressing markers such as the α-SMA and vimentin and enhance their ECM remodelling functions by modulating ECM deposition (through the production of ECM components such as collagen I) and degradation (through the expression of metalloproteinases such as MMP2 and MMP9) (Kalluri, 2016; Liu *et al.*, 2019). However, CAFs are extremely heterogeneous and subpopulations expressing other markers in addition to, or instead of, those above-mentioned have been identified (Puram *et al.*, 2017; Liu *et al.*, 2019). This observation can be explained by the diversity of the cell types from which CAFs originate and by the type of stimuli which trigger their formation (Petersen *et al.*, 2001; Fukino *et al.*, 2004; Öhlund *et al.*, 2017; Philippeos *et al.*, 2018; Biffi *et al.*, 2019). Nevertheless, the activation of fibroblasts into CAFs, which could be considered as the first step of the bidirectional interaction between malignant cells and CAFs, is instrumental to foster a pro-tumorigenic microenvironment. Indeed, CAFs are corrupted fibroblasts induced to express and release a broad spectrum of pro-tumorigenic factors such as cytokines, chemokines, growth factors, ECM components and metalloproteinases (Orimo *et al.*, 2005; Kobayashi *et al.*, 2010; Yu *et al.*, 2013; Bates *et al.*, 2015; Ershaid *et al.*, 2019).

The role of metalloproteinases within cancer is crucial due to their contribution to ECM remodelling (mainly through matrix metalloproteinases, known as MMPs, and a disintegrin and metalloproteinase domain with trombospondin motifs, known as ADAMTS) (Cal and López-Otín, 2015; Quintero-Fabián *et al.*, 2019) and modulation, by ectodomain shedding, of cytokines, growth factors and cell surface proteins (mainly through ADAMs) (Murphy, 2008).

In this context, ADAMs play a fundamental role in regulating both autocrine and paracrine functions within tumours. For instance, ADAM17 has been shown to be upregulated in colon cancer cells and some stromal cells, mainly endothelial-like, and to exert autocrine/paracrine proangiogenic functions via endothelial-EGFR activation (Blanchot-Jossic *et al.*, 2005). However, due to its broad spectrum of substrates and to its ubiquitous and elevated expression in a variety of cancers, usually associated with worse outcome, ADAM17 has been widely and mostly characterised as a factor intrinsic to cancer cells, in the context of EMT and cancer development and progression, neglecting its potential role as a CAF-derived determinant (Fabre-Lafay *et al.*, 2005; Sinnathamby *et al.*, 2011; Zheng *et al.*, 2012; Li *et al.*, 2014; Cai *et al.*, 2015). Only recently, ADAM17 studies have been conducted in CAFs, paving the way for new perspectives in cancer therapies. It has been shown that high levels of ADAM17 in CAFs derived from breast cancer patients correlate with high levels of tumour necrosis factor alpha (TNF-α) that in turn promote cancer cell proliferation (Gao *et al.*, 2013) and that its aberrant expression in CAFs derived from colorectal cancer (CRC) patients is associated with the induction of a desmoplastic reaction (DR) pattern (Mochizuki *et al.*, 2019). Nevertheless, its role in the TME, particularly why and how ADAM17 is upregulated in CAFs and its distinct roles in CAFs and CAF-mediated cancer progression, requires further investigation.

Therefore, the work in this chapter aimed to investigate the role of ADAM17 in the crosstalk between CAF and cancer cells. To simplify the study, the aim was subdivided in multiple objectives:

1. Characterise the phenotype of CAFs and NOFs upon incubation with the conditioned medium (C.M.) derived from OSCC cell lines.
2. Determine whether indirect co-culture of OSCC cancer cells (i.e. H357 and H376) with stromal fibroblasts (NOFs and CAFs) could alter ADAM17 levels and activity in both

indolent normal oral fibroblasts (NOFs) and CAFs. ADAM17 levels would be assessed by western blot, qPCR and ELISA assays.

3. Determine whether ADAM17 could play a role in mediating the CAF-like phenotype, by depleting ADAM17 in both NOFs and CAFs using a small interfering RNA (siRNA) and assessing CAF markers by qPCR and western blot assays and
4. Assess whether ADAM17 could influence the bidirectional interaction between CAFs and cancer cells, by performing migration and invasions assay using the C.M. derived from ADAM17-depleted NOFs and CAFs on OSCC cell lines.

To answer the first objectives, supported by evidence of the role of the conditioned medium derived from cancer cells in activating indolent fibroblasts (Guo *et al.*, 2008; Henriksson *et al.*, 2011), indirect co-culture experiments were set up using the conditioned media (C.M.) derived from OSCC cell lines to stimulate NOFs and CAFs (Figure 3.1).

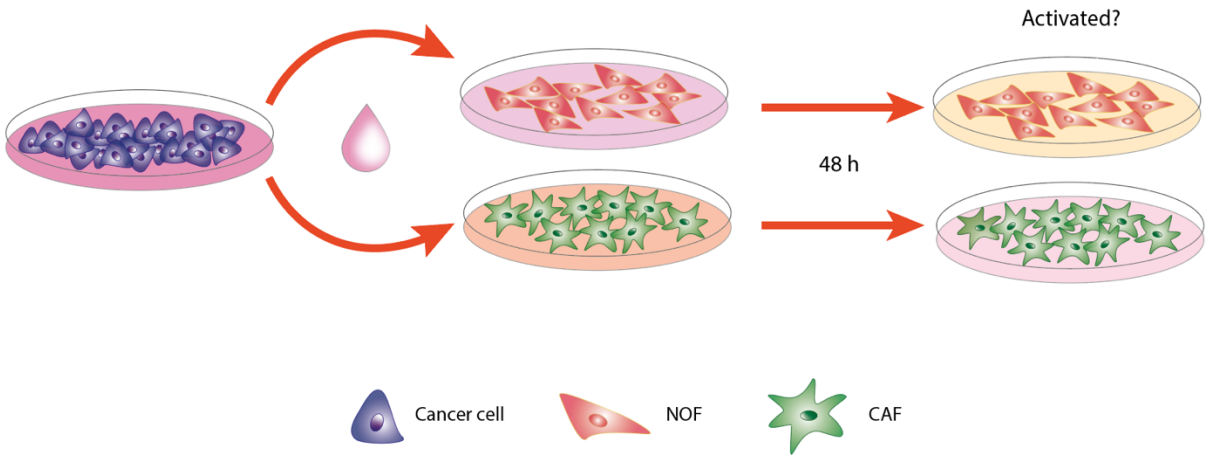

Figure 3.1 Schematic representation of the indirect co-culture experiment performed using OSCC-cell -derived C.M.

To pursue the second aim, supported by studies demonstrating that CAFs, although in a context-dependent manner (e.g. based on the type of cancer or CAFs in close proximity to cancer cells), can induce cancer cell migration in a paracrine manner (Henriksson *et al.*, 2011; Principe *et al.*, 2018; Sun *et al.*, 2019), indirect co-culture experiments were performed using the C.M. derived from CAFs and NOFs to treat H357 and H376 and determine its impact on

cancer cell behaviour (proliferation and migration). In this context, the C.M. used was derived from both NOFs and CAFs conditioned with OSCC-cell derived C.M. (henceforward referred to as conditioned NOFs/CAFs, cNOFs and cCAFs respectively) along with unconditioned controls (Figure 3.2). In addition, this experimental set up aimed to address the question whether, upon paracrine stimulation by cancer cells, cNOF could acquire CAF-like features and mimic their functions.

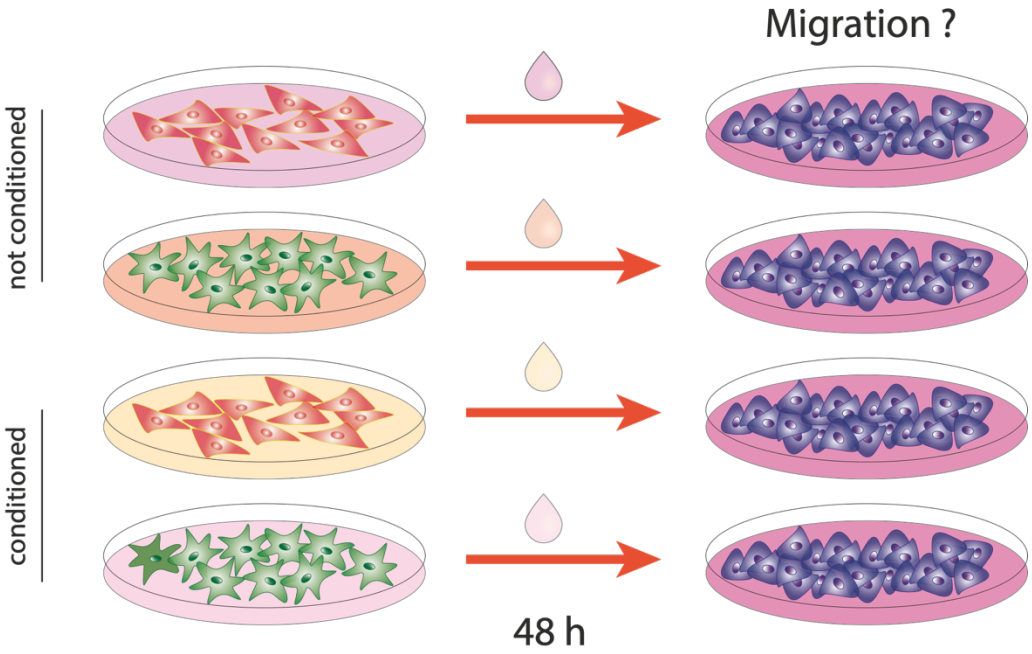

Figure 3.2 Schematic representation of the concept behind the experimental design requiring indirect incubation of OSCC cell lines with NOF- and CAF-derived C.M. to determine its impact on cancer cell behaviour.

3.2 Results

3.2.1 In vitro stimulation of NOFs and CAFs with OSCC-cell derived C.M. induces CAF-like markers in NOFs and reinforces them in CAFs

To investigate the contribution of cancer cells to the cancer cell -stromal fibroblast crosstalk, an indirect co-culture experiment was performed to determine the effect of cancer cell-derived C.M. on both NOFs and CAFs. Thus, low passage NOFs and CAFs were seeded into 6 well plates with and without coverslips and incubated with C.M. derived from two OSCC-cell lines, H357 and H376, for 48 h. At the end of the incubation, cell lysates and RNA extracts were harvested to evaluate the expression of a panel of CAF markers. CAFs consist of heterogeneous

cellular subpopulations expressing different sets of biomarkers which may or may not be shared (Sahai *et al.*, 2020). A further layer of complication stems from the observation that some biomarkers, such as Il-6 and HGF, can be lost during *ex vivo* culturing (Puram *et al.*, 2017).

Three commonly used markers, shown to be expressed by CAF subpopulations, mainly myofibroblast-like (myCAFs), in multiple cancer types, were assessed to analyse the response of fibroblasts to the C.M. derived from cancer cells. These markers were α-smooth muscle actin (α-SMA) and fibroblast activation protein (FAP) (identifying the mesenchymal lineage) and collagen type I (also referred to as COL1A1) (Chen, McAndrews and Kalluri, 2021). Upon stimulation, both NOFs and CAFs showed an increase of some of these CAF markers, though NOFs appeared more responsive. At the RNA level (Figure 3.2 A), compared to control, NOFs displayed a significant increase of collagen type I by 2.44±0.51-fold ($p<0.005$) and 1.95±0.29-fold ($p<0.05$) when treated with H357-derived and H376-derived C.M. respectively, while no change was detected in α-SMA levels. Likewise, compared to control, CAFs RNA levels for collagen type I increased by 1.8 ± 0.06-fold ($p<0.0001$) and 1.8±0.07-fold ($p<0.0001$) when treated with H357-derived and H376-derive C.M. respectively while no change was detected in α-SMA expression. Similarly, compared to control, protein levels increased in NOFs for collagen type I by 4.3±1.74-fold ($p=0.1582$) and 5.5±2.73-fold ($p=0.0599$), for FAP by 4.3±0.28-fold ($p<0.005$) and 7±0.85-fold ($p<0.0001$), for α-SMA by 1.7±0.1-fold ($p=0.0001$) and 1.6±0.07-fold ($p<0.0001$) when treated with H357-derived and H376-derived C.M., respectively. CAFs displayed increased levels for collagen type I by 1.7±0.3-fold ($p<0.05$) and 1.5±0.24-fold ($p=0.0652$), for FAP by 2.3±0.26-fold ($p<0.0005$) and 1.8±0.2-fold ($p<0.005$), while no change was detected for α-SMA when treated with H357-derived and H376-derived C.M. respectively (Figure 3.2 B-D).

This effect on NOFs phenotype could also be observed by microscopy. Upon stimulation, NOFs displayed a spindle-shaped phenotype typical of activated fibroblasts such as CAFs (Chen and Song, 2019) (Figure 3.2 E) and a noticeable cytoskeletal reorganisation as indicated by the presence of more stretched filamentous actin (F-Actin) fibres (Figure 3.2 F). Indeed, by measuring the area of NOFs for each condition, it increased in conditioned NOFs by 1.4±0.17-fold ($p<0.05$) and 1.7±0.31-fold (p) when treated with the C.M. from H357 and H376 respectively (Figure 3.2. G). On the contrary, stimulated CAFs did not exhibit any obvious change in their morphology.

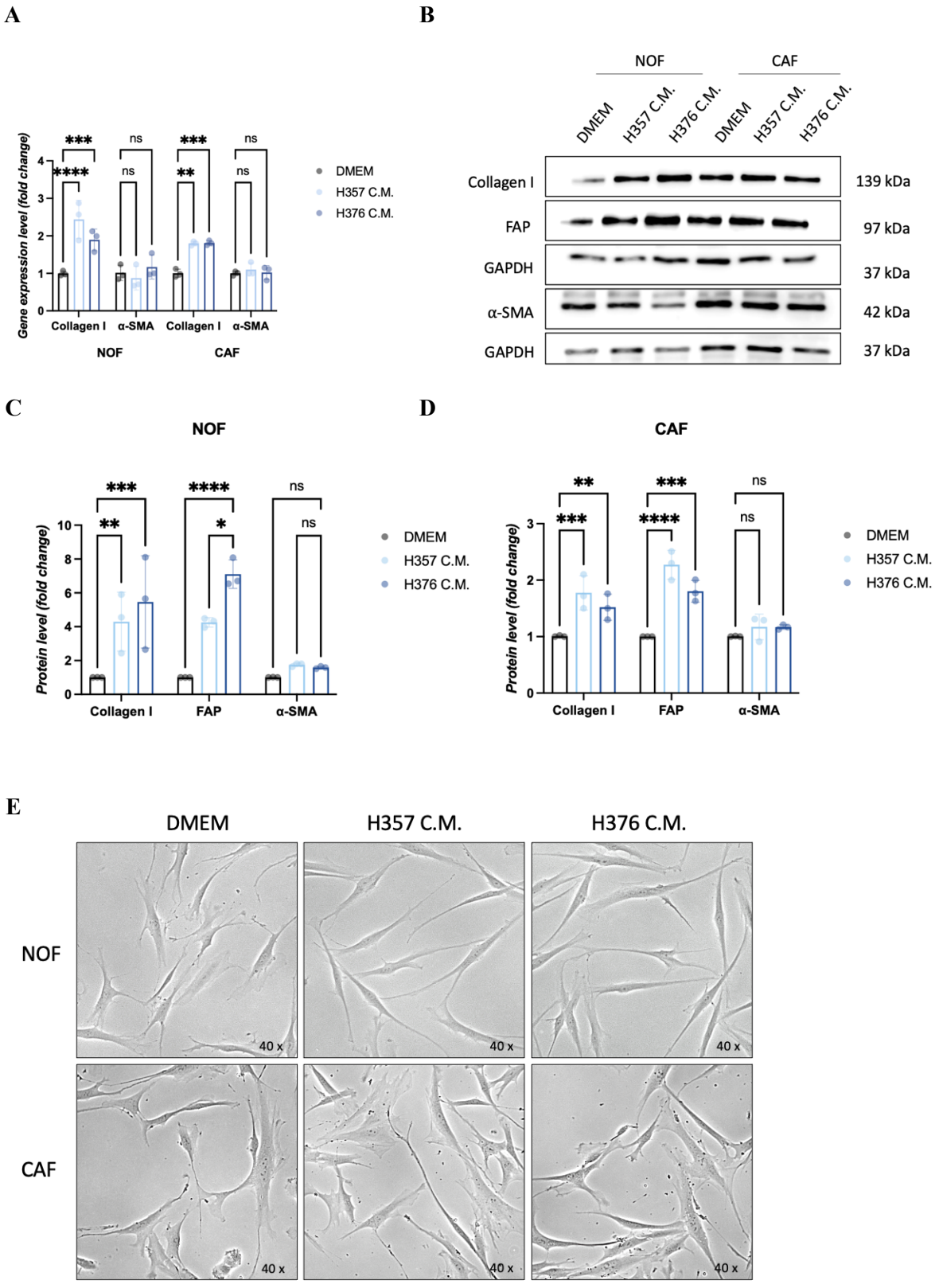
A
Gene expression level (fold change)
Collagen I
α-SMA
Collagen I
α-SMA
NOF
CAF
DMEM
H357 C.M.
H376 C.M.
B
NOF
CAF
DMEM
H357 C.M.
H376 C.M.
DMEM
H357 C.M.
H376 C.M.
Collagen I
FAP
GAPDH
α-SMA
GAPDH
139 kDa
97 kDa
37 kDa
42 kDa
37 kDa
C
NOF
Protein level (fold change)
Collagen I
FAP
α-SMA
DMEM
H357 C.M.
H376 C.M.
D
CAF
Protein level (fold change)
Collagen I
FAP
α-SMA
DMEM
H357 C.M.
H376 C.M.
E
DMEM
H357 C.M.
H376 C.M.
NOF
CAF
40 x

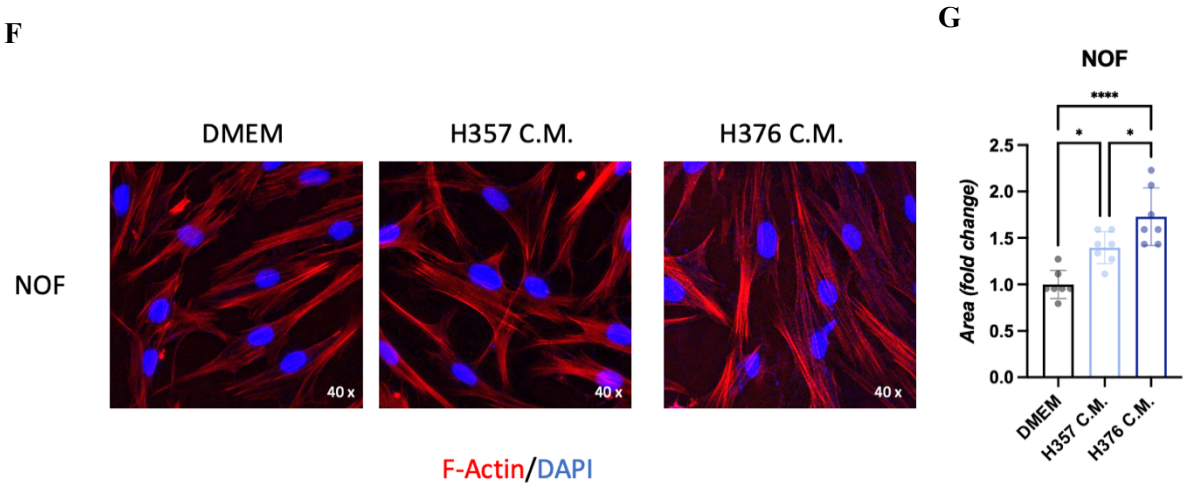

Figure 3.2 Stimulation of NOF and CAF with the C.M. derived from OSCC cell lines elicits CAF-markers upregulation.

*(**A**) Representative qPCR showing Collagen Type I and α-SMA gene expression levels in NOFs and CAFs upon incubation with OSCC cell-derived C.M. for 48 h (n=3 t=3). (**B**) Representative western blot showing Collagen Type I, FAP and α-SMA protein levels in both NOF and CAF upon 48 h of incubation with OSCC cell-derived C.M. (n=3 t=3). (**C-D**) Quantification of B by densitometry. Each data represents the mean ± SD from three independent experiments. P values were calculated via ordinary one-way ANOVA (∗P ≤ 0.05, ∗∗P ≤ 0.01, ∗∗∗P ≤ 0.001, , ∗∗∗∗P ≤ 0.0001). (**E**) Representative microscopy acquisitions of both NOF and CAF with and without OSCC-cell derived C.M.. The images were acquired at 40x magnification using the Olympus CKX41 inverted microscope. (**F**) Representative immunofluorescence images for NOFs stained for F-Actin upon the incubation with OSCC cell-derived C.M.. Cells were viewed using a Zeiss Axioplan 2 fluorescence light microscope, at 40x, setting the filter for Excitement/Emission between 578 and 600. Images were acquired using Proplus7.0.1 image software. (**G**) Quantification of F. P values were calculated via ordinary one-way ANOVA (∗P ≤ 0.05, ∗∗P ≤ 0.01, ∗∗∗P ≤ 0.001, , ∗∗∗∗P ≤ 0.0001).*

3.2.2 In vitro stimulation of NOFs and CAFs with OSCC-cell derived C.M. does not alter cell proliferation

To evaluate the effect on cell proliferation, cells were also seeded in duplicate onto coverslips in 12 well plates and treated as in section 3.2.1. After 48 h, cells were incubated for 4 to 6 h with EdU, a thymidine analogue which is incorporated into newly synthesised DNA, and then processed according to the manufacturer's protocol. The proliferation rate of each sample was

determined by counting the number of the cells which stained positive for EdU by microscopy. Stimulation with the C.M. derived from the cancer cells did not significantly alter the proliferation rate of either NOFs or CAFs (Figure 3.3).

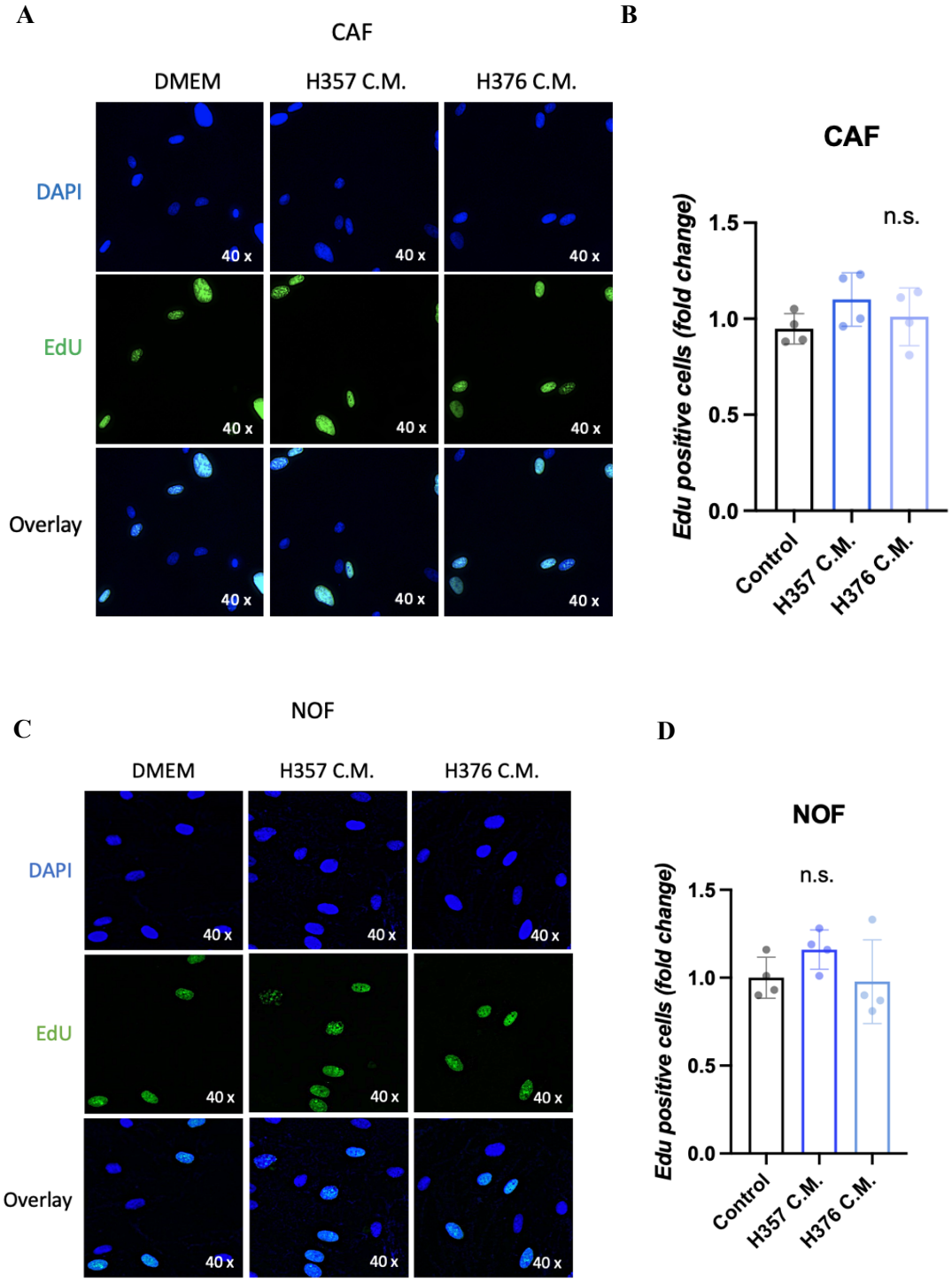

Figure 3.3 Stimulation of NOF and CAF with OSCC-cell derived C.M. does not alter cell proliferation.

*(**A**) and (**C**) Representative EdU proliferation assays in NOF and CAF respectively (n=3 t=3). Cells were viewed using a Zeiss Axioplan 2 fluorescence light microscope, at 20-40x, setting the filter for Excitement/Emission between 491 and 520. Images were acquired using Proplus 7.0.1 image software and analysed with FIJI by randomly picking four different areas and counting the EdU positive cells. The results were normalised to the control (untreated cells) and data reported as ratio between treated sample and its control. (**B**) and (**D**) Quantification of A and C respectively. P values were calculated via ordinary one-way ANOVA.*

3.2.3 In vitro stimulation of NOFs and CAFs with OSCC-cell derived C.M. induces ADAM17 upregulation

Cancer cells modulate the expression of tumour-promoting factors such as proteases (MMPs and ADAMs) in the surrounding cells including fibroblasts. Amongst these proteases, ADAM17 is frequently one of the most dysregulated (Fabre-Lafay *et al.*, 2005; McGowan *et al.*, 2007; Murphy, 2008; VanSchaeybroeck *et al.*, 2014; Walkiewicz *et al.*, 2016; Jiao *et al.*, 2018). Thus, ADAM17 levels were assessed in the same samples described in section 3.2.1. Upon stimulation with OSCC-cell derived C.M. both NOFs and CAFs showed a significant increase of ADAM17 at both transcriptional and translational levels compared to control (Figure 3.4). In NOFs, ADAM17 protein levels increased by 2.5±0.58-fold ($p<0.05$) and 3.5±1.1-fold ($p<0.01$) when treated with the C.M. derived from H357 and H376 respectively, whereas in CAFs it increased by 2.9±0.57-fold ($p<0.01$) and 3.7±0.81-fold ($p<0.001$) when treated with the C.M. derived from H357 and H376 respectively. Likewise at transcriptional level NOFs showed an increase of ADAM17 by 2.5±0.1-fold ($p<0.0001$) and 1.5±0.07-fold ($p<0.01$) and CAF by 3.7±0.14 ($p<0.001$) and 1.9±0.17($p<0.01$) when treated with the C.M. derived from H357 and H376 respectively.

Further support to this data was obtained by determining the ADAM17 activity levels via an enzyme-linked immunosorbent assay (ELISA) for one of the substrates commonly shed by ADAM17, the heparin-binding EGF-like growth factor (HB-EGF) (Mullooly *et al.*, 2016). NOFs and CAFs were initially seeded in 6 well plates and incubated for 48 h with or without the C.M. medium from H357/H376 cells. Next, they were transfected using either a control plasmid or one expressing HB-EGF. After 6 h the transfection mix was removed and replaced with complete culture medium and cells incubated for further 48 h. Since the basal levels of ADAM17-mediated release of HB-EGF are very low in absence of stimuli and thus difficult to detect, both NOFs and CAFs, prior C.M. harvesting, were treated for 40 minutes with 200

ng/ml of the phorbol-12-myristat-13-acetate (PMA), a non-physiological activator of protein kinase C (PKC) widely reported as stimulator of ADAM17 sheddase activity (Lorenzen *et al.*, 2016). NOFs showed an increase of HB-EGF shedding of 2.5±6.83-fold ($p<0.01$) and 4.2±7.05-fold ($p<0.01$) whereas in CAFs it increased by 3.9±16.5-fold ($p<0.0001$) and 5.3±49.86-fold ($p<0.0001$) when treated with the C.M. derived from H357 and H376 respectively.

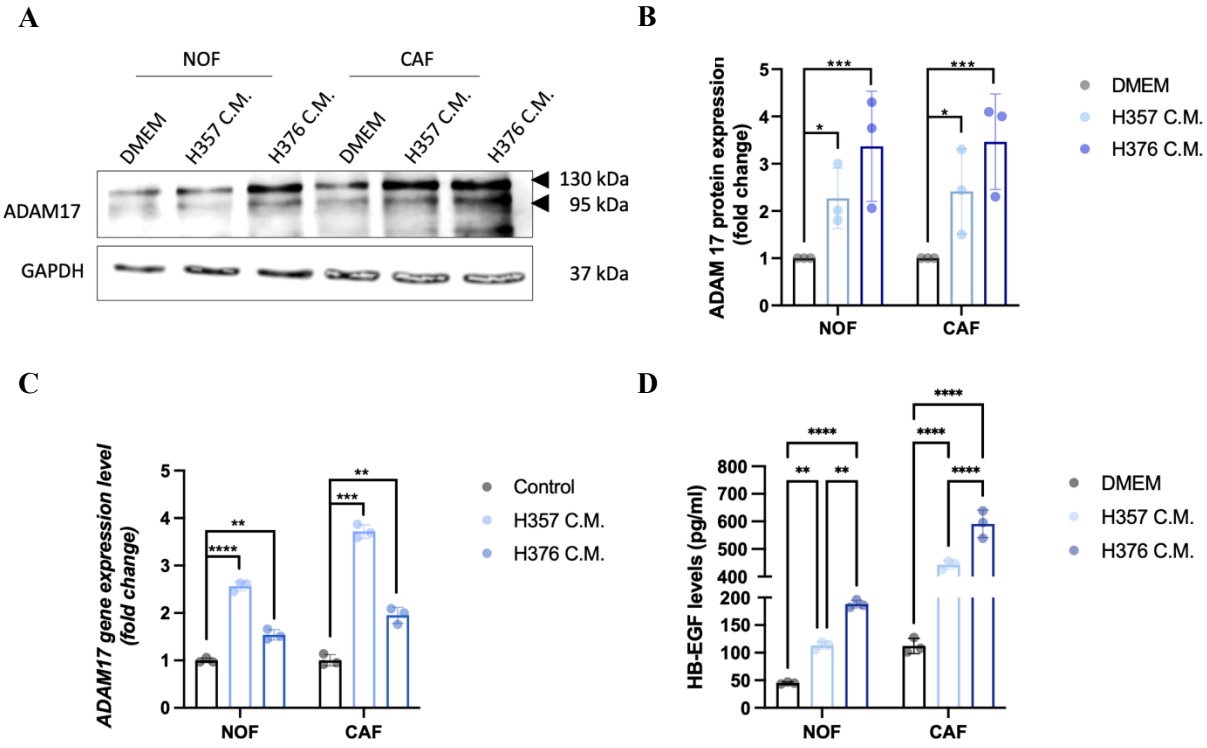

Figure 3.4 Stimulation of NOFs and CAFs with OSCC-cell derived C.M. upregulates ADAM17 levels.

*(**A**) Representative western blot showing ADAM17 protein levels in NOFs and CAFs incubated for 48 h with and without H357 and H376 derived C.M. (n=3 t=3). (**B**) Quantification of A by densitometry. (**C**) Representative qPCR for ADAM17 gene in NOFs and CAFs incubated for 48 h with and without H357 and H376 derived C.M. (n=3 t=3). (**D**) Representative ELISA showing HB-EGF levels in NOFs and CAFs incubated with OSCC-cell derived C.M. (n=3, t=1). NOFs and CAFs were seeded in six well plates and incubated with or without OSCC-cell derived C.M. for 48 h. Next cells were transfected with a scramble or with the HB-EGF plasmid. Following 6 h from the transfection, the medium was replaced with a complete culture medium and cells incubated for 48 h. Before C.M. harvesting, cells were stimulated with 200 ng/ml of PMA for 40 minutes to stimulate ADAM17 shedding activity. Then the media were harvested, centrifuged and filtered and used for the ELISA assay. Each data represents the*

*mean ± SD from three independent experiments. P values were calculated via ordinary one-way ANOVA (*P ≤ 0.05, **P ≤ 0.01, ***P ≤ 0.001, **** P ≤ 0.0001).*

3.2.4 Incubation of OSCC-derived cells with the C.M. originating from activated stromal fibroblasts promotes cancer cell migration

After having investigated the first part of the bidirectional interaction between cancer cells and stromal fibroblasts in sections 3.2.1-3, the second part was analysed in this section by investigating whether stromal fibroblasts could, in turn, influence cancer cells' migratory ability in a paracrine fashion. To determine the impact of stromal fibroblast-derived C.M. on cancer cell migration, a transwell migration assay was carried out on H357 and H376 using the C.M derived from NOFs, cNOFs and CAFs. This experimental set up also begins to address the question of whether the CAF-like phenotype observed by the expression of CAF markers by cNOFs (section 3.2.2) is reflected by functional CAF-like behaviour. Therefore, cancer cells were initially incubated for 48 h with either normal culture medium or with the C.M. derived from the different fibroblasts previously described in section 3.2.1. Next, cancer cells were seeded on transwell inserts in serum-free medium and placed in a 24 well plate containing complete culture medium. The plate was then incubated for 48 h. Cancer cells treated with the C.M. derived from NOFs did not show any change in their migratory ability as compared to the control. On the other hand, the H357 cells incubated with the C.M. derived from cNOFs showed an increase of their migration ability by 1.6±0.08-fold ($p<0.001$) and 1.9±0.17-fold ($p<0.001$) when incubated with CAF-derived C.M., whereas the H376 cells increased their migration by 1.4±0.05-fold ($p<0.01$) and 1.7±0.11-fold ($p<0.001$) (Figure 3.5 A-C). Interestingly, no influence of fibroblast-derived C.M. on cancer cell proliferation was detected by the EdU incorporation assay for any of the tested conditions (Figure 3.5 D-E).

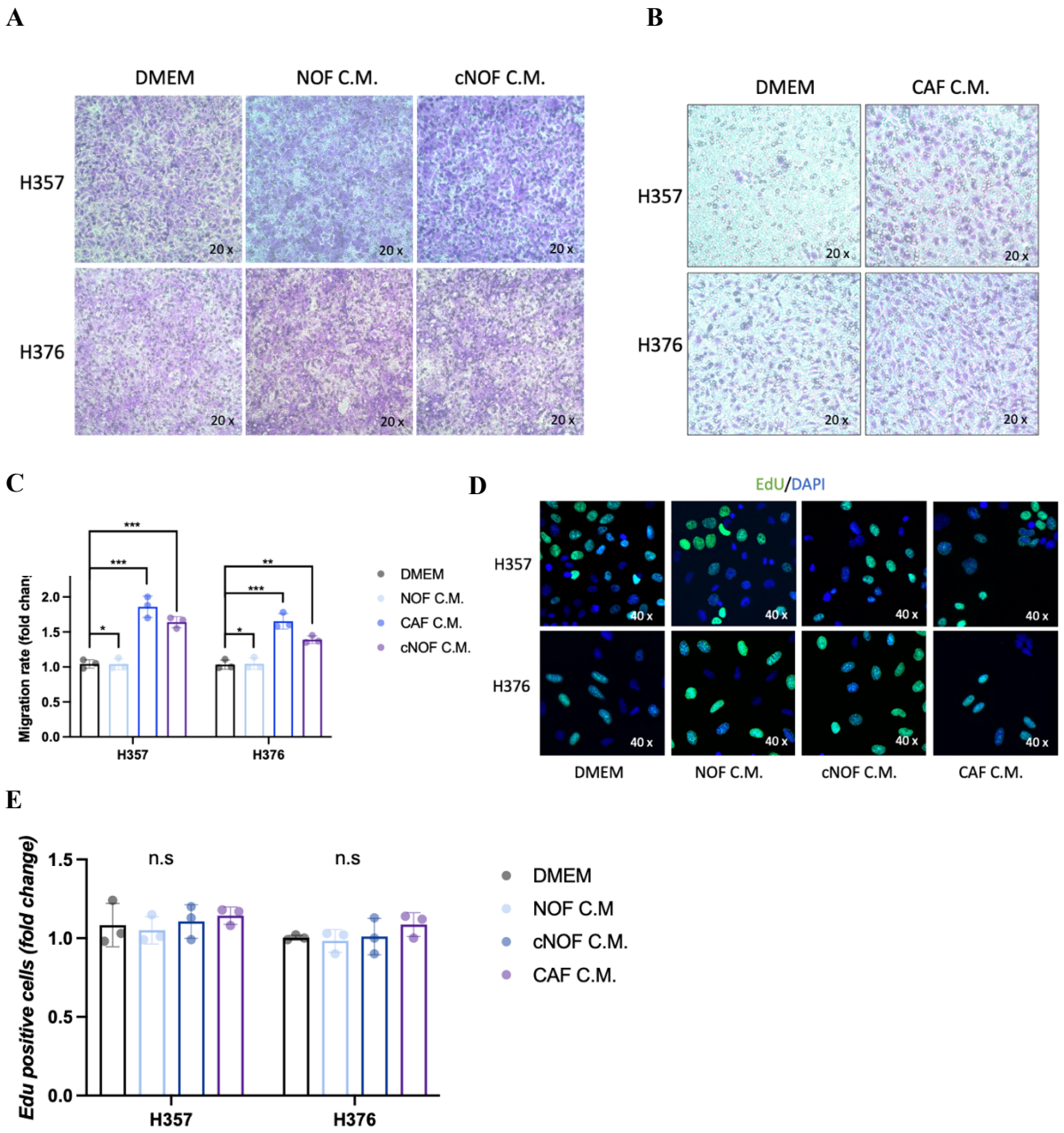

Figure 3.5 OSCC-derived cancer cells treated with C.M. derived from cNOF and CAF migrate more compared to control and to those treated with NOF-derived C.M, but proliferation is unchanged.

*(**A-B**) Transwell migration assay of H357 and H376 treated with and without NOF-, cNOF- and CAF-derived C.M. (n=3 t=3). Cells were initially seeded in 6 well plates and challenged or not with the desired C.M. for 48 h. Next, cells were seeded in transwells in a 24 well plate. To determine their migratory potential, cells were kept in serum-free medium while a complete culture medium was kept in the well where each Transwell was located. Cells were incubated for 48 h. (**C**) Quantification of A and B. Each data represents the mean ± SD from three independent experiments. (**D**) EdU proliferation*

*assay in H357 and H376 with and without the C.M. derived from NOF, cNOF and CAF. Cells were seeded in duplicate per condition. Cells were viewed using a Zeiss Axioplan 2 fluorescence light microscope, at 20-40x, setting the filter for Excitement/Emission between 491 and 520. Images were acquired using Proplus 7.0.1 image software and analysed with FIJI by randomly picking four different areas and counting the EdU positive cells. The results were normalised to the control (untreated cells) and data reported as ratio between treated sample and its control. (**E**) Quantification of D. Each data represents the mean ± SD from three independent experiments. P values were calculated via ordinary one-way ANOVA (∗P ≤ 0.05, ∗∗P ≤ 0.01, ∗∗∗P ≤ 0.001, ∗∗∗∗ P ≤ 0.0001).*

3.2.5 Downregulation of ADAM17 via small interfering RNA (siRNA) resulted in reduced CAF-marker expression in NOFs and CAFs

Having observed that stimulation of both NOFs and CAFs with C.M. derived from the OSCC cell line H357 and H376 triggered a CAF-like phenotype along with upregulating ADAM17 at both transcriptional and translational levels, the next step was to examine whether ADAM17 is involved in the acquisition of a CAF-like phenotype. The CAF-like phenotype includes not just the acquisition of a distinctive morphology and structure, which can be identified by the detection of markers such as those assessed in the previous section, but also the acquisition of functional properties exerted in a paracrine manner through the release of molecules able to act on other cells (secretome) (Chen and Song, 2019; Chen, McAndrews and Kalluri, 2021). Indeed, the pro-tumorigenic effects of CAFs have been described in diverse types of cancer though the underlying mechanisms are not universal (Sahai *et al.*, 2020). Along with a direct role in supporting cancer progression and especially metastasis via extracellular matrix (ECM) remodelling (Gaggioli *et al.*, 2007; Sahai *et al.*, 2020), CAFs can exert their role in a paracrine fashion too (O'Connell *et al.*, 2011; Servais and Erez, 2013; Tao *et al.*, 2017), as also evidenced in the previous section by incubating OSCC cancer cells with the C.M. derived from stromal fibroblasts (previously activated by exposure to cancer cell-derived C.M.). In addition, consistent with the literature, these activated fibroblasts were shown to have increased ADAM17 expression compared to their indolent counterparts (Gao *et al.*, 2013; Ishimoto *et al.*, 2017; Mochizuki *et al.*, 2019). Hence, considering the role of ADAM17 as master regulator of more than 80 substrates, some of which are cleaved and released within the stroma, NOFs and CAFs treated with C.M. derived from cancer cells, or fresh culture medium as a control, were depleted of ADAM17 by siRNA. Subsequently, the culture medium was harvested,

filtered and stored at -20° C while cell lysates and RNA were extracted and processed to obtain samples to use for the determination of ADAM17 levels and CAF markers.

To confirm the successful downregulation of ADAM17 in NOFs and CAFs, both western blot and qPCR assays were performed. At protein level, siRNA targeting of ADAM17 decreased ADAM17 levels by 3±0.12-fold, 1.9±0.33-fold ($p<0.05$) and 2.4±0.16-fold ($p<0.01$) compared to their respective control (DMEM, H357 C.M. and H376 C.M. respectively) (Figure 3.6 A-B). Similarly, upon siRNA-mediated silencing, ADAM17 transcriptional levels decreased in both NOFs and CAFs: in NOFs ADAM17 decreased by 2.6±0.05-fold, 6.3±0.05-fold ($p<0.0001$) and 6.3±0.05 ($p<0.0001$) compared to their respective control (DMEM, H357 C.M. and H376 C.M. respectively), whereas in CAF it decreased by 2.9±0.05-fold, 7.4±0.1-fold ($p<-0.0001$) and 7.3±0.06-fold ($p<0.0001$) compared to their respective control (DMEM, H357 C.M. and H376 C.M. respectively) (Figure 3.6 C-D).

Since ADAM17 has sheddase properties and cleaves a plethora of transmembrane substrates (Murphy, 2008; Zunke and Rose-John, 2017), to determine whether ADAM17 knock-down (KD) resulted in a reduced sheddase activity too, HB-EGF levels in the C.M. of CAFs were assayed via ELISA. NOFs and CAFs were seeded in 6 well plates and incubated until reached 50-60 % of confluency. Next, they were transfected with a control or with an ADAM17-targeting siRNA in combination with a plasmid for the HB-EGF expression. After 6 h of incubation, the transfection mix was discarded and fresh culture medium was added to the cells and plates incubated for 48 h. Prior to the harvest of the C.M., both NOFs and CAFs were treated with 200 ng/ml of PMA for 40 minutes. The ELISA showed a significant downregulation of ADAM17 sheddase activity upon siRNA-mediated silencing which in NOFs was 9.3±0.7-fold ($p<0.0001$) whereas in CAFs was 6.6±6.53-fold ($p<0001$) (Figure 3.6 E-F).

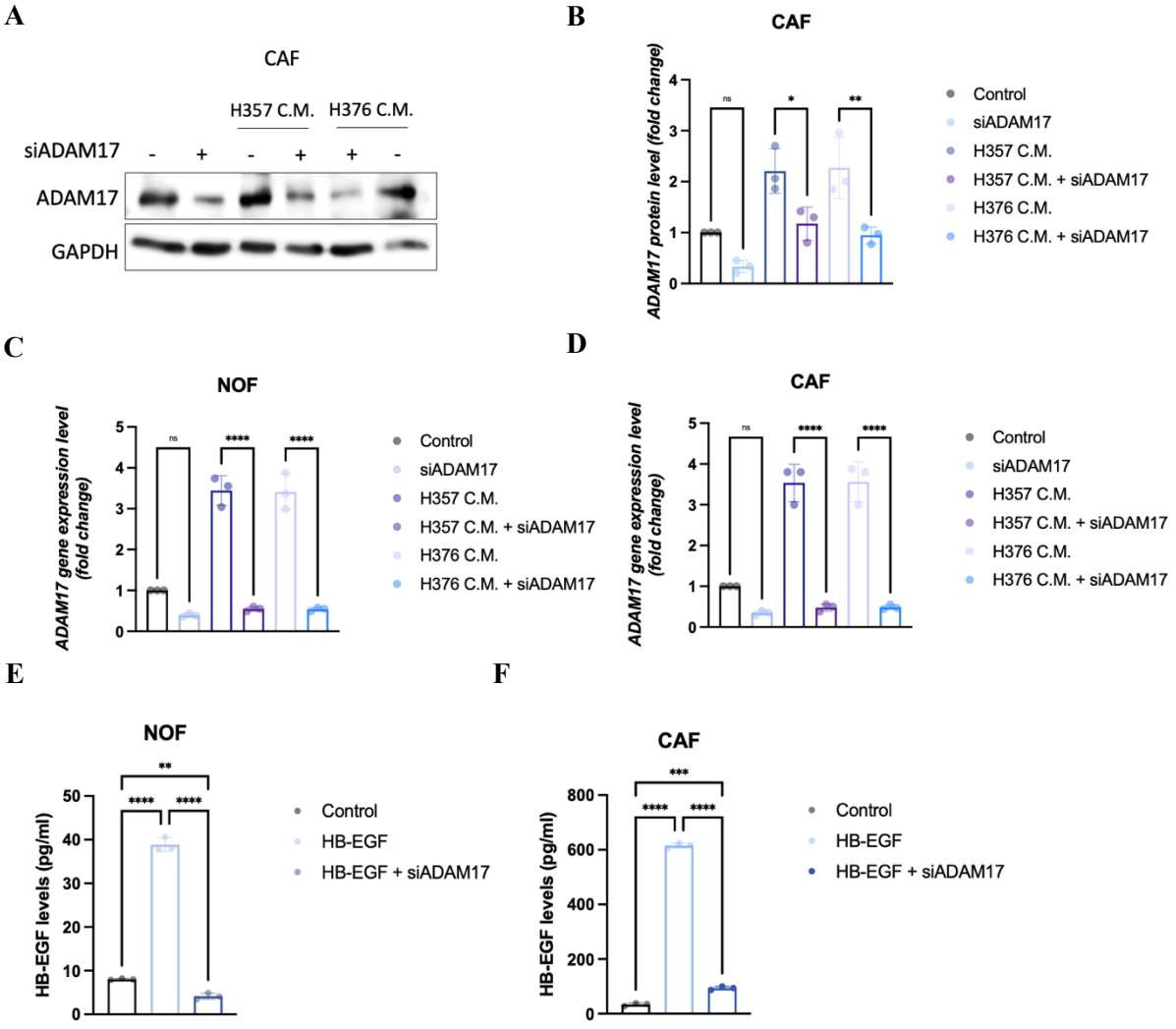

Figure 3.6 Targeting of ADAM17 with siRNA in NOFs and CAFs successfully downregulates ADAM17 levels and activity.

*(**A**) Representative western blot showing ADAM17 protein levels in CAFs upon ADAM17 depletion via siRNA in CAFs incubated with or without OSCC-derived C.M.. CAFs were seeded in 6 well plates and incubated with or without OSCC-cell derived C.M. for 48 h. Then the cells were transfected with or without siRNA targeting ADAM17 or with the control plasmid for further 48 h (n=3 t=3). (**B**) Quantification of A by densitometry. (**C**) and (**D**) Representative qPCR showing ADAM17 gene expression levels in NOFs and CAFs respectively. NOFs and CAFs were treated as above-mentioned. (**E**) and (**F**) ELISA showing ADAM17 activity in NOFs and CAFs upon ADAM17 depletion via siRNA. NOFs and CAFs were seeded and treated as above-mentioned. In addition, a plasmid to overexpress HB-EGF was transfected along with the siRNA against ADAM17. After 6 h the transfection mix was removed and cells incubated with fresh complete culture medium for 48 h. Prior to harvest of the C.M. both NOFs and CAFs were stimulated with 200 ng/ml of PMA for 40 minutes. Next, the medium was centrifuged and filtered. Each data represents the mean ± SD from three independent experiments. P*

*values were calculated via ordinary one-way ANOVA (*P ≤ 0.05, **P ≤ 0.01, ***P ≤ 0.001, **** P ≤ 0.0001).*

Following confirmation of successful ADAM17 knock-down in both NOFs and CAFs, western blot assay and qPCR assay were performed to evaluate both protein and transcript levels for some of the CAF markers. Interestingly, upon ADAM17 depletion there was a decrease of some of these markers in both NOFs and CAFs, though their expression varied between the two cell types. In NOFs there was a slight and not statistically significant decrease in Collagen I and FAP at protein levels (Figure 3.7 A-B), with the exception of FAP in NOFs treated with H376-derived C.M. and depleted of ADAM17, which decreased by 2±0.2-fold ($p<0.05$) compared to their control (NOFs treated with H376-derived C.M.). On the other hand, CAFs showed a more remarkable decrease in FAP levels compared to NOFs. Indeed, FAP levels decreased by 1.3±0.05-fold, 1.9±0.49-fold ($p<0.01$) and 2.2±0.16-fold ($p<0.01$) in CAFs depleted of ADAM17 compared to their respective controls (Figure 3.7 C-D). This trend was also confirmed in unstimulated NOFs and CAFs by qPCR, which confirmed a different response of CAF markers expression to ADAM17 depletion between NOFs (less responsive) and CAFs (more responsive). In NOFs, upon ADAM17 depletion the CAF markers decreased by 1.3±0.1-fold ($p<0.05$) and 1.3±0.04-fold ($p<0.001$) for α-SMA and Collagen I respectively, whereas Vimentin did not show any change. In CAFs the same markers decreased by 1.3± 0.03-fold($p<0.001$), 1.25±0.06-fold ($p<0.01$) and 1.4±0.03-fold ($p<0.0001$) for α-SMA, Vimentin and Collagen I respectively (Figure 3.7 E).

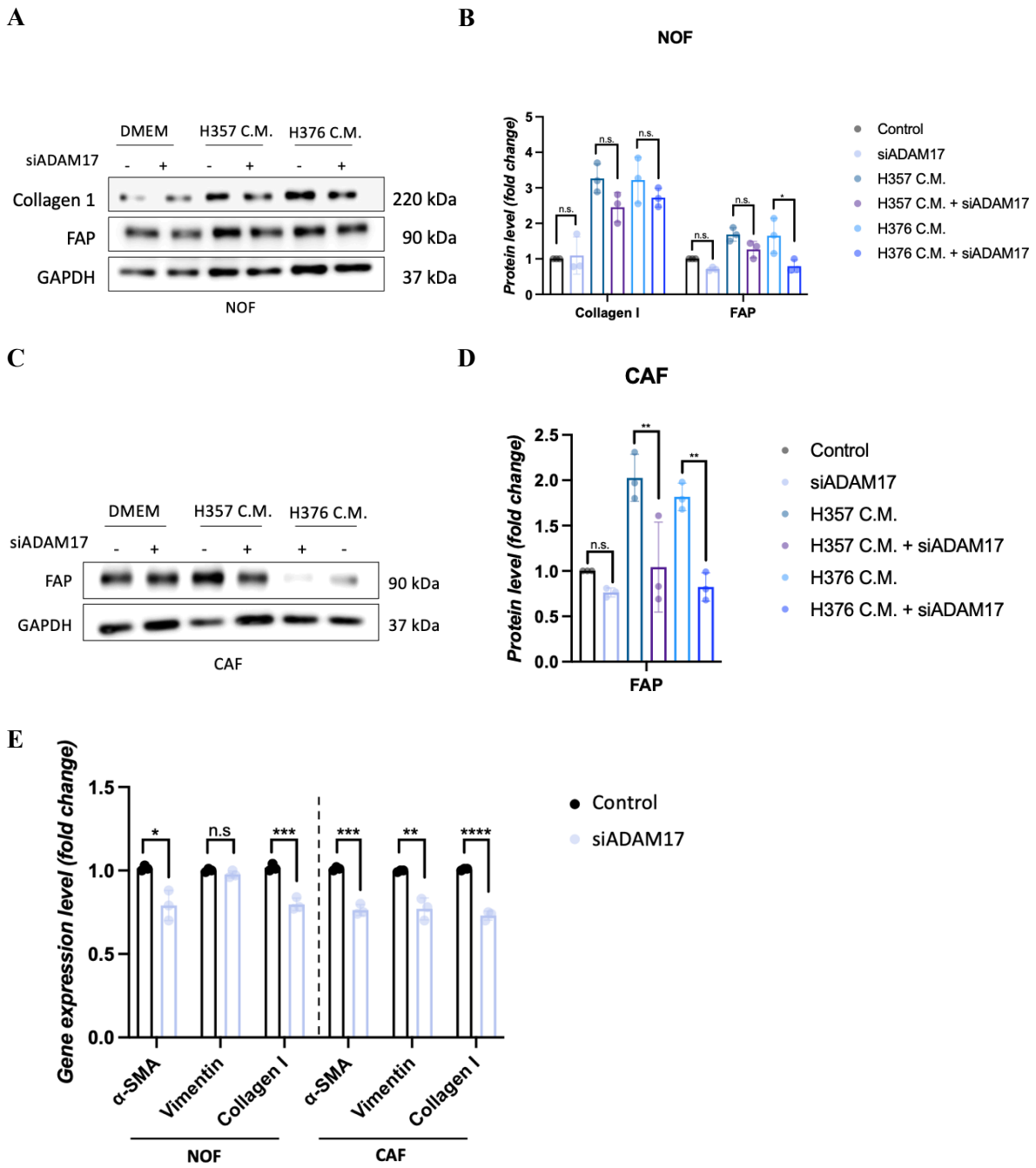

Figure 3.7 ADAM17 depletion in stimulated NOF and CAF could downregulate CAF markers.

*(**A**) and (**C**) Representative western blot showing the levels of Collagen I and FAP in NOFs and CAFs respectively. (**B**) and (**D**) Quantification by densitometry of A and C respectively. Each data represents the mean ± SD from three independent experiments. P values were calculated via ordinary one-way ANOVA (*P ≤ 0.05, **P ≤ 0.01, ***P ≤ 0.001, **** P ≤ 0.0001). (**E**) Representative qPCR showing CAF markers expression level in NOFs and CAFs respectively. Each data represents the mean ± SD*

from three independent experiments. P values were calculated via unpaired t test (∗P ≤ 0.05, ∗∗P ≤ 0.01, ∗∗∗P ≤ 0.001, ∗∗∗∗ P ≤ 0.0001).

3.2.6 Downregulation of ADAM17 in NOFs and CAFs did not alter their proliferation

To assess whether silencing ADAM17 could affect cell proliferation, the EdU incorporation assay was performed in both NOF and CAF for each condition as previously described in section 3.2.5. The results show that silencing ADAM17 in NOFs and CAFs did not significantly alter cell proliferation in either cell type (Figure 3.8).

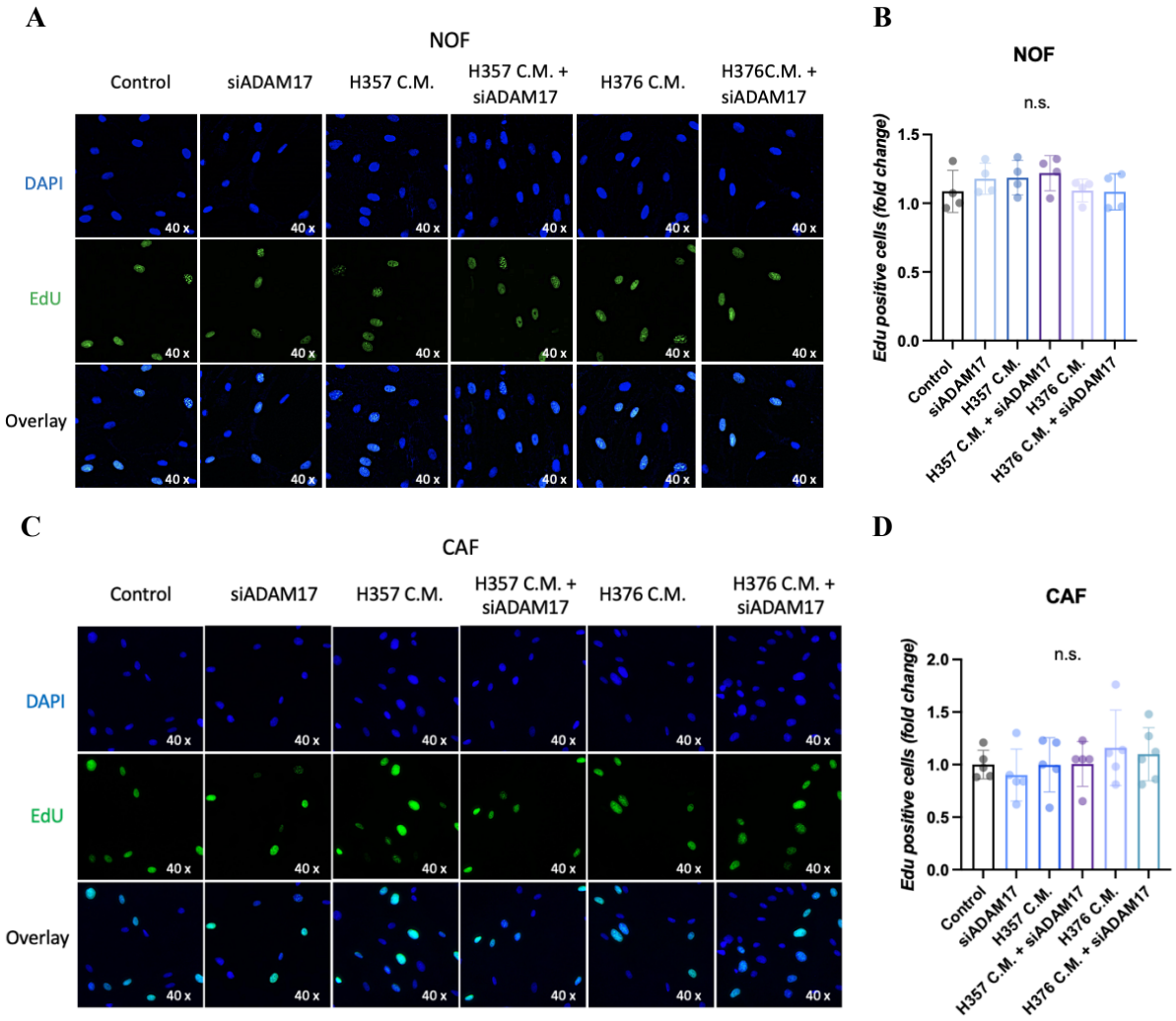

Figure 3.8 ADAM17 downregulation in NOFs and CAFs does not alter cell proliferation.

*(**A**) and (**C**) Representative EdU proliferation assay in NOFs and CAFs respectively (n=3 t=3). Cells were seeded in duplicate per condition in 6 well plates and incubated with or without OSCC-cell derived C.M. for 48 h. After 48 h, when 50-60 % confluent, cells were transfected with or without the siRNA targeting ADAM17 for further 48 h. Next, cells were incubated with the EdU for 4-6 h. Cells were viewed using a Zeiss Axioplan 2 fluorescence light microscope, at 20-40x, setting the filter for Excitement/Emission between 491 and 520. Images were acquired using Proplus 7.0.1 image software and analysed with FIJI by randomly picking four different areas and counting the EdU positive cells. The results were normalised to the control (untreated cells) and data reported as ratio between treated sample and its control. (**B**) and (**D**) Quantification of A and C respectively. Each data represents the mean ± SD from three independent experiments. P values were calculated via ordinary one-way ANOVA (*P ≤ 0.05, **P ≤ 0.01, ***P ≤ 0.001, **** P ≤ 0.0001).*

3.2.7 ADAM17 downregulation in NOFs and CAFs can restrain OSCC-cancer cell migration and invasion in a paracrine manner

Having shown that ADAM17 depletion in both NOFs and CAFs negatively NOFs and CAFs negatively regulated several CAF markers, the next step was to assess whether the C.M. derived from ADAM17-depleted fibroblasts could have a different effect on H357 and H376 cells. To evaluate this aspect, both the migratory and invasive potentials of both cell lines were analysed by wound healing and transwell migration assays, to determine the migration rate, and Matrigel coated transwell assays to analyse invasion. The migratory potential, which indicates the overall motile capacity of cancer cells, can be determined by wound healing assay, which is a 2D system not requiring a chemotactic response, and by transwell assay, which measures the motility of cells through an uncoated membrane in the presence of a chemotactic stimulus (Kramer *et al.*, 2013). On the other hand, the invasion assay, which indicates the capacity of cancer cells to move across the ECM by degrading it through metalloproteinases, can be performed using a transwell system wherein the membrane is coated with a thin layer of ECM (e.g. collagen, Matrigel etc.), in the presence of a chemotactic stimulus (Kramer *et al.*, 2013). Thus, H357 and H376 cell lines were seeded in 6 well plates and incubated for 48 h with or without the C.M. derived from stromal fibroblasts, previously conditioned or not with the C.M. derived from OSCC cell lines. Once the cells were 90% confluent, they were trypsinised and seeded for the next experiments. Some of them were seeded onto Matrigel coated transwell inserts in serum free medium, the inserts were then placed in a 24 well plate containing complete culture medium and incubated for 48 h. The same procedure was applied to perform the transwell migration assay ensuring that the transwell inserts were not coated. Lastly, to perform the wound healing assay, a straight scratch was performed by using a 200 µl tip and acquiring pictures at three time points (0, 6 h and 24 h).

Cancer cells treated with the conditioned medium from both NOFs and CAFs depleted of ADAM17 showed a reduced migratory phenotype compared to their respective controls. In H376, compared to control, the migration rate measured by wound healing assay decreased by 2.3±0.2-fold ($p<0.01$) and 2±0.13-fold ($p<0.01$) when treated with the C.M. derived from NOF depleted of ADAM17 (respectively referred to as NOF ADAM17 low, hence after NOF^{A17low} and conditioned NOF ADAM17 low, hence after $cNOF^{A17low}$) (Figure 3.9 A-B). Similarly, a decreased migration ability was detected by transwell migration assay in both H357 and H376 for the same conditions. In H357 the migration rate decreased by 1.8±0.1-fold ($p<0.001$) and

1.8±0.06-fold ($p<0.0001$) when treated with the C.M. derived from NOF^{A17low} and $cNOF^{A17low}$ respectively, whereas in H376 decreased by 1.45±0.08-fold ($p<0.001$) and 1.3±0.05-fold ($p<0.001$) for the same conditions (Figure 3.9 C-F).

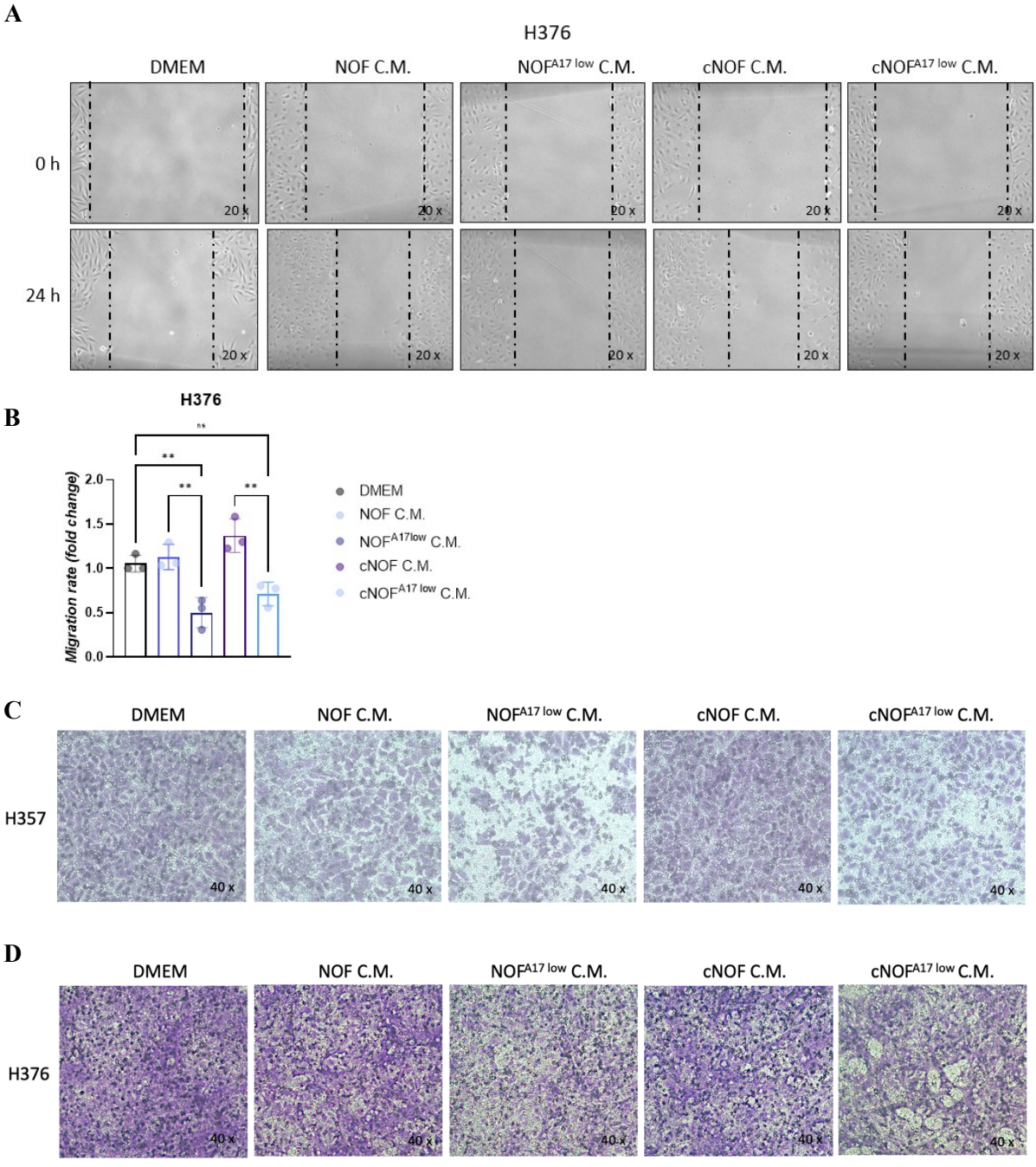

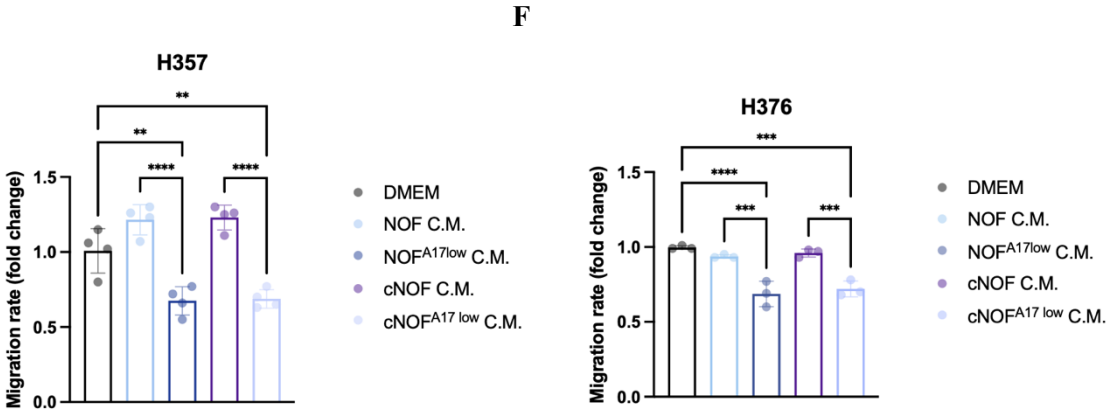

Figure 3.9 H357 and H376 migratory phenotype is restrained in the presence of conditioned medium from NOFs depleted of ADAM17.

*(**A**) Representative wound healing assay in H376 cells. Cells were seeded in 6 well plates and incubated with NOF-derived conditioned medium for 48 h. Afterwards, a scratch was created and the medium was replaced with fresh culture medium. The pictures were acquired at time 0, 6 h and 24 h. The area delimited by the scratch was measured using Fiji and data analysed in Prism by subtracting the area at 24 h from the one at time 0 and comparing it to the control as fold change (n=3 t=3). (**B**) Quantification of A. (**C**) and (**D**) Representative transwell migration assay for H357 and H376 respectively. Cells were initially seeded in 6 well plates and challenged or not with NOF-derived C.M. for 48 h. Then, cells were seeded in transwells in a 24 well plate. To determine their migratory potential, cells were kept in serum-free medium while a complete culture medium was kept in the well where each Transwell was located. Cells were incubated for 48 h (n=3 t=2). (**E**) and (**F**) Quantification of C and D respectively. Each data represents the mean ± SD from three independent experiments. P values were calculated via ordinary one-way ANOVA (*P ≤ 0.05, **P ≤ 0.01, ***P ≤ 0.001, **** P ≤ 0.0001).*

Migration and invasion abilities were then assessed in the same cancer cell lines using the C.M. derived from CAFs. Similar migratory and invasive restraining responses were observed in cancer cells treated with the C.M. derived from CAFs depleted of ADAM17 (CAF ADAM17 low and conditioned CAF ADAM17 low hence after referred to as CAF^{A17low} and $cCAF^{A17low}$). Compared to control, the migration rate evaluated via wound healing assay in H357 decreased by 1.67±0.05-fold ($p<0.01$) and 1.85±0.06-fold ($p<0.0001$) when treated with the C.M. derived from CAF^{A17low} and $cCAF^{A17low}$ respectively whereas in H376 it decreased by 1.8±0.14-fold ($p<0.01$) and 1.4±0.13-fold ($p<0.05$) for the same conditions (Figure 3.10 A-D). Likewise, the invasive ability in H357 decreased by 1.8±0.06-fold ($p<0.05$) while in H376 it decreased by 1.9±0.07-fold ($p<0.01$) when treated with the C.M. derived from CAF^{A17low} (Figure 3.10 E-F).

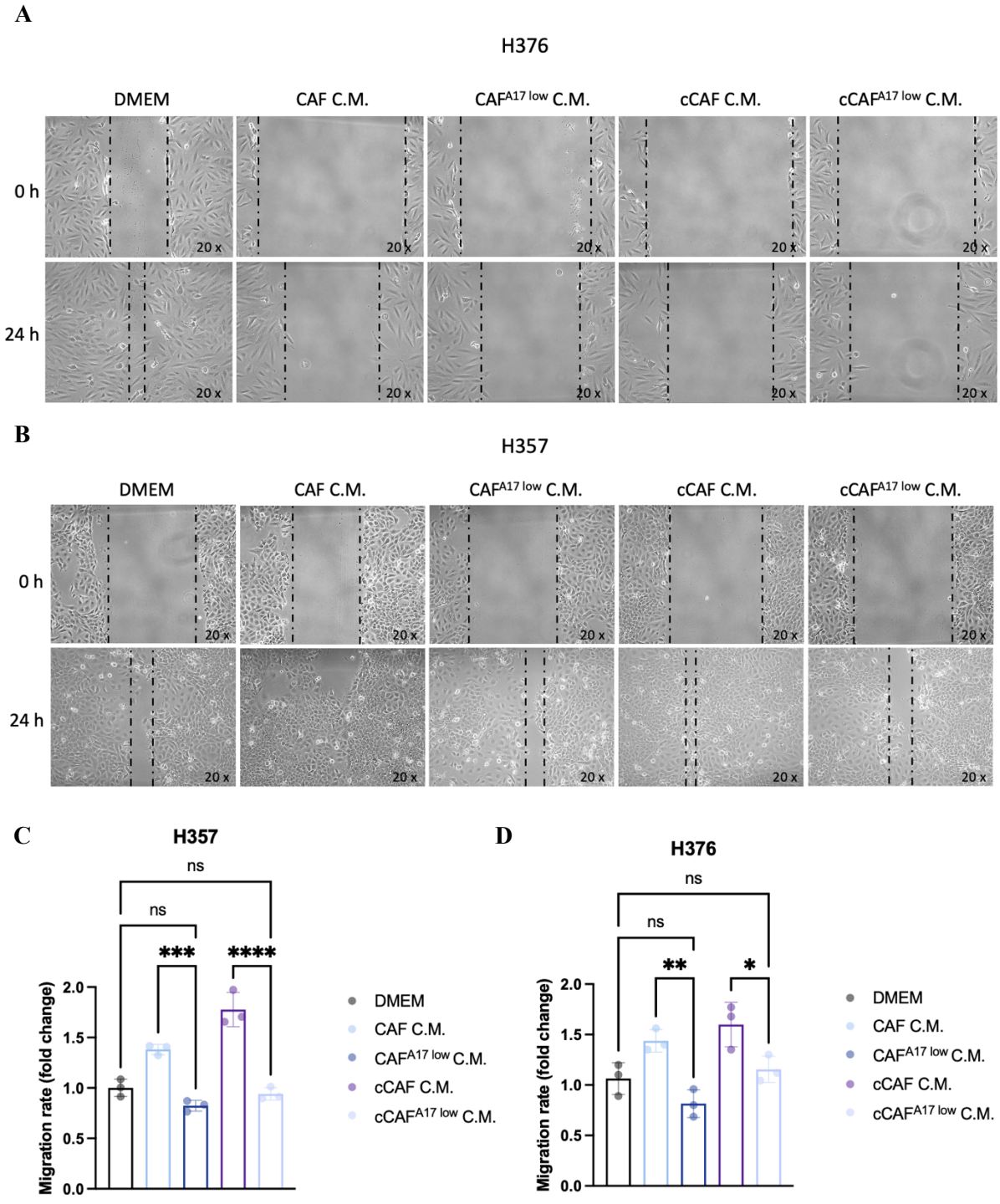
A
H376
DMEM
CAF C.M.
CAF$^{A17\ low}$ C.M.
cCAF C.M.
cCAF$^{A17\ low}$ C.M.
0 h
24 h
20 x
B
H357
C
H357
ns
***
****
Migration rate (fold change)
2.0
1.5
1.0
0.5
0.0
DMEM
CAF C.M.
CAF$^{A17\ low}$ C.M.
cCAF C.M.
cCAF$^{A17\ low}$ C.M.
D
H376
**
*

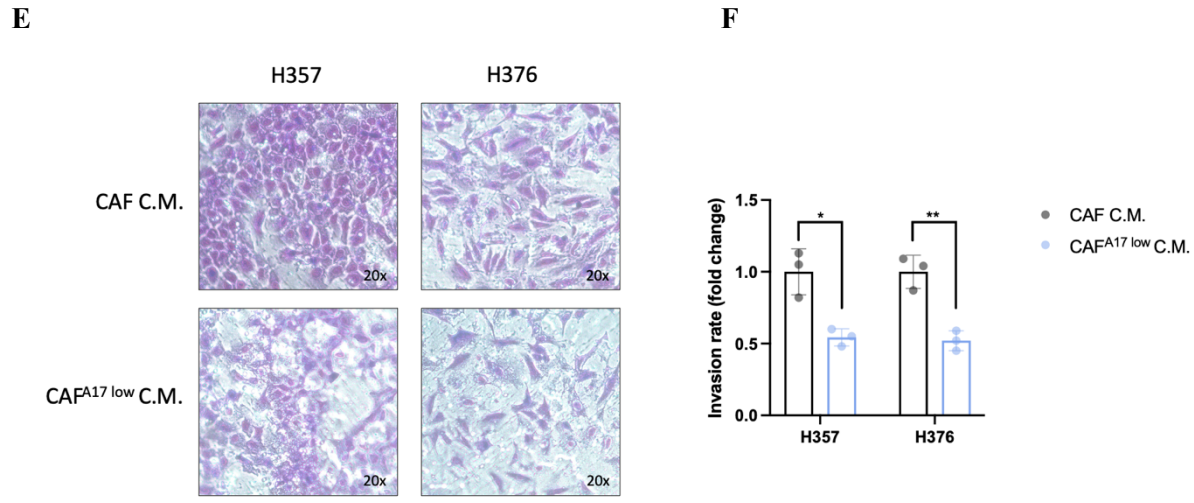

Figure 3.10 H357 and H376 migratory phenotype is restrained in the presence of conditioned medium from CAFs depleted of ADAM17.

*(**A**) and (**B**) Representative wound healing assay in H357 and H376 cells respectively. Cells were seeded in 6 well plates and incubated with CAF-derived conditioned medium for 48 h. Afterwards, a scratch was created and medium was replaced with fresh culture medium. The pictures were acquired at time 0, 6 h and 24 h. The area delineated by the scratch was measured by Fiji and data analysed in Prism as mentioned in Figure 6.1 (n=3 t=3). (**C**) and (**D**) Quantification of A and B respectively. (**E**) Representative transwell invasion assay for H357 and H376 respectively. Cells were initially seeded in 6 well plates and challenged or not with CAF-derived C.M. for 48 h. Then, cells were seeded in transwells coated with Matrigel in a 24 well plate. To determine their invasive potential, cells were kept in serum-free medium while a complete culture medium was kept in the well where each Transwell was located. Cells were incubated for 48 h (n=3 t=1). (**F**) Quantification of E for H357 and H376 respectively. Each data represents the mean ± SD from three independent experiments. P values were calculated via ordinary one-way ANOVA (for A-D) and unpaired t test (for E-G) (*P ≤ 0.05, **P ≤ 0.01, ***P ≤ 0.001, **** P ≤ 0.0001).*

Importantly, to rule out the influence of proliferation on the migratory and invasive phenotype of the challenged OSCC cells, the EdU assay was performed. Both H357 and H376 cells were seeded onto coverslips in 12 well plates and were treated for the same conditions as previously described (due to time constraints, the only conditions missing were cNOF C.M. and

cNOF^{A17low}). As reported in Figure 3.11, there was no difference in the proliferation rate amongst the samples suggesting that the restrained migratory and invasive behaviour are independent of the cell proliferation rate.

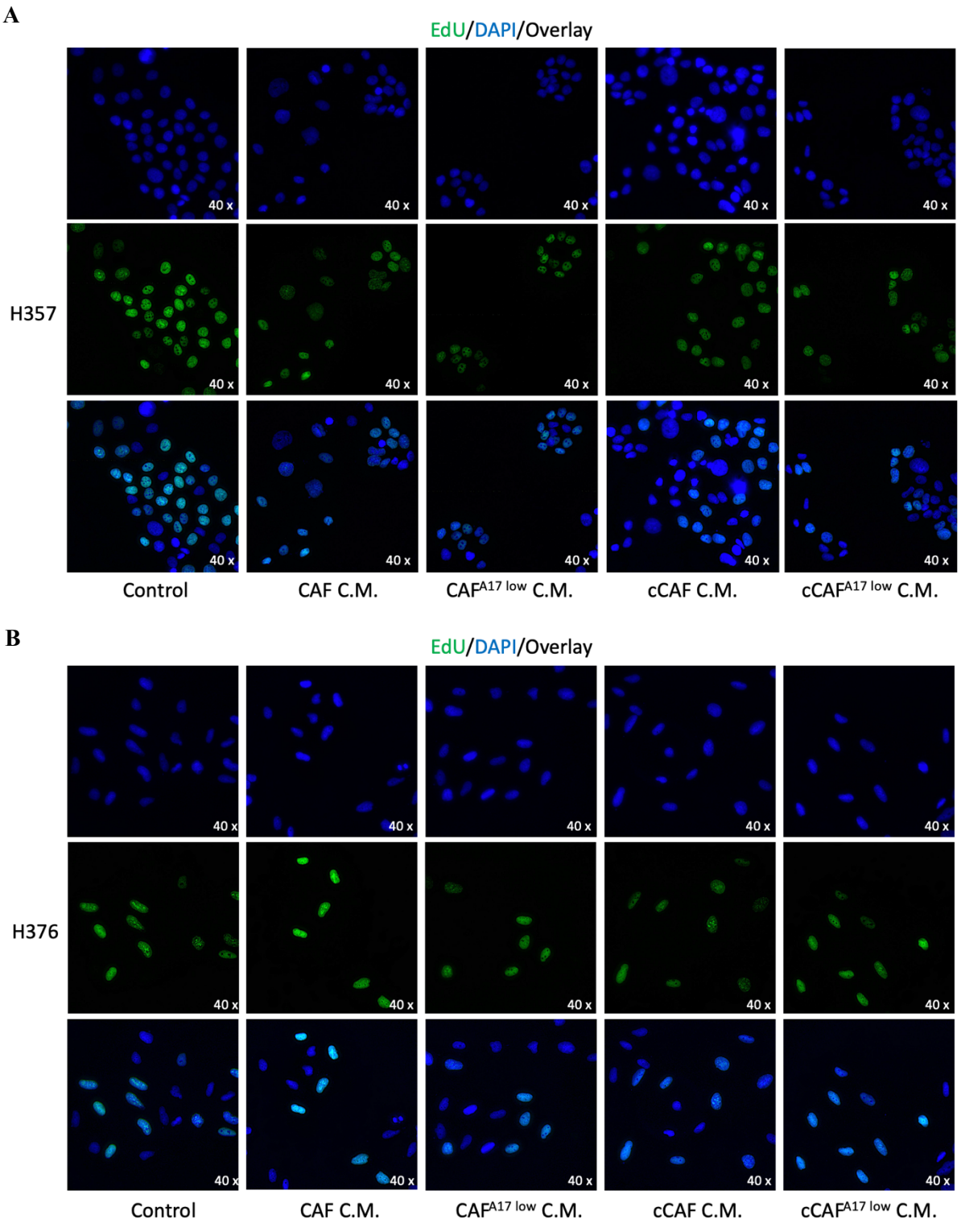

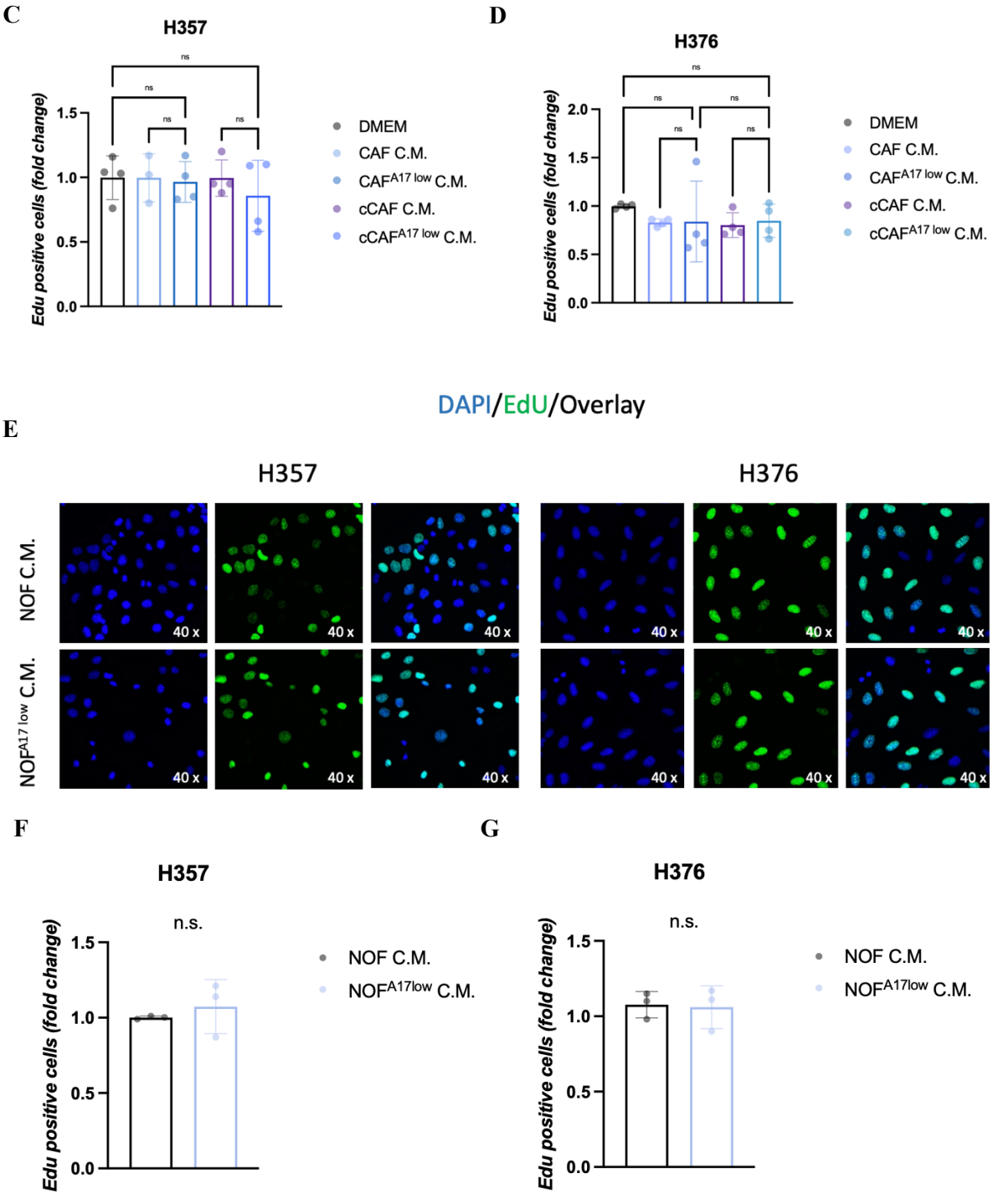
C
H357
Edu positive cells (fold change)
1.5
1.0
0.5
0.0
ns
DMEM
CAF C.M.
CAF A17 low C.M.
cCAF C.M.
cCAF A17 low C.M.
D
H376
Edu positive cells (fold change)
2.0
1.5
1.0
0.5
0.0
ns
DMEM
CAF C.M.
CAF A17 low C.M.
cCAF C.M.
cCAF A17 low C.M.
DAPI/EdU/Overlay
E
H357
H376
NOF C.M.
NOF A17 low C.M.
40 x
F
H357
n.s.
Edu positive cells (fold change)
1.5
1.0
0.5
0.0
NOF C.M.
NOF A17low C.M.
G
H376
n.s.
Edu positive cells (fold change)
1.5
1.0
0.5
0.0
NOF C.M.
NOF A17low C.M.

Figure 3.11 Conditioned medium derived from NOFs and CAFs depleted of ADAM17 does not alter H357 and H376 proliferation.

(**A**) and (**B**) Representative EdU proliferation assay in H357 and H376 cells respectively. Cells were seeded in duplicate onto coverslips in 12 well plates and incubated with CAF-derived conditioned medium for 48 h. Then the cells were incubated with EdU for 4-6 h before determining the EdU incorporation within the DNA by fluorescent microscopy. Cells were viewed using a Zeiss Axioplan 2 fluorescence light microscope, at 20-40x, setting the filter for Excitement/Emission between 491 and 520. Images were acquired using Proplus 7.0.1 image software and analysed with Fiji by randomly picking four different areas and counting the EdU positive cells. The results were normalised to the control (untreated cells) and data reported as ratio between treated sample and its control (n=3 t=3). (**C**) and (**D**) Quantification of A and B respectively. (**E**) Representative EdU proliferation assay in H357 and H376 treated with NOF-derived C.M.. The experiment was set up as described for A and B (n=3 t=2). (**F**) and (**G**) Quantification of (E). Each data represents the mean ± SD from three independent experiments. P values were calculated via ordinary one-way ANOVA (for A-D) and unpaired t test (for E-G) (∗P ≤ 0.05, ∗∗P ≤ 0.01, ∗∗∗P ≤ 0.001, ∗∗∗∗ P ≤ 0.0001).

3.2.8 Recombinant TGF-β1 can generate myofibroblast trans-differentiation in vitro and induce ADAM17 upregulation

Within neoplastic lesions, CAFs can originate from quiescent fibroblasts in response to cues such as the TGF- β1 derived from cancer cells, similarly to the transdifferentiation of resting fibroblasts into myofibroblasts during wound healing (Ronnov-Jessen and Petersen, 1993; Löhr *et al.*, 2001; Penn, Grobbelaar and Rolfe, 2012; Öhlund, Elyada and Tuveson, 2014).
Indeed, recombinant TGF-β1 has been widely used as an *in vitro* inducer of myofibroblasts, which have been reported to share features with CAFs, therefore also referred to as experimentally induced CAFs (eCAFs) (Evans *et al.*, 2003; Midgley *et al.*, 2013; Abidin *et al.*, 2021). Thus, to understand whether, beyond the acquisition of molecular myofibroblast biomarkers such as α-SMA and collagen I, this experimental model could recapitulate the functional phenotype observed so far for CAFs and cNOFs in section 3.2.1 and 3.2.4 (i.e. ADAM17 upregulation and paracrine-mediated regulation of cancer cell migration), NOFs were treated with human recombinant TGF-β1 followed by the investigation of ADAM17 according to the same protocol previously applied to study the effect of the C.M. derived from cancer cells on NOFs and CAFs.

To do so, low passage NOFs were seeded in 6-well plates followed by 24 h serum-starvation. After 24-h starvation, NOFs cells were incubated with recombinant TGF-β1 at 0, 0.25, 0.5, 1, 2.5 and 5 ng/ml. At the end of the incubation, protein and RNA were extracted and TGF-β1-signalling markers were assessed by western blot and qPCR assays. Markers of myofibroblast differentiation and TGF-β1-signalling, collagen I and phospho-SMAD3 respectively, were significantly up-regulated in a dose-dependent fashion upon TGF-β1 stimulation reaching their peak at 2.5 ng/ml (Figure 3.12 A-B). Collagen I increased by 5.5±1.4-fold ($p>0.05$), 12.88±3.01-fold ($p<0.01$), 15±2.1-fold ($p<0.001$), 21.7±4.13-fold ($p<0.0001$) and 20.57±3.9-fold ($p<0.0001$) in NOFs treated with TGF- β1 at 0.25 ng/ml, 0.5 ng/ml, 1 ng/ml, 2.5 ng/ml and 5 ng/ml respectively whereas the phosphorylated form of SMAD3 increased by 1.7±0.16-fold ($p>0.05$), 2.25±0.5-fold ($p<0.01$), 3.5±0.5-fold ($p<0.0001$), 5.4±0.21-fold ($p<0.0001$) and 5.3±0.26-fold ($p<0.0001$) for the same conditions (Figure 3.12 B). The same trend was observed by qPCR when assessing the RNA levels for alpha smooth muscle actin (α-SMA) and Collagen I. Indeed, α-SMA RNA levels increased by 1.8±0.63-fold ($p>0.05$), 2.3±0.6-fold ($p<0.05$), 6.9±0.01-fold ($p<0.0001$), 7.9±0.43-fold ($p<0.0001$) and 9.2±0.321-fold ($p<0.0001$) in NOFs treated with TGF- β1 at 0.25 ng/ml, 0.5 ng/ml, 1 ng/ml, 2.5 ng/ml and 5 ng/ml respectively whereas Collagen I transcript levels increased by 1.3±0.2-fold ($p>0.05$), 3.3±0.17-fold ($p<0.0001$), 6.8±0.2-fold ($p<0.0001$), 7.7±0.07-fold ($p<0.0001$) and 7.9±0.18-fold ($p<0.0001$) for the same conditions (Figure 3.12 C-D). These data were also confirmed through immunofluorescence by staining NOFs, treated or not with TGF- β1 at 2.5 ng/ml, for α-SMA and F-Actin (Figure 3.12 E-F). Altogether these data suggest that the use of TGF-β1 at 2.5 ng/ml is optimal for further *in vitro* studies in NOFs.

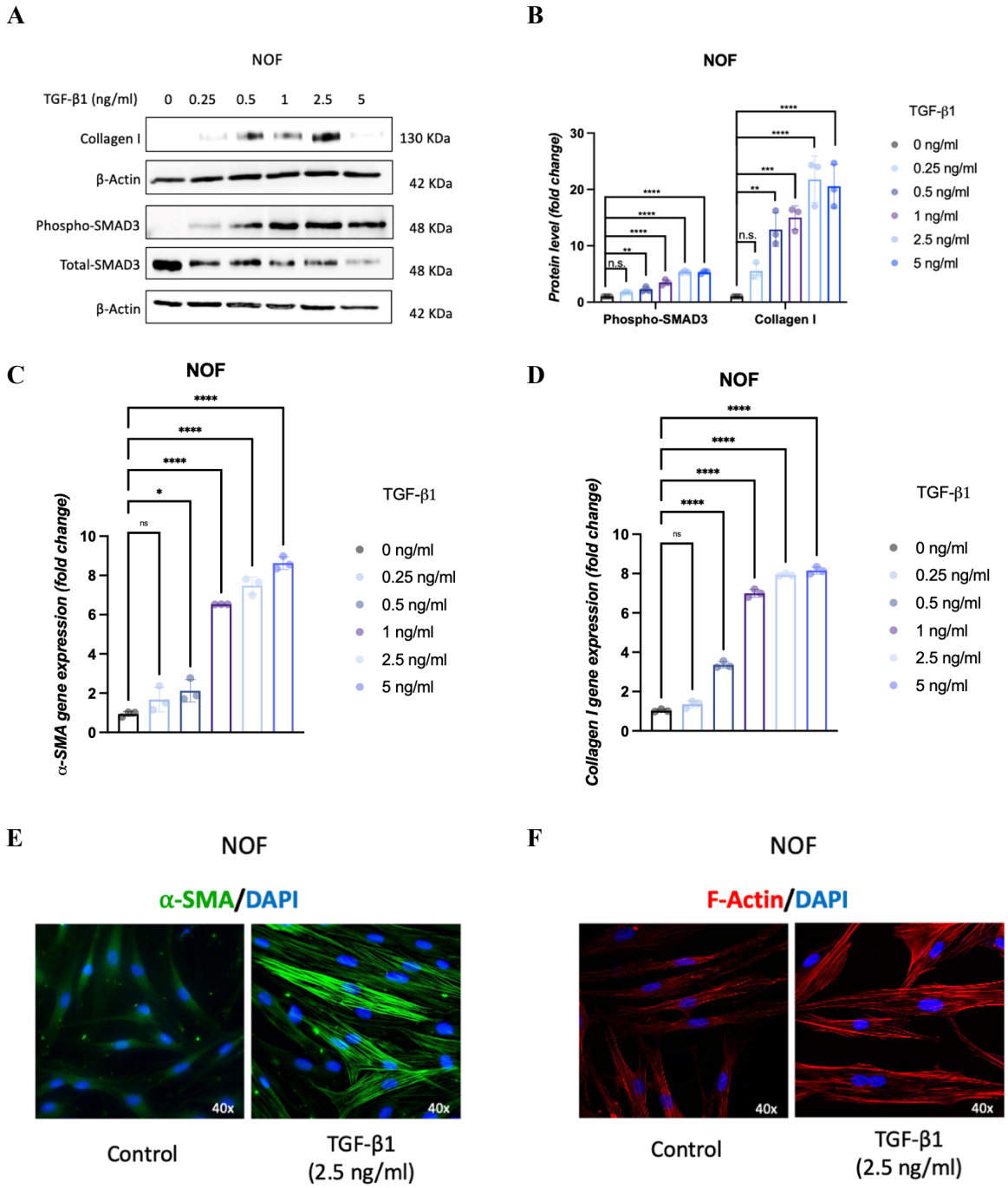

Figure 3.12 Low TGF-β1 concentrations can induce myofibroblast activation in a dose dependent manner in NOFs.

*(**A**) Representative western blot showing upregulation of Collagen I and phospho-SMAD3 in serum-starved NOFs treated with TGF-β1. NOFs were treated with TGF-β1 at 0, 0.25, 0.5, 1, 2.5 and 5 ng/ml for 24h (n=3 t=3). (**B**) Quantification of A by densitometry. (**C-D**) Representative qPCR showing α-SMA and Collagen I RNA levels in NOF with and without TGF-β1 (n=3 t=3). (**E**) Immunofluorescence staining showing α-SMA in NOF with and without TGF-β1 (n=3 t=3). (**F**) Immunofluorescence staining*

*of actin stress fibres (Actin Filaments or F-Actin) in NOFs with and without TGF-β1 (n=3 t=2). Each data represents the mean ± SD from three independent experiments. P values were calculated via ordinary one way Anova (*P ≤ 0.05, **P ≤ 0.01, ***P ≤ 0.001, **** P ≤ 0.0001).*

To characterise the impact of TGF-β1 on ADAM17 expression during TGF-β1-induced myofibroblasts generation, ADAM17 protein levels were evaluated by western blot and qPCR assays (Figure 3.13 A-C). Similarly to that observed for myofibroblasts markers, ADAM17 showed a concentration dependent up-regulation throughout TGF-β1 treatment, increasing by 1.4±0.11-fold ($p>0.05$), 1.75±0.06-fold ($p<0.01$), 1.9±0.13-fold ($p<0.001$), 2±0.3-fold ($p<0.0001$) and 2±0.26-fold ($p<0.0001$) in NOFs treated with TGF- β1 at 0.25 ng/ml, 0.5 ng/ml, 1 ng/ml, 2.5 ng/ml and 5 ng/ml respectively (Figure 3.13 A-B). An increase by 2±0.34-fold ($p<0.01$) of ADAM17 levels was also detected by qPCR in NOFs treated with TGF- β1 at 2.5 ng/ml compared to control (|Figure 3.13 C).

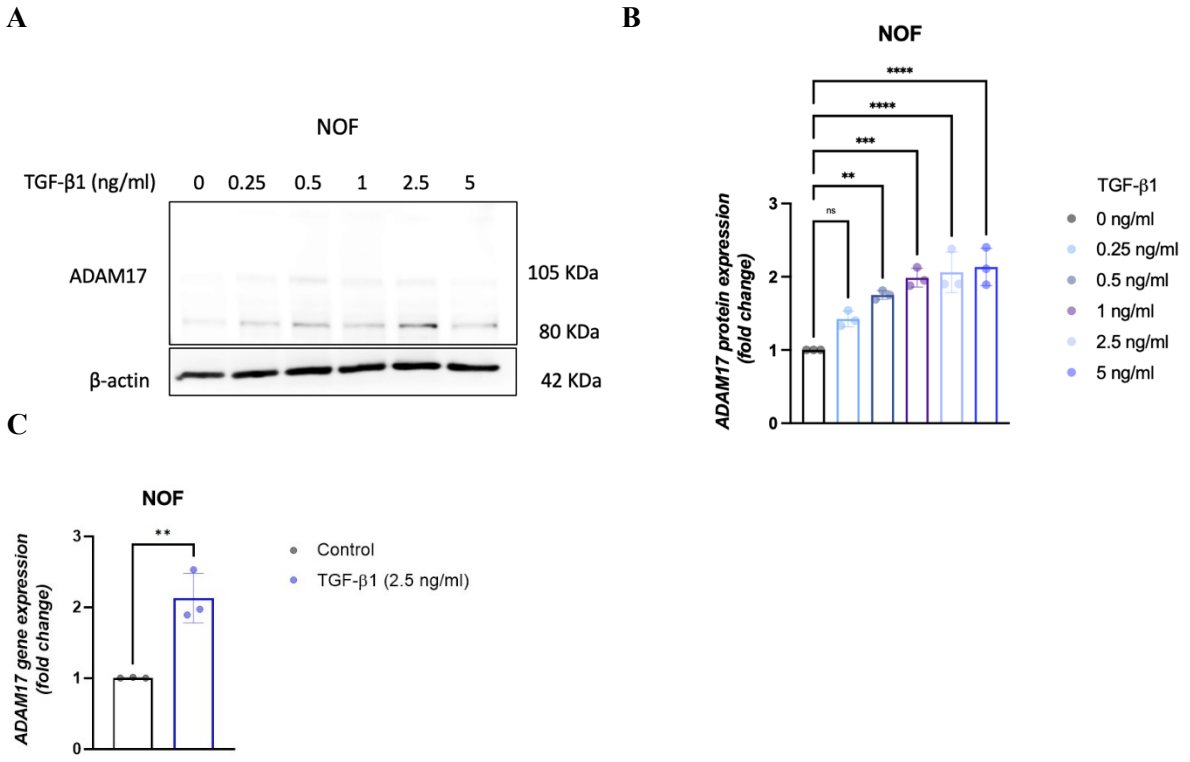

Figure 3.13 Low TGF-β1 concentrations can induce ADAM17 upregulation in a dose dependent manner in NOFs.

*(**A**) Representative western blot showing upregulation of ADAM17 in NOFs treated with TGF-β1. NOF were treated with TGF-β1 at 0, 0.25, 0.5, 1, 2.5 and 5 ng/ml for 24 h (n=3 t=3). (**B**) Quantification of*

*A by densitometry. (**C**) Representative qPCR showing ADAM17 levels upon treatment of NOFs with TGF-β1 at 2.5 ng/ml for 24 h (n=3 t=3). Each data represents the mean ± SD from three independent experiments. P values were calculated via ordinary one way Anova (3.13 B) and unpaired t test (3.13 C) (∗P ≤ 0.05, ∗∗P ≤ 0.01, ∗∗∗P ≤ 0.001, ∗∗∗∗ P ≤ 0.0001).*

3.2.9 Depletion of ADAM17 via siRNA in TGF-β1-induced myofibroblasts downregulates myofibroblast markers

Having established the optimal conditions for the TGF-β1-induced myofibroblast generation, different low passage NOFs were incubated with 2.5 ng/ml of recombinant TGF-β1 for 48 h. Subsequently, cells were transfected with 50 nM of siRNA targeting ADAM17 or control, non-targeting, siRNA for 48 h. Conditioned media, cell lysates and RNA extracts were harvested to evaluate secretome, myofibroblast and TGF-β1-signalling markers. ADAM17 KD caused more than 50% reduction of ADAM17 compared to control, at both protein and gene expression levels, as shown by western blot and qPCR analysis respectively (Figure 3.14 A-B, E). Indeed, ADAM17 protein levels decreased by 2.7±0.07-fold ($p<0.0001$) when comparing NOFs treated with TGF- β1 to ADAM17-depleted NOFs treated with TGF- β1 (Figure 3.14 A-B) whereas its RNA levels decreased by 2.2±0.07-fold ($p<0.001$) and by 3±0.03-fold ($p<0.0001$) in ADAM17-depelted NOFs with and without TGF-β1 respectively (Figure 3.14 E). Similarly, the phosphorylated SMAD3 protein levels decreased by 1.5±0.06-fold ($p<0.001$) when comparing NOFs treated with TGF- β1 to ADAM17-depleted NOFs treated with TGF-β1 (Figure 3.14 A-B), suggesting that ADAM17 contributes to regulation of the TGF-β1 signalling pathway. Moreover, ADAM17 knock-down induced a significant, although marginal, decrease of myofibroblast markers at both protein and RNA levels (Figure 3.14 C-D). Indeed, at protein level, when comparing ADAM17-depleted NOFs with and without TGF-β1 to their respective controls, α-SMA decreased by 1.3±0.09-fold ($p>0.05$) and 1.6±0.1-fold ($p<0.001$) whereas at RNA level it decreased by 1.2±0.15-fold ($p<0.001$) in ADAM17-depleted NOFs compared to control while it did not change between NOFs treated with TGF-β1in the presence or not of ADAM17 depletion (Figure 3.14 C-D, F). Similarly, Collagen I showed a significant although minimal decrease at both protein and RNA levels (Figure 3.14 C-D, F).

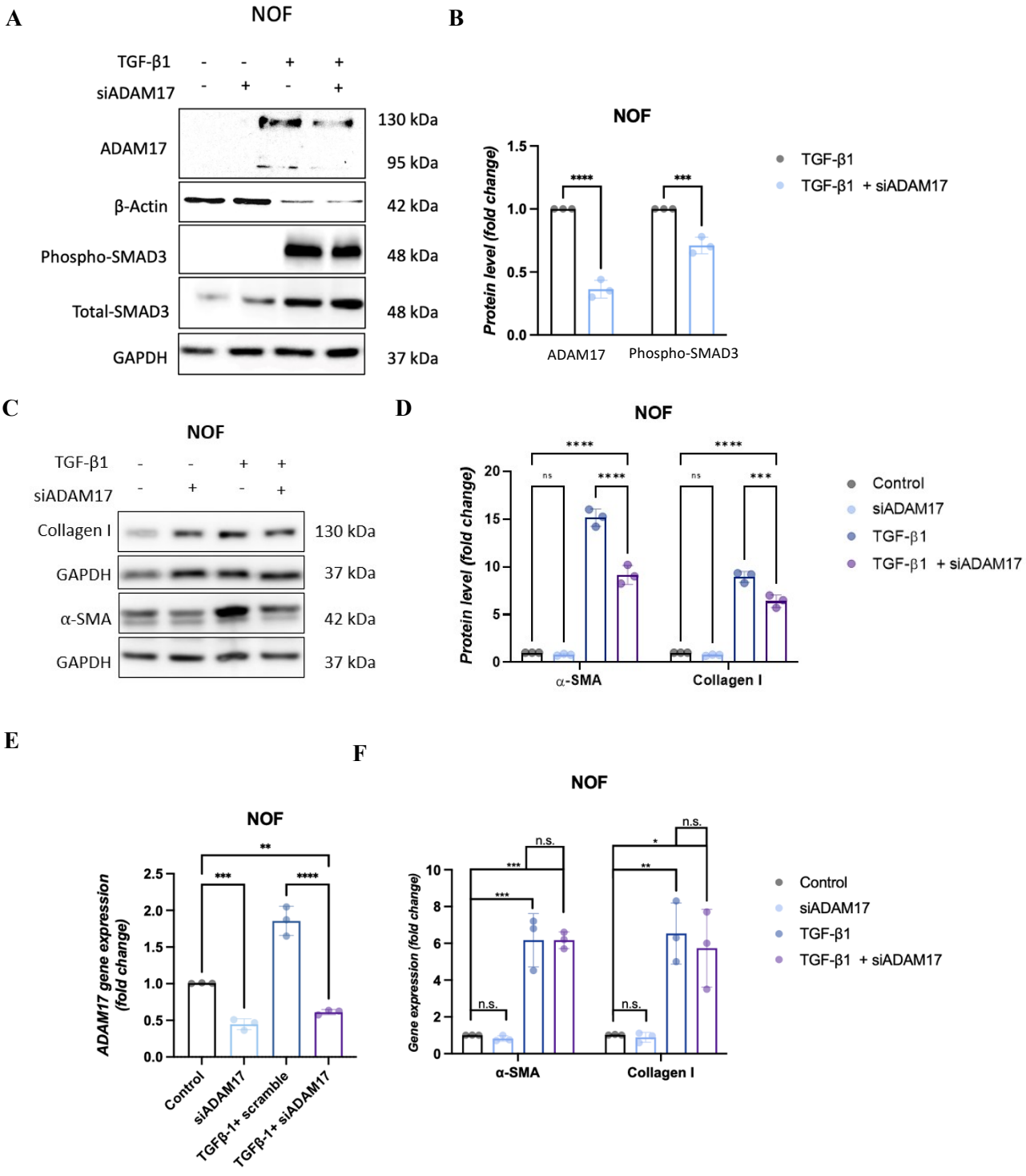

Figure 3.14 ADAM17 knock-down in TGF-β1-induced myofibroblasts downregulates TGF-β1 signalling pathway and marginally affects myofibroblast marker expression.

(A) Representative western blot showing ADAM17 and SMAD3 levels in NOFs depleted of ADAM17 upon treatment with TGF-β1. NOFs were seeded in six well plates and once attached they were treated

*with 2.5 ng/ml of TGF-β1 for 48 h. When the cells were 50-60% confluent ADAM17 was depleted via siRNA transfection and cells were incubated for 48 h (n=3 t=3). (**B**) Quantification of A by densitometry. Each data represents the mean ± SD from three independent experiments. (**C**) Representative western blot showing α-SMA and Collagen I protein levels in NOFs depleted of ADAM17 upon treatment with TGF-β1 (n=3 t=3). (**D**) Quantification of C by densitometry. (**E**) Representative qPCR showing ADAM17 levels in NOFs depleted of ADAM17 upon treatment with TGF-β1 (n=3 t=3). (**F**) Representative qPCR showing RNA levels of α-SMA and Collagen I in NOF depleted of ADAM17 upon treatment with TGF-β1 (n=3 t=3). Each data represents the mean ± SD from three independent experiments. P values were calculated via t test for B and ordinary one-way ANOVA for D-F(*P ≤ 0.05, **P ≤ 0.01, ***P ≤ 0.001, **** P ≤ 0.0001).*

Next, to test whether ADAM17 knock-down in NOFs could alter their proliferation, an EdU incorporation assay was performed for all the conditions. In line with what was observed for CAFs and NOFs in section 3.2.4, ADAM17 KD in NOFs did not affect cell proliferation as shown by EdU proliferation assay (Figure 3.15).

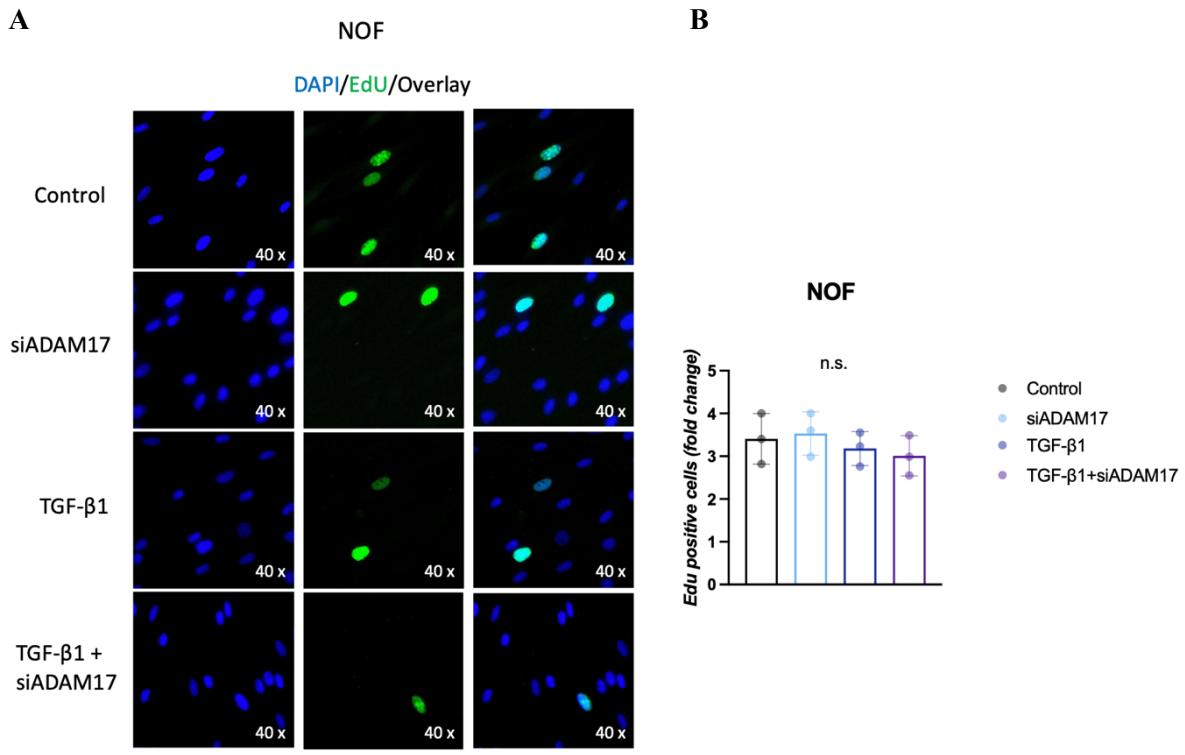

Figure 3.15 ADAM17 knock-down in TGF-β1-induced myofibroblasts does not alter NOF proliferation.

*(**A**) Representative EdU proliferation assay in NOFs depleted of ADAM17 upon treatment with TGF-β1. NOFs were seeded in twelve well plates and once attached they were treated with 2.5 ng/ml of TGF-*

*β1 for 48 h. When the cells were 50-60% confluent ADAM17 was depleted via siRNA transfection and cells were incubated for 48 h. At the end of the 48 h, cells were incubated with EdU for 4-6 h before proceeding with the assay according to the manufacturer's recommendations (n=3 t=3). (**B**) Quantification of A. Each data represents the mean ± SD from three independent experiments. P values were calculated via ordinary one-way ANOVA (∗P ≤ 0.05, ∗∗P ≤ 0.01, ∗∗∗P ≤ 0.001, ∗∗∗∗ P ≤ 0.0001).*

3.2.10 Conditioned media from TGF-β1-induced myofibroblasts upon ADAM17 knock-down reduces migratory phenotype in H357 cell line

Having demonstrated in section 3.2.9 that depletion of ADAM17 in TGF-β1-induced myofibroblasts could negatively regulate the expression of myofibroblast markers, the next step was to determine whether ADAM17 depletion could also affect their functions. Thus, the effect of the C.M. derived from myofibroblasts with ADAM17-deficiency was tested on H357 cancer cells. H357 cells were seeded in 6-well plates and incubated for 48 h with the C.M. derived from myofibroblasts (hereafter also referred to as eCAF) with and without ADAM17. While the C.M. from TGF-β1-induced myofibroblasts rendered the cells with increased migratory phenotype compared to untreated NOF, the C.M. from myofibroblasts depleted of ADAM17 impaired this response (Figure 3.16 A). Indeed, the migration rate decreased by 1.6±0.07-fold ($p>0.05$) and 1.7±0.3-fold ($p<0.01$) in $NOF^{A17\ low}$ and $eCAF^{A17\ low}$ respectively (Figure 3.16 B). To ensure that the gap closure was not due to cellular proliferation, a proliferation assay was performed via EdU DNA incorporation assay. The EdU proliferation assay showed no difference amongst the conditions confirming that the migration rate changes depending on the paracrine effect induced by ADAM17 depletion in NOFs (see Figure 3.16 C-D).

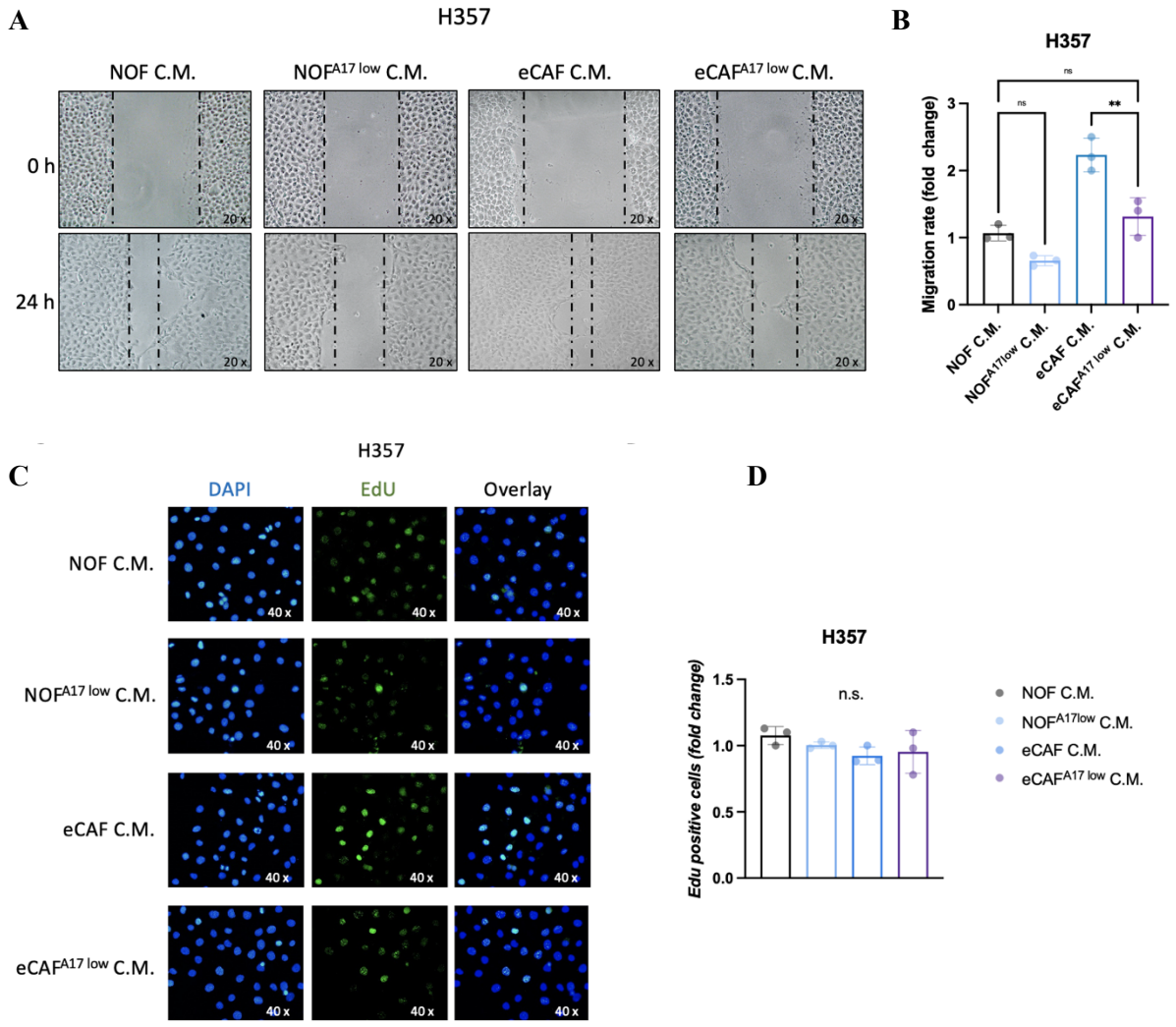

Figure 3.16 ADAM17 knock-down derived conditioned media prevent H357 cell migration.

*(**A**) Representative wound healing assay of H357 cell line incubated with C.M. from TGF-β1-induced myofibroblasts with and without ADAM17. H357 cells were seeded in six well plates and incubated for 48 h with the C.M. derived from NOFs depleted of ADAM17 upon treatment with TGF-β1. Once the cells were 90% confluent a scratch was performed and picture acquired at time 0, 6 h and 24 h (n=3 t=3). (**B**) Quantification of A. (**C**) Representative EdU proliferation assay of H357 cells treated as above described (n=3 t=3). (**D**) Quantification of C. Each data represents the mean ± SD from three independent experiments. P values were calculated via ordinary one-way ANOVA (*P ≤ 0.05, **P ≤ 0.01, ***P ≤ 0.001, **** P ≤ 0.0001).*

3.3 Discussion

The tumour microenvironment (TME) represents a complex and dynamic system wherein cancer cells are engaged in a constant crosstalk with its surrounding cells, both adjacent and

distant (Maman and Witz, 2018; Chen, McAndrews and Kalluri, 2021). This crosstalk allows cancer cells to shape the microenvironment at each stage in order to fulfil its demands by inducing indolent cells to turn into tumour supporting players, such as the cancer associated fibroblast (CAFs) (Shiga *et al.*, 2015; Maman and Witz, 2018; Sahai *et al.*, 2020). Indeed, CAFs contribute to most of the pro-tumorigenic functions within the TME, from remodelling the extracellular matrix (ECM) to secreting factors and remodulating metabolism. In this regard, the potential of cancer cells in influencing the TME in a paracrine manner was tested by an indirect co-culture using the conditioned medium (C.M.) derived from cancer cells to treat stromal fibroblasts such as NOFs and CAFs. As expected, both cell types were responsive to the cancer-derived C.M. though the extent of their responses differed. Indeed, NOFs seemed to be more sensitive and reactive to the cancer-derived C.M. displaying a major increase at both transcriptional and translational level of the CAF markers. Except for α-SMA, which showed not a significant nor considerable change, compared to CAFs, NOFs increase was nearly twofold for Collagen I RNA level whereas it was between two- to threefold at protein level. Similarly, FAP levels were between two- to fourfold higher in NOFs than CAFs. Altogether these data suggest that the C.M. derived from cancer cells can affect the stromal fibroblast behaviour *in vitro* and that this response might depend on the nature of the surrounding cells. In other words, unlike CAFs, which are reactive fibroblasts, perhaps bestowed of high basal levels of CAF-markers, primary fibroblast such as NOFs are more susceptible to the C.M. maybe because of their indolent nature and lower basal levels of CAF-markers. This conclusion is further supported by the microscopic observation of NOFs and CAFs treated or not with cancer cell-derived C.M.. While NOFs seem to change their morphology upon the treatment with the C.M., displaying a more elongated and spindle-like structure compared to control, CAFs do not.

The TME is a kaleidoscopic system wherein cells of diverse origins coexist and constantly rearrange the surrounding stroma by secreting a plethora of molecules and by modifying the ECM (Mueller and Fusenig, 2004; Maman and Witz, 2018). Key players in these processes are metalloproteinases such as the ADAMs, which have been reported to be upregulated not just in cancer cells but also in the stromal cells including CAFs (Gao *et al.*, 2013; Mochizuki *et al.*, 2019). Thus, the next question addressed in this chapter was whether the C.M. derived from cancer cells could trigger the expression of ADAM17 in the activated stromal fibroblasts.

As illustrated in Figure 3.4, upon treatment with cancer derived C.M. both NOFs and CAFs significantly upregulated ADAM17 transcript and protein levels along with ADAM17 proteolytic activity. In contrast to CAF marker expression, ADAM17 upregulation in CAFs

was more remarkable than NOFs, as evidenced by the ELISA for HB-EGF wherein, regardless higher proteolytic levels of ADAM17 in CAFs, the overall increase of ADAM17 sheddase function was between the four-to sixfold compared to the basal levels against an increase between two- to fourfold compared to basal levels in NOFs. Altogether these data indicate a clear involvement of cancer cells in influencing the stromal fibroblast acquisition of CAF-associated markers and ADAM17 upregulation, without affecting their proliferation rate as shown in Figure 3.3, the extent of this response might depend on the nature of the fibroblasts (indolent or reactive).

CAFs are the most abundant cellular component within the TME and play a crucial role in mediating cancer initiation, progression, spread throughout the organism and resistance to therapies (Cirri and Chiarugi, 2012; Chen, McAndrews and Kalluri, 2021). These pro-tumorigenic functions can be exerted in multiple ways including via their secretome enriched with a broad spectrum of molecules ranging from growth factors to proteinases, from substrates to their receptors, from nucleic acids to metabolites and vesicles. Altogether these factors regulate indirectly or directly cancer cells behaviour within the TME (Cirri and Chiarugi, 2012; Sahai *et al.*, 2020). In line with what is already reported in the literature (Hu *et al.*, 2013; Steinbichler *et al.*, 2016; S. Yu *et al.*, 2019), the C.M. derived from the reactive fibroblasts (cNOFs and CAFs) positively regulated cancer cell migration compared to the C.M. derived from indolent fibroblasts (NOFs). Moreover, there was a slight difference, although not significant, between the efficacy of CAFs and cNOFs in regulating cancer cell migration. Indeed, cancer cells incubated with the C.M. derived from CAFs migrated slightly more than their counterpart treated with the C.M. derived from cNOFs. This result could be once again due to the nature of the fibroblast type, with CAFs being a consolidated reactive fibroblast derived directly from a cancer patient whereas cNOFs result from the stimulation of primary fibroblasts derived from a healthy donor. Nevertheless, this result does not diminish the value of the finding, on the contrary it demonstrates that cancer cells can quickly and profoundly hijack an indolent fibroblast to turn it into a powerful ally in malignancy progression. Thus, identifying the mechanisms behind this detrimental loop could lead to a better therapeutic design to intervene at the very beginning of tumour initiation. Moreover, the results presented in this chapter indicate a different response between cancer cells to the C.M. derived from both cNOFs and CAFs. As compared to H357 cells, H376 migration seemed to increase to a less extend, though not remarkable, which might be explained by H376 cells being a metastatic cell line thus more migratory by nature whereas H357 cells are not (Prime *et al.*, 1990; Prime,

Gamel, *et al.*, 1994; Prime, Matthews, *et al.*, 1994). Of note, cancer cells did not show any alteration of their proliferation status upon treatment with the C.M. from stromal fibroblasts.

ADAMs are metalloproteinases with proteolytic domain involved in a variety of biological processes including diseases such as cancer (Murphy, 2008; Lambrecht, Vanderkerken and Hammad, 2018). In this scenario, ADAM17 represents one of the best and most studied members though some of its functions and properties remain elusive (Gooz, 2010; Zunke and Rose-John, 2017; Düsterhöft, Lokau and Garbers, 2019). ADAM17 is an important sheddase known to regulate the availability of substrates and their receptors, most of which play a key role in essential signalling pathways (Gooz, 2010). Moreover, ADAM17 activation occurs exclusively in response to stimuli such as those triggering diseases like cancer. Indeed, ADAM17 hyperactivation has been evidenced in cancer cells and the TME, thus making ADAM17 a potential candidate for cancer therapy (Moss and Minond, 2017b). In this context and following the results showing ADAM17 upregulation in activated fibroblasts, the next question addressed was to whether targeting ADAM17 in stromal fibroblasts could have any impact on their features. Firstly, silencing of ADAM17 in both NOFs and CAFs induced a mild decrease of CAF markers expression with a similar extent at RNA levels whereas it varied at protein levels with CAFs showing a more remarkable decrease of FAP protein levels compared to NOFs. More specifically, this decrease was observed in the context of CAFs previously incubated with the C.M. derived from cancer cells (cCAFs), where cCAFs depleted of ADAM17 ($cCAF^{A17\,low}$) showed lower levels of FAP compared to cCAFs, whereas FAP levels in $cCAF^{A17\,low}$ were like those of CAFs alone. These data seem to suggest that ADAM17 silencing might help mitigate the further activation of CAFs in response to cancer cell secretome. A similar trend was observed in cNOFs for FAP levels, although the response varied amongst conditions, whereas Collagen Type I protein levels in cNOFs upon ADAM17 depletion did not resume the basal levels of the unstimulated NOFs.

After having demonstrated the effect of activated fibroblasts (cNOFs, CAFs and cCAFs) in positively regulating cancer cell migration *in vitro* in a paracrine fashion, the next step was to analyse the same phenomenon upon ADAM17 depletion in stromal fibroblasts. A better understanding of this aspect is fundamental considering both the role of ADAM17, known to shed over 90 substrates most of which are released as secreted factors by the cells (Gooz, 2010; Moss and Minond, 2017b; Düsterhöft, Lokau and Garbers, 2019) and given that stromal fibroblasts represent one of the major sources of soluble factors within the TME (Chen, McAndrews and Kalluri, 2021). Here it has been demonstrated that ADAM17 depletion in stromal fibroblasts can mitigate their pro-tumorigenic paracrine effect on cancer cells by

restraining cancer cell migratory potential. Although neither NOFs nor cNOFs could trigger a stronger migratory response in cancer cells, this negative effect on H357 and H376 cell migration was reproducible amongst all the ADAM17-depleted fibroblasts studied, independently of their activation status. Moreover, the decreased cancer cell migration was statistically significant, also with the C.M. derived from activated fibroblasts, shown here to have elevated levels of ADAM17 expression and activities (see section 3.2.3). This suggests that ADAM17 targeting in the stromal fibroblast could be a potentially good candidate when designing therapies addressing tumours at their primary stage, in order to prevent or delay their evolution as metastatic tumours, or advanced tumours to delay the further dissemination of cancer cells. In addition, the C.M. derived from ADAM17-depleted stromal fibroblasts did not alter cancer cell proliferation.

A crosstalk between TGF-β1 and ADAM17 has been reported, wherein they mutually regulate each other's expression and activity, either positively or negatively, in a context-dependent manner (Borrell-Pagès *et al.*, 2003; C. Liu *et al.*, 2009; Malapeira *et al.*, 2010). Thus, another important aspect investigated in this chapter was the response of NOFs to TGF-β1, known to be a driver of myofibroblasts and CAFs generation released by cancer cells (Sahai *et al.*, 2020), and whether ADAM17 silencing in NOFs could interfere with this process. Firstly, in line with the literature (Abidin *et al.*, 2021) it was observed a significant response to TGF-β1, even at low concentrations (starting at 0.25 ng/ml) as evidenced by western blot analysis of the TGF-β1 and CAF markers. Moreover, both the phosphorylated form of SMAD3 and Collagen Type I increased significantly and robustly in a dose dependent manner reaching the peak at 2.5 ng/ml. The same trend was observed at RNA level for both Collagen Type I and α-SMA. Secondly, keeping with what observed for NOFs treated with OSCC cell derived C.M. in section 3.2.3, NOF treatment with TGF-β1 displayed a significant and dose dependent upregulation of ADAM17 protein levels, suggesting that TGF-β1 can mimic the effect of the C.M. derived from cancer cells. Next, it was observed that upon ADAM17 silencing in eCAFs the levels of phosphorylated SMAD3 significantly decreased compared to control along with α-SMA and Collagen I, although their change was detected at protein level and not at RNA level, suggesting that their regulation might occur at post-translational level, either by mediating their production or their turn-over. Nevertheless, these data indicate that ADAM17 silencing in eCAFs can negatively regulate the TGF- β1 signalling pathway, as previously described in the literature (Xu *et al.*, 2016).

Chapter 4: Investigation of the molecular regulator(s) behind the restrained migration in OSCC-derived cancer cells upon treatment with the C.M. from ADAM17-depleted stromal fibroblasts

4.1 Aims and objectives

Following the observation of the restrained migratory and invasive capacity associated with depletion of fibroblast ADAM17 in an indirect co-culture assay, further analyses were required to investigate how ADAM17 could exert this function, focussing on the identification of the cancer cell-intrinsic molecular mechanism(s) triggered. Thus, to address this question, the following analyses were performed:

1. Assessment of the protein and RNA levels of a panel of markers associated with cancer cell migration by western blot and qPCR assays respectively.
2. Pharmacological targeting of the molecular player(s) potentially involved in the ADAM17-mediated paracrine regulation of the cancer cell migration.
3. Investigation of the effect of ADAM17 depletion in OSCC cell lines.

4.2 Results

4.2.1 The paracrine effect of ADAM17 on OSCC-cancer cells migration might function by modulating N-cadherin in cancer cells.

Several lines of evidence show that targeting of ADAM17 in cancer cells restrains cancer cell migration and invasion and that ADAM17 can promote EMT in gastric cancer cells via the TGF-β signalling pathway, which in turn induces the up-regulation of markers such as Snail, vimentin and N-cadherin (Kenny and Bissell, 2007; Xu *et al.*, 2016; W. Li *et al.*, 2019). Likewise, lung adenocarcinoma cells with high ADAM17 levels displayed an EMT-associated cell invasion which was reversed upon silencing of ADAM17, followed by the decrease of the EMT markers N-cadherin and vimentin (Cai *et al.*, 2015).

Thus, to assess whether a similar mechanism could have been triggered in cancer cells in response to the exposure to the C.M. derived from activated stromal fibroblasts, H357 and H376 cells were seeded in six well plates and challenged with the C.M. derived from NOFs and CAFs depleted of ADAM17 and, following an incubation of 48 h, a panel of four markers (Snail, Slug, Twist and N-cadherin) associated with the acquisition of a migratory behaviour

by cancer cells was evaluated by qPCR assay. The only marker that showed a significant and consistent downregulation in both H357 and H376 treated with the C.M. derived from ADAM17-depleted NOFs and CAFs was N-cadherin. N-cadherin, which is an important mesenchymal marker and biomechanical effector upregulated in metastatic cells (Vilchez Mercedes *et al.*, 2021), showed a decrease by 1.3±0.05-fold ($p>0.05$) and 1.8±0.1-fold ($p<0.0001$) in H357 treated with $NOF^{A17\ low}$ and $cNOF^{A17\ low}$ respectively, compared to NOF and cNOF (Figure 4.1 A) whereas in H376 it decreased by 1.4±0.1-fold ($p<0.05$) and 1.4±0.02-fold ($p<0.0001$) for the same conditions (Figure 4.1 B). Similarly, when treated with ADAM17-depleted NOF-derived C.M. N-cadherin decreased by 1.7±0.10-fold ($p<0.001$) and 1.6±0.24-fold ($p<0.001$) in H357 treated with $CAF^{A17\ low}$ and $cCAF^{A17\ low}$ respectively, compared to CAFs and cCAFs (Figure 4.1 C), whereas in H376 it decreased by 1.5±0.03-fold ($p<0.01$) and 1.9±0.11-fold ($p<0.0001$) for the same conditions (Figure 4.1 D).

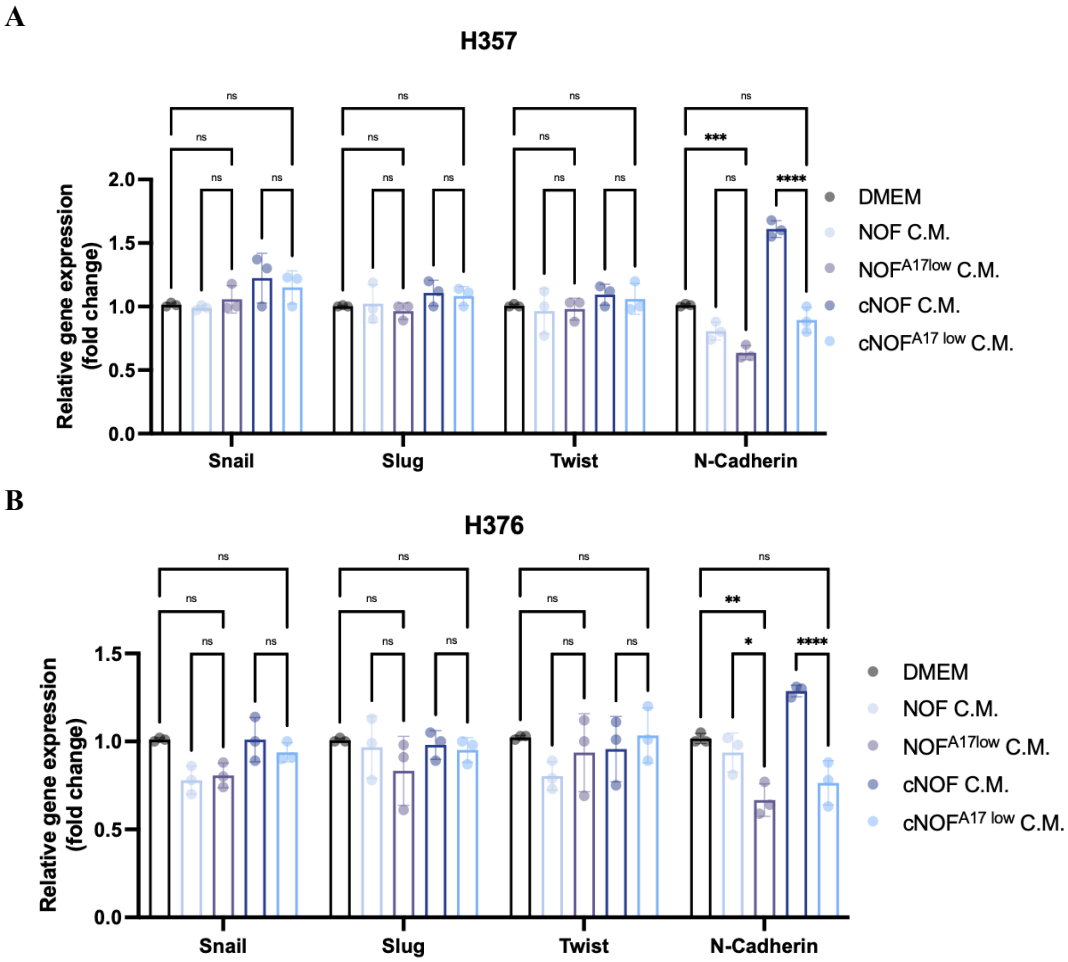

C

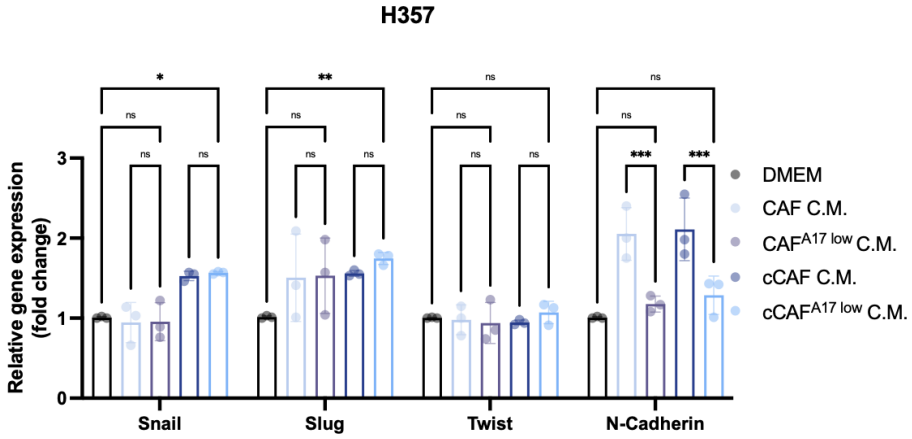

D

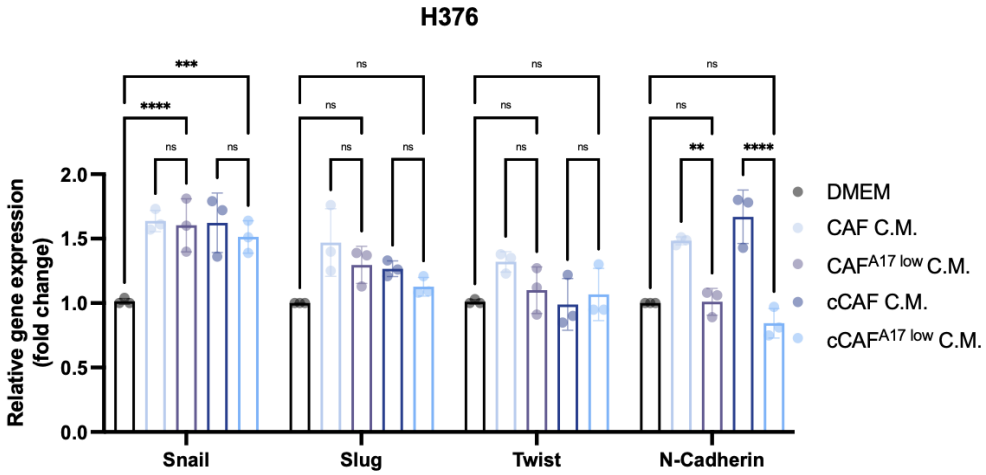

Figure 4.1 OSCC cells treated with the conditioned medium derived from NOFs and CAFs depleted of ADAM17 display a reduction of N-cadherin gene levels.

*(**A-B**) Representative qPCR showing Snail, Slug, Twist and N-cadherin gene expression levels in H357 and H376 challenged with the C.M. derived from NOFs. Cells were seeded in 6 well plates and incubated with and without the C.M. derived from NOFs (NOF, NOF$^{A17\ low}$, cNOF and cNOF$^{A17\ low}$) for 48 h (n=3 t=3). (**C-D**) Representative qPCR showing Snail, Slug, Twist and N-cadherin gene expression levels in H357 and H376 challenged with the C.M. derived from CAFs. Cells were seeded in 6 well plates and incubated with and without the C.M. derived from CAFs (CAF, CAF$^{A17\ low}$, cCAF and cCAF$^{A17\ low}$) for 48 h (n=3 t=3). Each data represents the mean ± SD from three independent experiments. P values were calculated via ordinary one-way ANOVA (*P ≤ 0.05, **P ≤ 0.01, ***P ≤ 0.001, **** P ≤ 0.0001).*

Thus, N-cadherin levels were also evaluated by western blot in both H357 and H376. Initially, N-cadherin levels were assessed in cancer cells challenged with the C.M. derived from NOFs, $NOF^{A17\ low}$, CAFs and $CAF^{A17\ low}$. Though only in H376, N-cadherin showed a downregulation also at protein levels when cells were incubated with $NOF^{A17\ low}$ and $CAF^{A17\ low}$ compared to their respective control (Figure 4.2 A). Next, N-cadherin protein levels were assessed in H357 and H376 for the same conditions investigated by qPCR. The results confirmed a significant decrease of N-cadherin in both cell lines when treated with the C.M. derived from NOFs and CAFs depleted of ADAM17 compared to their control, confirming the trend observed by qPCR. In H357 N-cadherin protein levels decreased by 2.5±0.3-fold ($p<0.01$) and 2.8±0.05-fold ($p<0.0001$) when treated with the C.M. derived from $CAF^{A17\ low}$ and $cCAF^{A17\ low}$ respectively, whereas in H376 it decreased by 1.9±0.07-fold ($p<0.05$) and 4.5±0.3-fold ($p<0.0001$) for the same conditions (Figure 4.2 B-E).

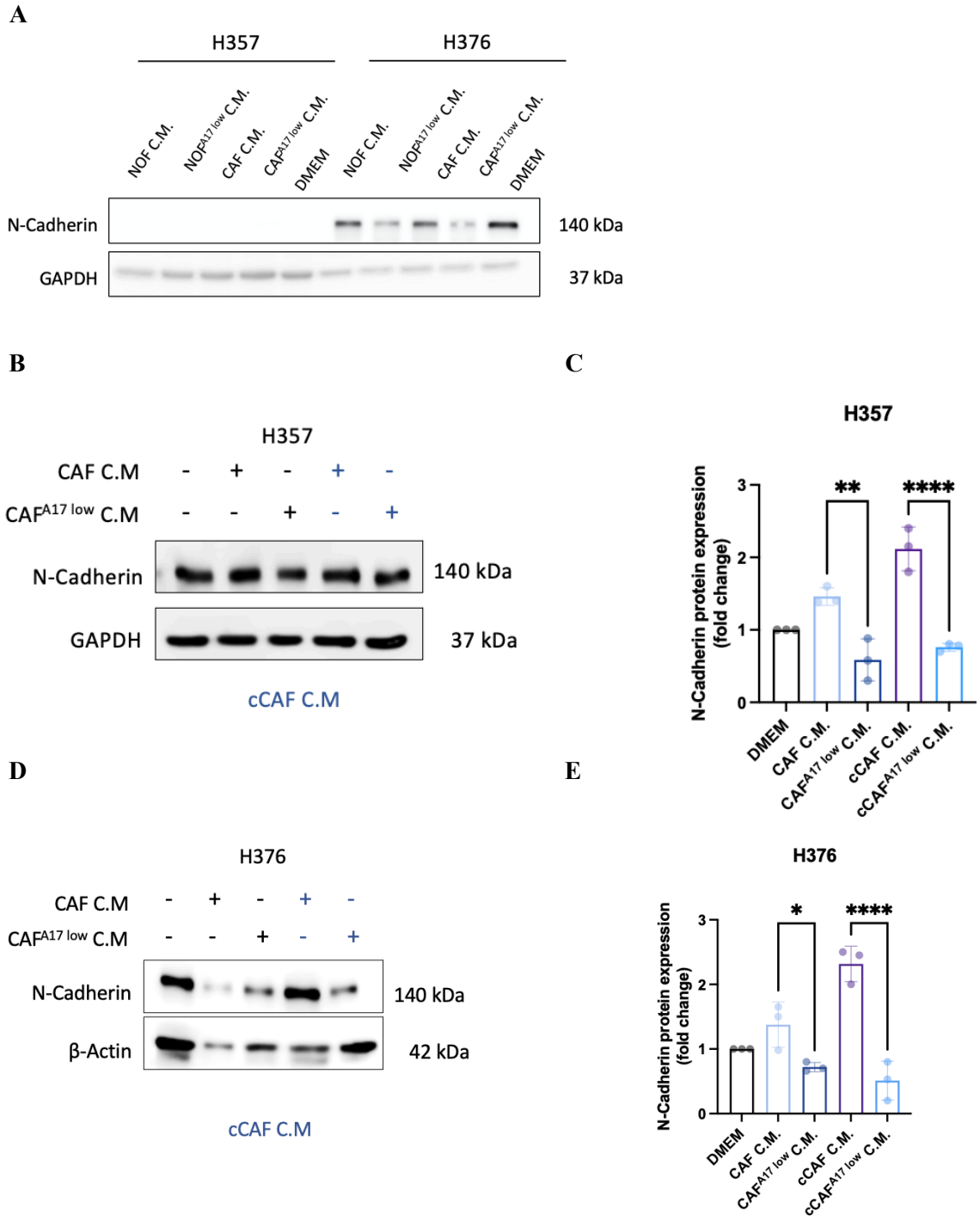

Figure 4.2 OSCC cells treated with the conditioned medium derived from NOFs and CAFs depleted of ADAM17 display a reduction of N-cadherin protein levels.

*(**A**) Representative western blot showing N-cadherin protein levels in H357 and H376 challenged with the C.M. derived from NOFs and CAFs, not conditioned with OSCC cell-derived C.M., depleted of ADAM17 (n=3 t=3). (**B**) Representative western blot showing N-cadherin protein levels in H357*

*treated with CAF-derived and cCAF-derived C.M. (n=3 t=3). Cells were seeded in 6 well plates and incubated with and without the C.M. derived from CAFs (CAF, $CAF^{A17\ low}$, cCAF and $cCAF^{A17\ low}$) for 48 h. (**C**) Quantification of B by densitometry. (**D**) Representative western blot showing N-cadherin protein levels in H376 treated with CAF-derived C.M. (n=3 t=3). Cells were seeded in 6 well plates and incubated with and without the C.M. derived from CAFs (CAF, $CAF^{A17\ low}$, cCAF and $cCAF^{A17\ low}$) for 48 h. (**E**) Quantification of D by densitometry. Each data represents the mean ± SD from three independent experiments. P values were calculated via ordinary one-way ANOVA (∗P ≤ 0.05, ∗∗P ≤ 0.01, ∗∗∗P ≤ 0.001, ∗∗∗∗ P ≤ 0.0001).*

Since N-cadherin acquisition is associated to the EMT process, characterised by the cadherin switching that leads to the loss of the epithelial marker E-cadherin in favour of the acquisition of mesenchymal markers such as N-cadherin (Huang *et al.*, 2019), E-cadherin levels were also assessed, although only H357 were positive since H376 are known to lack its expression (Jenkinson *et al.*, 2011). E-cadherin levels did not show any change either at protein or at transcriptional level (Figure 4.3).

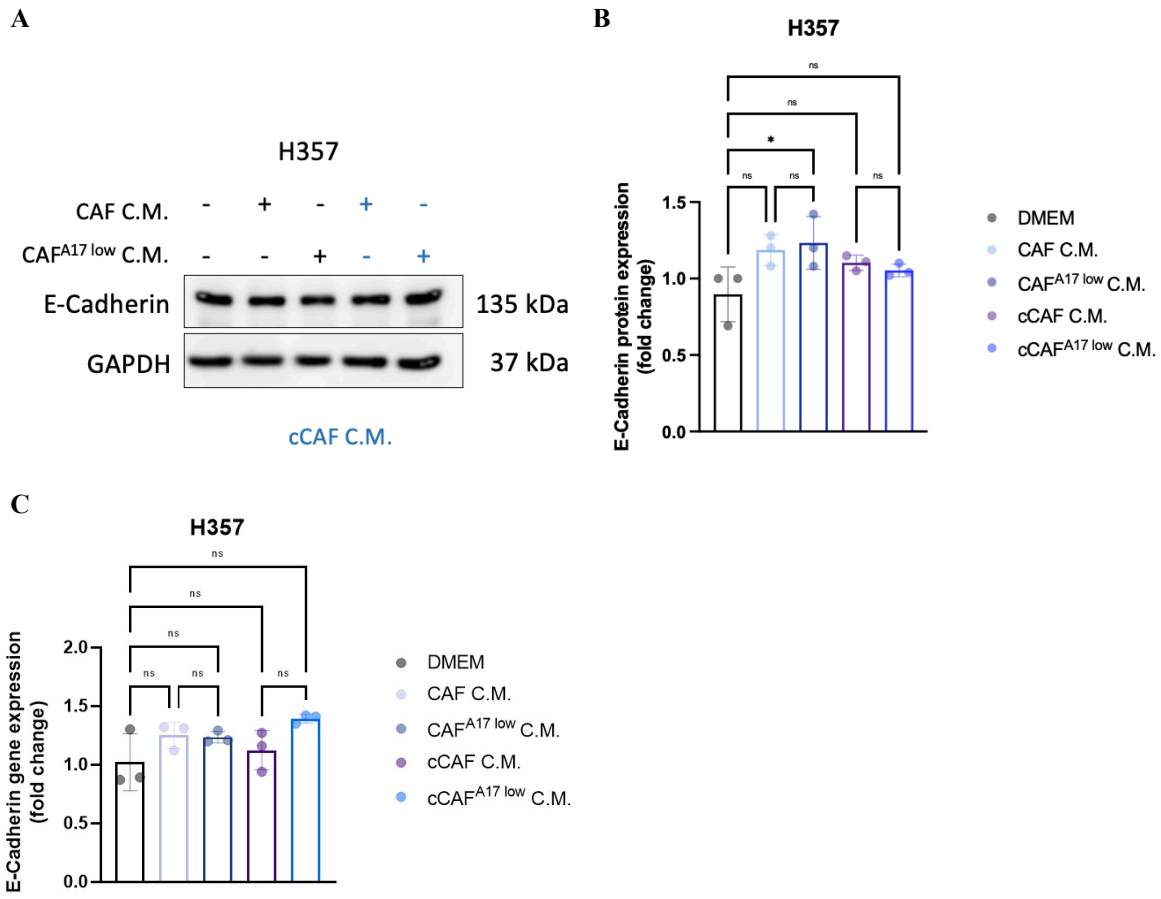

Figure 4.3 OSCC cells treated with the conditioned medium derived from CAFs depleted of ADAM17do not display alteration of E-cadherin levels.

*(**A**) Representative western blot showing E-cadherin protein levels in H357 treated with CAF-derived C.M. (n=3 t=3). Cells were seeded in 6 well plates and incubated with and without the C.M. derived from CAFs (CAF, CAF$^{A17\ low}$, cCAF and cCAF$^{A17\ low}$) for 48 h. Control blot is the same reported in Figure 4.2 B since E-cadherin and N-cadherin were blotted on the same membrane. (**B**) Quantification of A by densitometry. (**C**) Representative qPCR showing E-cadherin gene expression levels in H357 challenged with the C.M. derived from CAFs (n=3 t=3). Each data represents the mean ± SD from three independent experiments. P values were calculated via ordinary one-way ANOVA (∗P ≤ 0.05, ∗∗P ≤ 0.01, ∗∗∗P ≤ 0.001, ∗∗∗∗ P ≤ 0.0001).*

Considering these results, to determine the role of N-cadherin in the migratory phenotype observed in OSCC derived cell lines, N-cadherin was inhibited in both H357 and H376 via ADH-1 treatment. ADH-1 is a small cyclic peptide known to be an N-cadherin antagonist,

currently in clinical trial for its antineoplastic activity (Williams *et al.*, 2000; W. Yu *et al.*, 2019).

H357 and H376 cells were seeded into six well plates with or without the C.M. derived from CAFs for 48 h. Next, when the cells reached at least a 90% of confluence, a scratch was created and the cells were treated with ADH-1 at 0.2 mg/ml or with DMSO. The concentration of ADH-1 used was selected as sub-cytotoxic after a dose-response assay in line with what already reported in the literature (Erez *et al.*, 2004; Shintani *et al.*, 2008; Lammens *et al.*, 2012). As reported in Figure 4.4, the migratory potential strongly and significantly decreased in both cell lines in the presence of ADH-1 compared to their respective controls. Of note, this impaired migratory ability was independent of the cell proliferation potential as no significant reduction in proliferation was observed in both H357 and H376 treated with ADH-1 in the presence of CAF-derived C.M. (only in H376 treated with C.M. derived from CAFs) and the extent of the reduction observed could not be sufficient to explain the substantial drop in cancer cell migration. In H357 the migration rate decreased by 3.7±0.01-fold ($p<0.0001$) and 4.6±0.01-fold ($p<0.0001$) when treated with ADH-1 in the presence or absence of CAF-derived C.M., whereas in H376 it decreased by 3.6±0.05-fold ($p<0001$) and 2.4±0.01-fold ($p<0.0001$), suggesting that N-cadherin plays a crucial role in migration in OSCC cell lines and that this could be a potential candidate through which depletion of ADAM17 might negatively modulate cancer cell migration in a paracrine manner.

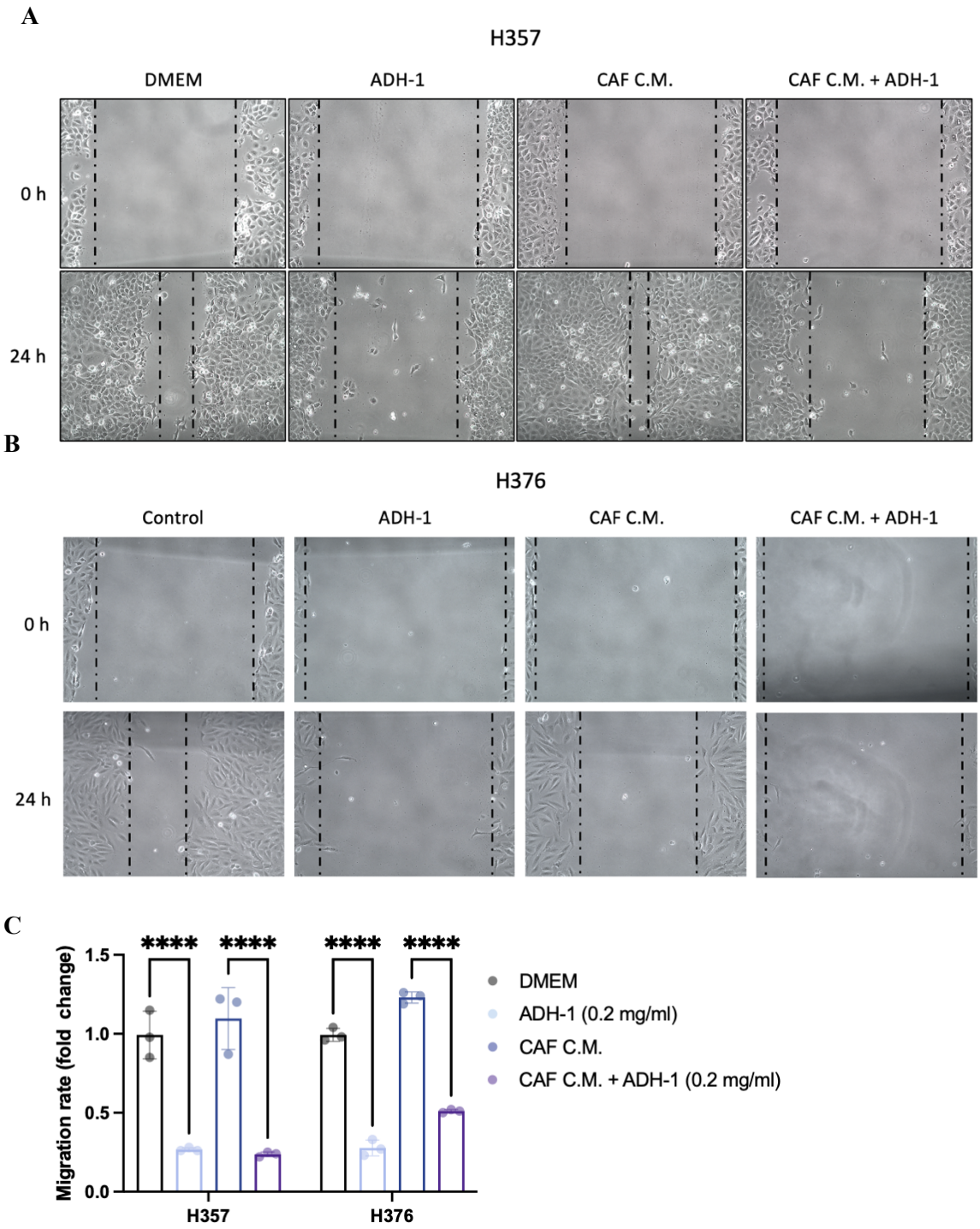
A
H357
DMEM
ADH-1
CAF C.M.
CAF C.M. + ADH-1
0 h
24 h
B
H376
Control
ADH-1
CAF C.M.
CAF C.M. + ADH-1
0 h
24 h
C
Migration rate (fold change)
1.5
1.0
0.5
0.0
****
****
****
****
H357
H376
DMEM
ADH-1 (0.2 mg/ml)
CAF C.M.
CAF C.M. + ADH-1 (0.2 mg/ml)

D

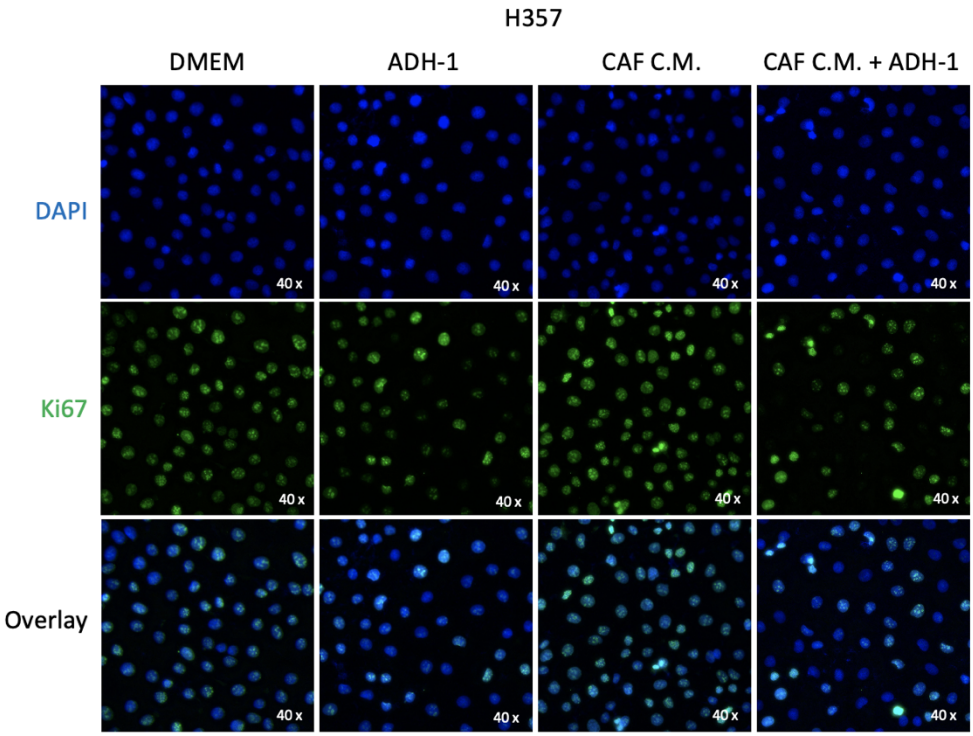
H357
DMEM
ADH-1
CAF C.M.
CAF C.M. + ADH-1
DAPI
Ki67
Overlay
40 x

E

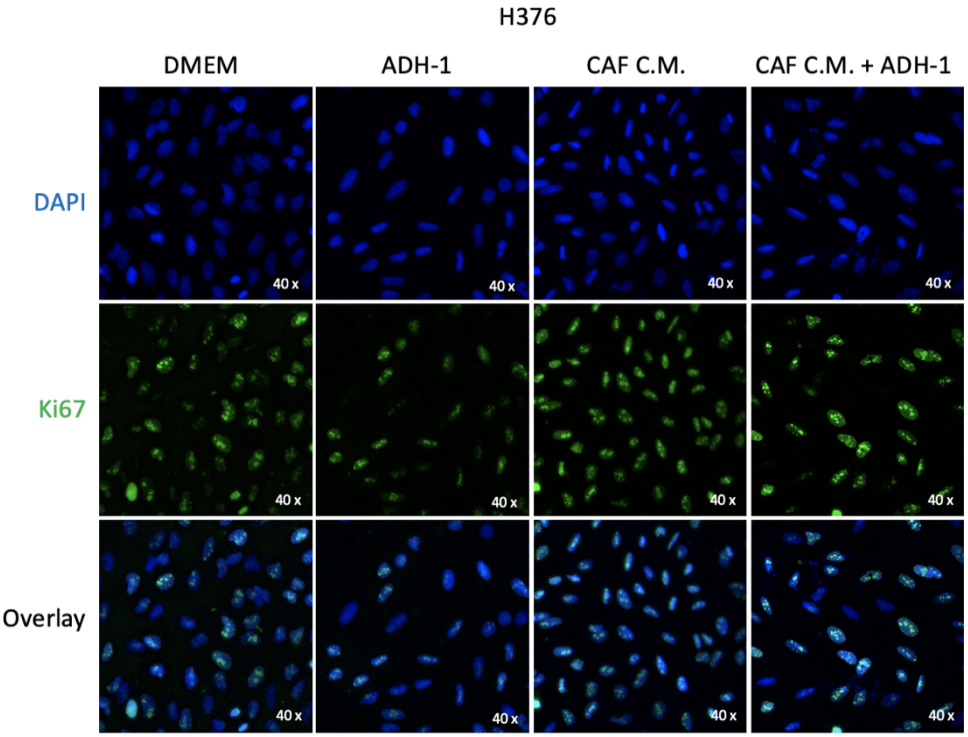
H376
DMEM
ADH-1
CAF C.M.
CAF C.M. + ADH-1
DAPI
Ki67
Overlay
40 x

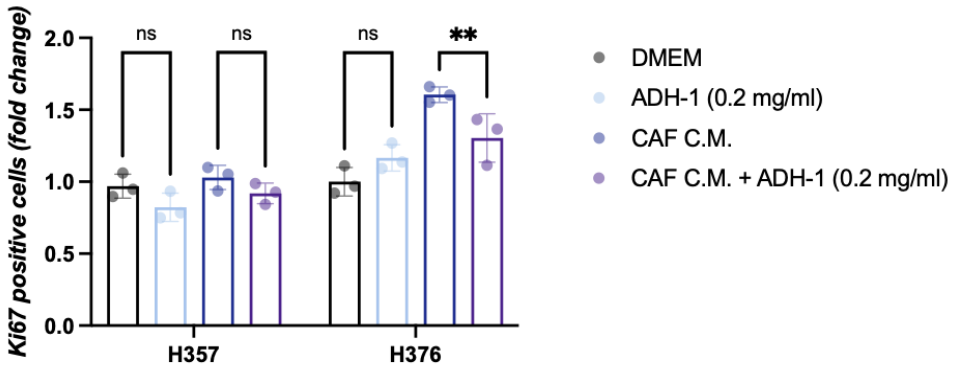

Figure 4.4 ADH-1-mediated N-cadherin inhibition in OSCC cell lines restrains cancer migration.

*(**A**) and (**B**) Wound healing assay in H357 and H376 cells, respectively, in the presence of ADH-1. Cells were seeded in 6 well plates and incubated with or without CAF-derived C.M. for 48 h. Afterwards, a scratch was created and medium was replaced with fresh culture medium containing either ADH-1 (0.2 mg/ml) or DMSO (n=3 t=2). The pictures were acquired at time 0, 6 h and 24 h. The area delimited by the scratch was measured by Fiji and data analysed in Prism. (**C**) Quantification of A and B. (**D-E**) Representative Ki67 immunofluorescence staining for H357 and H376 respectively. The cells were seeded onto coverslips and treated as above-mentioned. Cells were viewed using a Zeiss Axioplan 2 fluorescence light microscope, at 20-40x, setting the filter for Excitement/Emission between 491 and 520. Images were acquired using Proplus 7.0.1 image software and analysed with Fiji by randomly picking four different areas and counting the Ki67 positive cells. The results were normalised to the control (untreated cells) and data reported as ratio between treated sample and its control (n=3 t=2). (**F**) Quantification of D and E. Each data represents the mean ± SD from three independent experiments. P values were calculated via ordinary one-way ANOVA (∗P ≤ 0.05, ∗∗P ≤ 0.01, ∗∗∗P ≤ 0.001, ∗∗∗∗ P ≤ 0.0001).*

4.2.2 Acute depletion of ADAM17 in H357 and H376 cell lines does not alter the migratory phenotype in an autocrine manner

Having identified a role for ADAM-17 in mediating, in a paracrine fashion, cancer cell migration through CAFs, it was fundamental to determine whether ADAM17 could have any impact when directly targeting it in cancer cells. ADAM17 has been shown to be upregulated in many human malignancies and enhances cancer cell migration and invasion in both a cell- and non-cell-autonomous manner (Kenny and Bissell, 2007; Cai *et al.*, 2015; Morancho *et al.*, 2015; W. Li *et al.*, 2019). Nevertheless, its functions vary accordingly cell type and microenvironment which requires clarification for whether it is applicable to all cancers. Thus,

to assess ADAM17 role in shaping cancer cell behaviour *in vitro*, H357 and H376 cells were depleted of ADAM17 and their proliferation and migration analysed.

H357 and H376 cells were sub-confluently seeded in 6 well and 12 well plates and transfected with si-ADAM17 or control siRNA for 48 h. Eventually, C.M., protein lysates and RNA were harvested. ADAM17 depletion via siRNA was successful in both cell lines, showing a decrease of ADAM17 RNA level by 2.7±0.2-fold ($p<0.0001$) in H357 and by 3.4±0.07-fold in H376 (Figure 4.5 A). Moreover, as observed for CAFs, ADAM17 silencing did not alter cell proliferation as reported by the EdU proliferation assay (Figure 4.5 B-D).

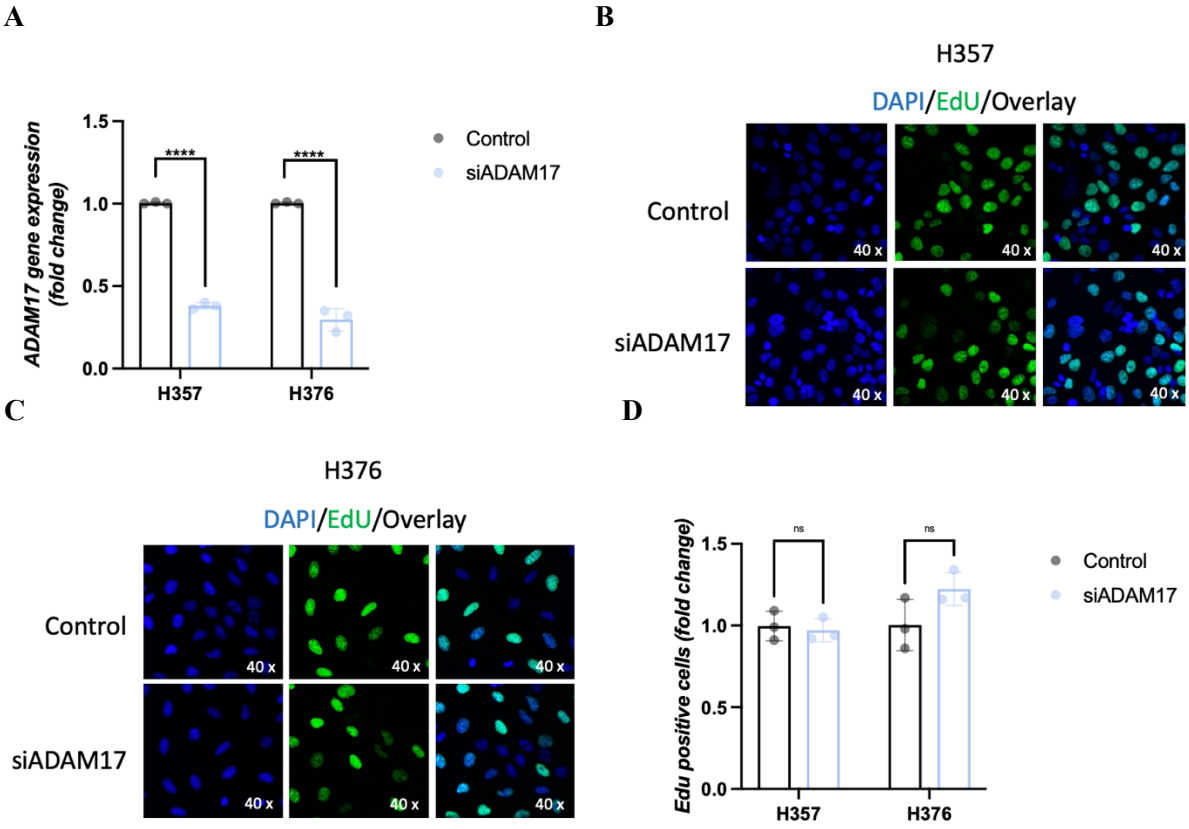

Figure 4.5 ADAM17 depletion in OSCC cell lines by siRNA.

*(**A**) Representative qPCR showing ADAM17 RNA levels in H357 upon ADAM17 KD by siRNA (n=3 t=2). (**B**) Representative immunofluorescence staining showing EdU proliferation assay in H357 upon ADAM17 KD. H357 cells were seeded in twelve well plates onto coverslips and once 50-60% confluent they were depleted of ADAM17 by siRNA. Cells were viewed using a Zeiss Axioplan 2 fluorescence light microscope, at 20-40x, setting the filter for Excitement/Emission between 491 and 520. Images were acquired using Proplus 7.0.1 image software and analysed with Fiji by randomly picking four*

*different areas and counting the EdU positive cells. The results were normalised to the control and data reported as ratio between ADAM17-depleted sample and its control (n=3 t=2). (**C**) Quantification of B. (**D**) Representative qPCR showing ADAM17 RNA levels in H376 upon ADAM17 KD by siRNA. ADAM17 silencing was performed according to the same protocol used for H357 cells (n=3 t=2). (**E**) Representative immunofluorescence staining showing EdU proliferation assay in H376 upon ADAM17 KD. The protocol applied was the same used for H357 cells (n=3 t=2). (**F**) Quantification of E. Each data represents the mean ± SD from three independent experiments. P values were calculated via Unpaired T Test (∗P ≤ 0.05, ∗∗P ≤ 0.01, ∗∗∗P ≤ 0.001, ∗∗∗∗ P ≤ 0.0001).*

To assess whether the C.M. derived from both cancer cell lines upon ADAM17 knock-down had the same migration inhibitory effect as observed when using that derived from ADAM17-deficient CAFs, a wound healing assay was performed for both cell lines and the protein levels of N-cadherin assessed by western blot assay (Figure 4.6).

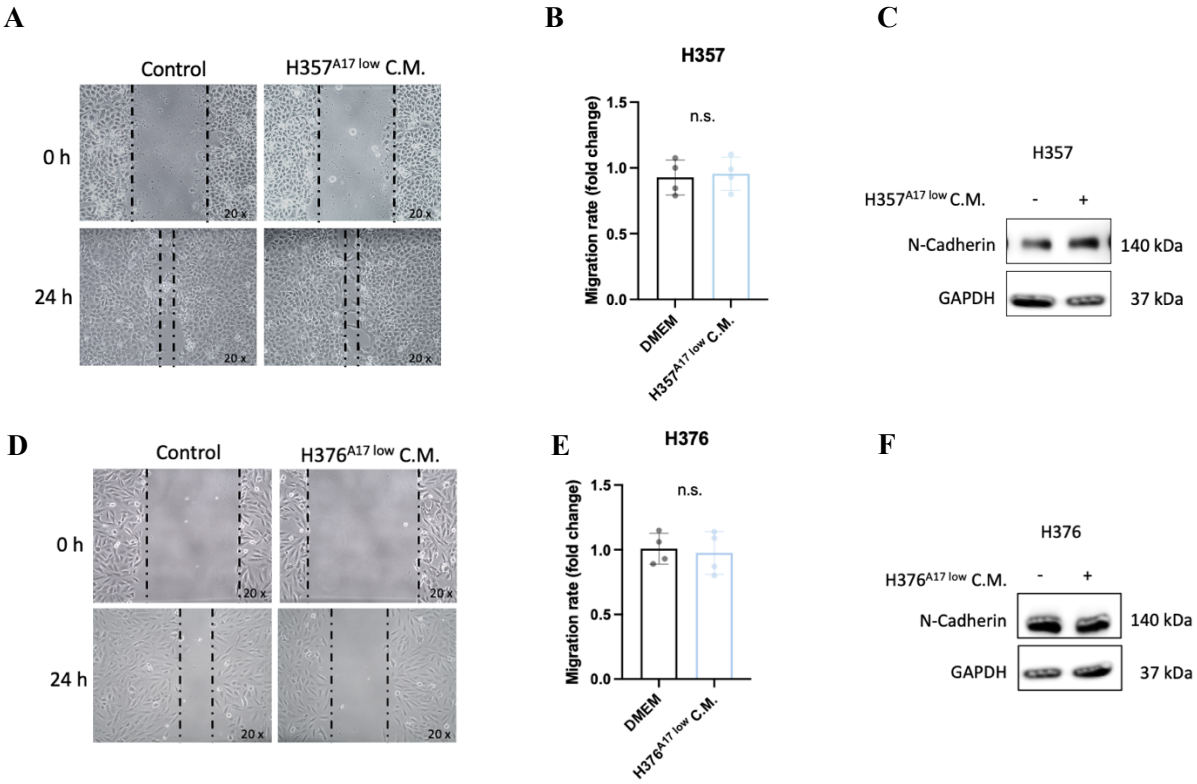

Figure 4.6 ADAM17 KD in OSCC cell lines does not affect cancer cell migration nor N-cadherin levels.

*(**A**) Representative wound healing assay in H357 treated with the C.M. from H357 depleted of ADAM17. H357 cells were seeded in six well plates and incubated for 48 h with or without the C.M.*

*from ADAM17-depleted H357 cells. Once the cells were 90% confluent a scratch was performed and the pictures acquired at time 0, 6 h and 24 h (n=3 t=2). (**B**) Quantification of A. (**C**) Representative western blot showing N-cadherin levels in H357 treated with and without the C.M. derived from ADAM17-depleted H357 cells (n=3 t=2). (**D**) Representative wound healing assay in H376 treated with the C.M. from H376 depleted of ADAM17. H376 cells were seeded in six well plates and incubated for 48 h with or without the C.M. from ADAM17-depleted H376 cells. Once the cells were 90% confluent a scratch was performed and the pictures acquired at time 0, 6 h and 24 h (n=3 t=2). (**E**) Quantification of D. (**F**) Representative western blot showing N-cadherin levels in H3576 treated with and without the C.M. derived from ADAM17-depleted H376 cells (n=3 t=2). Each data represents the mean ± SD from three independent experiments. P values were calculated via Unpaired T Test (∗P ≤ 0.05, ∗∗P ≤ 0.01, ∗∗∗P ≤ 0.001, ∗∗∗∗ P ≤ 0.0001).*

4.3 Discussion

Cancer motility is a fundamental property acquired by cancer cells to leave their primary site and metastasise to distant organs (Paul, Mistriotis and Konstantopoulos, 2016; Weiss, Lauffenburger and Friedl, 2022). Following the observation, reported in Chapter 3, that OSCC cells' migratory potential is negatively regulated when incubated with the C.M. derived from ADAM17 depleted fibroblasts, here in this chapter, the molecular player underpinning this cancer migration restriction was investigated by evaluating a panel of markers known to be involved in EMT and cancer migration (Yang *et al.*, 2020; J. shun Wu *et al.*, 2021). The results obtained by qPCR showed firstly that both H357 and H376 are more responsive to CAF-derived C.M. than to that derived from NOFs, which displayed on average an increase of their RNA levels, although it was mostly non-significant statistically and it varied across the genes analysed. Secondly, none of the markers analysed changed across conditions apart from N-cadherin. Indeed, N-cadherin RNA levels significantly decreased in H357 and H376 treated with the C.M. derived from ADAM17 depleted fibroblasts. The same trend was observed at protein levels suggesting that ADAM17 might play a role in regulating N-cadherin levels in cancer cells in a paracrine way and that, regardless the activation status of the fibroblasts, ADAM17 depletion exerts its negative regulation on cancer motility. Thus, to validate these data, N-cadherin was inhibited in cancer cells and the migratory potential assessed. The data illustrated that targeting N-cadherin in cancer cells recapitulates the effect exerted by the C.M. derived from ADAM17 depleted fibroblasts, although the underlying mechanism requires

further investigation. Of note, E-cadherin levels were also assessed in H357 cells, since H376 are known to be E-cadherin-deficient (Jenkinson *et al.*, 2011), and there was no change detected, suggesting that either there is no cadherin switch, which is one of the traits of the EMT process (Huang *et al.*, 2019), and that N-cadherin promotes cancer cell migration regardless of E-cadherin loss, as previously reported in the literature (Nieman *et al.*, 1999; Huang *et al.*, 2019), or that E-cadherin loss might happen in a second time, as consequence of the EMT program (Nilsson *et al.*, 2014), and that the window of time considered here is not enough to exclude this option. However, the first speculation might be more plausible considering that H376 cells lack E-cadherin and that show the same response of the H357 cell line to the treatment with the C.M. derived from ADAM17-deficient CAFs.

In chapter 3 it was demonstrated that ADAM17-depletion in stromal fibroblast can restrain cancer cell motility and, in this chapter, that this cancer migration restriction might function via N-cadherin regulation in cancer cells. Hence, it was investigated whether the C.M. derived from ADAM17 depleted cancer cells could recapitulate the same phenomenon. Moreover, it was observed that ADAM17 depletion in cancer cells did not influence their proliferation. More importantly neither H376 nor H357 treated with the C.M. derived from ADAM17-depleted cancer cells showed any migratory ability alteration. Moreover, N-cadherin levels did not change, as reported by western blot assay, suggesting that the N-cadherin paracrine regulation mediated by ADAM17 might be peculiar to fibroblasts and indicating new approaches to investigate its function within the TME as regulator of CAF-cancer cell crosstalk are required.

Chapter 5: Determination of the CAF-associated mechanism(s) underpinning the ADAM17-mediated paracrine regulation of OSCC cell migratory potential

5.1 Aims and objectives

Having observed a clear implication of ADAM17 in mediating the crosstalk between cancer cells and CAFs, it was fundamental to identify which changes were triggered upon the genetic inhibition of ADAM17 in CAFs and how these could impact on the cancer cell migratory potential. The last decades witnessed unprecedented strides in the development of therapeutics, also beyond the cancer field, thanks to the identification of molecular networks and their players through the large-scale protein analysis (also known as proteomics analysis) obtained by mass spectrometry (MS) techniques (Kwon *et al.*, 2021). Indeed, MS-based technologies allow the detection and identification of changes in the abundance of proteins within cells under any condition. Nonetheless, good and common practice at the end of any proteomics assay is the validation of the candidates by the traditional molecular techniques. Therefore, to gain a deeper insight into the protein landscape in CAFs upon silencing ADAM17 and eventually determine which proteins could be relevant to explain the phenotype observed so far, the investigative approach applied was as follows:

1. Proteomics analysis performed via Label-Free Mass Spectrometry (LFMS) to identify the differentially expressed proteins between control CAFs and ADAM17-depleted CAFs.
2. *In vitro* validation of the resulting protein candidates, by either pharmacological or genetic targeting in CAFs, followed by functional analysis by using the C.M. derived from CAFs to test the impact on cancer cell behaviour.

5.2 Results

5.2.1 Proteomics analysis of CAFs upon ADAM17-KD

To identify the proteins which could be responsible for the N-cadherin mediated migration of cancer cells when incubated with the C.M. from ADAM17-deficient CAFs observed in Chapter 4, the protein pellets from different CAF samples were processed by mass spectrometry. Firstly, to gain an insight of the biological significance and of the trend within the dataset, obtained by using three different biological replicates and two technical replicate per condition (i.e. to assess the response of the different biological samples, which are three different CAF samples obtained from different donors, to the same treatment, which is ADAM17 depletion), a Principal Component Analysis (PCA) was performed. PCA is an unsupervised multivariate

statistical method which visualises the samples as clusters based on their similarity (Lever, Krzywinski and Altman, 2017). As reported in Figure 6.1 A, the PCA plot showed mainly two clusters representing the control-CAFs (SC) group in cyan and the ADAM17-depleted CAFs (KD) group in pink. The two groups seemed to separate along the first principal component (PC1) which accounts for the 65.1 % of variation, though the samples 5SC and 6SC, and 3KD and 4 KD show a slightly different trend, with the SC (5 and 6) samples in the negative quarter of the PC1, not very distant from its KD (5 and 6) counterpart, whereas the KD (3 and 4) seem to separate along the second principal component (PC2) which accounts for the 12.5 % of variation (Figure 5.1 A). Moreover, the analysis of the protein abundance distribution within the two groups (SC vs KD) showed a similar variation from the median (19 % and 20 % respectively), as indicated by the sample of coefficient variation plots, suggesting that the number of proteins identified and interrogated was quite similar within the two groups (Figure 5.1 B).

A further interrogation of the dataset resulted in 38 out of 2702 proteins (1.41 % of the proteins identified, Log_2 FC > 0.5, FDR < 0.05) being differentially expressed across all conditions between the two groups (Figure 5.1 C).

Following an initial analysis of the dataset through the open-source REACTOME, amongst the significantly up-regulated proteins in the ADAM17-depleted CAFs (KD), there were proteins involved in the immune response (i.e. IFIT1, TAP1, JMJD6), in the cytoprotection by HMOX1 (i.e. CARM1, CASK, COX7A2L), in the metabolism (i.e. ACOX1, CARM1, PXN) and in insulin regulation (i.e. PXN, ATP6V1D) (Figure 5.1 C).

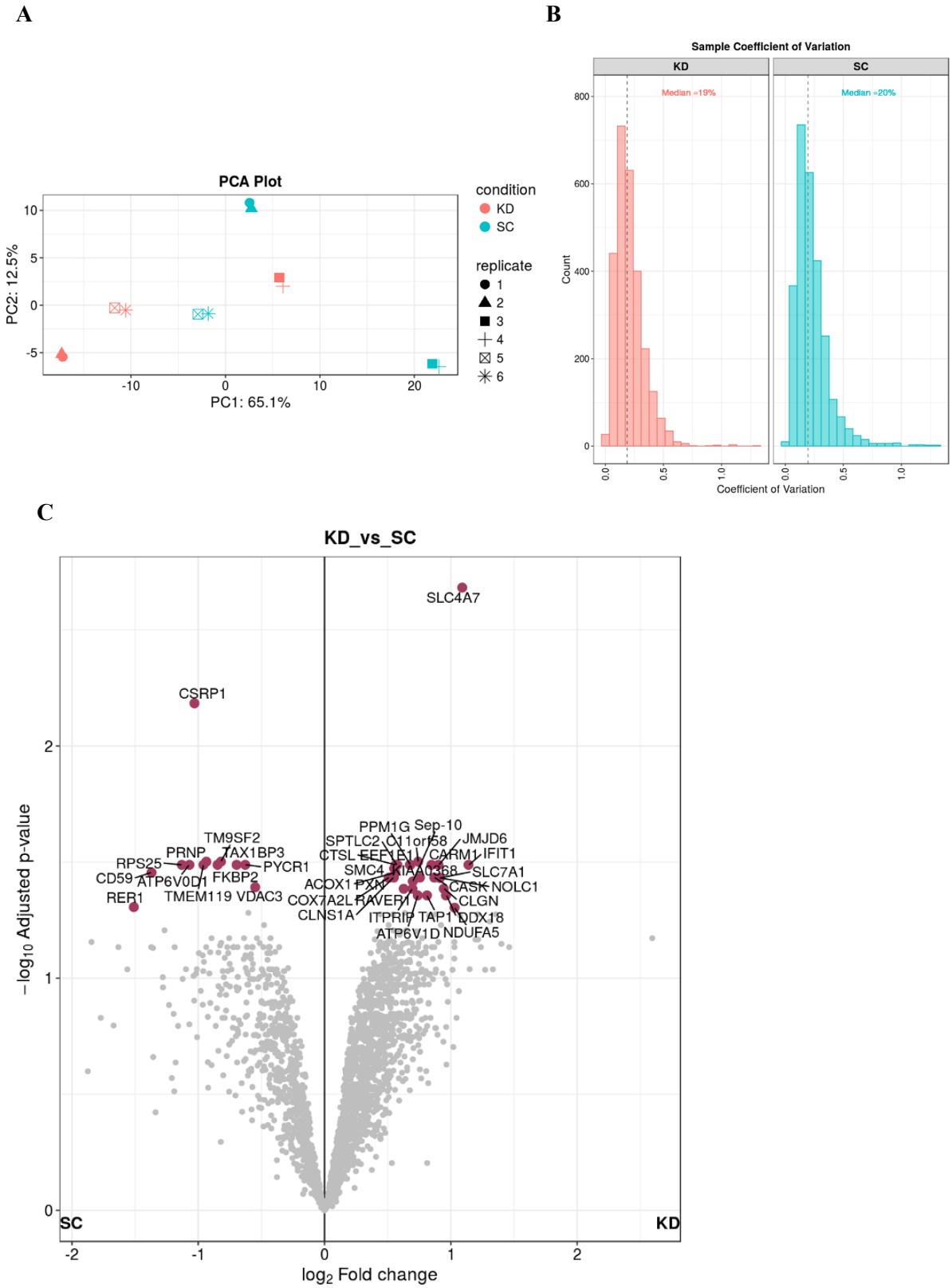

Figure 5.1 Proteomics analysis of CAF (SC) vs CAF$^{A17\ low}$ (KD).

*(**A**) PCA plot showing the groups distribution as clusters. (**B**) Histogram plot showing the distribution of protein abundance within the groups in function of their respective coefficient of variation (CV). (**C**)*

Volcano plot showing the Differentially Expressed Proteins (DEP) in CAFs upon ADAM17 downregulation. The raw data files were analysed using MaxQuant to obtain protein identifications and their respective label-free quantification values using in-house standard parameters. Of note, the data were normalization based on the assumption that most proteins do not change between the different conditions. Statistical analysis was performed using an in-house generated R script based on the ProteinGroup.txt file. First, contaminant proteins, reverse sequences and proteins identified "only by site" were filtered out. In addition, proteins that have been only identified by a single peptide and proteins not identified/quantified consistently in the same condition have been removed as well. The LFQ data was converted to log2 scale, samples were grouped by conditions and missing values were imputed using the 'Missing not At Random' (MNAR) method, which uses random draws from a left-shifted Gaussian distribution of 1.8 StDev (standard deviation) apart with a width of 0.3. Protein-wise linear models combined with empirical Bayes statistics were used for the differential expression analyses. The limma package from R Bioconductor was used to generate a list of differentially expressed proteins for each pair-wise comparison. A cutoff of the adjusted p-value of 0.05 (Benjamini-Hochberg method) along with a log2 fold change of 1 was applied to determine significantly regulated proteins in each pairwise comparison.

Amongst the up-regulated proteins, some are known to be regulated by JAK/STAT signalling pathway, such as IFIT1, SLC4A7 and others that were not statistically significant (MX1, OAS3, IFIT3, COL5A1, GBP1, data not shown). Of note, SLC4A7, IFIT3 and COL5A1 have been reported to be negatively regulated by STAT3 (Bharadwaj *et al.*, 2016). This observation was in line with western blot analysis of CAFs depleted of ADAM17 showing a decreased phosphorylation of STAT3 upon ADAM17 KD (Figure 5.2 A) and was consistent with previous *in vivo* studies which showed that mice deficient for ADAM17 displayed a reduced STAT3 phosphorylation (Chalaris, Adam, *et al.*, 2010). More specifically, the phosphorylated levels of STAT3 decreased by 1.5±0.15-fold ($p<0.05$), 1.6±0.2-fold ($p<0.05$) and 1.6±0.07-fold ($p<0.01$) in CAF002, CAF003 and CAF004 respectively, upon ADAM17 depletion compared to control (Figure 5.2 A and C). Considering that STAT1 is involved in the positive regulation of the above-mentioned targets and that STAT3 and STAT1 can negatively modulate each other, with STAT3 known to inhibit the antiviral-response mediated by the Type I Interferon (represented by the upregulated proteins MX1, OAS3, IFIT1 and IFIT3) (Wang, Levy and Lee, 2011) STAT1 and STAT2 signalling activation was assessed by western blot. Both STAT1 and STAT2 were phosphorylated in $CAF^{A17\ low}$ compared to control, confirming the hypothesis of a switch within the STAT pathway in favour of the STAT1-STAT2 signalling cascade (Figure 5.2 B). The levels of the phosphorylated form of STAT1 increased by 8±5-

fold ($p<0.001$), 5.8±0.4-fold ($p<0.5$) and 7±2.7-fold ($p<0.01$) in $CAF^{A17\ low}$ and $cCAF^{A17\ low}$, respectively, compared to control, whereas the phosphorylated form of STAT2 increased by 3.2±1.3-fold ($p>0.05$), 2.7±1.1-fold ($p>0.5$) and 7±1.7-fold ($p<0.01$) in $CAF^{A17\ low}$ and $cCAF^{A17\ low}$, respectively, compared to control (Figure 5.2 B and D).

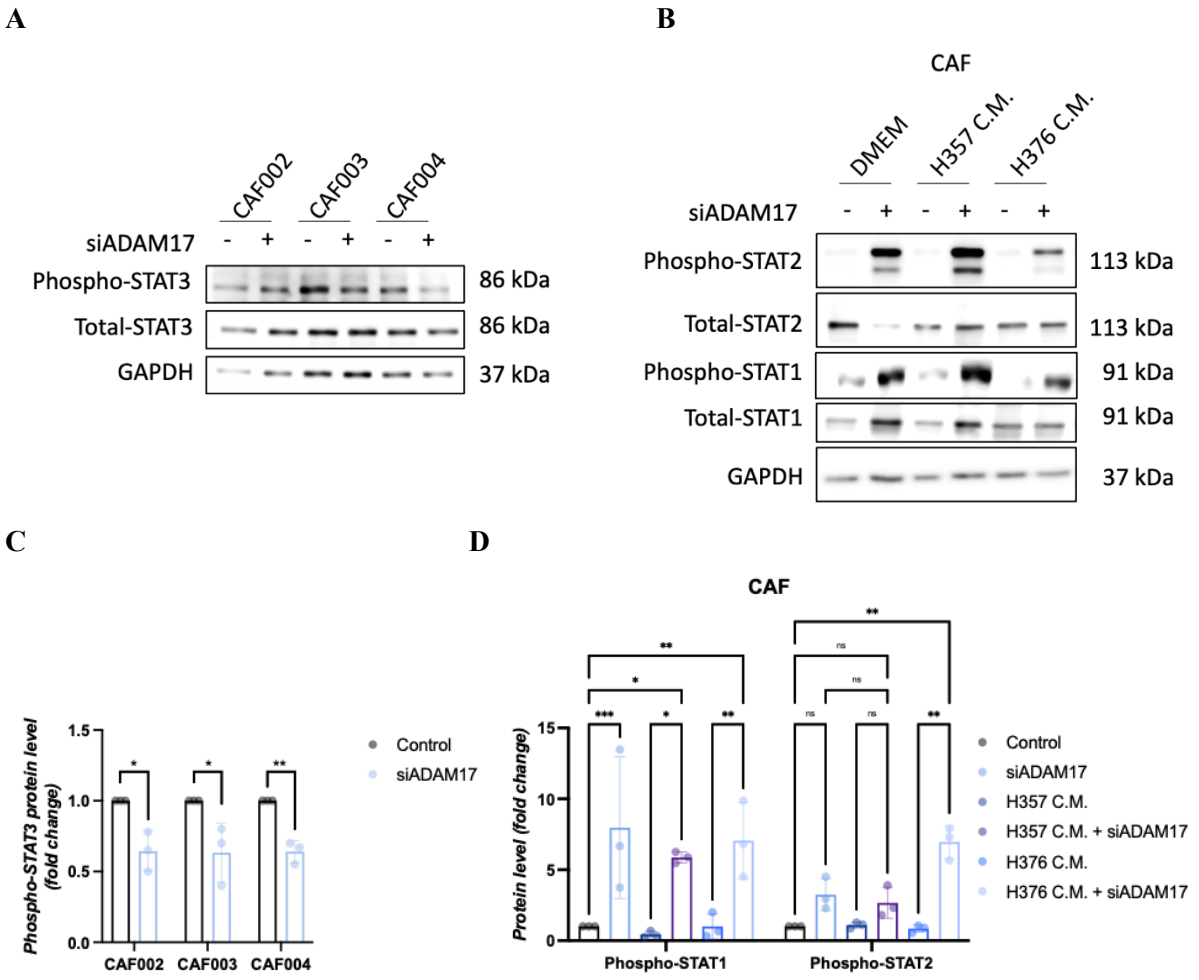

Figure 5.2 ADAM17 downregulation in CAFs reduces STAT3 phosphorylation and promotes STAT1-STAT2 signalling activation.

*(**A**) Representative western blot showing STAT3 levels in three different biological replicates for CAFs with and without ADAM17 depletion (n=3 t=3). (**B**) Representative western blot showing STAT1 and STAT2 levels in control CAFs and ADAM17-depleted CAFs (n=3 t=3). (**C**) and (**D**) Quantification of A and B respectively. Each data represents the mean ± SD from three independent experiments. P values were calculated via unpaired t test for C and ordinary one-way ANOVA for D (*P ≤ 0.05, **P ≤ 0.01, ***P ≤ 0.001, **** P ≤ 0.0001).*

As above-mentioned, some of the upregulated proteins in $CAF^{A17\ low}$ are involved in the antiviral-response mediated by the Type I Interferon signalling pathway. To validate this observation, a panel of Type I Interferon markers was assessed at gene expression level via qPCR. As shown in Figure 5.3 A, the Type I Interferon genes were transcriptionally upregulated, confirming the proteomics data. Indeed, compared to control, Interferon β 1 (IFNB1) increased by 2.9±0.1-fold (P<0001), OAS2 by 4.5±0.31-fold (p<0.0001), MX1 by 3.8±0.33-fold (p<0.0001), CCL5 by 4±0.52-fold (p<0.0001), Interleukin β (Il-β) by 2.37±0.3-fold (p<0.0001), CXCL2 by 4.4±0.36-fold (p<0.0001), IRF1 by 2.3±0.4-fold (p<0.0001) and IRF9 by2.7±0.18-fold (p<0.0001) (Figure 5.3 A). On the contrary, Interleukin 6 (Il-6), known to be a STAT3 activator, upon ADAM17 depletion in CAFs decreased by 2±0.015-fold (p<0.05). In line with this observation, in $cCAF^{A17\ low}$, previously conditioned with the C.M. derived from H376 cells, an increase of 2.6±1.02-fold (p<0.05) was detected at protein level by western blot analysis of MX1 compared to cCAF previously incubated with the C.M. from H376 cells (Figure 5.3 B-C). The same trend was observed in $cCAF^{A17\ low}$ which were previously conditioned or not with the H357-derived C.M. (Figure 5.3 D).

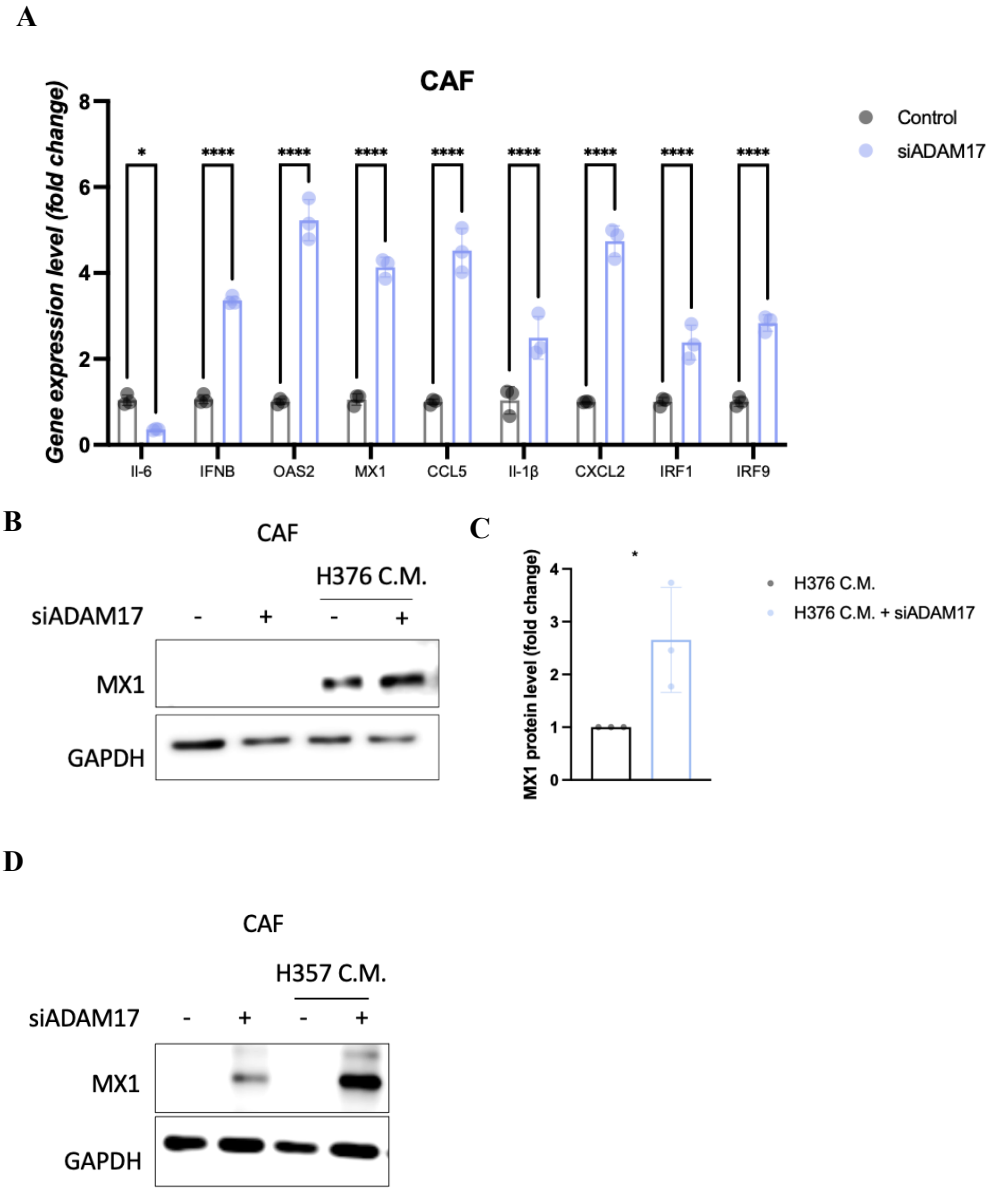

Figure 5.3 ADAM17 depletion in CAFs induces the activation of the Interferon Type I-mediated antiviral-response.

*(**A**) Representative qPCR showing some of the Interferon Type I genes upregulated in Adam7-depleted CAFs. CAFs were seeded in 6 well plates and, once at 50-60% confluent, depleted of ADAM17 by transfection with a siRNA targeting ADAM17 (n=3 t=3). (**B**) and (**D**) Representative western blot showing MX1 protein levels in CAFs. CAFs were seeded in six well plates and incubated or not with OSCC-derived C.M. for 48 h. Once cells were 50-60 % confluent, ADAM17 was depleted via siRNA. (n=3 t=3). (**C**) Quantification of B. Each data represents the mean ± SD from three independent experiments. P values were calculated via Student T-Test (∗P ≤ 0.05, ∗∗P ≤ 0.01, ∗∗∗P ≤ 0.001, ∗∗∗∗ P ≤ 0.0001).*

5.2.2 STAT3 and STAT2 downregulation in CAFs does not restrain cancer migration

The proteomics data, validated by qPCR and western blot assays, showing an upregulated Interferon Type I signalling signature in CAFs upon ADAM17 depletion, led us to investigate any potential involvement of interferon signalling in the reduced migration of OSCC cells treated with the conditioned medium derived from $CAF^{A17\ low}$. This aim was supported by existing studies reporting a direct and indirect role of interferons (IFNs) in regulating tumour progression in all its aspects, from cell proliferation, differentiation, migration to survival (Parker, Rautela and Hertzog, 2016; Doherty *et al.*, 2017).

In this regard, to determine the role of STATs in CAF-mediated cancer cells migration, a STAT3 and STAT2 downregulation in CAFs was performed by targeting STAT3 and STAT2 via siRNA. In both scenarios, STAT3 and STAT2 silencing was performed in conditioned and non-conditioned CAFs, according to the same protocol adopted for ADAM17 depletion. After harvesting the conditioned medium, protein lysates and RNA were collected and processed and STAT2 and STAT3 levels assessed by western blot and qPCR assays respectively. The genetic silencing of both genes was successful, showing an average of 80% of knock-down efficiency. Upon silencing, the protein levels of STAT2 decreased by 1.5±0.15-fold ($p<0.01$), 1.8±0.11-fold ($p<0.001$) and 4.5±0.1-fold ($p<0.0001$) in CAFs and cCAFs (previously incubated with the C.M. derived from H357 and H376 cells), respectively, compared to controls (Figure 5.4 A-B). Similarly, it was observed by qPCR that STAT2 RNA levels decreased by 11±0.02-fold ($p<0.001$), 6.4±0.20-fold ($p<0.001$) and 7±0.01-fold ($p<0.001$) for the same conditions (Figure 5.4 C).

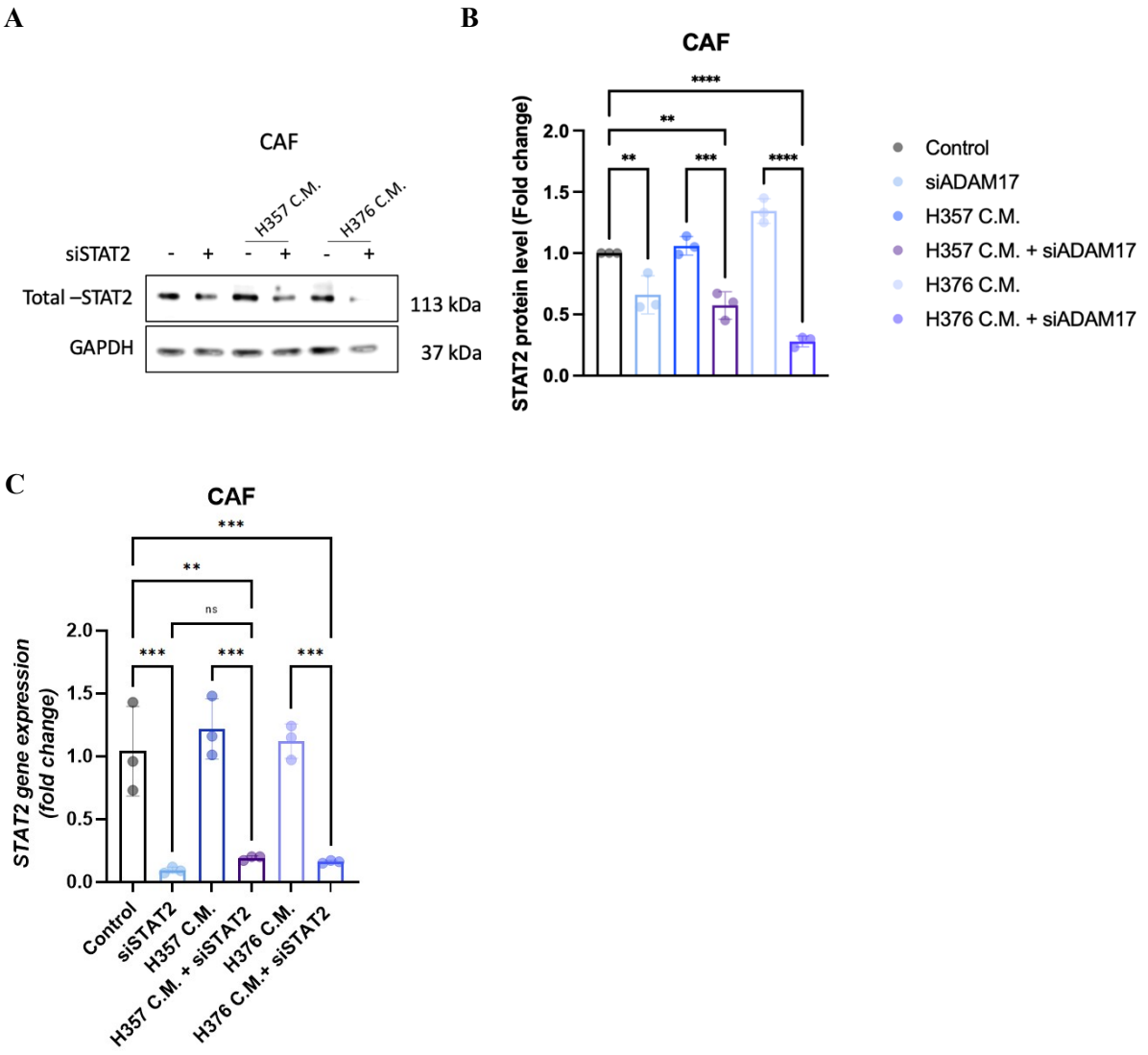

Figure 5.4 STAT2 downregulation via siRNA in stimulated and unstimulated CAFs.

*(**A**) Western blot showing STAT2 protein levels upon knock down in CAFs (n=3 t=1). (**B**) Quantification of A. (**C**) qPCR showing gene levels of STAT2 in CAFs upon knock-down (n=3 t=1). Each data represents the mean ± SD from three independent experiments. P values were calculated via ordinary one-way ANOVA (*P ≤ 0.05, **P ≤ 0.01, ***P ≤ 0.001, **** P ≤ 0.0001).*

The same outcome was obtained upon silencing STAT3, which showed protein levels decreased by 3.3±0.04-fold ($p<0.0001$) and 6.8±0.04-fold ($p<0.0001$) in CAFs and cCAFs respectively, compared to controls (Figure 5.5 A-B). Similarly, it was observed by qPCR that STAT3 RNA levels decreased by 3.8±0.02-fold ($p<0.001$), 6.7±0.02-fold ($p<0.001$) and 7±0.01-fold ($p<0.001$) for the same conditions (Figure 5.5 C).

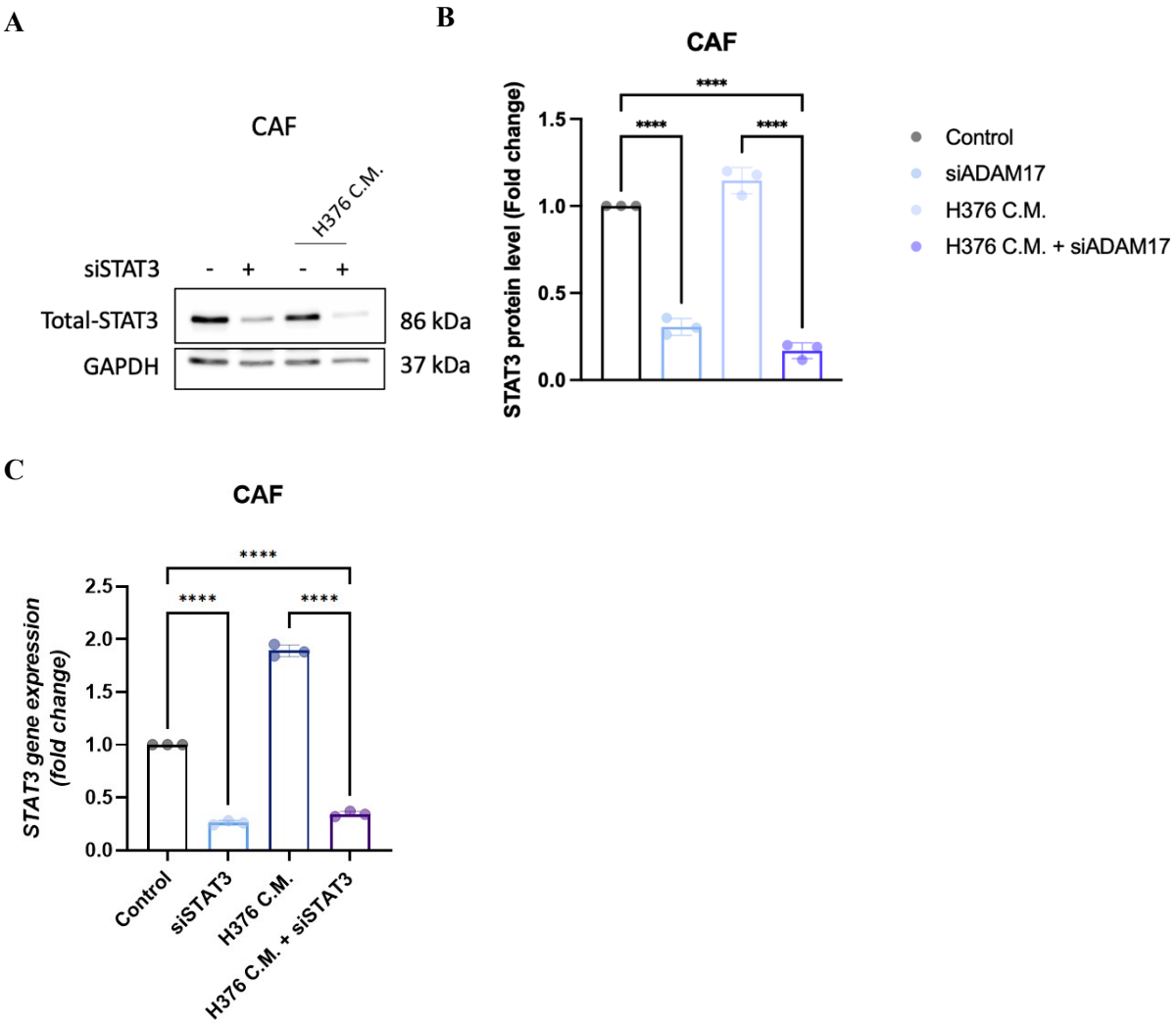

Figure 5.5 STAT3 downregulation via siRNA in stimulated and unstimulated CAFs.

*(A) Western blot showing STAT3 protein levels upon knock down in CAFs (n=3 t=1). (B) Quantification of A.(C) qPCR sowing gene levels of STAT3 in CAFs upon knock-down (n=3 t=1). Each data represents the mean ± SD from three independent experiments. P values were calculated via ordinary one-way ANOVA (*P ≤ 0.05, **P ≤ 0.01, ***P ≤ 0.001, **** P ≤ 0.0001).*

Next, the C.M. derived from CAFs was used to determine the impact on cancer cell migration by performing a wound healing assay.

Firstly, the C.M. derived from STAT2-deficient CAFs ($CAF^{STAT2\ low}$) was tested on OSCC cell lines. H376 cells were seeded in six well plates and incubated with CAF-derived C.M. for 48. Some cells were used for protein and RNA extraction to perform western blot and qPCR analysis of N-cadherin levels. Other cells were used for the wound healing assay.

As reported in Figure 5.6, cancer cell migration did not change in cells treated with the C.M. derived from CAF$^{STAT2\ low}$ nor N-cadherin levels showed any difference across the same conditions. Thus, these data seemed to rule out an implication of STAT2 in mediating cancer cell migration and N-cadherin expression. Nonetheless, this experiment was performed only once due to time constraints, therefore calling for further repeats to corroborate the results.

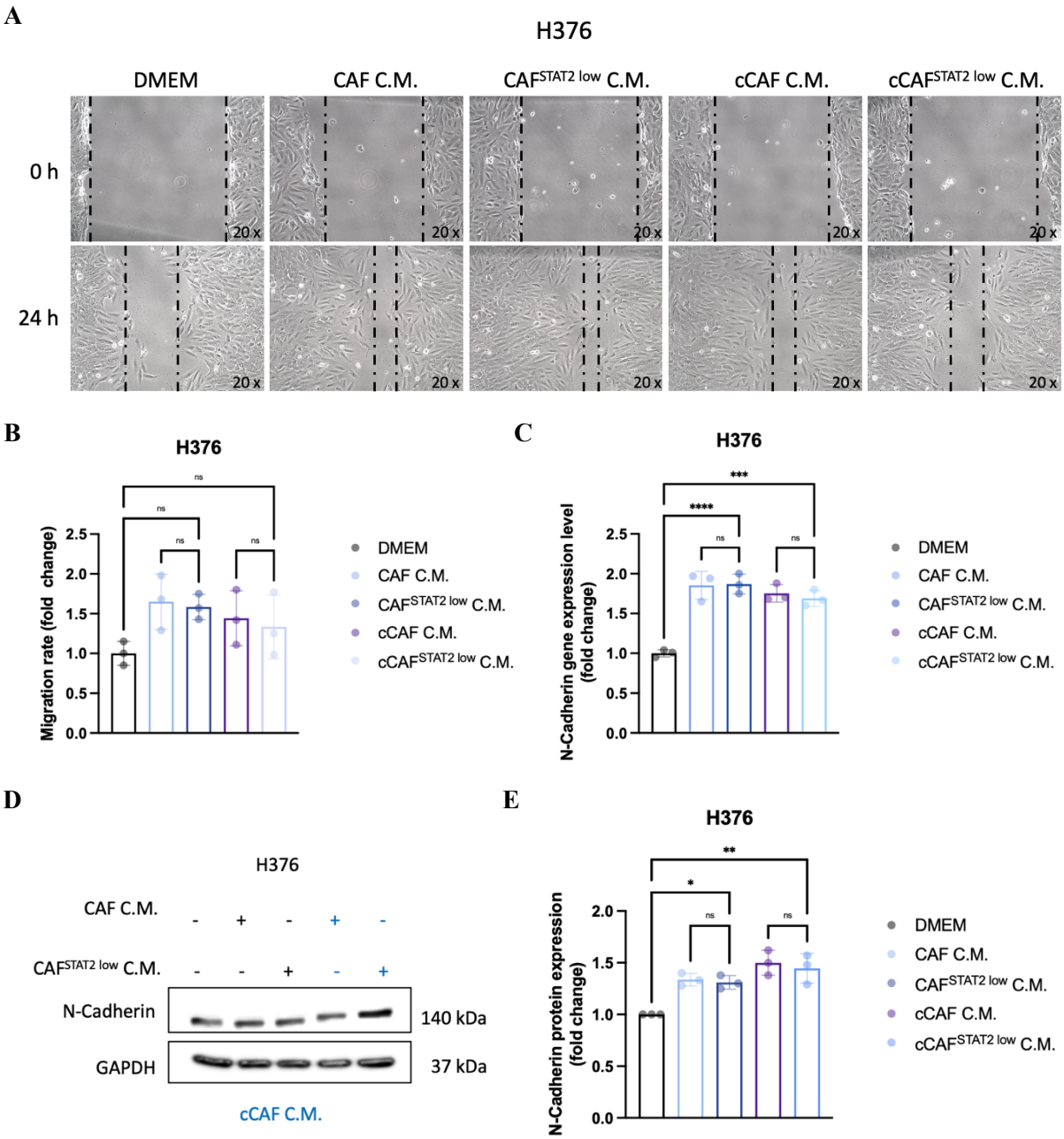

Figure 5.6 Assessment of the impact of CAF$^{STAT2\ low}$ -derived C.M. on H376 migration.

*(**A**) Wound healing assay in H376 challenged with CAF-derived C.M. H376 cells were seeded in six well plates and incubated for 48 h with the C.M. derived from stimulated and unstimulated CAF with and without STAT2 (n=3 t=1). (**B**) Quantification of A. (**C**) Representative qPCR assay showing N-cadherin levels in H376 challenged with CAF-derived C.M. (n=3 t=1). (**D**) Western blot representing N-cadherin level in H376 challenged with CAF-derived C.M (n=3 t=1). (**E**) Quantification of D by densitometry. Each data represents the mean ± SD from three independent experiments. P values were calculated via ordinary one-way ANOVA (*P ≤ 0.05, **P ≤ 0.01, ***P ≤ 0.001, **** P ≤ 0.0001).*

Next, the same experiment, using the same experimental design, was performed in H376 using the C.M. derived from STAT3-deficient CAFs (CAF$^{STAT3\ low}$). As observed for STAT2, also STAT3 downregulation in CAFs did not impact on H376 migration (Figure 5.7 A). Likewise, N-cadherin levels did not change across the same conditions (Figure 5.7 C and D). Altogether, these data suggest that STAT3 is not involved in paracrine mediation of cancer cell migration and N-cadherin expression. Also in this case, further repeats are needed since this experiment was performed only once due to time constraints.

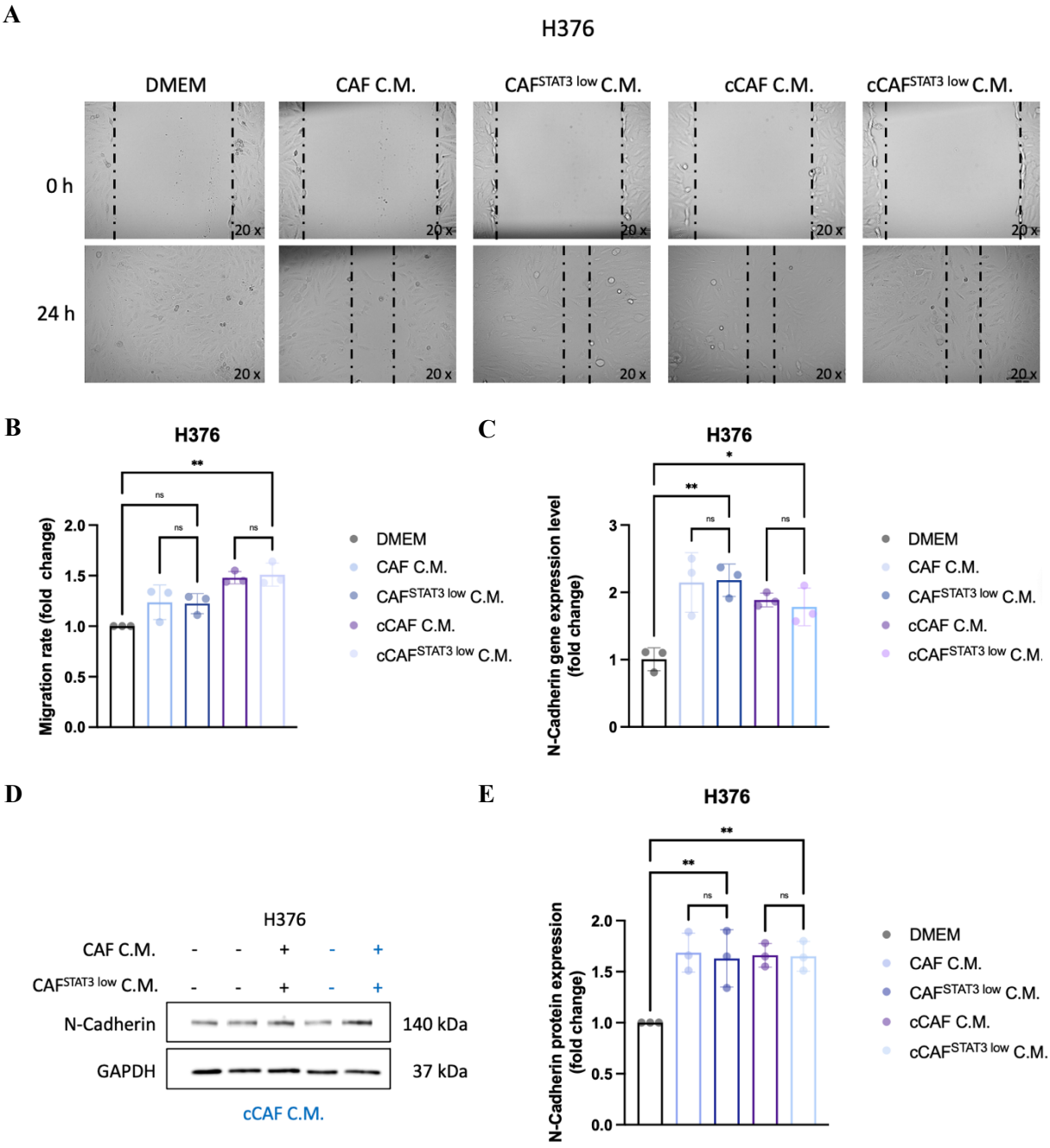

Figure 5.7 Assessment of the impact of CAF$^{STAT3\ low}$ -derived C.M. on H376 migration.

*(**A**) Wound healing assay in H376 challenged with CAF-derived C.M. H376 cells were seeded in six well plates and incubated for 48 h with the C.M. derived from stimulated and unstimulated CAF with and without STAT3 (n=3 t=1). (**B**) Quantification of A. (C) Representative qPCR assay showing N-cadherin levels in H376 challenged with CAF-derived C.M. (n=3 t=1). (**D**) Western blot representing N-cadherin level in H376 challenged with CAF-derived C.M (n=3 t=1). (**E**) Quantification of D by densitometry. Each data represents the mean ± SD from three independent experiments. P values were calculated via ordinary one-way ANOVA (*P ≤ 0.05, **P ≤ 0.01, ***P ≤ 0.001, **** P ≤ 0.0001).*

5.2.3 cGAS downregulation in CAFs does not restrain cancer migration

Having generated evidence that STAT2 and STAT3 might not be involved in the ADAM17-mediated paracrine regulation of cancer cell migration, the next step was to determine whether there were other candidates, involved in the Interferon Type I activation, that could explain the observed phenotype. Following a further analysis of the differentially expressed proteins obtained by mass spectrometry, there were some potential candidates known to be involved in the activation of the Interferon Type I signalling cascade such as TAP1, SLC4A7, NDFUFA5, ITPRIP, ACOX1. Most of these proteins are known to play a role directly or indirectly in the DNA-damage response (DDR), for example by interacting with DDR mediators (TAP1) (Dai *et al.*, 2021) or by intracellular ROS production (NDUFA5, ACOX1) (Rak and Rustin, 2014; Zeng *et al.*, 2017) and pH regulation (SLC4A7) (Lee *et al.*, 2014). Thus, the approach adopted was to investigate the most important mediator of the Interferon Type I activation, the second messenger cyclic GMP-AMP (cGAS) (Hopfner and Hornung, 2020). The hypothesis was that under cellular stress induced by dysregulated ROS or increased intracellular pH, the DNA could be damaged, released within the cytoplasm and, once recognised and bound by cGAS, trigger the activation of the cGAS-STING pathway, known to engage the interferon response. In the first instance, cGAS levels were assessed in stimulated and unstimulated CAFs upon ADAM17 knock down. The cGAS protein levels in $CAF^{A17\ low}$ showed a mild and non-significant increase compared to their respective controls. Indeed, cGAS increased by 1.3±0.07-fold ($p>0.05$) when comparing CAFs to $CAF^{A17\ low}$ whereas it increased by 1.3±0.26-fold ($p>0.05$) when comparing cCAFs to $cCAF^{A17\ low}$ (Figure 5.8 A-B). Moreover, compared to CAFs, cGAS decreased by 1.4±0.1-fold ($p>0.05$) when CAFs were conditioned with the C.M. derived from H376 cells (Figure 5.8 A-B). Nevertheless, supported by the proteomics data and by the literature which describes the cooperation of cGAS and autophagy in inducing Type I Interferon activation (Zhang *et al.*, 2021), the next step was to determine whether autophagy could be involved in cGAS and/or Interferon Type I activation. Thus, a panel of autophagy markers was evaluated in CAFs upon treatment with chloroquine, a well-known autophagic flux inhibitor which blocks lysosomes, widely used in autophagy studies (Mauthe *et al.*, 2018). Of note, while autophagy-related gene 3 (ATG3) and autophagy-related gene 5 (ATG5) markers, essential for the delivery of the autophagic cargo to the lysosomes, increased in ADAM17-deficient CAFs, the gold standard light chain 3 B II (LC3B II), lipidated form of the phagosome which eventually fuses with the lysosome, did not show any variation (Figure

5.8 C-E) (Dikic and Elazar, 2018). ATG3 protein levels increased by 1.44±0.25-fold ($p<0.01$) and 1.4±0.2-fold ($p<0.5$) in $CAF^{A17\ low}$ and $cCAF^{A17}$ low (combining the cells with and without the treatment with chloroquine) compared to control, whereas, in the same conditions, ATG5 levels increased by 1.3±0.12-fold ($p<0.0001$) and 1.37±0.17-fold ($p>0.5$) compared to control (Figure 5.8 C-D). These data, though suggesting a potential autophagy induction as represented by ATG3 and ATG5, would require a further validation to confirm the initial hypothesis.

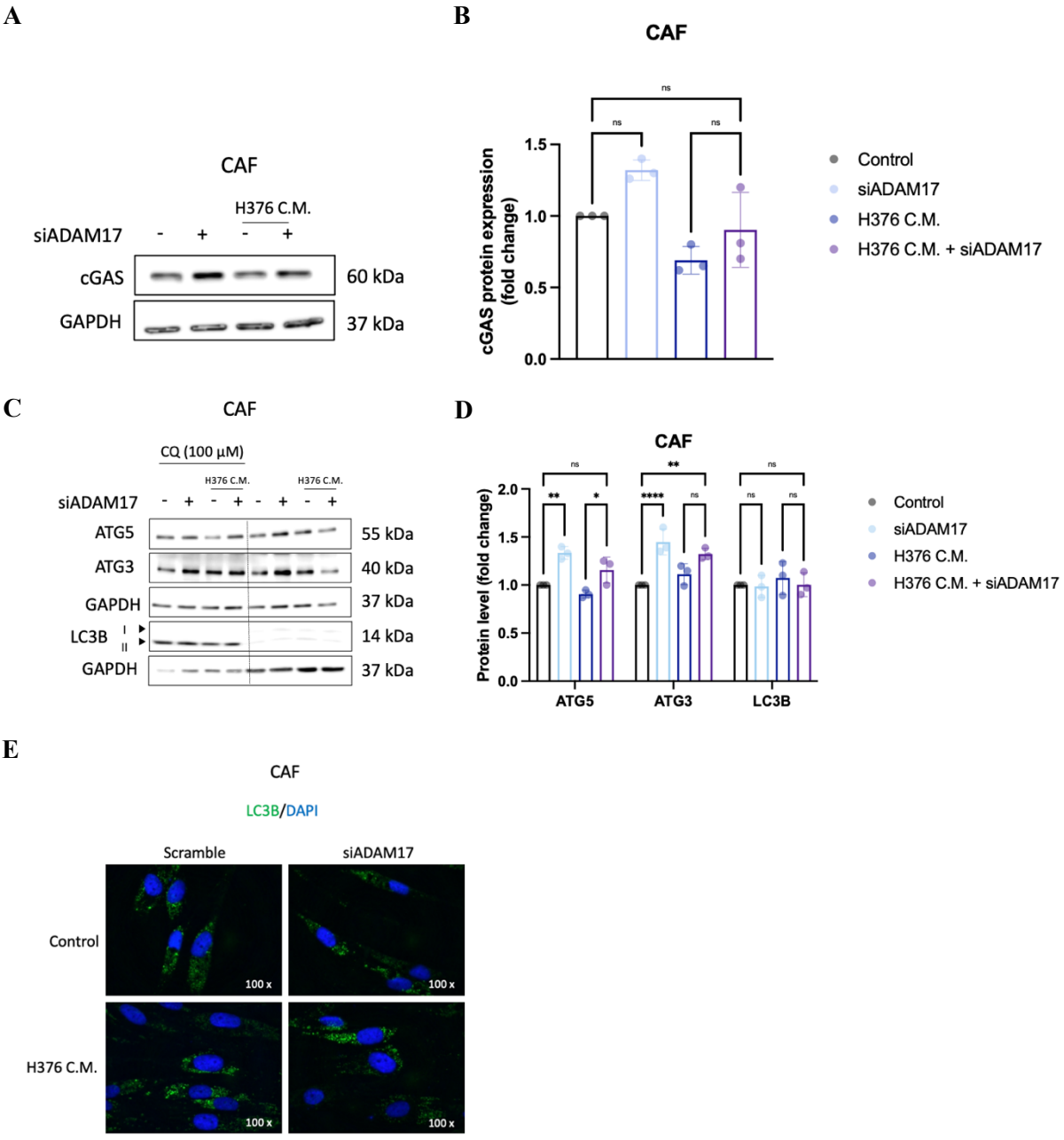

Figure 5.8 ADAM17 downregulation in CAFs induces upregulation of cGAS and ATG3 and ATG5 autophagy markers.

*(**A**) Representative western blot showing cGAS protein levels in stimulated and unstimulated CAFs upon ADAM17 knock-down (n=3 t=3). (**B**) Quantification of A by densitometry. Each data represents the mean ± SD from three independent experiments. P values were calculated via ordinary one-way ANOVA. (**C**) Western blot showing autophagy markers in stimulated and unstimulated CAFs upon ADAM17 knock-down. CAFs were initially challenged with the C.M. derived from H376 and*

*subsequently depleted of ADAM17 via siRNA. Cells were kept in culture for 48 h. This experimental layout was designed in duplicate. Next, 24 h before terminating the experiment, some CAFs were treated with 100 μM of Chloroquine for 24h. Cells were then processed for either protein lysis or immunofluorescence staining (n=3 t=2). (**D**) Quantification of C. (**E**) Immunofluorescence staining for LC3B in CQ-treated CAFs. Each data represents the mean ± SD from three independent experiments. P values were calculated via ordinary one-way ANOVA (∗P ≤ 0.05, ∗∗P ≤ 0.01, ∗∗∗P ≤ 0.001, ∗∗∗∗ P ≤ 0.0001).*

Next, to shed light on a possible role of cGAS in mediating the paracrine restriction of cancer cell migration, cGAS function was further investigated in stimulated and unstimulated CAFs. In this regard, cGAS was genetically downregulated by siRNA in conditioned and unconditioned CAFs and the derived C.M. was tested on H376 cells to assess any role in cancer cell migration. The experiment set up was the same described in section 5.2.2. The cGAS knock down in CAFs was successful (more than 80% of protein reduction and more than 60% of RNA reduction), thus the C.M. derived from the same CAFs was tested on H376 via wound healing assay (Figure 5.9). At protein level, cGAS decreased by 5±0.1-fold ($p<0001$), 4.8±0.3-fold ($p<0001$), 5.2±0.05-fold ($p<0001$) and 5.2±0.35-fold ($p<0001$) in $CAF^{cGAS\ low}$, $CAF^{cGAS/A17\ low}$, $cCAF^{cGAS\ low}$ and $CAF^{cGAS/A17\ low}$, respectively, compared to control (Figure 5.9 A-B). Similarly, at RNA levels cGAS decreased by 2.5±0.25-fold ($p<0001$), 2.3±0.2-fold ($p<0001$), 2.8±0.03-fold ($p<0001$) and 2.8±0.02-fold ($p<0001$) in $CAF^{cGAS\ low}$, $CAF^{cGAS/A17\ low}$, $cCAF^{cGAS\ low}$ and $CAF^{cGAS/A17\ low}$, respectively, compared to control (Figure 5.9 A-B).

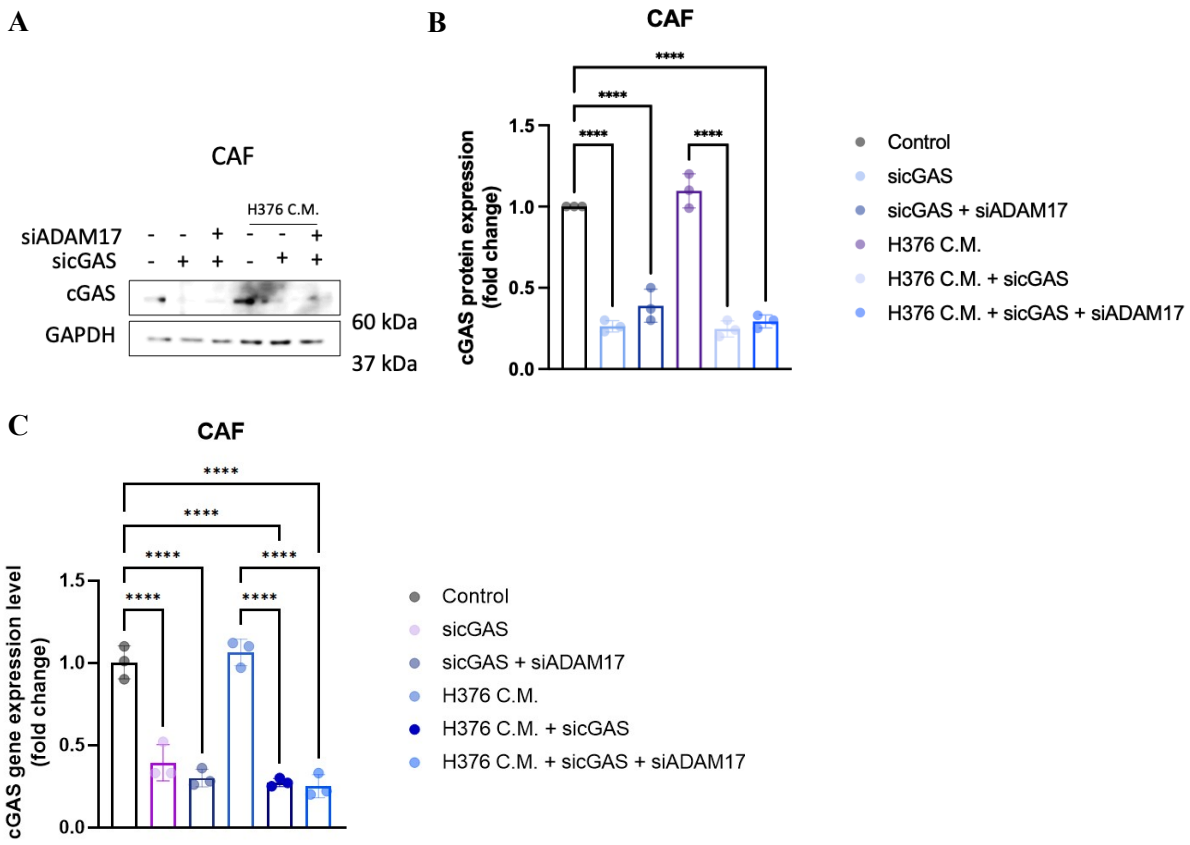

Figure 5.9 cGAS levels in CAFs upon siRNA-mediated silencing.

*(**A**) Western blot showing cGAS levels in conditioned and unconditioned CAFs upon cGAS down-regulation. CAFs were seeded in six well plates and incubated with or without H376-derived CM. for 48 h. Once 50-60% confluent they were transfected with or without the siRNA targeting cGAS and/or siADAM17 for further 48 h (n=3 t=1). (**B**) Quantification of A. (**C**) Representative qPCR showing cGAS RNA levels in CAFs upon cGAS down-regulation (n=3 t=1). Each data represents the mean ± SD from three independent experiments. P values were calculated via ordinary one-way ANOVA (*P ≤ 0.05, **P ≤ 0.01, ***P ≤ 0.001, **** P ≤ 0.0001).*

The H376 cells were seeded and treated as previously described for the same assay (section 5.2.2). cGAS downregulation in CAFs did not induce an increased migration of H376 (there was a minimal and non-significant reduction in the H376 challenged with the C.M. derived from CAF$^{cGAS\ low}$ and cCAF$^{cGAS\ low}$) (Figure 5.10 A). This observation was in line with the N-cadherin protein levels which show no change upon the treatment (Figure 5.10 C-D). Altogether, these data rule out any implication of cGAS in a paracrine mediation of cancer cell

migration and N-cadherin expression. Nevertheless, further repeats will be needed to corroborate the results.

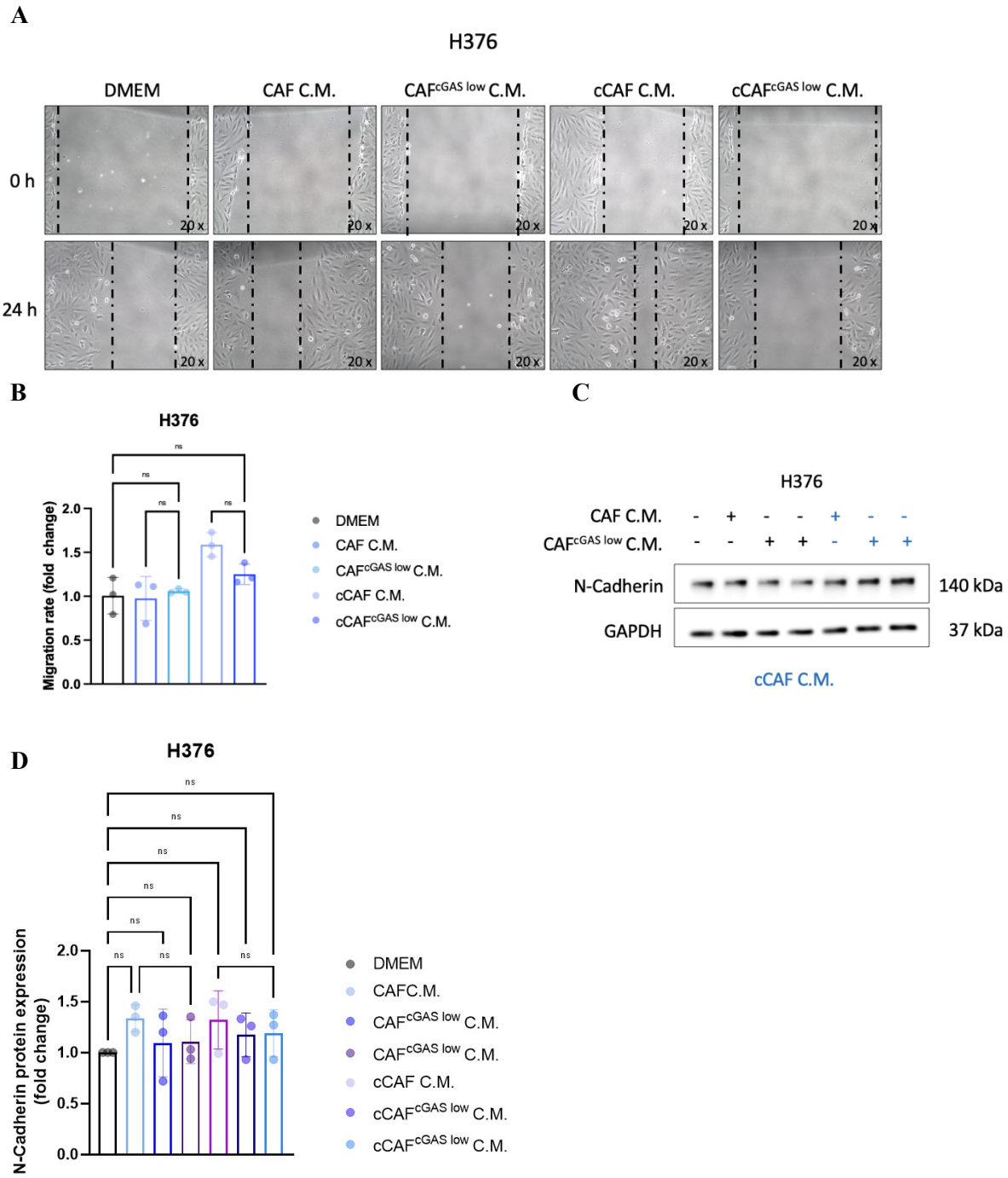

Figure 5.10 Assessment of the impact of cGAS-deficient CAF-derived C.M. on H376 migration.

*(**A**) Wound healing assay in H376 challenged with CAF-derived C.M. H376 cells were seeded in six well plates and incubated for 48 h with the C.M. derived from stimulated and unstimulated CAFs with and without cGAS (n=3 t=1). (**B**) Quantification of A. (**C**) Western blot representing N-cadherin level in H376 challenged with CAF-derived C.M. (n=3 t=1). (**D**) Quantification of C. Each data represents*

the mean ± SD from three independent experiments. P values were calculated via ordinary one-way ANOVA.

5.2.4 AKT downregulation in CAFs does not restrain cancer cell migration

Since none of the hypotheses pursued were proved, another investigative approach was adopted to address the same question. In the previous characterisation of cCAF$^{A17\ low}$, another pathway, AKT signalling, was identified as potentially altered upon ADAM17 depletion. Indeed, an increase of AKT protein levels was observed in cCAF$^{A17\ low}$ (Figure 5.11). AKT, also known as protein kinase B (PKB), is a serine/threonine protein kinase regulating a broad range of biological processes such as metabolism, cell differentiation and survival, through the PI3K/AKT signalling cascade, therefore representing one of the major targeted proteins for anticancer therapy, including CAF-targeted therapies (F. Wu *et al.*, 2021; He *et al.*, 2021). Thus, to assess whether AKT could contribute to mediate in a paracrine manner the cancer cell migration, as observed upon ADAM17 knock down in CAFs, a genetic down-regulation of AKT was performed in CAFs via siRNA, in both stimulated and unstimulated conditions.

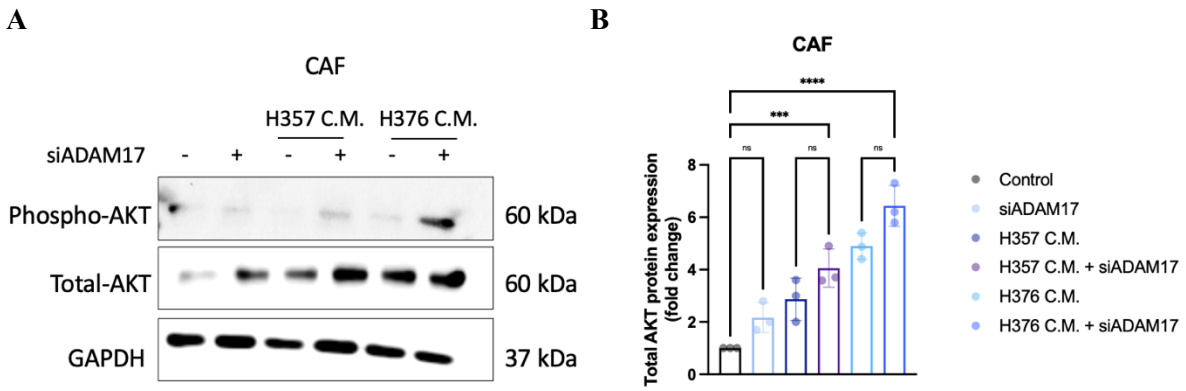

Figure 5.11 AKT signalling activation in CAF$^{A17\ low}$ and cCAF$^{A17\ low}$.

*(**A**) Representing western blot showing AKT protein levels in CAFs conditioned with OSCC cell-derived C.M. followed by ADAM17 depletion. Cells were seeded in six well plates and incubated for 48 h with or without OSCC-cell derived C.M. until 50-60% confluent. Then, cells were depleted of ADAM17 by transfection (n=3 t=3). (**B**) Quantification of A. Each data represents the mean ± SD from three independent experiments. P values were calculated via ordinary one-way ANOVA (∗P ≤ 0.05, ∗∗P ≤ 0.01, ∗∗∗P ≤ 0.001, ∗∗∗∗ P ≤ 0.0001).*

As previously described, CAFs were initially incubated for 48 h with or without the C.M. derived from cancer cells. When the cells were 50-60 % confluent AKT was silenced via

siRNA. At the end of the experiment, proteins and RNA were harvested and processed and the derived conditioned medium harvested. The siRNA-mediated AKT downregulation was successful, showing more than 50% of efficacy at protein level and more than 80% at RNA level. Specifically, the protein levels decreased by 2±0.05-fold (p) and 2.4±0.07-fold (p) in $CAF^{AKT\ low}$ and $cCAF^{AKT\ low}$ respectively, compared to controls (Figure 5.12 A-B), whereas the RNA levels decreased by 3.2±0.01-fold (p) and 3.5±0.01-fold (p) for the same conditions (Figure 5.12 C).

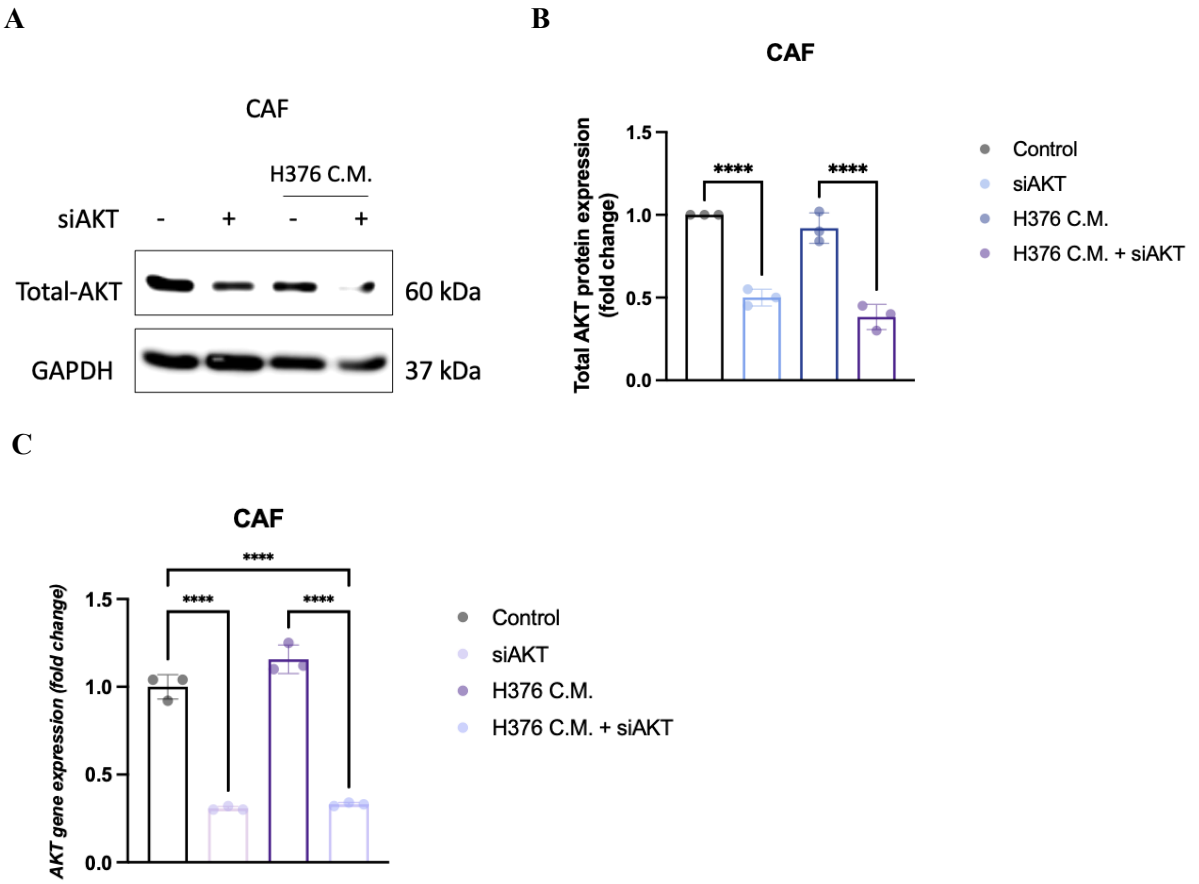

Figure 5.12 AKT levels in CAFs upon siRNA-mediated silencing.

*(**A**) Western blot showing AKT protein levels in stimulated and unstimulated CAFs upon AKT depletion. Cells were seeded in six well plates and incubated with or without H376-derived C.M. for 48 h. Once the cells were 50-60% confluent AKT was depleted via transfection using a siRNA. After 6 h, the transfection mix was removed and replaced with fresh culture medium and cells incubated for 48 h (n=3 t=1). (**B**) Quantification of A. (**C**) qPCR showing AKT RNA levels in CAFs upon AKT depletion (n=3 t=1). Each data represents the mean ± SD from three independent experiments. P values were calculated via ordinary one-way ANOVA (*P ≤ 0.05, **P ≤ 0.01, ***P ≤ 0.001, **** P ≤ 0.0001).*

Next, to assess the effect of the C.M. derived from AKT-deficient CAFs on cancer cell migration, a wound healing assay was performed using H376 cells. H376 cells were seeded in six well plates and incubated for 48 h with and without the C.M. derived from $CAF^{AKT\ low}$ and $cCAF^{AKT\ low}$. When the cells were 90% confluent a scratch was created and pictures acquired at time 0, 6 h and 24 h. Of note, AKT downregulation in CAFs did not alter H376 migration (Figure 5.13 A-B). This observation was in line with the N-cadherin protein levels which show no change upon the treatment (Figure 5.13 C-D). Altogether, these data suggest AKT is not involved in paracrine mediation of cancer cell migration and N-cadherin expression, although further repeats will be needed to confirm this initial finding.

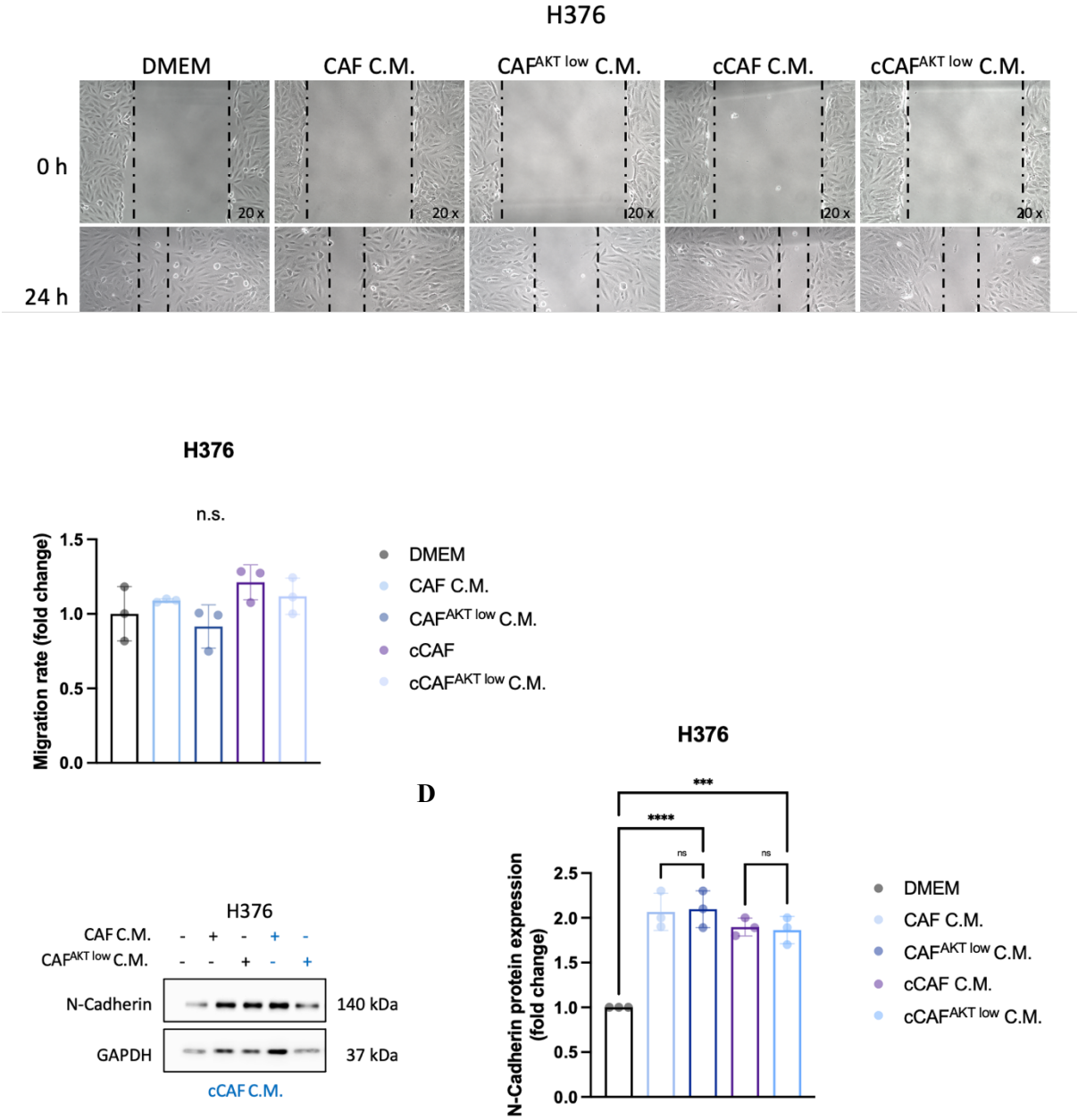

Figure 5.13 Assessment of the impact of AKT-deficient CAF-derived C.M. on H376 migration.

(**A**) Wound healing assay in H376 challenged with the C.M. derived from AKT-depleted CAF. H357 cells were seeded in six well plates and incubated for 48 h with C.M. derived from CAFs with and without AKT. When cells were 90% confluent a scratch was performed and the pictures acquired at time 0, 6 h and 24 h (n=3 t=1). (**B**) Quantification of A. (**C**) Western blot representing N-cadherin protein levels in H376 challenged with CAF-derived C.M. (n=3 t=1). (**D**) Quantification of C. Each data represents the mean ± SD from three independent experiments. P values were calculated via ordinary one-way ANOVA (*P ≤ 0.05, **P ≤ 0.01, ***P ≤ 0.001, **** P ≤ 0.0001).

Interestingly, as observed for CAFs, also for NOFs ADAM17 depletion induced an increased phosphorylation of AKT and a concomitant downregulation of STAT3 phosphorylation, suggesting a conserved role of ADAM17 in modulating these signalling pathways (Figure 5.14). The phosphorylated form of STAT3 decreased by 1.6±0.17-fold ($p>0.5$) and 2.8±0.32-fold ($p<0001$) in $NOF^{A17\ low}$ and $eNOF^{A17\ low}$ respectively, compared to controls for NOF804, whereas it decreased by 2±0.15-fol ($p<0.05$) and 1.6±0.24-fold ($p<0.05$) in $NOF^{A17\ low}$ and $eNOF^{A17\ low}$ respectively, compared to controls for NOF806 and by 2.2±0.3-fold ($p<0.05$) and 2.6±0.2-fold ($p<0.0001$) in $NOF^{A17\ low}$ and $eNOF^{A17\ low}$ respectively, compared to controls for NOF343 (Figure 5.14 A-B). On the other hand, the phosphorylated form of AKT increased by 1.8±0.2-fold ($p<0.05$) and 1.3±0.4-fold ($p>0.05$) in $NOF^{A17\ low}$ and $eNOF^{A17\ low}$ respectively, compared to controls for NOF804, whereas it increased by 1.7±0.3-fold ($p>0.05$) and 1.9±0.8-fold ($p<0.0001$) in $NOF^{A17\ low}$ and $eNOF^{A17\ low}$ respectively, compared to controls for NOF806 and by 1.2±0.05-fold ($p>0.05$) and 1.5±0.6-fold ($p>0.05$) in $NOF^{A17\ low}$ and $eNOF^{A17\ low}$ respectively, compared to controls for NOF343 (Figure 5.14 A-B).

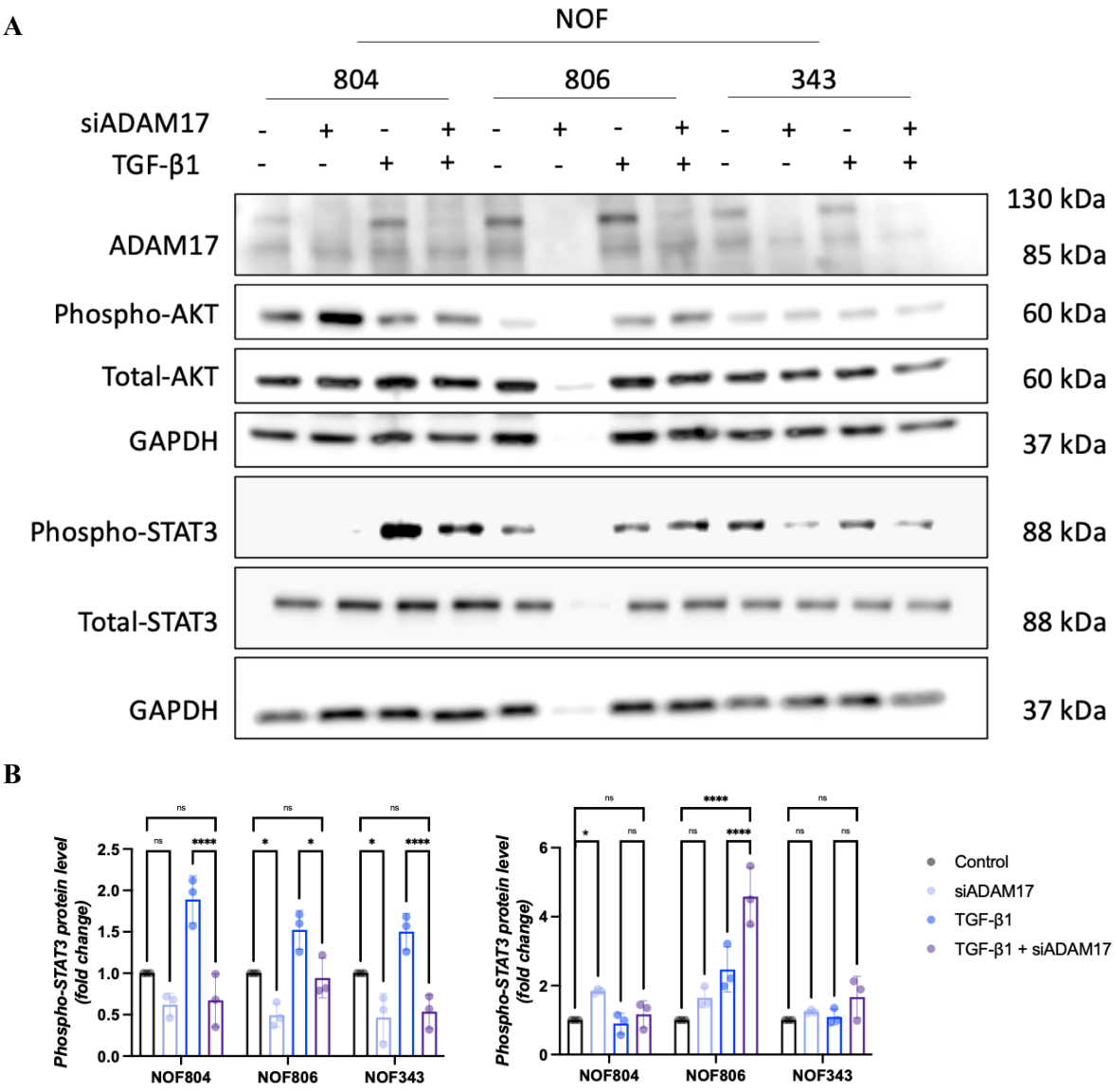

Figure 5.14 ADAM17 knock-down in TGF-β1-induced myofibroblasts downregulates STAT3 and upregulates AKT pathways.

*(**A**) Representative western blot showing protein levels of AKT and STAT3 pathways in TGF-β1-induced myofibroblasts upon ADAM17 depletion (n=3 t=3). (**B**) Quantification of A. Each data represents the mean ± SD from three independent experiments. P values were calculated via ordinary one-way ANOVA (*P ≤ 0.05, **P ≤ 0.01, ***P ≤ 0.001, **** P ≤ 0.0001).*

5.2.5 Confirmation and identification of candidate targetable proteins through a second proteomics analysis in CAFs upon ADAM17 KD

To gain further insights on the protein landscape in CAFs upon ADAM17 depletion, a second proteomics analysis was performed as described in section 5.2.1. This time, the samples compared included also CAFs conditioned with the C.M. derived from H357 and H376 thus, to process the 18 samples at the same time, the three biological replicates per condition were pooled together to obtain six final samples which were processed in duplicate. However, due to the inconclusive nature of the results obtained from cCAF and cCAF^{A17low}, in this section the data reported are only those relative to CAF (CTRL) and CAF^{A17low} (KD). As shown by the PCA plot, the control-CAF (CTRL) group in orange and the ADAM17-depleted CAF (KD) group in pink aligned as two distinct clusters separated along the PC1 which accounts for the 71.2 % of variation, confirming that ADAM17 depletion causes a molecular shift within CAFs (Figure 5.15 A). Moreover, the analysis of the protein abundance distribution within the two groups (CTRL vs KD) showed a similar variation from the median (5 % and 8 % respectively), suggesting that the number of proteins identified and interrogated is similar within the two groups (Figure 5.15 B).

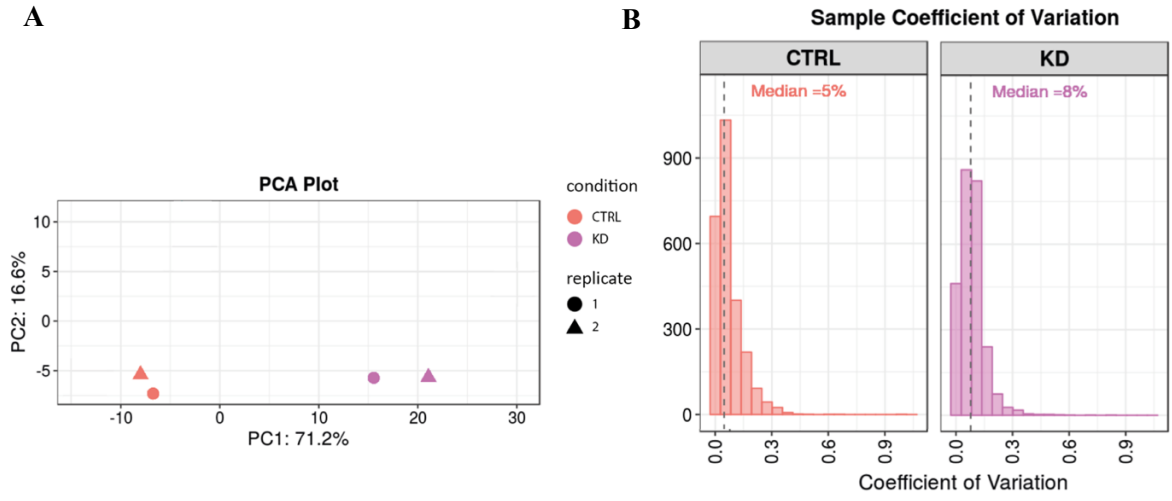

Figure 5.15 Proteomics analysis of control-CAFs (CTRL) vs ADAM17-depleted CAFs (KD).

*(**A**) PCA plot showing the groups distribution as clusters. (**B**) Histogram plot showing the distribution of protein abundance within the groups in function of their respective coefficient of variation (CV). A cutoff of the adjusted p-value of 0.05 (Benjamini-Hochberg method) along with a log2 fold change of 1 was applied to determine significantly regulated proteins in each pairwise comparison.*

To determine whether the differentially expressed proteins identified within this second mass-spectrometry analysis matched with the data extrapolated from the first attempt, a meticulous screening was performed by comparing the two lists of proteins and picking those whose expression changed in both lists, independently of the p values. This choice derived from the idea that proteins whose expression changed consistently in both the independent experiments could have been more molecularly significant and useful to outline a reliable molecular landscape associated with ADAM17 depletion than picking those showing a significant p value but an opposite trend. Using this approach, the number of proteins that were differentially expressed between the CTRL and KD groups accounted for 181 proteins, of which 36 were downregulated in $CAF^{A17\ low}$ whereas 145 were upregulated. Through the interrogation of the open source REACTOME using the list of upregulated proteins, those involved in the Interferon Type I (IFIT1, IFIT5, IFI35, OAS2, OAS3, HLA-C and SAMHD1 etc.), immunity and antigen presentation (TAP1, TAP2, HLA-C, PSAT1, PSME2 etc.), mitochondrial activity and metabolism (AARS, AARS2, MRPL3, LARS, CARS2, ABCD3, GYG1 etc.) were confirmed, in line with the first analysis (Table 5.1). Of note, these data were consistent with first *in vivo* studies characterising the role of ADAM17 in engineered mouse models, which reported that mice lacking ADAM17 displayed up-regulation of genes involved in host defence and interferon-mediated immunity (Chalaris, Adam, *et al.*, 2010).

Table 5.1 Up-regulated proteins in CAFs upon ADAM17 depletion.

The list comprises of 145 proteins that showed the same trend between the two independent experimental set up and whose average of the Log2 fold change, combining the Log2 fold change of both datasets, was ≥ 0.2.

Proteins up-regulated in ADAM17 depleted CAFs									
Gene name	Fold change	Gene name	Fold change	Gene name	Fold change	Gene name	Fold change	Gene name	Fold change
AAK1	0.74	DDX39A	0.28	IFIT1	1.28	PCBP2	0.77	TGM2	0.35
AARS	0.27	DHX30	0.75	IGF2R	0.27	PLA2G4A	0.83	TMF1	0.94
ACOX1	0.46	DNAJB2	0.89	IMPDH1	0.84	PLCD1	0.84	TMTC3	0.75
ACAD9	0.49	DNMBP	0.75	KIAA1524	0.75	PPIC	0.73	TNPO3	0.63
ANPEP	0.44	DOCK10	0.96	KPNA6	0.44	PPIH	0.50	TOMM70A	0.31
APOL2	0.22	DPP7	0.72	LARS	0.39	PPP2R5D	0.70	TRMT112	0.83
ATP61D	0.74	DSP	0.67	LEPREL4	0.45	PRPSAP2	1.12	TUBA1C	0.49
BCAS2	0.74	ECE1	0.73	LRRC15	0.55	PSAT1	0.46	TXN	0.41
CACNA2D1	0.83	EDC3	0.72	LSM6	0.91	PSME2	0.36	WDR61	0.48
CARS2	0.69	EDF1	0.31	MKI67	0.97	PTRH2	0.71	YAP1	0.69
CCDC47	0.52	EFTUD1	0.65	MRI1	0.99	RAB3B	0.40	ZCCHC8	0.84
AKT1S1	0.26	EMC3	0.89	MRPL1	0.75	RAD21	1.06	ZPR1	0.87
CD97	1.22	FAM3C	0.42	MRPL3	0.68	RHOC	0.33	NUDCD1	0.49
CDC42BPB	0.57	FDXR	0.66	MRPL37	0.80	RPL27A	0.69	AARS2	0.55
CEMIP	0.88	FTO	0.84	MTA2	1.04	S100A10	0.68	ABI1	0.62
CETN2	0.83	GBF1	0.27	MTMR6	0.85	S100A16	0.54	AHR	1.16
CHERP	0.77	GFM1	0.49	MTX2	0.50	ALDH4A1	0.73	NT5E	0.30
CIAPIN1	0.85	GFM2	0.88	MYADM	0.29	SAMHD1	0.74	OAS2	1.04
CLNS1A	0.83	GFPT2	0.84	NFKB1	0.79	SLC25A13	0.90	SYAP1	0.34
CLPTM1	0.92	GLRX3	0.31	NFKB2	0.78	SMCHD1	1.05	TAP1	0.86
CLPTM1L	0.67	GNA13	1.07	NOC3L	0.90	SMTN	0.68	TAP2	1.25
CNOT1	0.63	GYG1	0.57	NOC4L	0.93	SNTB2	0.87	DDX18	0.76
COMMD1	0.44	HEATR1	0.32	NT5C	0.98	SNW1	0.71	CASK	0.86
COMT	0.43	HGH1	0.66	NUP50	0.99	SPR	0.92	NOLC1	1.07
COPG2	0.28	HLA-C	0.75	NUP88	0.74	SRPR	0.76	PPM1G	0.43
COPS5	0.69	HSPB7	0.78	OAS3	1.49	STK38	0.85	EEF1E1	0.54
CRIP2	0.35	HTRA2	0.71	OTUD6B	0.67	SUB1	1.04	A0A0B4J203	0.64
CUL3	0.62	IFI35	0.88	PARP14	0.98	TACC1	0.90	AKR1C3	0.55
CUL5	0.69	IFIT3	0.82	PBK	0.86	TBC1D9B	0.86	ABCD3	0.62

Using the open-source Search Tool for the Retrieval of Interacting Genes (STRING), which allows to determine both the direct (physical) and indirect (functional) interactions amongst proteins, it was possible to identify 6 clusters, each involved in a specific biological/molecular activity. Globally, from a first analysis, the obtained protein-protein interaction (PPI) network showed more interactions than expected for a random dataset, meaning that the proteins are at least partially biologically connected as a group (p value =1.21e-09). This is an important aspect to highlight since the proteins were picked in an unbiased manner and from two independent experiments. Two out of the six clusters were enriched with proteins known to regulate the immune response. One cluster enriched with proteins involved in antigen processing and presentation of endogenous peptide antigen via major histocompatibility complex I (MHCI) and interferon-mediated immunity whereas, the other cluster consisted of proteins engaged with the regulation of the inflammatory response through NFκB (see Figure

5.16 A and B). More specifically, the second cluster displayed proteins (CUL3, COMMD1 and PSME2) involved in the ubiquitin-mediated proteasomal degradation of target proteins including NFκB, whose regulation occurs also via NFKB1 and NFKB2 (Maine *et al.*, 2007; Savinova, Hoffmann and Ghosh, 2009; Xu *et al.*, 2015).

A

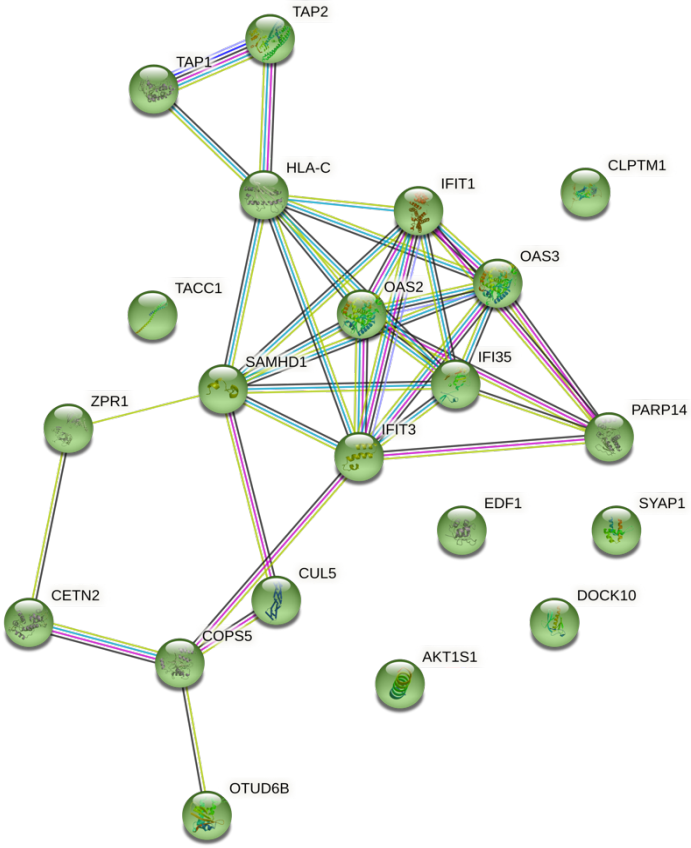

B

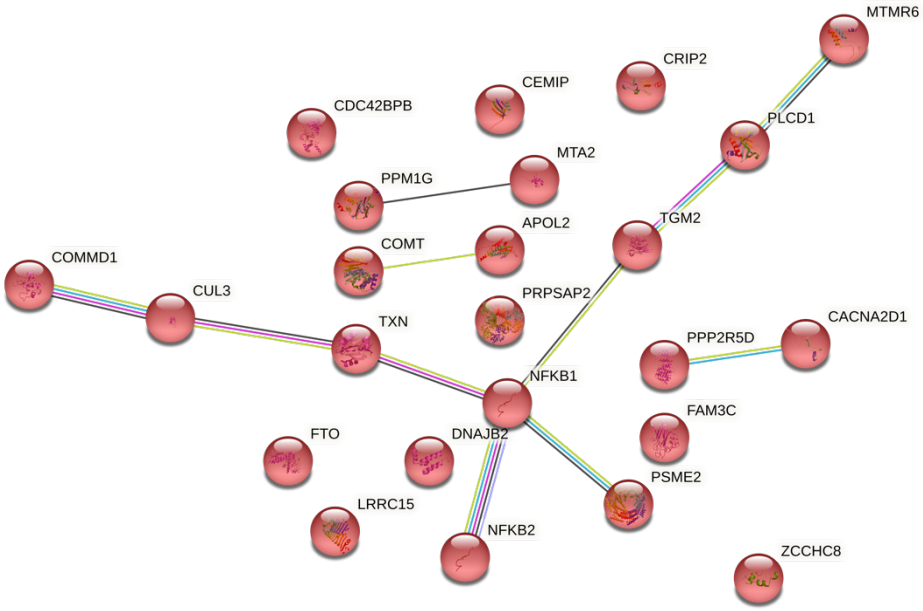

Figure 5.16 Protein-protein interaction (PPI) network of proteins up-regulated in ADAM17-depleted CAFs identifying immune response related proteins.

*(**A**) PPI network representing proteins involved in antigen processing and presentation and interferon mediated immune response. (**B**) PPI networks illustrating proteins involved in NFκB-mediated inflammatory response.*

Unlike the above-mentioned data, which were supported by previous literature, a third cluster was enriched with proteins involved in mRNA processing, mainly pre-mRNA splicing, mRNA degradation and export out of the nucleus (NOLC1, LSM6, BCAS2, CLNS1A, PPIH, AAK1, CNOT1, EDC3, DDX39A and DHX30), for the first time associated with a potential role of ADAM17 in their regulation (Figure 5.17).

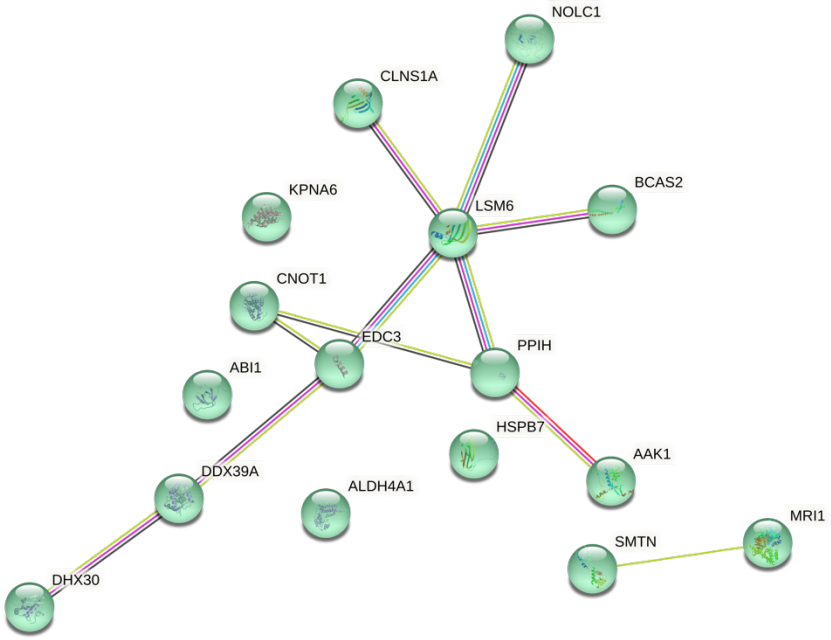

Figure 5.17 Protein-protein interaction (PPI) network of proteins up-regulated in ADAM17-depleted CAFs, identifies proteins involved in mRNA processing.

The other three PPI networks are represented by proteins engaged with potentially overlapping biological processes. These processes include mitochondrial translation and elongation (e.g. MRPL1, MRPL3, MRPL37, GFM1, GFM2, RPL27A), translation and RNA/DNA processing (e.g. NT5E, EFTUD1, NOC3L, NOC4L) (Figure 5.18 A), translation and DNA damage response (DDR) (e.g. EEF1E1, AARS, LARS, TRMT112, CIAPIN1, CARS2) (Figure 5.18 B), regulation of the Golgi network, RHO GTPase pathway (e.g. GNAI13, GFB1, COPG2,

RHOC, ABCD3), protein transport (e.g. TOMM70A, MTX2, NUP50, NUP88, TBC1D9B) (Figure 5.18 C). Also in the case of these three PPI networks, there is no evidence of a clear or direct implication of ADAM17 in their regulation.

A

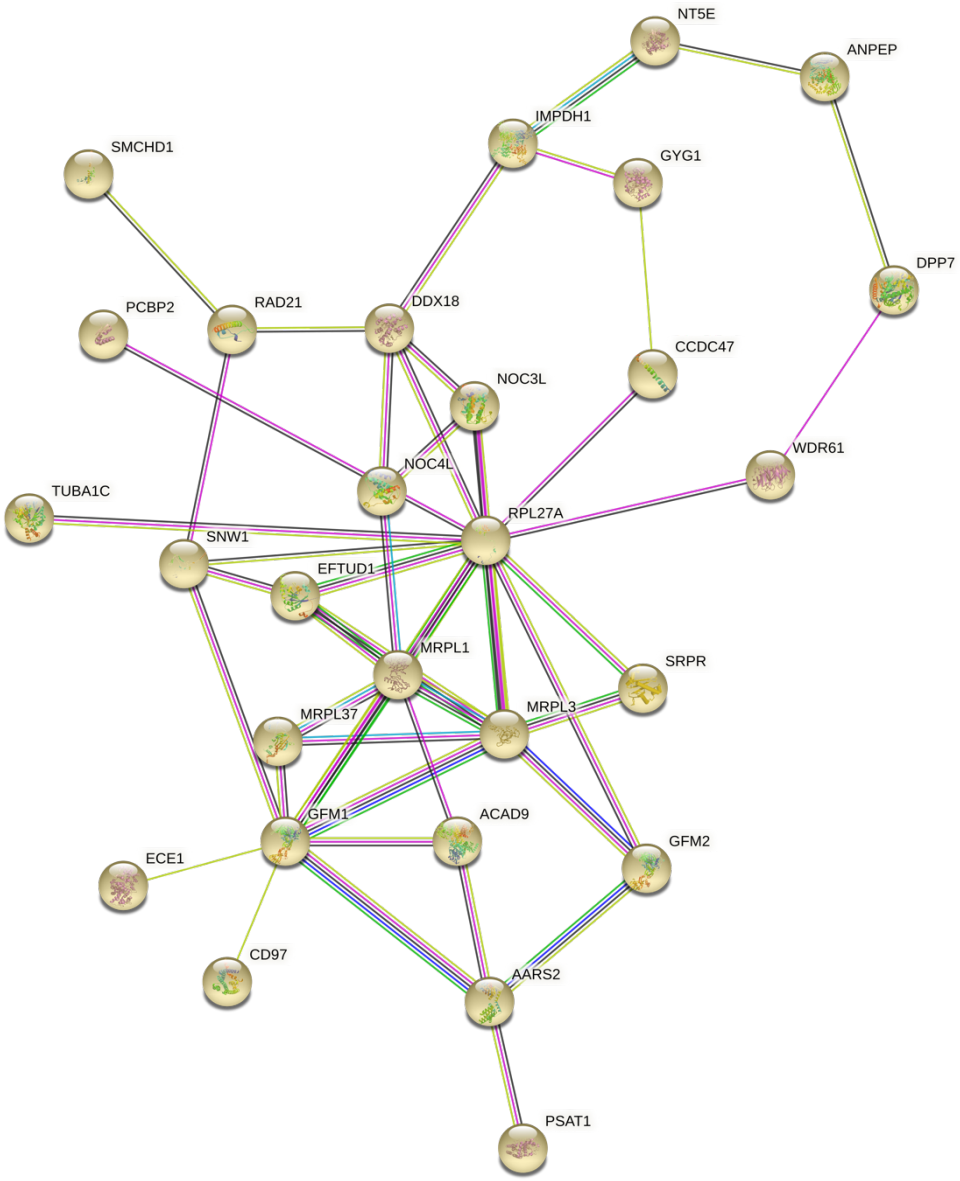

B

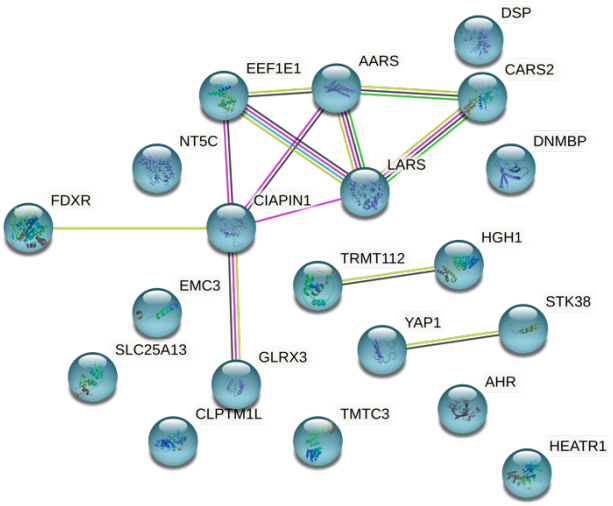
DSP
EEF1E1
AARS
CARS2
NT5C
DNMBP
LARS
FDXR
CIAPIN1
HGH1
TRMT112
EMC3
STK38
YAP1
SLC25A13
GLRX3
AHR
CLPTM1L
TMTC3
HEATR1

C

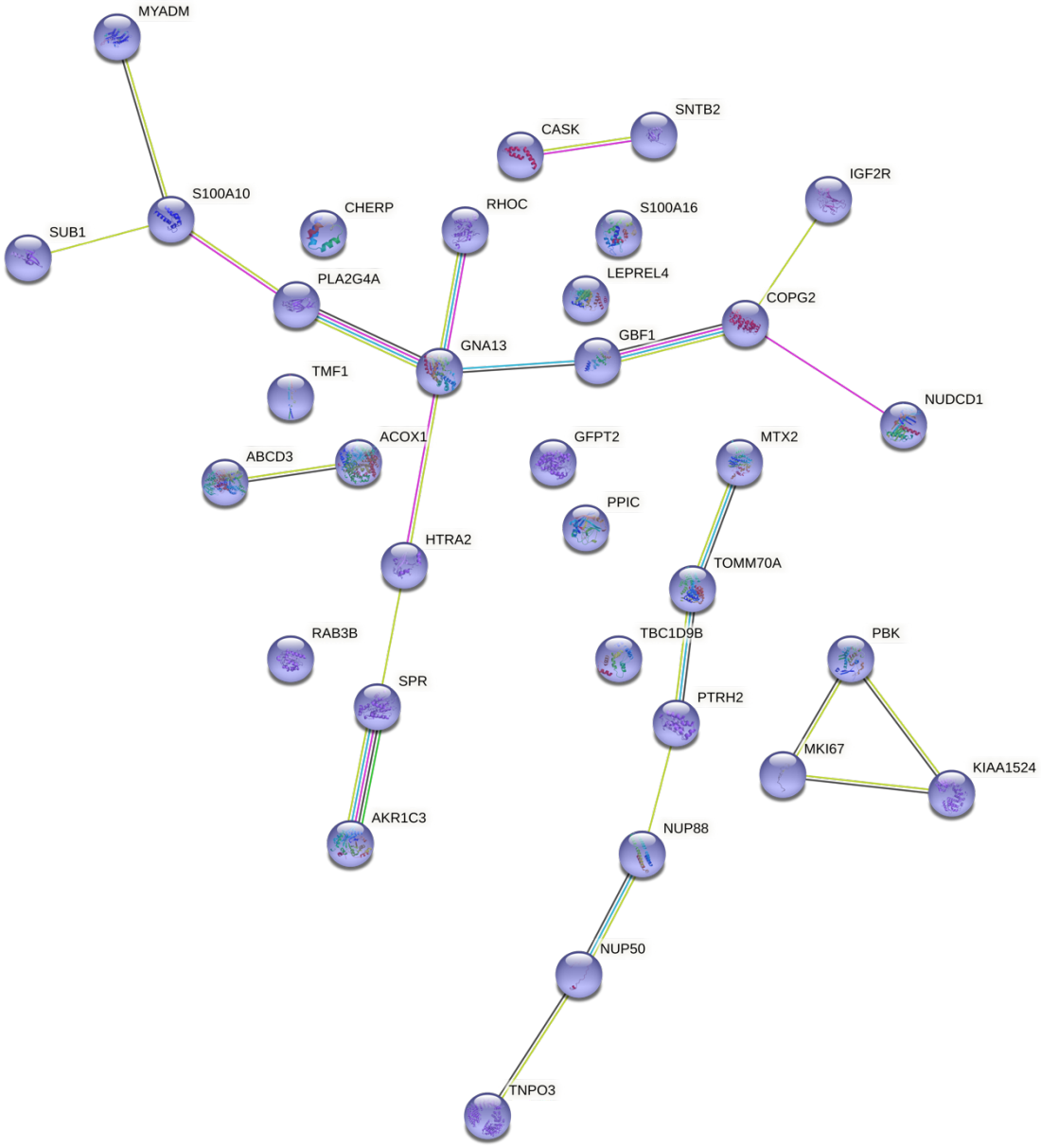
MYADM
SNTB2
CASK
IGF2R
S100A10
CHERP
RHOC
S100A16
SUB1
LEPREL4
PLA2G4A
COPG2
GNA13
GBF1
TMF1
NUDCD1
ACOX1
GFPT2
MTX2
ABCD3
PPIC
HTRA2
TOMM70A
RAB3B
TBC1D9B
PBK
SPR
PTRH2
MKI67
KIAA1524
AKR1C3
NUP88
NUP50
TNPO3

Figure 5.18 Protein-protein interaction (PPI) networks of up-regulated proteins in ADAM17 depleted CAFs.

To identify the most significant pathways negatively regulated upon ADAM17 depletion in CAFs, the same approach was used to analyse those that were positively regulated for the same conditions, uploading the list of down-regulated proteins upon ADAM17 depletion in CAFs (Table 5.2).

Table 5.2 Down-regulated proteins in CAFs upon ADAM17 depletion.

The list comprises of 36 proteins that showed the same trend between the two independent experimental set up and whose Log2 fold change average, combining the Log2 fold change of both datasets, was ≥ 0.2.

Proteins down-regualted in ADAM17 depleted CAFs			
Gene name	Fold change	Gene name	Fold change
ACTN4	0.48	HMGB1	0.37
CSRP1	1.02	HMGB2	0.31
AKAP12	0.80	LAMA4	0.17
ALDOC	0.31	LIMS1	0.45
CALD1	0.79	NES	0.88
CALM2	0.71	NUDC	0.58
CNBP	0.50	NUTF2	1.18
COL12A1	0.31	PTGS1	0.60
COL1A1	0.21	RECQL	0.61
CSRP2	0.59	RPS11	0.35
CSTB	0.67	S100A6	0.76
ERLIN1	0.25	SERPINB2	0.70
FBN1	0.77	TXNL1	0.30
FBN2	0.86	UBE2N	0.46
FGF2	0.24	PDGFRA	0.85
FHL1	0.60	CD59	0.82
FHL2	0.71	RPS25	0.63
HEBP2	0.48	ATP6V0D1	0.65

Consistent with *in vivo* studies reporting that ADAM17 deficient mice displayed reduced renal interstitial collagen deposition with reduced fibrosis (Kefaloyianni *et al.*, 2016) and skin defects (Horiuchi *et al.*, 2009; Franzke *et al.*, 2012), amongst the proteins negatively regulated upon ADAM17 depletion there were those involved in collagen degradation, elastic fibres and

multimeric structures formation and non-integrin membrane-ECM interactions (FBN1, FBN2, COL1A1, COL12A1, LAMA4, FGF2) (Figure 5.19). In addition, there were proteins engaged with other biological processes such as regulation of gap-junction activity (ACTN4), PDGFR signalling pathway (PDGFRA), EGFR signalling pathway (PDGFRA, AKAP12), apoptosis-induced DNA fragmentation (HMGB1, HMGB2), neutrophil degranulation (ALDOC, CD59, CSTB, HEBP2, HMGB1, SERPINB2), RND2 GTPase cycle (NUDC, TXNL1), cytoplasmic translation (RPS11, RPS25), FGFR pathway (FGF2) and cytoskeleton organisation (CSRP1, CSRP2, ACTN4) (Figure 5.19).

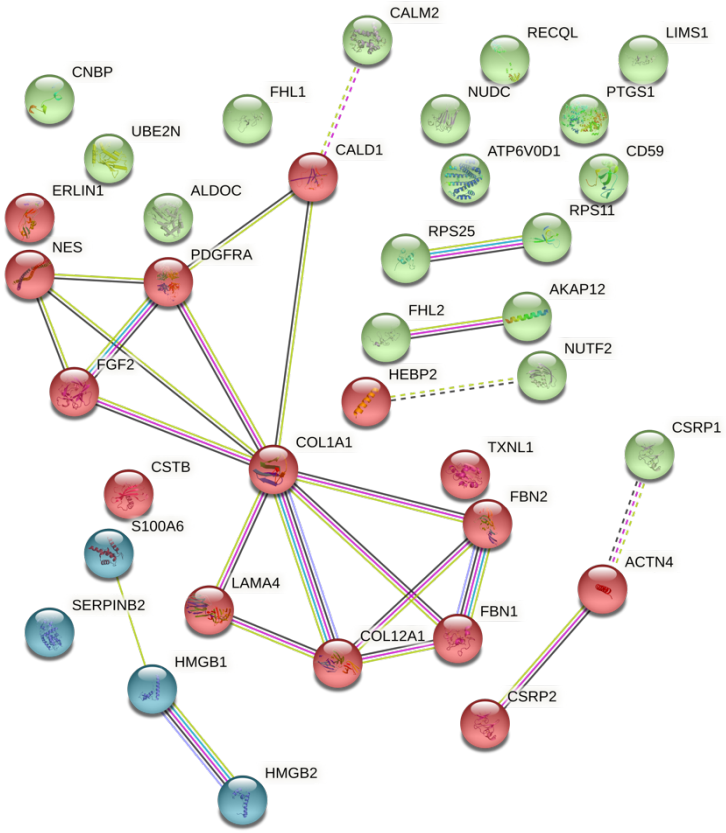

Figure 5.19 Protein-protein interaction (PPI) network of proteins down-regulated in ADAM17-depleted CAFs.

To gain a deeper insight, each cluster was separately analysed by STRING by evidencing the pathways within each network. A first cluster was made up of proteins involved in the ECM organisation (PDGFRA, FGF2, CALD1, LAMA4, COL12A1, COL1A1, FBN1, FBN2, NES, ACTN4, CSRP2), processed involved in the skeletal development (PDGFRA, FGF2, CALD1,

LAMA4, COL12A1, COL1A1, FBN1, FBN2, NES, ACTN4, CSRP2) and TGF-β1 sequestration within the ECM (FBN1 and FBN2) (Figure 5.20).

Amongst the proteins, nestin (NES) has been shown to be regulated by FGF2 in glioma cells (Chang *et al.*, 2013) and to modulate the proliferative and invasive capacities of gastrointestinal stromal tumour cells by regulating mitochondrial functions (J. Wang *et al.*, 2015). Moreover, NES and TGF-β1 positively and reciprocally regulate each other in pancreatic cancer cells (Su *et al.*, 2013).

The platelet derived growth factor receptor alpha (PDGFRA) is mainly expressed by mesenchymal tissues and used as a fibroblast marker (Farahani and Xaymardan, 2015). Studies showed its crucial role in cardiac fibroblast maintenance and survival (Asli *et al.*, 2019; Ivey *et al.*, 2019), whereas its expression can be positively regulated by FGF2, as reported in another study conducted in glioma cells (Chen *et al.*, 2013).

The protein caldesmon 1 (CALD1) has been reported to be a marker of CAFs in bladder cancer patients and to associate with disease progression and poor prognosis by promoting the infiltration of immunosuppressive cells, such as macrophages M2 and $CD8^+$ T cells (Du *et al.*, 2021). In another study, the CALD1 expression of stromal fibroblasts, within colorectal cancer, was found to be regulated by TGF-β1 (Calon *et al.*, 2015).

In line with in vivo studies using engineered mouse models to conditionally inactivate ADAM17, which reported bone defects and an osteoporosis-like phenotype in mice lacking ADAM17 (represented by bone loss due to a reduction of both the trabecular and cortical bones) (Horiuchi *et al.*, 2009), one of the prominent biological process negatively affected upon ADAM17 depletion in CAFs was that related to skeletal morphogenesis and development. As shown by the interaction diagram, the proteins engaged with this process are FBN1, FBN2, COL1A1, COL12A1, PDGFRA, FGF2, NES (Figure 5.20). In addition, CSTB, which was not reported to interact with any protein within the cluster, has been shown regulate the bone metabolism, as observed in *Cstb*$^{-/-}$ mice which, unlike the *ADAM17*$^{-/-}$ mice, had thicker and more mineralised trabecular bones whereas no change was observed in the cortical bone (Manninen *et al.*, 2015).

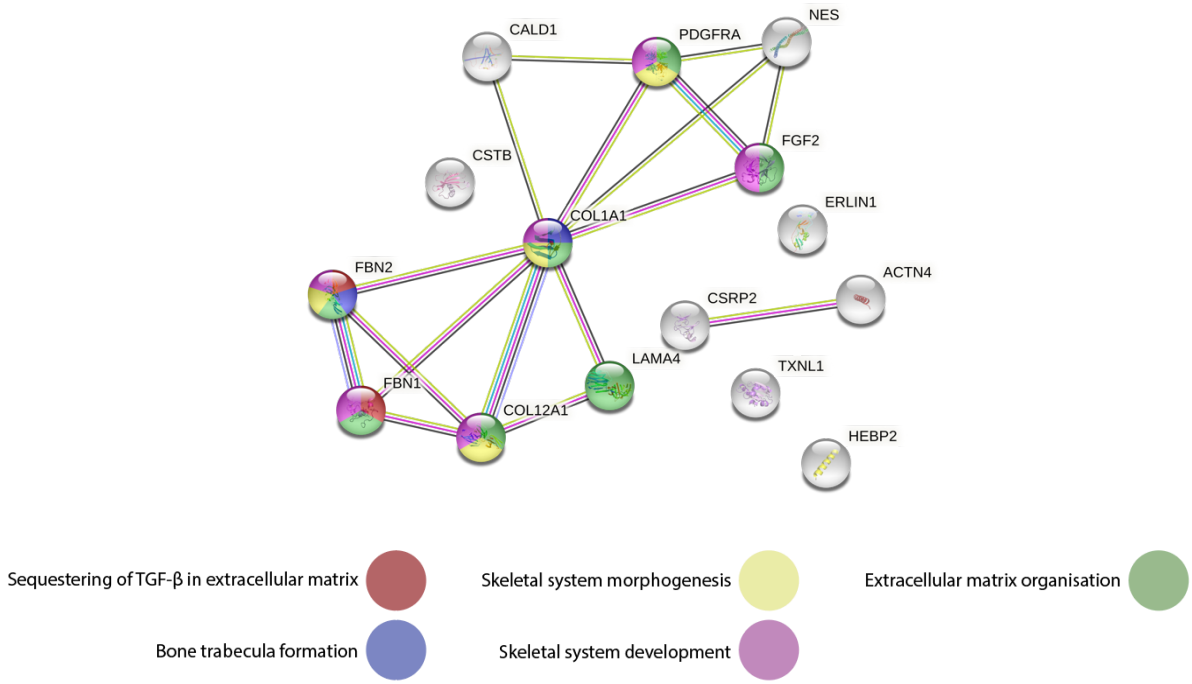

Figure 5.20 Interaction network of proteins involved in bone-associated processes, ECM organisation and TGF-β1 sequestration

A second cluster displayed proteins which functions are related to cell-cell interaction and communication, with some proteins involved in more than one function, such as LIMS1, CD59, FHL2, AKAP12, FHL1 involved in focal adhesion, cell junction and cytoplasm, whereas CSRP1, RPS11 also in extracellular exosomes. The rest of the proteins were mainly associated with cytoplasm, extracellular exosome and cell junction (CNBP, PTGS1, ALDOC, UBE2N, NUTF2, ATP6V0D1, RECQL, CALM2, NUDC and RPS25) (Figure 5.21).

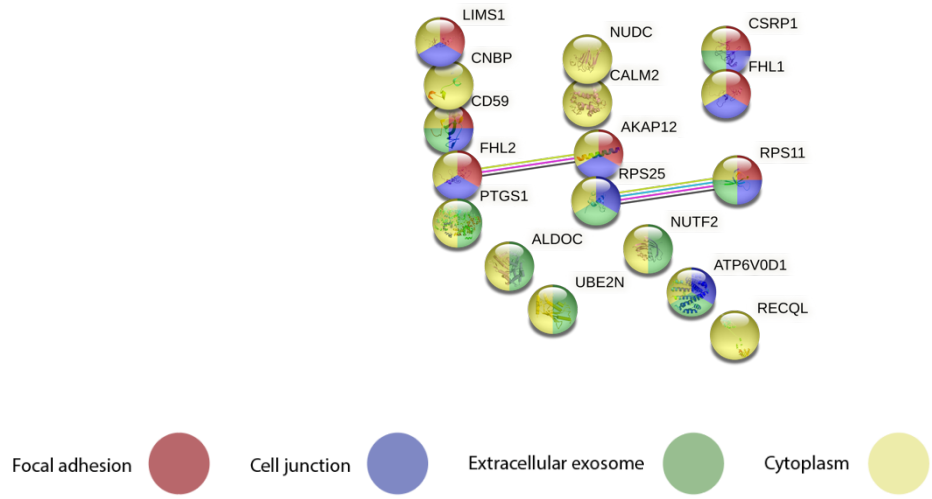

Figure 5.21 Interaction network of proteins involved in intercellular communication.

The third and last cluster was made up by proteins engaged with DNA-related functions and inflammatory response to antigenic stimuli (SERPINB2, HMGB1 and HMGB2) (Figure 5.22). The ubiquitous nuclear protein high mobility group box 1 (HMGB1) has been shown to be secreted by CAFs in non-small cell lung cancer and to promote malignancy progression and metastasis by the activation of the NFκB pathway (Ren *et al.*, 2021).

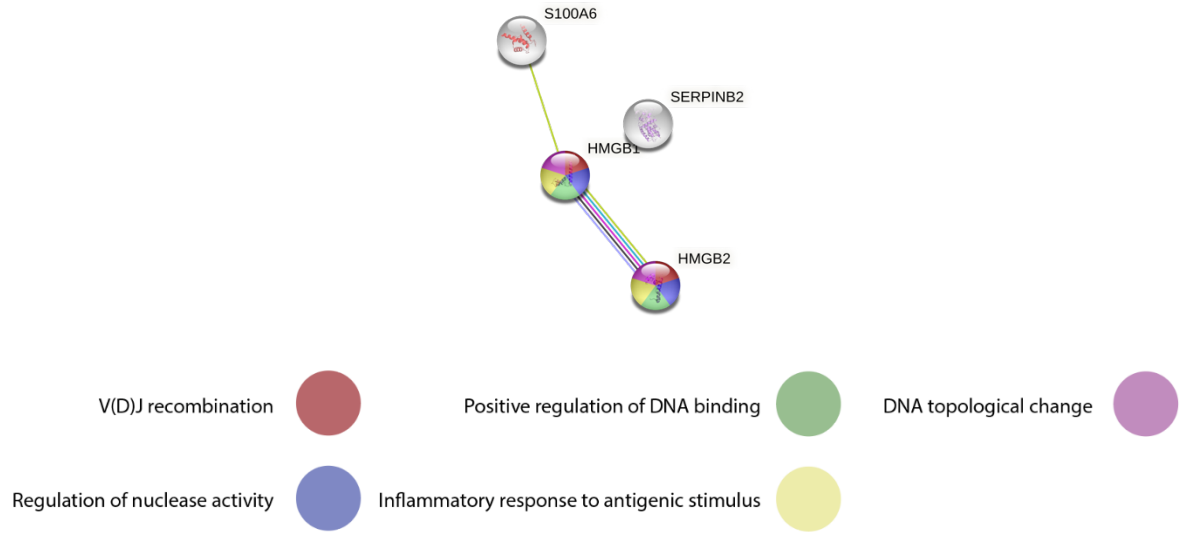

Figure 5.22 Interaction network of proteins involved in DNA-associated processes

5.2.6 EGFR signalling pathway does not influence N-cadherin levels in OSCC-derived cells

ADAM17 is known to regulate the activity and availability of a plethora of molecules through its sheddase activity (Gooz, 2010)(Gooz, 2010). Moreover, it is well documented to function as a regulator of the cell surface tyrosine kinase Epidermal Growth Factor Receptor (EGFR) signalling cascade through the shedding of EGFR-ligands (such as transforming growth factor alpha, amphiregulin, epiregulin and heregulin) (Sahin *et al.*, 2004). Moreover, as indicated in the proteomics data reported in section 5.2.5, amongst the downregulated proteins in CAFs upon ADAM17 depletion there were the platelet-derived growth factor receptor A (PDGFRA), known to be involved in a reciprocal transactivation with the EGFR signalling pathway (He *et al.*, 2001; Chakravarty *et al.*, 2017) and the A-kinase anchoring protein 12 (AKAP12) which participates in the EGFR transactivation through TGF-alpha (Cao *et al.*, 2019). Moreover, ADAM17 has been demonstrated to be activated by the PDGFRB and to mediate the crosstalk between PDGFRB and EGFR (Mendelson *et al.*, 2010). Thus, another approach to determine the potential mechanism underlying the ADAM17-mediated regulation of cancer cell migration via CAFs was to assess the role of the EGFR signalling pathway in both H357 and H376 as follows:

1. Stimulation of the EGFR pathway via EGF treatment of H357 and H376 cells.
2. EGFR pathway inhibition via Gefitinib treatment of H357 and H376 cells.

3. Evaluation of the N-cadherin levels in H357 and H376 under the above-mentioned conditions.

Both H357 and H376 cells were seeded in six well plates and when 70-80% confluent they were treated with Gefitinib (at 5μM or 10μM) (Liu *et al.*, 2017) or DMSO for 4 h before stimulating them with EGF (at 10ng/ml) (Son *et al.*, 2013) for 1 h. Afterwards the cells were lysed to harvest proteins and RNA and to assess N-cadherin levels. EGF treatment triggered the activation of the EGFR pathway as shown by the strong phosphorylation of the EGFR protein whereas Gefitinib was shown to be effective by the decrease of EGFR phosphorylation (Figure 5.23 A-B). The decrease was dose dependent though it was possible to detect it only in the H357 cells (Figure 5.23 A-B). Hence, when evaluating N-cadherin levels, neither H357 nor H376 seemed to have any change across the conditions, suggesting that EGFR pathway does not play a role in its regulation (Figure 5.23 A-C).

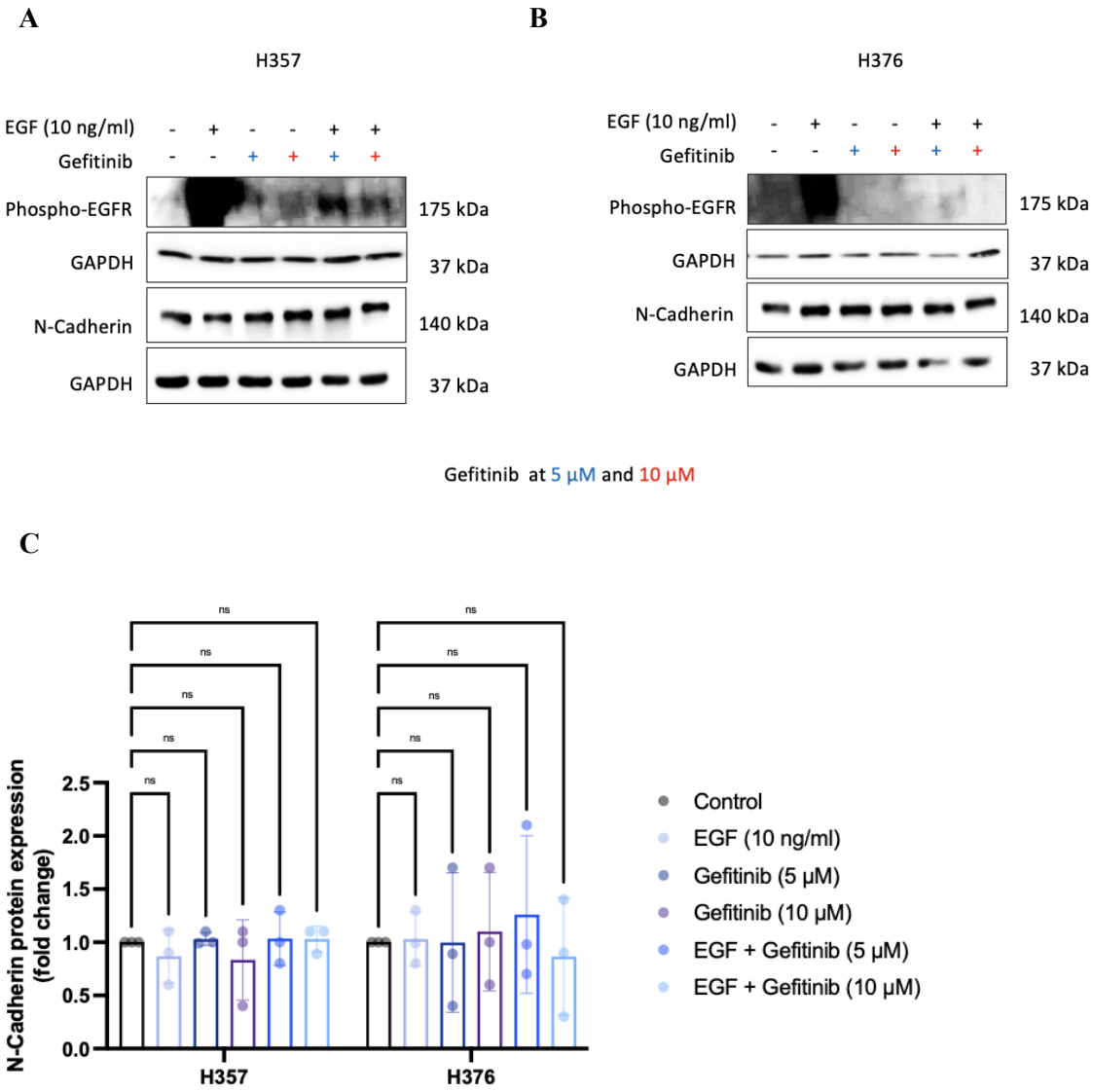

Figure 5.23 EGFR signalling assessment in OSCC cell lines.

*(**A-B**) Representative western blot showing EGFR pathway activation and N-cadherin levels in H357 and H376 cells respectively. Cells were seeded in six well plates until 70-80% confluent. Then, the cells were treated with Gefitinib at two different concentrations (5 µM and 10 µM) for 4 h. Next, cells were stimulated with the recombinant EGF at 10 ng/ml for 1 h before harvesting both proteins and RNA (n=3 t=2). (**C**) Quantification of A and B by densitometry. Each data represents the mean ± SD from three independent experiments. P values were calculated via ordinary one way Anova (*P ≤ 0.05, **P ≤ 0.01, ***P ≤ 0.001, **** P ≤ 0.0001).*

5.2.7 FGFR regulates cancer cell migration

In addition to the EGFR signalling, CAFs contribute to generate a protumorigenic environment by activating the FGFR in cancer cells through the release of FGFR ligands (FGFs) (Y. Sun *et al.*, 2017; Sahai *et al.*, 2020). In this scenario, ADAM17 can participate to the FGFR regulation through its substrates, known to interact with FGFR, such as Tumour Necrosis Factor alpha (TNF-α), Klotho, NCAM and others (D'Amici *et al.*, 2013; Zivotic *et al.*, 2018; Saar-Kovrov, Donners and van der Vorst, 2021). More importantly, as evidenced by the proteomics analysis, another important downregulated protein, although the extent of its downregulation was not significant, was the fibroblast growth factor 2 (FGF2), one of the family of ligands known to activate the FGFR pathway (Xie *et al.*, 2020). Hence, to investigate the FGFR involvement in cancer cell migration the following approach was applied:

1. FGFR pathway inhibition via the FGFR inhibitor SSR128129E in cancer cells and the evaluation of the effect on their migration by wound healing assay.
2. Determination of the N-cadherin levels under the above-mentioned conditions.

As per the EGFR pathway investigation, the approach applied to examine the role FGFR in OSCC cells migration was similar. H376 and H357 cells were seeded in six well plates in the presence or not of the C.M. derived from CAFs the cells were 90% confluent, a scratch was performed and the cells were treated with SSR128129E (at 2.5µg/ml, 5µg/ml or 10 µg/ml) (Guccini *et al.*, 2021) or DMSO for 24 h. The pictures were acquired at the microscope at time 0, 6 h and 24 h. Afterwards the cells were lysed to harvest proteins and RNA and to assess N-cadherin levels. The treatment with the FGFR inhibitor (FGFRi) SSR128129E showed a restriction of the migratory potential in H376 cells both in the presence and absence of the C.M. derived from CAFs. Indeed, the migration rate decreased by 1.4±0.09-fold ($p>0.05$), 1.39±0.12-fold ($p>0.05$) and 1.9±0.07-fold ($p<0.05$) in H376 treated with the FGFRi at 2.5µg/ml, 5µg/ml and 10µg/ml respectively, compared to control whereas, it decreased by 3.5±0.05774-fold ($p<0.0001$) and 3.4±0.05-fold ($p<0.0001$) in H376 treated with the FGFR inhibitor (FGFRi) SR128129E at 2.5µg/ml and 5µg/ml respectively, in the presence of CAF C.M. compared to H376 treated with only CAF C.M. (Figure 5.204A-B).

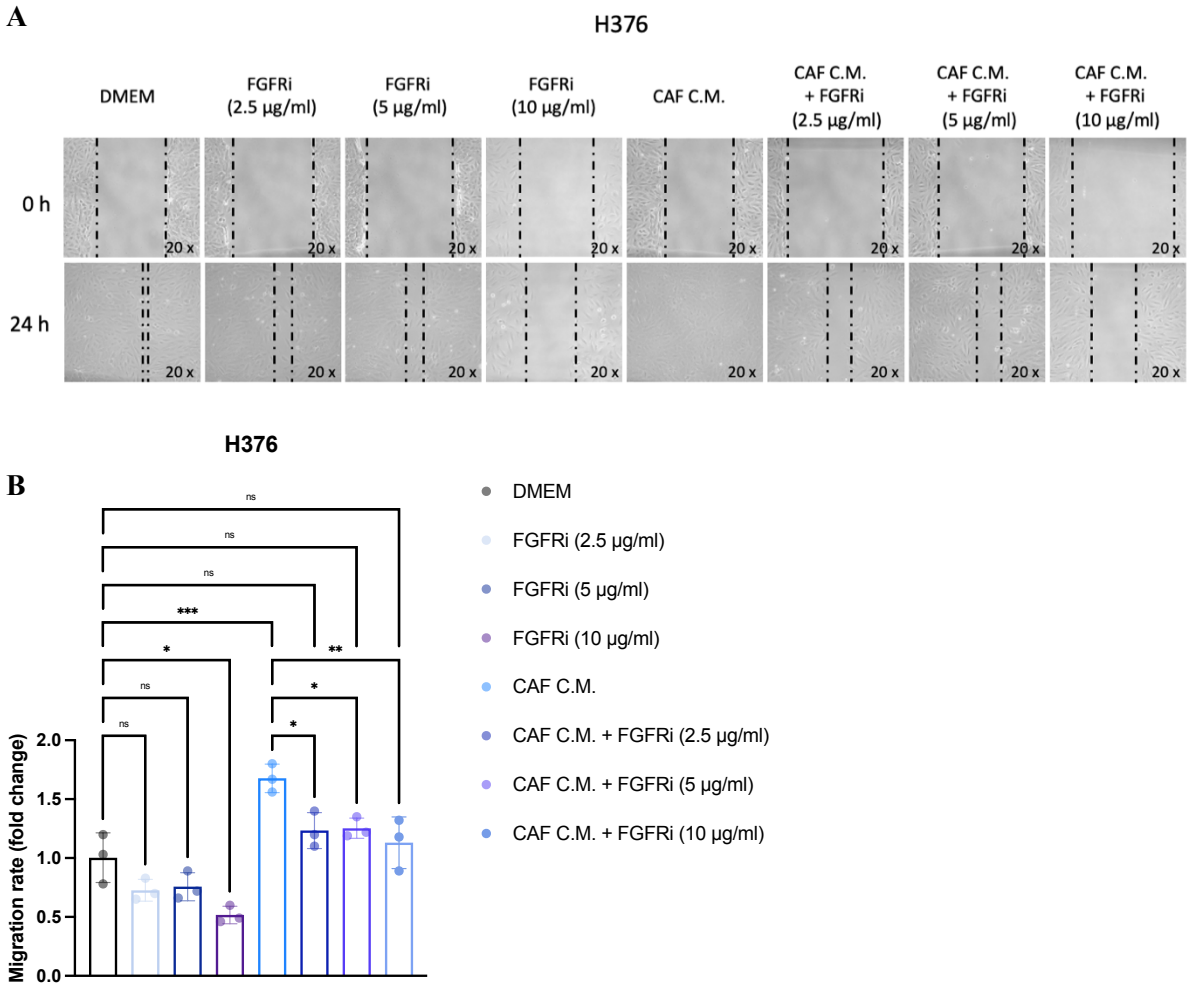

Figure 5.24 FGFR signalling assessment in H376 cells.

*(**A**) Wound healing assay showing the effect of the FGFRi SR128129E on H376. Cells were seeded in six well plates with and without the C.M. derived from CAF. When the cells were 90% confluent a scratch was performed, the FGFRi was added were needed and pictures acquired at time 0, 6 h and 24 h (n=3 t=1). (**B**) Quantification of A. (**C**) Western blot showing N-cadherin levels in H376 upon treatment with the FGFRi as above-mentioned (n=1 t=1). (**D**) Ki67 immunofluorescence staining in H376 upon treatment with the FGFRi. Cells were viewed using a Zeiss Axioplan 2 fluorescence light microscope, at 20-40x, setting the filter for Excitement/Emission between 491 and 520. Images were acquired using Proplus 7.0.1 image software and analysed with Fiji by randomly picking four different areas and counting the Ki67 positive cells. The results were normalised to the control (untreated cells) and data reported as ratio between treated sample and its control (n=3 t=1). (b) Quantification of D. Each data represents the mean ± SD. P values were calculated via ordinary one way Anova (*P ≤ 0.05, **P ≤ 0.01, ***P ≤ 0.001, **** P ≤ 0.0001).*

Next, the levels of N-cadherin were assessed by qPCR assay which showed a decrease in a dose dependent manner (Figure 5.24 A). The N-cadherin levels decreased by 1.5±0.05-fold

(p>0.05), 1.7±0.04-fold (p>0.05) and 2.1±0.03-fold (p>0.05) in H376 treated with the FGFRi at 2.5μg/ml, 5μg/ml and 10μg/ml respectively compared to control, whereas it decreased by 1.2±0.2-fold (p<0.01), 2.3±0.23-fold (p<0.001) and 2.5±0.24-fold (p<0.0001) in H376 treated with the FGFRi at 2.5μg/ml and 5μg/ml respectively, in the presence of CAF C.M. compared to H376 treated with only CAF C.M. (Figure 5.25A). Nevertheless, the proliferation rate did not change across the conditions indicating that the restriction of the migration ability is independent of an alteration of the cellular division (Figure 5.25 B-C). However, the experiment was performed only once thus further repeats are required to validate these results.

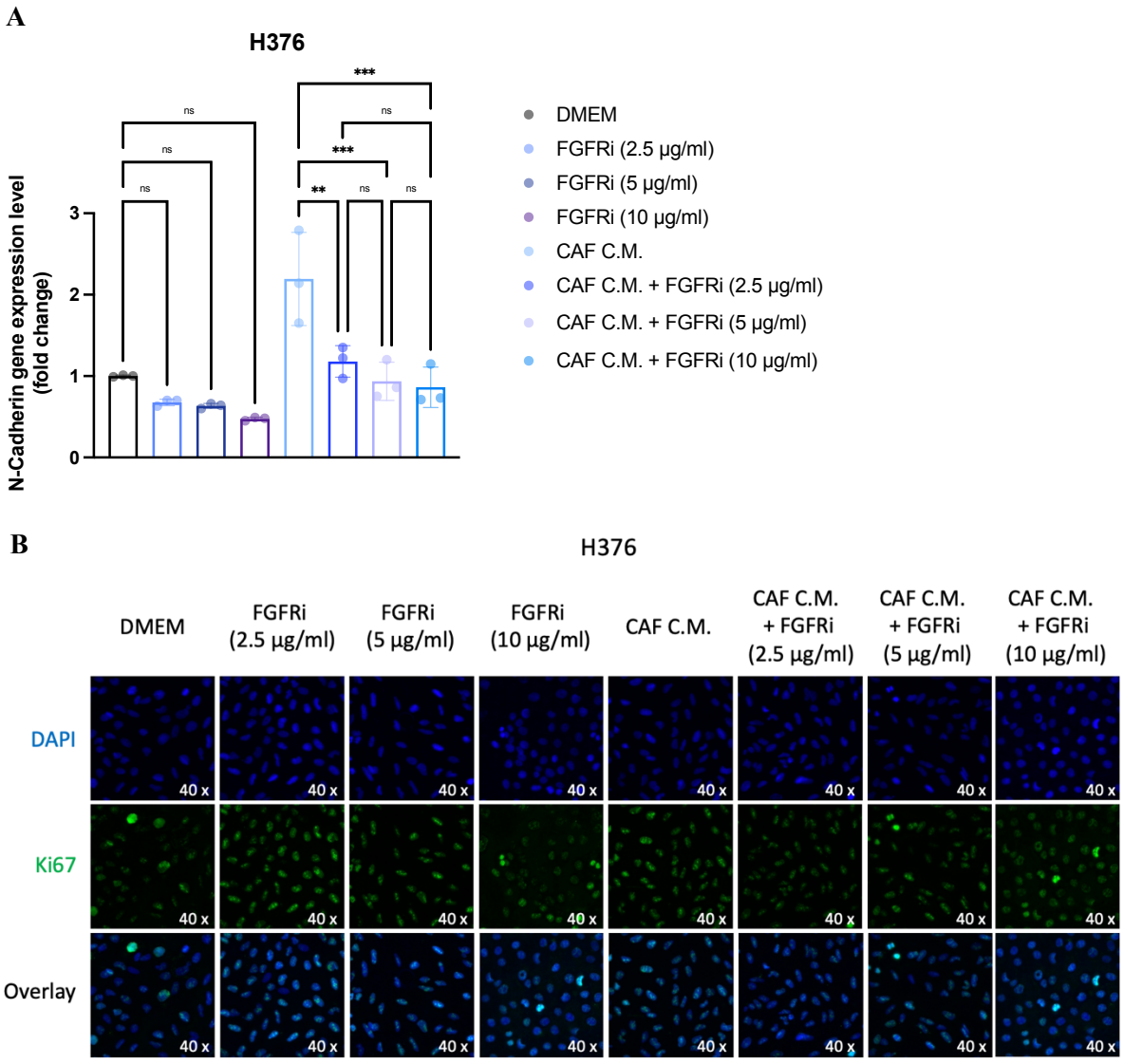

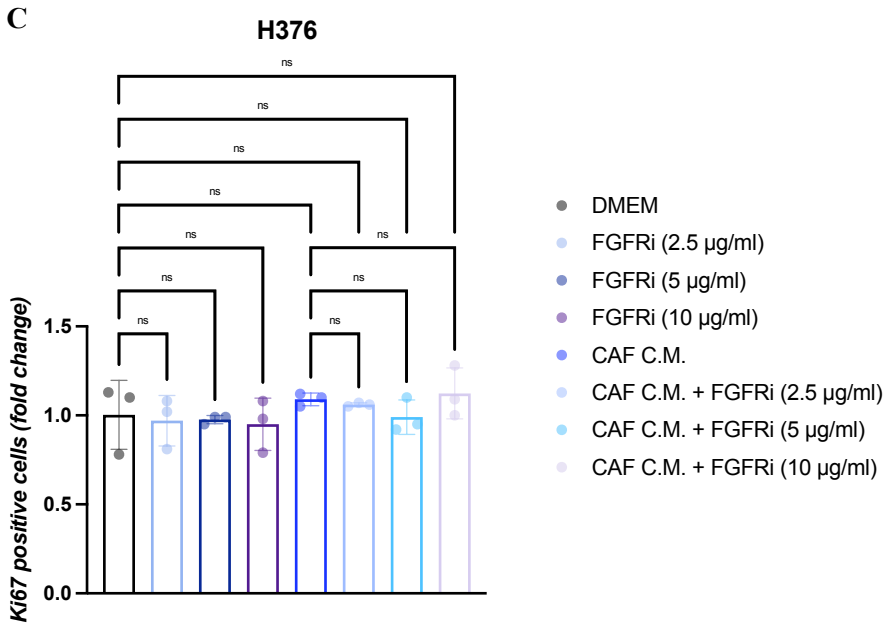

Figure 5.25 FGFR inhibition decreases N-cadherin levels in H376 cells.

*(**A**) Representative qPCR showing N-cadherin levels in H376 upon treatment with the FGFRi as above-mentioned (n=3 t=1). (**B**) Ki67 immunofluorescence staining in H376 upon treatment with the FGFRi. Cells were viewed using a Zeiss Axioplan 2 fluorescence light microscope, at 20-40x, setting the filter for Excitement/Emission between 491 and 520. Images were acquired using Proplus 7.0.1 image software and analysed with Fiji by randomly picking four different areas and counting the Ki67 positive cells. The results were normalised to the control (untreated cells) and data reported as ratio between treated sample and its control (n=3 t=1). (**C**) Quantification of B. Each data represents the mean ± SD. P values were calculated via ordinary one way Anova (*P ≤ 0.05, **P ≤ 0.01, ***P ≤ 0.001, **** P ≤ 0.0001).*

Similarly to what observed for H376 cells, also H357 cell migration decreased upon treatment with SSR128129E (Figure 5.26 A-B). The migration rate decreased by 1.6±0.07-fold ($p<0.01$) and 1.3±0.12-fold ($p>0.05$) in H357 treated with the FGFRi at 5µg/ml and 10µg/ml respectively, compared to control whereas, it decreased by 1.4±0.12-fold ($p<0.01$) and 1.4±0.15-fold ($p<0.01$) in treated with the FGFR inhibitor (FGFRi) SR128129E at µg/ml and 10µg/ml respectively, in the presence of CAF C.M. compared to H3757 treated with only CAF C.M. (Figure 5.26 A-B).

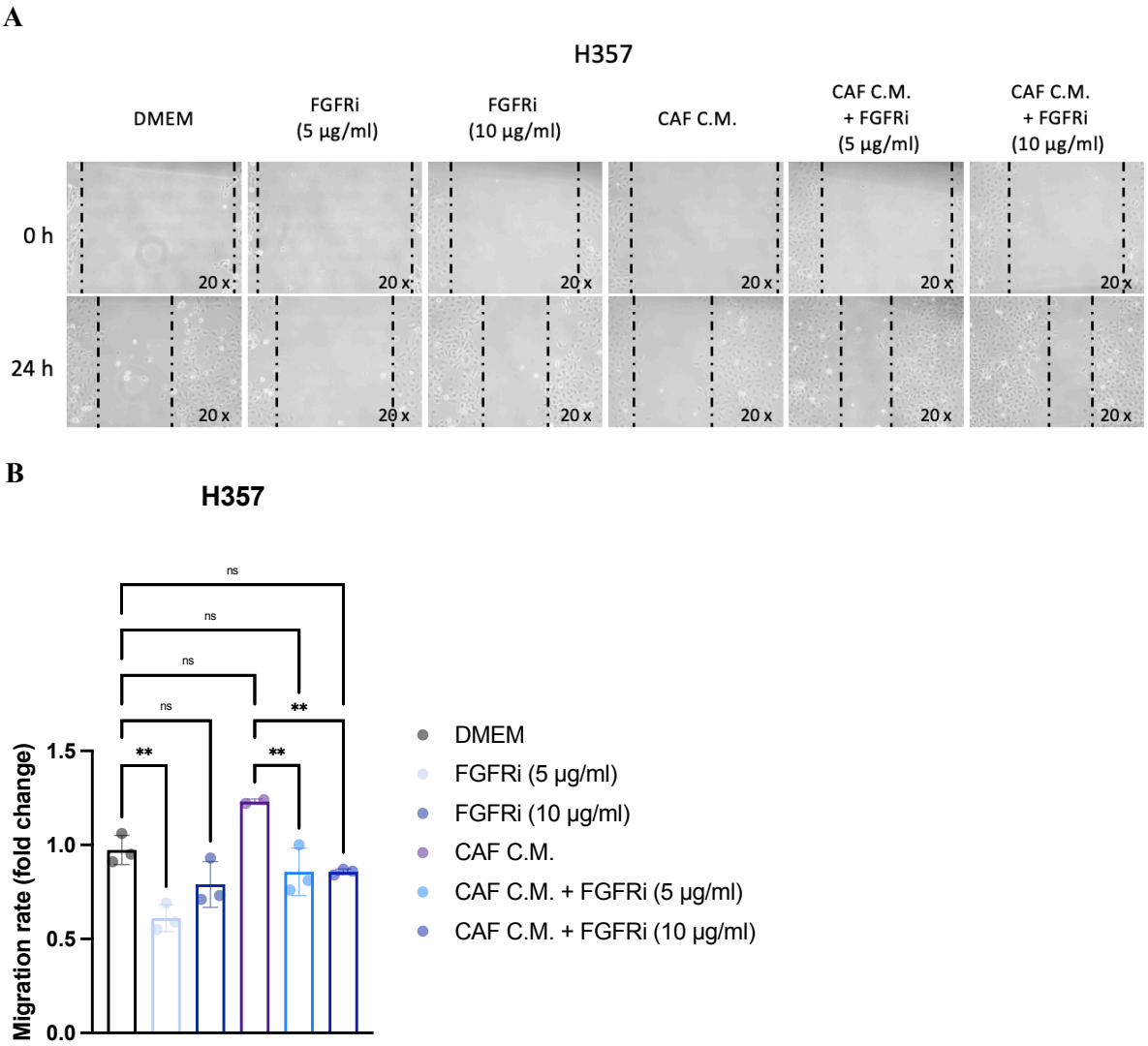

Figure 5.26 FGFR signalling assessment in H357 cells.

*(**A**) Wound healing assay showing the effect of the FGFRi SR128129E on H357. Cells were seeded in six well plates with and without the C.M. derived from CAF. When the cells were 90% confluent a scratch was performed, the FGFRi was added were needed and pictures acquired at time 0, 6 h and 24 h (n=3 t=1). (**B**) Quantification of A. P values were calculated via ordinary one way Anova (∗P ≤ 0.05, ∗∗P ≤ 0.01, ∗∗∗P ≤ 0.001, ∗∗∗∗ P ≤ 0.0001).*

Similarly to what observed for H376 cell line, the levels of N-cadherin assessed by qPCR assay showed a decrease in H357 upon treatment with the FGFR inhibitor (Figure 5.27 A). The N-cadherin levels decreased by 3.5±0.12-fold ($p<0.01$), 3.5±0.16-fold ($p<0.01$) and 2.7±0.17-fold ($p<0.01$) in H357treated with the FGFRi at 2.5µg/ml, 5µg/ml and 10µg/ml respectively compared to control, whereas it decreased by 2.8±0.12-fold ($p<0.001$), 5.4±0.02-fold ($p<0.0001$) and 3.6±0.16-fold ($p<0.0001$) in H357 treated with the FGFRi at 2.5µg/ml and 5µg/ml respectively, in the presence of CAF C.M. compared to H357 treated with only CAF

C.M. (Figure 5.27 A). Nevertheless, the proliferation rate did not change across the conditions indicating that the restriction of the migration ability is independent of an alteration of the cellular division (Figure 5.27 B-C) However, as mentioned for H376 cells, the experiment was performed only once, thus further repeats are required to validate these results.

A

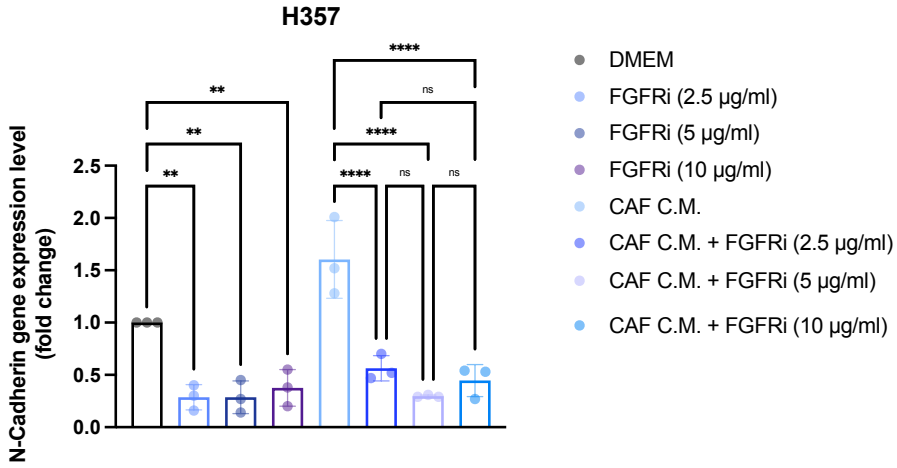

B

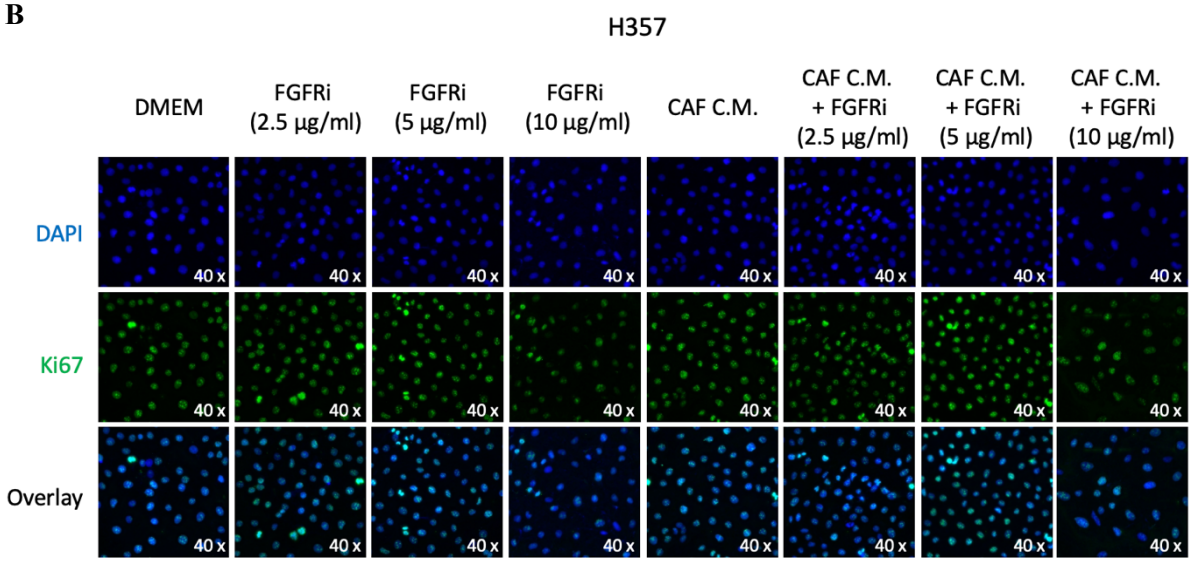

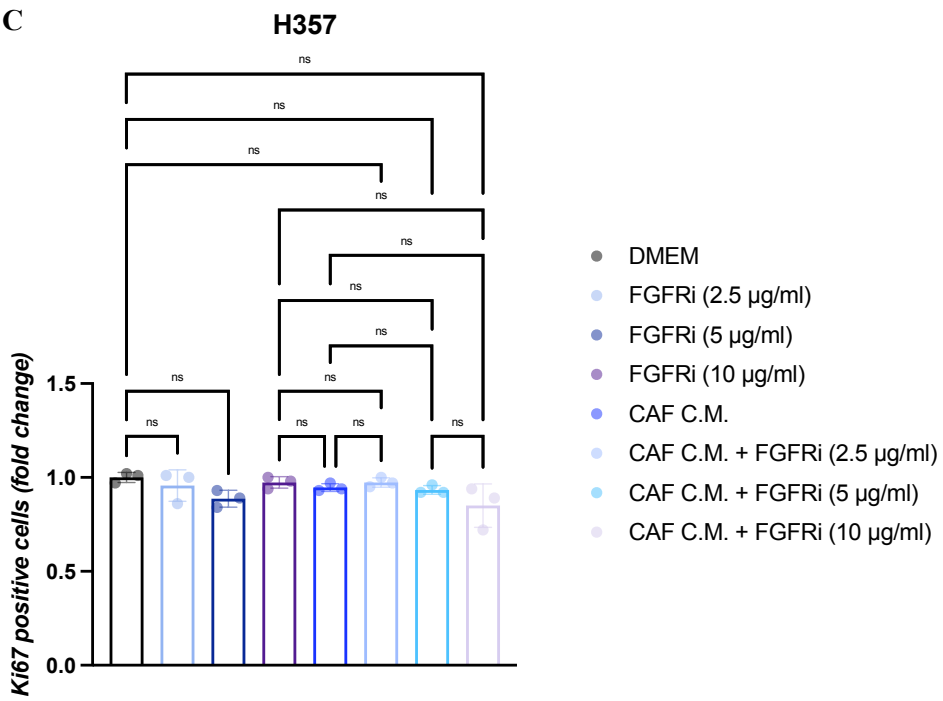

Figure 5.27 Determination of N-cadherin levels and proliferation status upon FGFR inhibition in H357 cells.

(**A**) qPCR showing N-cadherin levels in H357 upon treatment with the FGFRi as above-mentioned (n=1 t=1). (**B**) Ki67 immunofluorescence staining in H357 upon treatment with the FGFRi. Cells were viewed using a Zeiss Axioplan 2 fluorescence light microscope, at 20-40x, setting the filter for Excitement/Emission between 491 and 520. Images were acquired using Proplus 7.0.1 image software and analysed with Fiji by randomly picking four different areas and counting the Ki67 positive cells. The results were normalised to the control (untreated cells) and data reported as ratio between treated sample and its control (n=3 t=1). (**C**) Quantification of B. Each data represents the mean ± SD. P values were calculated via ordinary one way Anova (∗P ≤ 0.05, ∗∗P ≤ 0.01, ∗∗∗P ≤ 0.001, ∗∗∗∗ P ≤ 0.0001).

Since in section 5.2.5, table 5.2, FGF2 was one of the downregulated proteins upon ADAM17 depletion in CAFs, FGF2 levels were validated by both western blot and qPCR assays. At protein level, as reported by western blot assay, it was observed a decrease of FGF2, although not significant, of 1.6±0.11-fold ($p>0.05$), 3.4±0.1-fold ($p>0.05$) and 1.86±1.75-fold ($p>0.05$) in $CAF^{A17\ low}$ and $cCAF^{A17\ low}$ (previously incubated with the C.M. from either H357 or H376 cells) respectively, compared to their controls (Figure 5.28 A-B). The same trend was observed at RNA level, as detected by qPCR, displaying a decrease of FGF2 RNA levels by 1.5±0.1-fold ($p<0.05$), 1.7± 0.11-fold ($p<0.001$) and 1.5± 0.1-fold ($p>0.05$) in $CAF^{A17\ low}$ and $cCAF^{A17}$

low (previously incubated with the C.M. from either H357 or H376 cells) respectively, compared to their controls (Figure 5.28 C).

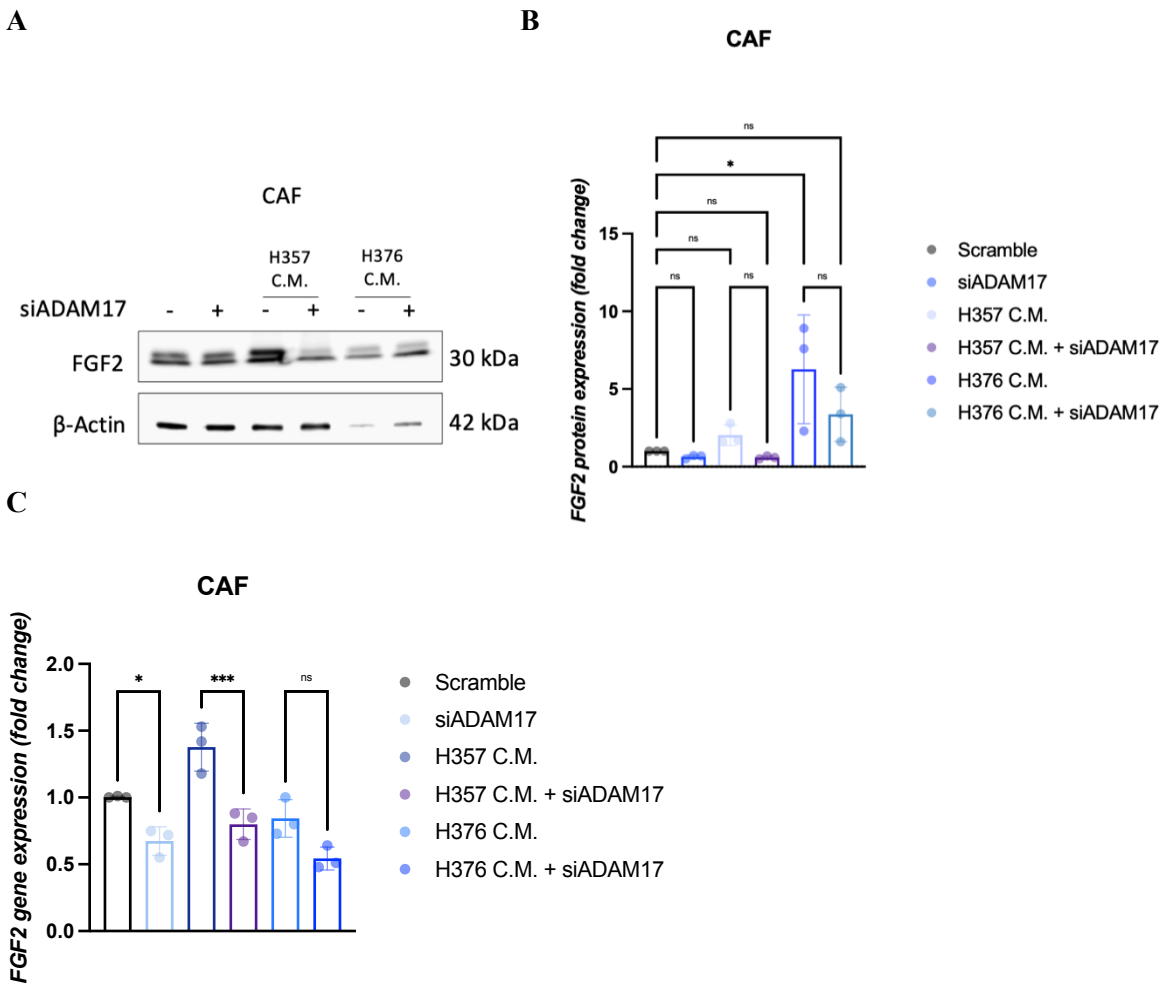

Figure 5.28 FGF2 validation in CAFs upon ADAM17 depletion.

*(**A**) Representative western blot showing FGF2 protein levels in CAFs conditioned with OSCC cell-derived C.M. followed by ADAM17 depletion. Cells were seeded in six well plates and incubated for 48 h with or without OSCC-cell derived C.M. until 50-60% confluent. Then, cells were depleted of ADAM17 by transfection (n=3 t=3). (**B**) Quantification of A. (**C**) Representative qPCR showing FGF2 RNA levels in CAFs conditioned with OSCC cell-derived C.M. followed by ADAM17 depletion (n=3, t=3). Each data represents the mean ± SD from three independent experiments. P values were calculated via ordinary one-way ANOVA (*P ≤ 0.05, **P ≤ 0.01, ***P ≤ 0.001, **** P ≤ 0.0001).*

To assess whether FGF2 could be involved in regulating the migratory property of cancer cells, both H357 and H376 cell lines were incubated with the C.M. derived from CAF$^{A17\ low}$ and then treated with 20 ng/ml of the recombinant protein FGF2 for 48 h (Lefèvre *et al.*, 2009). At the end of this incubation, cells were treated with the FGFR inhibitor, following the same protocol

used for Figures 5.24 and 5.27. Upon stimulation with the recombinant protein FGF2, the migratory potential of the cancer cells incubated with the C.M. derived from $CAF^{A17\ low}$ was comparable to that of the control but did not resemble that of the cancer cells incubated with the C.M. derived from ADAM17 proficient CAFs (Figure 5.29 A-C). Moreover, once the cancer cells treated with the recombinant protein FGF2 were challenged with the FGFR inhibitor, the migratory potential was restricted and its levels comparable to those observed in OSCC cell incubated with the C.M. derived from $CAF^{A17\ low}$ (Figure 5.29 A-C). Indeed, the migration rate in H376 cells decreased by 1.7±0.1-fold ($p<0.05$), 1.35±0.13-fold ($p>0.05$) and 1.25±0.15-fold ($p>0.05$) when incubated with $CAF^{A17\ low}$, $CAF^{A17\ low}$ and FGF2 followed by 5µg/ml of FGFRi, and $CAF^{A17\ low}$ and FGF2 followed by 10µg/ml of FGFRi compared to control (Figure 5.29 C). On the contrary, the migration rate increased by 1.8±0.13-fold ($p<0.01$) in H376 incubated with $CAF^{A17\ low}$ and FGF2 compared to those incubated with $CAF^{A17\ low}$ alone (Figure 5.29 C).

The same trend was observed for H357. Indeed, the migration rate decreased by 1.7±0.1-fold ($p<0.05$), 1.9±0.21-fold ($p<0.05$) and 1.75±0.25-fold ($p<0.05$) when incubated with $CAF^{A17\ low}$, $CAF^{A17\ low}$ and FGF2 followed by 5µg/ml of FGFRi, and $CAF^{A17\ low}$ and FGF2 followed by 10µg/ml of FGFRi compared to control (Figure 5.29 C). On the contrary, the migration rate increased by 1.8±0.08-fold ($p<0.05$) in H357 incubated with $CAF^{A17\ low}$ and FGF2 compared to those incubated with $CAF^{A17\ low}$ alone (Figure 5.29 C). Nevertheless, due to time constraints the experiment was performed only once thus, the results obtained are preliminary and require further repeats.

A

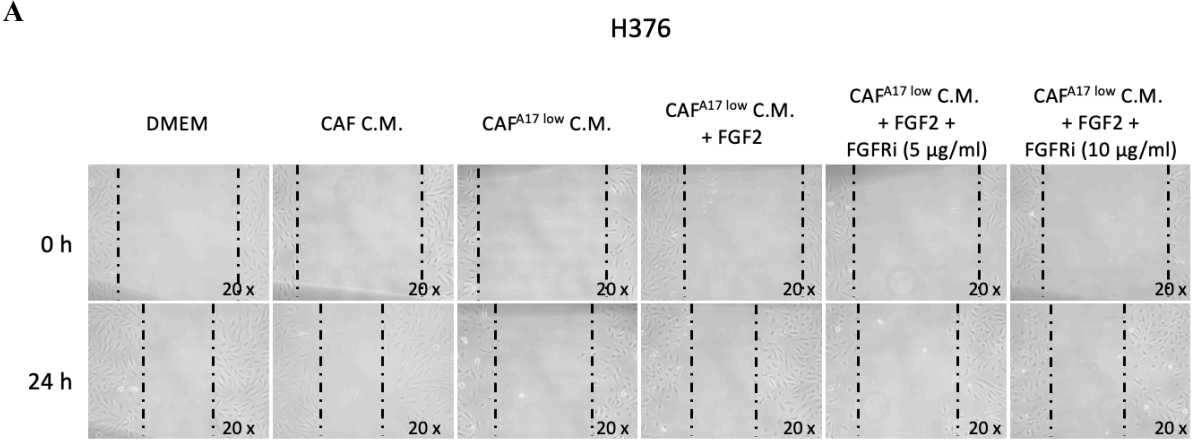

B

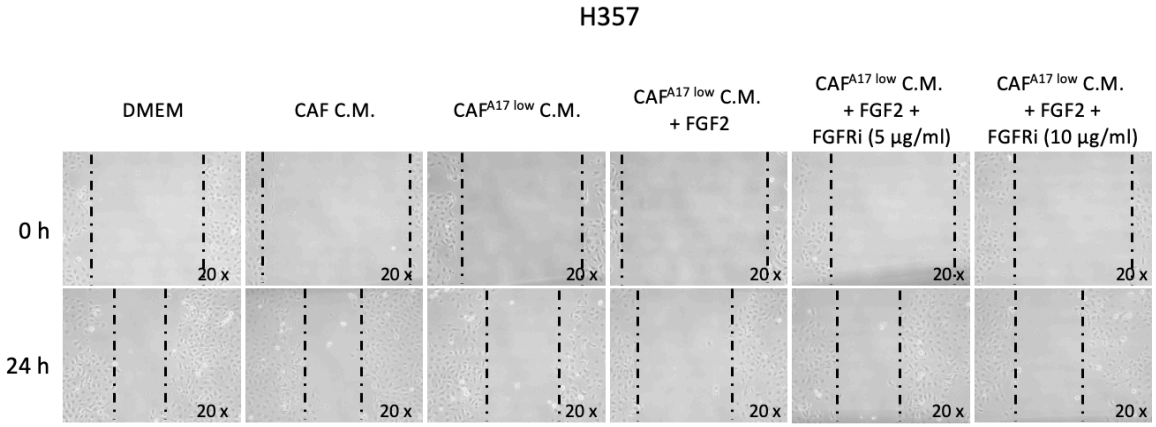

C

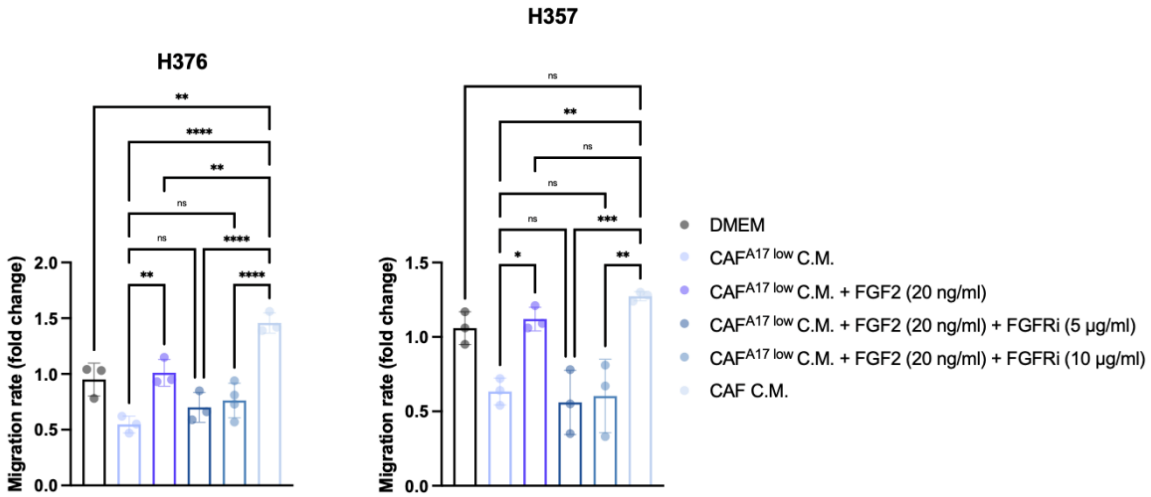

Figure 5.29 Determination of the influence of FGF2 on the migratory behaviour of OSCC cell lines.

*(**A**) and (**B**) Representative wound healing assays of H376 and H357 cells, respectively, upon incubation with the recombinant protein FGF2. Both cell lines were seeded in 6 well plates and after an incubation of 48 h with the C.M. derived from CAF$^{A17\ low}$ and 20ng/ml of the recombinant protein FGF2, the cells were treated with the FGFR inhibitor as previously described (n=3, t=1). (**C**) Quantification of A and B respectively. P values were calculated via ordinary one-way ANOVA (∗P ≤ 0.05, ∗∗P ≤ 0.01, ∗∗∗P ≤ 0.001, ∗∗∗∗ P ≤ 0.0001).*

The proliferation status of both H357 and H376 cells was determined by Ki67 immunofluorescence staining and it showed that there was not a significant change across the conditions when compared to their respective controls (Figure 5.30 A-C).

A

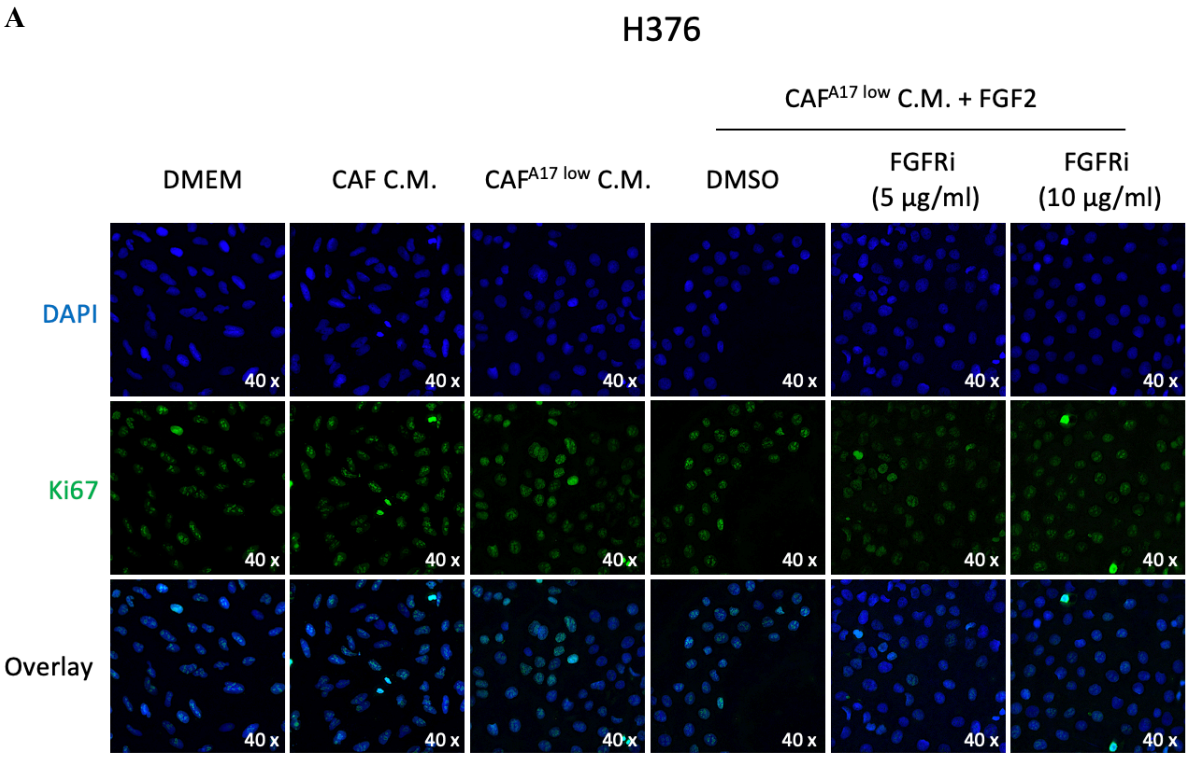
H376
CAF$^{A17\ low}$ C.M. + FGF2
DMEM
CAF C.M.
CAF$^{A17\ low}$ C.M.
DMSO
FGFRi (5 µg/ml)
FGFRi (10 µg/ml)
DAPI
Ki67
Overlay
40 x

B

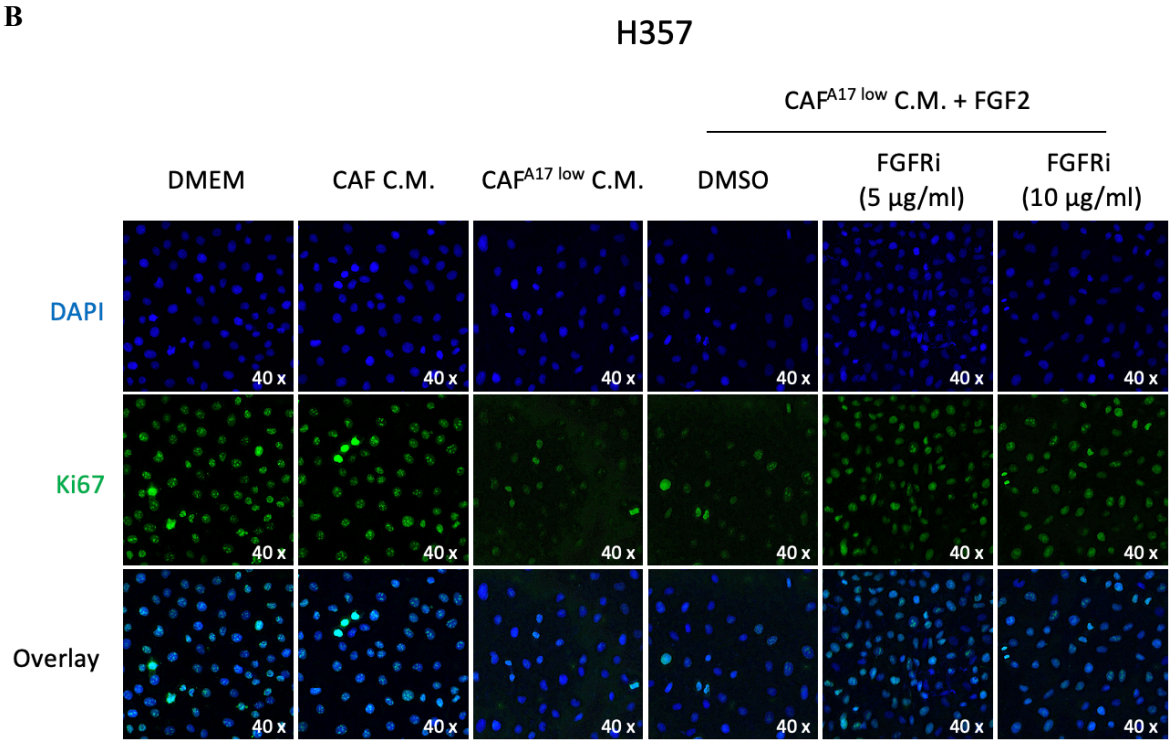
H357
CAF$^{A17\ low}$ C.M. + FGF2
DMEM
CAF C.M.
CAF$^{A17\ low}$ C.M.
DMSO
FGFRi (5 µg/ml)
FGFRi (10 µg/ml)
DAPI
Ki67
Overlay
40 x

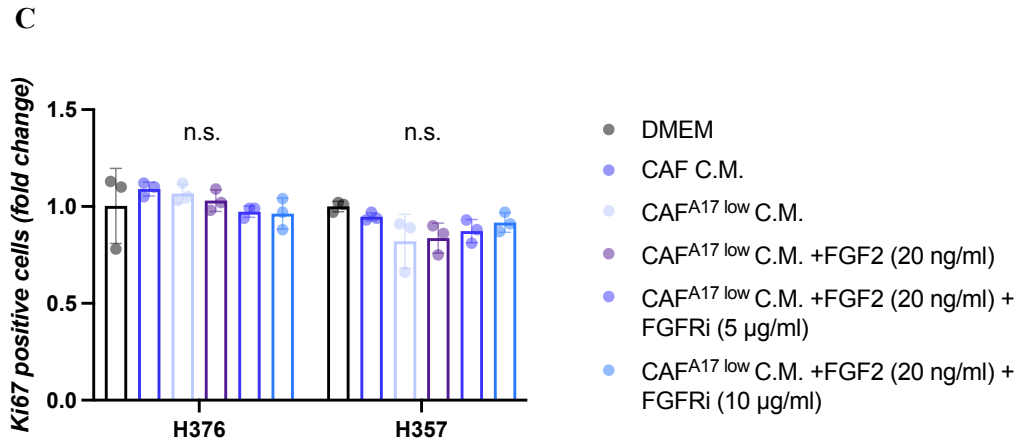

Figure 5.30 Proliferation status assessed by Ki67 immunofluorescence staining in H376 and H357 cells upon treatment with the recombinant protein FGF2.

*(**A**) and (**B**) Representative Ki67 immunofluorescence staining of H376 and H357 cells respectively, upon treatment with 20ng/ml of the recombinant protein FGF2. The cells were seeded and treated as describe in Figure 5.24 (n=3 t=1). (**C**) Quantification of A and B respectively. P values were calculated via ordinary one-way ANOVA (*P ≤ 0.05, **P ≤ 0.01, ***P ≤ 0.001, **** P ≤ 0.0001).*

5.3 Discussion

To get a deeper insight into the fibroblast response to ADAM17 depletion, proteomics analysis was performed and the differentially expressed proteins were examined. Amongst the proteins which were significantly upregulated in CAF$^{A17\ low}$ there were some involved, directly or indirectly, in the Interferon Type I signalling pathway (TAP1, SLC4A7, NDFUFA5, ITPRIP, ACOX1). Although it was validated the upregulation of the Interferon Type I by assessing its markers by both western blot and qPCR assays, it was not involved in regulating the cancer cell migratory ability as shown by wound healing assay for cancer cells treated with the C.M. derived from CAFs depleted of STAT3 and STAT2. Moreover, the levels of N-cadherin did not change suggesting that ADAM17-mediated regulation of cancer cell migration does not exploit the STAT signalling pathway.

Considering the presence of proteins engaged in both the DDR and Interferon Type I response, the role of the DNA sensor receptor cGAS as potential mediator in the ADAM17-regulated cancer cell migration was investigated. The protein levels of cGAS seemed to slightly increase upon ADAM17 depletion, albeit that silencing in CAF did not recapitulate the effect observed with ADAM17 depletion as shown by wound healing assay of H376 cells treated with the C.M.

derived from CAF$^{cGAS\ low}$. The N-cadherin levels did not change either indicating that cGAS does not play a role in cancer cell migration.

Another pathway investigated was AKT (AKT1) because of its upregulation in CAFs upon ADAM17 depletion. As per the above-mentioned pathway, also AKT silencing in CAFs did not mimic the effect of ADAM17 depletion indicating that AKT has no role in regulating cancer cell migration in a paracrine manner. Altogether, these data seem to rule out the engagement of STAT2, STAT3, cGAS and AKT in the paracrine regulation of cancer cells by CAFs, contrary to what observed for CAF$^{A17\ low}$ and cCAF$^{A17\ low}$, thus implying further investigation to determine the mechanism underpinning the ADAM17-N-cadherin axis behind cancer cell migration. However, these data need further validation since the siRNA experiments were performed only once due to time constraints and further cancer cell lines would be needed to strengthen the reliability of these findings.

Moreover, after a second mass spectrometry analysis, performed using the samples generated from a second independent experiment and according to the same conditions as per the first attempt, a comprehensive examination was carried out on the two datasets originated from both the proteomics assays. In doing so, the datasets were screened and combined in order to create a unique list containing the proteins which show a consistent differential expression. This confirmed some of the proteins shortlisted in the first attempt (IFIT1, TAP1, CD59 etc.) and pointed out novel potential targets (FGF2, NES, PDGFRA etc.). In both cases, some of these proteins have been reported to be associated, directly or indirectly, with ADAM17 functions, such as those involved in fibrosis and immune response (e.g. FBN1, FBN2, COL1A1, CSTB etc.) (Chalaris, Adam, *et al.*, 2010; Chalaris, Gewiese, *et al.*, 2010; Kefaloyianni *et al.*, 2016; Tholen *et al.*, 2016) whereas others have no previous documentation supporting this correlation (NES, CALD1, CD59, OAS2, IFIT1 etc.), thus meaning that further analyses will be necessary to validate and elucidate this aspect and the mechanisms underpinning their ADAM17-mediated regulation. In addition, FGF2 has been demonstrated to negatively regulate the anti-viral immune response hence potentially explaining the upregulated anti-viral response observed in CAFs upon ADAM17 depletion (Liu, Luo and Yang, 2015).

Cancer cell motility can be triggered by diverse stimuli which in turn activate signalling pathways such as the EGFR and FGFR signalling cascades (Qian *et al.*, 2013; Paul, Mistriotis and Konstantopoulos, 2016; Weiss, Lauffenburger and Friedl, 2022). EGFR and FGFR can be activated respectively by their ligands EGF and FGF, known to be two of the multitude of factors secreted by CAF (Sahai *et al.*, 2020; Chen, McAndrews and Kalluri, 2021) and shown

to be, directly or indirectly, regulated by ADAM17 (Baumgart *et al.*, 2010; D'Amici *et al.*, 2013; Zunke and Rose-John, 2017; Zivotic *et al.*, 2018). Thus, supported by the proteomics finding which suggested downregulation of FGF2, albeit inconclusively validated by western blot and qPCR assay, and PDGFRA, known to modulate key pathways such as the EGFR and the FGFR, in this chapter it was investigated whether the EGFR or the FGFR signalling pathways could play a role in the ADAM17/N-cadherin axis within the CAF-cancer cells crosstalk. Firstly, both H357 and H376 were treated with human recombinant EGF in the presence or absence of the EGFR inhibitor Gefitinib. The western blot data showed no change in N-cadherin protein levels suggesting that EGFR may not be involved in the ADAM17/N-cadherin axis. However, these results do not exclude a role of EGFR in regulating cancer cell migration since no migration assay was performed to assess this property.

Secondly, to investigate the role of FGFR, both H357 and H376 cells were treated with the FGFRi SR128129E at three concentrations for 24 h. The wound healing assay evidenced a clear and significant restriction of both H376 and H357 cell migratory ability, though there was no difference between the two concentrations. The negative regulation of cancer migration was also observed when treated with the C.M. derived from CAFs, suggesting that FGFR inhibition is enough to counteract the pro-migratory effect derived from CAF conditioned medium. Consistently with this observation, the N-cadherin RNA levels show a clear and consistent decrease in both H357 and H376 treated with the FGFRi.

In addition, to determine the role of FGF2 in mediating the cancer cell motility, both H357 and H376 incubated with the C.M. derived from ADAM17-deficient CAFs were then treated with FGF2. These experiments showed that cancer migration was restored, nearly resuming the levels of those cells incubated with the C.M. from ADAM17-proficient CAFs. Altogether, these findings potentially corroborate the hypothesis of the involvement of CAF-derived FG2 in restricting cancer cell migration.

However, due to time constraints the experiment was conducted only once thus requiring further repeats to validate and optimise the findings.

Chapter 6: Discussion

6.1 Overview

Cancer is a chronic disease and is the second leading cause of death globally. Despite the rapid and effective advances in cancer research, cancer burden is constantly rising thus posing not just a threat to life but also a significant strain on the healthcare systems (WHO, 2020).

After decades of a cancer-centric view focussed on dissecting malignant features regardless the environmental context within it is harboured, the last 20 years have been characterised by an intense and growing interest in investigating the surrounding and, more recently, distant but finely interconnected environments (tumour microenvironment-TME- and tumour environment/tumour organismal environment-TE/TOE- respectively) paving the way to a more comprehensive approach in cancer research (Laplane *et al.*, 2018, 2019b; Maman and Witz, 2018; Jin and Jin, 2020). This modern approach is the result of a gradual and constant process stemming from the failure of tackling cancer through the canonical therapeutic strategies, tailored largely exclusively on neoplastic-intrinsic features, along with the increasing awareness of the pivotal role played by non-malignant cells during tumorigenesis and metastasis (McAllister and Weinberg, 2014; Laplane *et al.*, 2018, 2019b; Jin and Jin, 2020). The focus on TME has helped explain aspects of tumour pathogenesis which are driven or influenced in a non-genetic and non-cell autonomous manner (McAllister and Weinberg, 2014; Lambert, Pattabiraman and Weinberg, 2017; Laplane *et al.*, 2019b; Hanahan, 2022). Thus, the TME components, as determinants of cancer progression and active players in the bidirectional interactions with the neoplastic cells, emerged as potential candidates to design more precise and more effective therapeutic strategies.

In this scenario, CAFs represent one of the most studied TME components although, due to their high heterogeneity in subpopulations and functions, their targeting, by reprogramming or by depletion in cancer therapy, remains challenging. Thus, to overcome this weakness, another approach would be to block the signals derived from CAFs or those deriving from neoplastic cells which promote their formation (Sahai *et al.*, 2020). For instance, targeting CAF-derived cytokines, growth factors and ECM components is a potential strategy to modulate cancer cell-CAFs crosstalk. Indeed, inhibition of the CXCL12 receptor on cancer cells increases the accumulation of T-cells thus allowing the clearance of cancer cells, and targeting PDGF-CC

derived from malignant cells inhibited CAFs recruitment and their induction of cancer growth and angiogenesis (Diop-Frimpong *et al.*, 2011; Feig *et al.*, 2013; Bai *et al.*, 2015). A fundamental part in cell:cell communication is played by the ADAMs, known to be upregulated in a variety of cancers and to modulate pro-tumorigenic functions in both an autocrine and paracrine manner, thus influencing the TME (Borrell-Pagès *et al.*, 2003; Garton, Gough and Raines, 2006; Kuefer *et al.*, 2006). However, most investigation of the ADAMs has focussed on cancer cells thus overlooking their contribution to ADAM-mediated influences on the TME. Within the ADAMs, ADAM17 is the most widely and deeply investigated of the ADAMs family, especially in cancer, although, due to its pleiotropic nature and functional redundancy with other metalloproteinases, its targeting is still challenging.

To date, despite a few studies characterising ADAMs expression in the stroma and showing upregulation of diverse ADAMs in CAFs, these findings point to a pivotal role of CAF-associated ADAMs in orchestrating cancer progression (Peduto *et al.*, 2006; Gao *et al.*, 2013; Ishimoto *et al.*, 2017; Mochizuki *et al.*, 2019). Nevertheless, the mechanisms underpinning both the upregulation of ADAMs in CAFs and the CAF-associated ADAMs modulation of cancer progression remain still elusive.

In this regard this project showed, for the first time, a potential mechanism underlying the upregulation of ADAM17 in CAFs and how this might contribute to a CAF-mediated exacerbation of malignant traits by cancer cells. Indeed, this project demonstrated that cancer cells induce the upregulation of ADAM17 in neighbouring fibroblasts which in turn sheds factors promoting the migration of cancer cells at least in part by upregulating N-cadherin. Targeting of CAF-associated ADAM17 and cancer cell-associated N-cadherin hinders this crosstalk and hampers cancer cell migration. Collectively, this study identified a novel ADAM17-N-cadherin axis contributing to pro-migratory CAF:cancer cell interactions.

6.2 Cancer cells induce ADAM17 upregulation in stromal fibroblasts to create a protumorigenic environment

Malignant progression lies in the well-established network engaged by neoplastic cells with stromal cells, especially with CAFs. CAFs in turn provide cancer cells with the cues to support cancer cell survival and progression under challenging conditions, such as anticancer therapy. Most of CAF functions are exerted in a paracrine fashion by releasing a broad range of molecules, from cytokines to growth factors and ECM components. To date, the majority of

the studies dedicated to understanding the cancer cell:CAF bidirectional interactions focussed on mainly two aspects: how cancer cells give rise to CAFs (first step within the crosstalk) and how CAFs support neoplasia (final step within the crosstalk). Although both approaches contributed to advances in therapeutic strategies, the current clinical treatments are still not thoroughly tackling disease. This state-of-the art could be possibly explained by the complexity of targeting cancer cells, which are genetically unstable and frequently overcome any targeted therapy in the long term, and by the complexity of CAFs, which are highly heterogeneous and each subset likely to contribute to cancer development in a specific and different manner, thus making it difficult identifying a definitive CAF-targeted therapy. Thus, considering that CAFs are genetically stable, a promising approach would be targeting the root cause of their versatile functions (intermediate step of the crosstalk). In this regard, the role of ADAMs might be central given that some members are sheddase proteins contributing to the activation and release of a large number of substrates involved in malignancies.

In this regard, ADAM17, known to shed over 80 substrates, including TNF-α, EGFR ligands, NOTCH ligands etc., would represent a promising candidate for a CAF-targeted therapy. Most of the studies about ADAM17, and in general on ADAMs, have been conducted in cancer cells, however, only a few recent studies shed light on ADAMs functions in CAFs. These studies have demonstrated a crucial role of ADAMs, including ADAM17, in CAFs as determinants to sustain cancer progression (Peduto *et al.*, 2006; Gao *et al.*, 2013; Ishimoto *et al.*, 2017; Mochizuki *et al.*, 2019). For instance, CAFs derived from breast cancer patients have been shown to express high levels of ADAM17, compared with the matched normal tissue, which cleaved TGF-α thus promoting cancer cell proliferation via AKT, ERK and EGFR signalling pathways (Gao *et al.*, 2013). Moreover, high levels of ADAM17 were found in CAFs derived from gastric cancer patients, compared with matched normal fibroblasts (NFs). ADAM17 was found to be activated by RHBDF2 and also expressed at higher levels in CAFs than NFs, resulting in promotion of CAF motility through the TGF-β1 signalling pathway, which conferred invasive properties to gastric cancer cells (Ishimoto *et al.*, 2017).

For the first time, in this PhD thesis it was shown that OSCC cancer cells can trigger the upregulation of ADAM17 levels (both transcriptional and translational) and activity in both CAFs and NOFs which in turn acquire pro-tumorigenic properties, eventually exploited by cancer cells. This observation coincided with the acquisition of CAF-like features by NOFs, therefore suggesting a potential involvement of ADAM17 in mediating a CAF-like phenotype under certain conditions, such as the (indirect) coculture with cancer cells. This novel aspect is

important and in line with a previous study which demonstrated, using an engineered mouse model, that loss of all four tissue inhibitor of metalloproteinases (TIMPs), some of which inhibit ADAM17, bestowed the normal fibroblasts with CAF-like traits, both at morphological and functional level (Shimoda *et al.*, 2014). Moreover, it has been reported that normal fibroblasts derived from gastric cancer patients acquire CAF-like traits when transfected with the RHBDF2 (also known as iRHOM2, a key regulator of ADAM17 (Adrain *et al.*, 2012)) plasmid, due to its activation of the TGF-β1 signalling pathway through ADAM17 (Ishimoto *et al.*, 2017). Similarly, another *in vivo* study showed that mice with inducible ADAM17 knock-out (KO) in proximal tubules were more protected against kidney fibrosis and displayed decreased fibrotic markers such as α-SMA and fibronectin along with a reduced collagen deposition in the kidney cortex (Kefaloyianni *et al.*, 2016). However, unlike the work of Shimoda *et al*. and Kefaloyianni *et al.* but in agreement with the work by Ishimoto et al., the findings reported in this thesis indicated that ADAM17 depletion in CAFs only marginally affected CAF morphology. This could be explained by the fact that other metalloproteinases and ADAMs are still functional thus contributing to the maintenance of a CAF-like morphology and that ADAM17 alone does not impinge on this aspect, despite its implication in regulating signalling pathways which are known to sustain such traits (i.e. TGF-β1) (Wang *et al.*, 2008; Malapeira *et al.*, 2010). In addition, in another study using a mouse model for cardiomyocyte-specific ADAM17 depletion, ADAM17 deficiency was associated with an enhanced myocardial fibrosis under pressure-overload due to increase and accumulation of integrin-β1, which otherwise would have been cleaved by ADAM17 and eventually cleared (Fan *et al.*, 2016). Altogether, these data suggest a further variable to ADAM17 contribution to fibrosis, which is the tissue specificity. This represents a fundamental aspect to consider when designing ADAM17 targeted therapy since, depending on the response of the tissue under treatment, the result could range from pro-tumorigenic (through an increase of fibrosis which, due to an exacerbated stiffness, might support cancer cell growth, angiogenesis and impede both the infiltration of anti-tumour immune cells and drug delivery) to anti-tumorigenic (reduction or clearance of fibrotic tissue) (Goetz *et al.*, 2011; Swartz and Lund, 2012; Acerbi *et al.*, 2015; Chandler *et al.*, 2019; Zaghdoudi *et al.*, 2020).

Nevertheless, ADAM17, through its sheddase activity, may represent a potential regulator of CAF-mediated cancer cell behaviour, as evidenced by migration and invasion assays of OSCC cells. This experiment showed that OSCC cancer cell migratory and invasive capacities increased when incubated with the C.M. derived from NOFs, which were previously

conditioned with the C.M. derived from cancer cells, and CAFs, whereas these effects were restrained when incubated with the C.M. derived from ADAM17-depleted CAFs. Of note, although the role of ADAM17 in cancer cell migration has been extensively investigated by its depletion in cancer cells, showing that ADAM17-depleted cells migrate and invade less than their respective controls (Das *et al.*, 2012; Lv *et al.*, 2014; Hong *et al.*, 2016), the data reported in this thesis are the first to illustrate a paracrine regulation of cancer cells migration and invasion mediated by CAF-associated ADAM17. Importantly, here it was also demonstrated, for the first time, that the ADAM17-mediated paracrine regulation of OSCC cancer cell migration might be a CAF specific property, since OSCC cells treated with the C.M. derived from ADAM17-depleted OSCC cells did not migrate less compared with their respective control. Nonetheless, contrary to what has been reported by most of the studies (Lv *et al.*, 2014; Hu *et al.*, 2018; Jiao *et al.*, 2018; Xiang *et al.*, 2020), ADAM17 depletion in cancer cells did not alter their proliferation, as evidenced by EdU incorporation assay. However, this observation was consistent with a few works characterising ADAM17 in other cancer cells and cell types, such as mouse colon carcinoma cells and lymphatic endothelial cells (LECs) (Das *et al.*, 2012; Mężyk-Kopeć *et al.*, 2015).

Neoplastic cells are thought to give rise to CAFs also through their secretome and, amongst the factors, TGF-β1 represents the most investigated (Casey *et al.*, 2008; Wen *et al.*, 2015; Yoon *et al.*, 2021). It has been reported that there is a mutual engagement/regulation between TGF-β1 and ADAM17 (C. Liu *et al.*, 2009; Wang *et al.*, 2009; Malapeira *et al.*, 2010; Ramdas *et al.*, 2013; Xu *et al.*, 2016). For instance, TGF-β1 engages ADAM17 to potentiate the downstream ErbB signalling in breast cancer cell lines (Wang *et al.*, 2009), whereas ADAM17 negatively regulates TGF-β1 by cleaving vasorin in breast cancer cells (Malapeira *et al.*, 2010) or activates it in gastric cancer cells (Xu *et al.*, 2016). Consistent with Ramdas *et al.*, who showed that TGF-β1 induces the upregulation of some ADAMs, including ADAM17, in a rat model of renal fibrosis, here in this PhD study it was demonstrated that TGF-β1 stimulation of NOFs triggered their transdifferentiation into eCAFs, as previously reported (Abidin *et al.*, 2021), and, more pertinently to this study and for the first time, to an increased expression of ADAM17, in a dose dependent fashion. Moreover, in line with Xu *et al.*, ADAM17 depletion in eCAFs negatively regulated TGF-β1 signalling, as shown by lower levels of the phosphorylated from of SMAD3 and, although mildly, the myofibroblastic phenotype as shown by a reduction of both α-SMA and collagen I levels. Therefore, these data indicate that TGF-β1 and ADAM17 may mutually regulate each others'functions, suggesting TGF-β1 as a

potential mediator of CAF-associated ADAM17 expression, even though it might not be the only factor responsible of it, and ADAM17 inhibition in CAFs as a valuable and alternative strategy for CAFs-targeted therapies.

6.3 Targeting ADAM17 in CAFs restrains cancer cell migration by negatively regulating N-cadherin in cancer cells maybe through the FGF2/FGFR signalling pathway

One of the most challenging aspects of cancer is metastasis. Considerable investments have been made and significant advances achieved in the development of new therapeutics and yet metastases still represent the major cause of death from solid tumours. Fundamental to the metastatic process it is the acquisition of an invasive and motile capacity by the malignant cells, which could be dependent or independent of EMT. ADAM17 has been implicated in regulating metastasis and invasion has been reported in cancer cells from a variety of tissues via diverse mechanisms of actions (Lv *et al.*, 2014; Xu *et al.*, 2016; Li *et al.*, 2018; Xiang *et al.*, 2020). On the other hand, less is known about the influence of CAF-associated ADAM17 on cancer cell motility and invasive features. To date, the only published work reporting a similar phenomenon associated, although indirectly, with ADAM17, shows that gastric cancer cells acquire an invasive capacity when directly co-cultured with CAFs overexpressing RHBDF2, possibly through the activation of ADAM17 (Ishimoto *et al.*, 2017). More importantly, the current thesis shows, unlike Ishimoto *et al.*, a potential mechanism underlying the CAF-associated ADAM17 regulation of cancer cell migration. Indeed, the cancer cells which were incubated with the C.M. derived from ADAM17-depleted CAFs migrated less as compared to their controls and expressed lower protein and RNA levels of N-cadherin, a key regulator of EMT and cancer migration (Hazan *et al.*, 2004). More importantly, N-cadherin levels were even higher in cancer cells incubated with the C.M. derived from CAFs, which were previously treated with the C.M. derived from cancer cells (cCAFs) and that were shown to express higher levels of ADAM17. Altogether these findings suggest that cancer cells induce the upregulation of ADAM17 in CAFs in order to sustain their pro-migratory activity by the upregulation of N-cadherin. In keeping with this observation, chemical targeting of cancer cell-associated N-cadherin by ADH-1 (an N-cadherin antagonist (Shintani *et al.*, 2008)) mirrored the effect of

the C.M. derived from ADAM17-depleted CAFs as shown by the impaired cancer cell migration.

Strikingly, upon mass-spectrometry analyses of CAFs with and without ADAM17, amongst the proteins differentially expressed between the two groups, there were some potentially involved in regulating cancer cell migration, in particular the fibroblast growth factor 2 (FGF2). Assessment of FGF2 levels by western blot and qPCR assays, under the same conditions, in CAFs showed a significant reduction of FGF2, thus prompting the investigation of its role in cancer cell migration. FGF2 is one of the ligands and activators of the FGF receptor (FGFR) tyrosine kinases, which are known to synergistically work with N-cadherin. Indeed, N-cadherin binds to and stabilises FGFR therefore preventing its internalisation and degradation (Suyama *et al.*, 2002). Moreover, in human pancreatic cancer xenografts, reduced cancer cell invasiveness was observed as a consequence of a decrease of N-cadherin levels upon inhibition of the FGFRs (Taeger *et al.*, 2011). In another study, N-cadherin and FGF2 have been shown to synergise and exacerbate the invasive potential of N-cadherin expressing breast cancer cells (Hazan *et al.*, 2000). FGF2 has been reported to be fundamental to CAF-mediated cancer progression as outlined in studies using breast cancer cell lines which proliferated, migrated and invaded more upon incubation with the C.M. derived from CAFs via the FGF2-FGFR1 axis (Suh *et al.*, 2020, 2022). In fact, in line with the literature, here in this thesis it was demonstrated that chemically inhibiting the FGFR signalling pathway hampered cancer cell migration also in cancer cells previously incubated with the C.M. derived from CAFs. In addition, the N-cadherin RNA levels showed a significant reduction which may indicate that the reduced migration upon FGFR inhibition is dependent on N-cadherin status. In line with this observation and with the hypothesis of a role of FGF2 in regulating cancer motility, the migratory ability of cancer cells incubated with the C.M. derived from $CAF^{A17\ low}$ was rescued upon treatment with the human recombinant protein FGF2. However, to further corroborate this speculation, the FGFR inhibitor concentration and incubation time should be optimised. Unfortunately, due to time constraints, the experiment was performed only once thus calling for further repeats to confirm the findings. Moreover, it would be necessary to include further cancer cell lines to determine whether these findings are consistent.

Nonetheless, these results are quite promising, especially compared to the attempts reported in Chapter 5, sections 5.2.2-4, to target signalling pathways and investigate other differentially expressed proteins obtained via mass-spectrometry analyses. Other proteins negatively regulated in ADAM17-depleted CAFs were PDGFRA, known to engage with EGFR in mutual

transactivation (He *et al.*, 2001; Chakravarty *et al.*, 2017) and A-kinase anchoring proteins 12 (AKAP12), which participates in EGFR transactivation by facilitating protein kinase A (PKA) mediated phosphorylation of naked cuticle homolog 2 (NKD2), ultimately favouring its binding to the EGFR activator TGF-α (Cao *et al.*, 2019). Thus, considering the role of EGFR in cancer (Damstrup *et al.*, 1998; Ritter and Arteaga, 2003; Zhen, Guanghui and Xiefu, 2014), this thesis investigated whether its targeting in cancer cells incubated with the C.M. derived from CAFs could hamper their migratory capacity. Unlike the result of of targeting the FGFR pathway, inhibition of EGFR did not show any influence on cancer cell behaviour. However, as per the FGFR inhibition experiment, further repeats would be required to confirm these findings since, due to time constraints, it was performed only twice and the exposure time might need to be extended to appreciate any differences across the conditions. However, these data were consistent with work showing that inhibition of the EGFR signalling in OSCC cell lines affected the migration in a cell-dependent manner, restraining it in some cell lines and sparing it in others (Ohnishi *et al.*, 2017).

6.4 CAF-associated ADAM17 may regulate the interferon type I signalling pathway

ADAM17 functions as a regulator of the immune response and inflammation is well known and has been extensively described (Moss and Minond, 2017b; Düsterhöft, Lokau and Garbers, 2019). Moreover, it has been proved to play a pivotal role in cancer disease also through the cleavage and release of pro-inflammatory cytokines (e.g. CD154 transmembrane cytokine, member of the TNF family, expressed primarily by the T cells (Yacoub *et al.*, 2013; Hassan, Stagg and Mourad, 2015)) and their receptors (e.g. IL6-R (Chalaris, Gewiese, *et al.*, 2010; Yousefi *et al.*, 2019)), chemokines and adhesion molecules (e.g. L-selectin on the neutrophils (Wang *et al.*, 2010; Watson *et al.*, 2019)).

In addition to the above-mentioned substrates, recent evidence has shown that ADAM17 can also regulate the availability of another class of cytokines, whose immunomodulator role in malignancies is well documented (Parker, Rautela and Hertzog, 2016): the interferons. Interferon γ (IFNγ or IFNG), which is the only interferon type 2, is known to exert anti-tumorigenic functions (Kaplan *et al.*, 1998), and has been reported to be proteolytically degraded by ADAM17 thus neutralising its antitumorigenic effects (Kanzaki *et al.*, 2016).

What is less well investigated is the potential of ADAM17 to regulate interferon type I (IFN-I) family, especially in the context of cancer. Indeed, most of the literature describes its role in the context of autoimmune diseases. For example, in a study using a model of the systemic lupus erythematous (SLE) autoimmune disease, it was demonstrated that IFN-I downregulated ADAM17 in Langerhans cells therefore leading to photosensitivity (T. M. Li *et al.*, 2019). In another study using macrophages, it was demonstrated that the stimulator of interferon genes (STING), an important endoplasmic reticulum (ER)-associated sensor implicated in DNA-induced immune signalling, activates ADAM17 which in turn promotes an inflammatory response by cleaving and releasing the plasma membrane protein semaphorin 4D (SEMA4D) (Motani and Kosako, 2018).

More importantly, it has been demonstrated that one of the mechanisms underpinning the refractiveness of solid tumours to conventional cancer immunotherapy, established by the creation of an immunosuppressive environment, can occur through inhibiting the anti-tumour type I interferon response by downregulating the receptor IFNAR1 within the stroma (the author focussed on the cytotoxic lymphocytes) (Katlinski *et al.*, 2017). Likewise, another study reported that CAFs, within colon and pancreatic ductal adenocarcinoma tumours, downregulate IFNAR1 therefore leading to stromagenesis and cancer progression (Cho *et al.*, 2020). More recently, it was observed that direct contact between cancer cells and CAFs triggered the interferon type I response upon the activation of the STING signalling cascade (Arwert *et al.*, 2020). However, to date no reports describe any role of CAFs in modulating the interferon response via ADAM17. Thus, the current PhD work is the first evidence of a potential role of ADAM17 in mediating an interferon type I signature within CAFs, whose effects on cancer are worthy of further investigation. Indeed, here it is reported that upon depletion of ADAM17 in CAFs, amongst the upregulated proteins there are some involved in the interferon type I response and anti-viral signalling such as OAS2, OAS3, IFIT1, IFIT3, IFI35, SAMHD1, TAP1, TAP2 and PARP14. However, unlike Arwert *et al.* who observed a similar signature mainly upon a direct co-culture between CAFs and cancer cells, explaining its upregulation with the activation of STING by the cytoplasm derived from cancer cells, here the interferon related genes were induced by simply depleting ADAM17 in CAFs. In addition, the activation of the interferon type I pathway was also supported by the increased phosphorylation of its key mediators STAT1 and STAT2.

Interestingly, some of the above-mentioned markers were validated by molecular analyses (qPCR and WB) and it was observed that, similarly to Arwert *et al*., upon stimulation with the

conditioned medium derived from cancer cells there was a strong upregulation of these markers but, more importantly, this was further exacerbated by ADAM17 depletion in CAFs. Although due to time constraints it was not possible to determine either the mechanism(s) underlying this phenomenon or its impact on the modulation of the immune response (for example by evaluating the interaction of immune cells with cancer cells incubated with the C.M. derived from ADAM17-depleted CAFs) , these data show for the first time a potential implication of CAF-associated ADAM17 in fine tuning interferon signalling which may be crucial in developing therapeutic strategies based on the interferon type I pathways and the anti-viral response. For example, trying to understand whether the upregulation of the antiviral signature could compromise the oncolytic virus anticancer therapy, as suggested by Arwert *et al.* (Arwert *et al.*, 2020).

6.5 Conclusions and significance of the study

Research into CAFs still represents one of the most promising avenues within the complex field of cancer research. Several attempts to target CAFs to date have failed due to poor efficacy or worsening of patient conditions (Catenacci *et al.*, 2015; Ramanathan *et al.*, 2019). The identification of new biomarkers, therefore, taking into account CAF heterogeneity and their role in the crosstalk with the other cell types within the TME, is critical and may lead to identification of new therapeutic strategies.

Amongst the diverse approaches suggested to advance the understanding of CAFs, those scrutinised within this thesis are:

1. Investigation of the signal(s) activating CAFs;
2. Investigation of the molecular player(s) underlying CAFs activation;
3. Investigation of the pro-tumorigenic signal(s) derived from CAFs;
4. Investigation of the molecular changes elicited within cancer cells by CAFs.

Although with some limitations, due to time constraints which did not allow definition of a complete mechanism behind some of these aspects, the current study is the first to explore the contribution of CAF-associated ADAM17 in the acquisition of cancer cell aggressive traits, such as invasion and migration. In brief, this thesis has shed light on a novel aspect of the bidirectional interaction between cancer cells and CAFs, by demonstrating that cancer cells do

not just convert indolent fibroblasts to CAFs but, more importantly, they instruct them, through their secretome (signal activating CAFs), to upregulate ADAM17. ADAM17 upregulation in CAFs contributes to strengthening of CAF features and exacerbate CAF protumorigenic functions (mechanism underlying CAF activation) at least *in vitro*. Hence, CAFs with high levels of ADAM17 may provide cancer cells with a special environment which renders them more aggressive and motile by inducing their upregulation of N-cadherin (change elicited in cancer cells).

Thus, the novel findings of the current study can be summarised as follows:

1. Cancer cell interaction with CAFs is instrumental in inducing tumour promoting CAFs and it can occur through a paracrine-mediated upregulation of ADAM17 expression and function in CAFs;
2. ADAM17 hyperactivation in CAFs contributes to the generation of a protumorigenic secretome which fosters cancer cell migration in an N-cadherin dependent manner, without affecting cell proliferation;
3. The upregulation of N-cadherin in cancer cells might be triggered by the release of FGFR ligands, such as FGF2, by CAFs expressing high levels of ADAM17;
4. Targeting the (CAF-associated) ADAM17: (cancer cell-associated) N-cadherin axis can restrain cancer cells from migrating and invading;
5. Targeting ADAM17 in CAFs may "convert" CAFs into a (perhaps) less tumour supportive CAF subtype (as shown by the downregulation of some CAF-associated markers, such as CALD1 and PDGFRA), whose properties need further investigation.

In addition to these findings, the work in this thesis also provides evidence that:

1. TGF-β1 might be one of the factors released by cancer cells to foster the formation of protumorigenic CAFs by upregulating ADAM17;
2. Cancer cell-associated ADAM17 does not mirror the functions exerted by CAF-associated ADAM17;
3. Targeting ADAM17 in CAFs plays a role in the modulation of the interferon type I signalling pathway.

Moreover, ADAM17 depletion in non-previously conditioned NOFs and CAFs was sufficient to impair cancer cell migration, suggesting that its targeting in stromal fibroblasts could form the basis of a preventive strategy. In other words, targeting ADAM17 in fibroblasts within incipient tumours could mean undermining a crucial player of the bidirectional interaction

between cancer cells and fibroblasts. Indeed, lowering ADAM17 levels in NOFs could prevent them from overexpressing ADAM17 and transdifferentiate into CAFs in response to cancer cell-derived stimuli. This, in turn, would impoverish their secretome of factors which could be, although to a lower extent compared to those released by CAFs, exploited by cancer cells for sustaining malignant progression.

6.7 Future work

As mentioned in the above section, time constraints were a major limitations, nonetheless, diverse aspects would be worth of elucidation to further strengthen the findings described within this thesis.

1. Dissecting the mechanisms behind the cancer cells-associated TGF-β1induction of ADAM17 in CAFs, for example by targeting TGF-β1 in CAFs (chemically or genetically) or by depleting cancer cell secretome from TGF-β1 (for example by using a neutralising antibody).
2. Translating the *in vitro* model into an *in vivo* experimental set up, either by xenografts using cancer cells previously incubated with the C.M. derived from ADAM17 proficient and deficient CAFs, thus evaluating their tumorigenic potential, or by using a genetically engineered mouse model of oral squamous cell carcinoma to selectively target ADAM17 in CAFs and assess its impact on cancer outcome. The latter approach could be exploited also to investigate the response to immunotherapy, given that ADAM17 depletion in CAFs induces an interferon type I and anti-viral signature (for example to understand the effects on the anticancer viral therapy).
3. Analysing the role of ADAM17 in CAFs derived from patients affected from other types of cancers, in order to understand whether ADAM17 upregulation in CAFs is a conserved strategy adopted by cancer cells.
4. Assessing the impact of the secretome derived from ADAM17-depleted CAFs on the immune cells. This aspect could be investigated accordingly two approaches:
    I. co-culturing cancer cells, previously incubated with the C.M. derived from ADAM17-depleted CAFs, with immune cells (for example NKs, macrophages) to evaluate the type of interaction engaged (are the immune cells attracted/recruited by cancer cells? Are the immune cells skewed towards a tumour-promoting type?);

II. immune cells incubation with the C.M. derived from ADAM17-depleted CAFs to analyse their phenotype (for example by flow cytometry to detect their distinctive signature) and functional properties (for example their lytic capacity when co-cultured with cancer cells).

5. Evaluation of ADAM17 levels within the stromal fibroblasts at different stages of the tumours through immunohistochemistry (IHC) staining of tissue microarrays (TMA);
6. Analysis of the RNA-sequencing data of CAFs vs. ADAM17-depleted CAFs obtained through MinION, a portable and real-time device purchased from Oxford Nanopore technologies, which has been prevented by the limited read depth;
7. Investigation of the role of ADAM17 in autophagy and mitochondrial activity. This stems from the data derived from the proteomics analysis, which showed the upregulation of proteins associated with both mitochondrial functions (MRPL1, MRPL3, MRPL37, GFM1, GFM2, RPL27A, TOMM70A etc.) and the DNA damage response (EEF1E1, AARS, LARS, TRMT112, CIAPIN1, CARS2 etc.), and the western blot indicating an increase of some markers of autophagy (ATG3 and ATG5) along with cGAS (data that require further investigation to corroborate the findings).

References

Abidin, S.A.I.Z. *et al.* (2021) 'Myofibroblast transdifferentiation is associated with changes in cellular and extracellular vesicle miRNA abundance', *PLOS ONE*, 16(11), p. e0256812. Available at: https://doi.org/10.1371/JOURNAL.PONE.0256812.

Abulaiti, A. *et al.* (2013) 'Interaction between non-small-cell lung cancer cells and fibroblasts via enhancement of TGF-β signaling by IL-6', *Lung Cancer* [Preprint]. Available at: https://doi.org/10.1016/j.lungcan.2013.08.008.

Acerbi, I. *et al.* (2015) 'Human breast cancer invasion and aggression correlates with ECM stiffening and immune cell infiltration', *Integrative Biology*, 7(10), pp. 1120–1134. Available at: https://doi.org/10.1039/C5IB00040H.

Adrain, C. *et al.* (2012) 'Tumor necrosis factor signaling requires iRhom2 to promote trafficking and activation of TACE', *Science*, 335(6065), pp. 225–228. Available at: https://doi.org/10.1126/SCIENCE.1214400/SUPPL_FILE/1214400.ADRAIN.SOM.PDF.

Aikawa, T. *et al.* (2008) 'Glypican-1 modulates the angiogenic and metastatic potential of human and mouse cancer cells', *The Journal of Clinical Investigation*, 118(1), pp. 89–99. Available at: https://doi.org/10.1172/JCI32412.

Alava, E. De *et al.* (2006) 'Neuregulin (NRG) expression modulates clinical response to trastuzumab in patients with metastatic breast cancer (MBC)', *https://doi.org/10.1200/jco.2006.24.18_suppl.10069*, 24(18_suppl), pp. 10069–10069. Available at: https://doi.org/10.1200/JCO.2006.24.18_SUPPL.10069.

Amour, A. *et al.* (1998) 'TNF-α converting enzyme (TACE) is inhibited by TIMP-3', *FEBS Letters* [Preprint]. Available at: https://doi.org/10.1016/S0014-5793(98)01031-X.

Anderson, N.M. and Simon, M.C. (2020) 'The tumor microenvironment', *Current Biology*, 30, pp. 905–931. Available at: https://doi.org/10.1016/j.cub.2020.06.081.

Anderson, R.L. *et al.* (2018) 'A framework for the development of effective anti-metastatic agents', *Nature Reviews Clinical Oncology 2018 16:3*, 16(3), pp. 185–204. Available at: https://doi.org/10.1038/s41571-018-0134-8.

Arwert, E.N. *et al.* (2020) 'STING and IRF3 in stromal fibroblasts enable sensing of genomic stress in cancer cells to undermine oncolytic viral therapy', *Nature Cell Biology 2020 22:7*, 22(7), pp. 758–766. Available at: https://doi.org/10.1038/s41556-020-0527-7.

Asli, N.S. *et al.* (2019) 'PDGFRα signaling in cardiac fibroblasts modulates quiescence,

metabolism and self-renewal, and promotes anatomical and functional repair', *bioRxiv*, p. 225979. Available at: https://doi.org/10.1101/225979.

Bai, Y.P. *et al.* (2015) 'FGF-1/-3/FGFR4 signaling in cancer-associated fibroblasts promotes tumor progression in colon cancer through Erk and MMP-7', *Cancer Science*, 106(10), pp. 1278–1287. Available at: https://doi.org/10.1111/CAS.12745.

Bates, A.L. *et al.* (2015) 'Stromal matrix metalloproteinase 2 regulates collagen expression and promotes the outgrowth of experimental metastases', *The Journal of Pathology*, 235(5), pp. 773–783. Available at: https://doi.org/10.1002/PATH.4493.

Baumgart, A. *et al.* (2010) 'ADAM17 regulates epidermal growth factor receptor expression through the activation of Notch1 in non-small cell lung cancer', *Cancer Research*, 70(13), pp. 5368–5378. Available at: https://doi.org/10.1158/0008-5472.CAN-09-3763/655865/P/ADAM17-REGULATES-EPIDERMAL-GROWTH-FACTOR-RECEPTOR.

Bernard, V. *et al.* (2019) 'Single-cell transcriptomics of pancreatic cancer precursors demonstrates epithelial and microenvironmental heterogeneity as an early event in neoplastic progression', *Clinical Cancer Research*, 25(7), pp. 2194–2205. Available at: https://doi.org/10.1158/1078-0432.CCR-18-1955/73940/AM/SINGLE-CELL-TRANSCRIPTOMICS-OF-PANCREATIC-CANCER.

Bharadwaj, U. *et al.* (2016) 'Small-molecule inhibition of STAT3 in radioresistant head and neck squamous cell carcinoma', *Oncotarget*, 7(18), p. 26307. Available at: https://doi.org/10.18632/ONCOTARGET.8368.

Biffi, G. *et al.* (2019) 'Il1-induced Jak/STAT signaling is antagonized by TGFβ to shape CAF heterogeneity in pancreatic ductal adenocarcinoma', *Cancer Discovery*, 9(2), pp. 282–301. Available at: https://doi.org/10.1158/2159-8290.CD-18-0710/42870/AM/IL-1-INDUCED-JAK-STAT-SIGNALING-IS-ANTAGONIZED-BY.

Blanchot-Jossic, F. *et al.* (2005) 'Up-regulated expression of ADAM17 in human colon carcinoma: Co-expression with EGFR in neoplastic and endothelial cells', *Journal of Pathology* [Preprint]. Available at: https://doi.org/10.1002/path.1814.

Blobel, C.P. (2005) 'ADAMs: Key components in egfr signalling and development', *Nature Reviews Molecular Cell Biology* [Preprint]. Available at: https://doi.org/10.1038/nrm1548.

Bohrer, L.R. *et al.* (2016) 'ADAM17 in tumor associated leukocytes regulates inflammatory mediators and promotes mammary tumor formation', *Genes & Cancer*, 7(7–8), p. 240. Available at: https://doi.org/10.18632/GENESANDCANCER.115.

Bonnans, C., Chou, J. and Werb, Z. (2014) 'Remodelling the extracellular matrix in development and disease', *Nature Reviews Molecular Cell Biology* [Preprint]. Available at:

https://doi.org/10.1038/nrm3904.

Borrell-Pagès, M. *et al.* (2003) 'TACE is required for the activation of the EGFR by TGF-α in tumors', *EMBO Journal* [Preprint]. Available at: https://doi.org/10.1093/emboj/cdg111.

Brechbuhl, H.M. *et al.* (2017) 'Fibroblast subtypes regulate responsiveness of luminal breast cancer to estrogen', *Clinical Cancer Research* [Preprint]. Available at: https://doi.org/10.1158/1078-0432.CCR-15-2851.

Cai, M. *et al.* (2015) 'Adam17, a Target of Mir-326, Promotes Emt-Induced Cells Invasion in Lung Adenocarcinoma', *Cellular Physiology and Biochemistry*, 36(3), pp. 1175–1185. Available at: https://doi.org/10.1159/000430288.

Cal, S. and López-Otín, C. (2015) 'ADAMTS proteases and cancer', *Matrix Biology*, 44–46, pp. 77–85. Available at: https://doi.org/10.1016/J.MATBIO.2015.01.013.

Calon, A. *et al.* (2015) 'Stromal gene expression defines poor-prognosis subtypes in colorectal cancer', *Nature Genetics 2015 47:4*, 47(4), pp. 320–329. Available at: https://doi.org/10.1038/ng.3225.

Calvo, F. *et al.* (2013) 'Mechanotransduction and YAP-dependent matrix remodelling is required for the generation and maintenance of cancer-associated fibroblasts', *Nature Cell Biology 2013 15:6*, 15(6), pp. 637–646. Available at: https://doi.org/10.1038/ncb2756.

Campbell, P.J. *et al.* (2010) 'The patterns and dynamics of genomic instability in metastatic pancreatic cancer', *Nature 2010 467:7319*, 467(7319), pp. 1109–1113. Available at: https://doi.org/10.1038/nature09460.

Cao, Z. *et al.* (2019) 'Protein kinase A-mediated phosphorylation of naked cuticle homolog 2 stimulates cell-surface delivery of transforming growth factor-α for epidermal growth factor receptor transactivation', *Traffic*, 20(5), pp. 357–368. Available at: https://doi.org/10.1111/TRA.12642/.

Casar, B. *et al.* (2011) 'Blocking of CDCP1 cleavage in vivo prevents Akt-dependent survival and inhibits metastatic colonization through PARP1-mediated apoptosis of cancer cells', *Oncogene 2012 31:35*, 31(35), pp. 3924–3938. Available at: https://doi.org/10.1038/onc.2011.555.

Casey, T.M. *et al.* (2008) 'Cancer associated fibroblasts stimulated by transforming growth factor beta1 (TGF-β1) increase invasion rate of tumor cells: A population study', *Breast Cancer Research and Treatment*, 110(1), pp. 39–49. Available at: https://doi.org/10.1007/S10549-007-9684-7/FIGURES/4.

Catenacci, D.V.T. *et al.* (2015) 'Randomized Phase Ib/II Study of Gemcitabine Plus Placebo or Vismodegib, a Hedgehog Pathway Inhibitor, in Patients With Metastatic Pancreatic Cancer',

Journal of Clinical Oncology, 33(36), p. 4284. Available at: https://doi.org/10.1200/JCO.2015.62.8719.

Chakravarty, D. *et al.* (2017) 'EGFR and PDGFRA co-expression and heterodimerization in glioblastoma tumor sphere lines', *Scientific Reports 2017 7:1*, 7(1), pp. 1–10. Available at: https://doi.org/10.1038/s41598-017-08940-9.

Chalaris, A., Gewiese, J., *et al.* (2010) 'ADAM17-mediated shedding of the IL6R induces cleavage of the membrane stub by γ-secretase', *Biochimica et Biophysica Acta (BBA) - Molecular Cell Research*, 1803(2), pp. 234–245. Available at: https://doi.org/10.1016/J.BBAMCR.2009.12.001.

Chalaris, A., Adam, N., *et al.* (2010) 'Critical role of the disintegrin metalloprotease ADAM17 for intestinal inflammation and regeneration in mice', *The Journal of experimental medicine*, 207(8), pp. 1617–1624. Available at: https://doi.org/10.1084/JEM.20092366.

Chambers, A.F., Groom, A.C. and MacDonald, I.C. (2002) 'Dissemination and growth of cancer cells in metastatic sites', *Nature Reviews Cancer 2002 2:8*, 2(8), pp. 563–572. Available at: https://doi.org/10.1038/nrc865.

Chandler, C. *et al.* (2019) 'The double edge sword of fibrosis in cancer', *Translational Research*, 209, pp. 55–67. Available at: https://doi.org/10.1016/J.TRSL.2019.02.006.

Chang, K.W. *et al.* (2013) 'Fibroblast growth factor-2 up-regulates the expression of nestin through the Ras–Raf–ERK–Sp1 signaling axis in C6 glioma cells', *Biochemical and Biophysical Research Communications*, 434(4), pp. 854–860. Available at: https://doi.org/10.1016/J.BBRC.2013.04.031.

Chen, D. *et al.* (2013) 'Better Prognosis of Patients with Glioma Expressing FGF2-Dependent PDGFRA Irrespective of Morphological Diagnosis', *PLOS ONE*, 8(4), p. e61556. Available at: https://doi.org/10.1371/JOURNAL.PONE.0061556.

Chen, S. *et al.* (2021) 'Single-cell analysis reveals transcriptomic remodellings in distinct cell types that contribute to human prostate cancer progression', *Nature Cell Biology 2021 23:1*, 23(1), pp. 87–98. Available at: https://doi.org/10.1038/s41556-020-00613-6.

Chen, S.H. *et al.* (2010) 'Up-regulation of fibronectin and tissue transglutaminase promotes cell invasion involving increased association with integrin and MMP expression in A431 cells', *Anticancer Research* [Preprint].

Chen, X. and Song, E. (2019) 'Turning foes to friends: targeting cancer-associated fibroblasts', *Nature Reviews Drug Discovery* [Preprint]. Available at: https://doi.org/10.1038/s41573-018-0004-1.

Chen, Y. *et al.* (2021) 'Type I collagen deletion in αSMA+ myofibroblasts augments immune

suppression and accelerates progression of pancreatic cancer', *Cancer Cell*, 39(4), pp. 548-565.e6. Available at: https://doi.org/10.1016/J.CCELL.2021.02.007.

Chen, Y., McAndrews, K.M. and Kalluri, R. (2021) 'Clinical and therapeutic relevance of cancer-associated fibroblasts', *Nature Reviews Clinical Oncology*. Nature Publishing Group, pp. 792–804. Available at: https://doi.org/10.1038/s41571-021-00546-5.

Cheung, K.J. and Ewald, A.J. (2016) 'A collective route to metastasis: Seeding by tumor cell clusters', *Science*, 352(6282), pp. 167–169. Available at: https://doi.org/10.1126/SCIENCE.AAF6546/ASSET/681C756C-EE6D-42BB-AE74-22520995CA99/ASSETS/GRAPHIC/352_167_F2.JPEG.

Cho, C. *et al.* (2020) 'Cancer-associated fibroblasts downregulate type I interferon receptor to stimulate intratumoral stromagenesis', *Oncogene 2020 39:38*, 39(38), pp. 6129–6137. Available at: https://doi.org/10.1038/s41388-020-01424-7.

Christova, Y. *et al.* (2013) 'Mammalian iRhoms have distinct physiological functions including an essential role in TACE regulation', *EMBO Reports* [Preprint]. Available at: https://doi.org/10.1038/embor.2013.128.

Cirri, P. and Chiarugi, P. (2012) 'Cancer-associated-fibroblasts and tumour cells: A diabolic liaison driving cancer progression', *Cancer and Metastasis Reviews*. Springer, pp. 195–208. Available at: https://doi.org/10.1007/s10555-011-9340-x.

Clarke, C.J. *et al.* (2016) 'The initiator methionine trna drives secretion of type II collagen from stromal fibroblasts to promote tumor growth and angiogenesis', *Current Biology* [Preprint]. Available at: https://doi.org/10.1016/j.cub.2016.01.045.

Cole, S.W. *et al.* (2015) 'Sympathetic nervous system regulation of the tumour microenvironment', *Nature Reviews Cancer*, 15(9), pp. 563–572. Available at: https://doi.org/10.1038/nrc3978.

Costa, A. *et al.* (2018) 'Fibroblast Heterogeneity and Immunosuppressive Environment in Human Breast Cancer', *Cancer Cell*, 33(3), pp. 463-479.e10. Available at: https://doi.org/10.1016/J.CCELL.2018.01.011.

Cowden Dahl, K.D. *et al.* (2008) 'Matrix metalloproteinase 9 is a mediator of epidermal growth factor-dependent E-cadherin loss in ovarian carcinoma cells', *Cancer Research* [Preprint]. Available at: https://doi.org/10.1158/0008-5472.CAN-07-5046.

Cox, J. *et al.* (2014) 'Accurate proteome-wide label-free quantification by delayed normalization and maximal peptide ratio extraction, termed MaxLFQ', *Molecular & cellular proteomics : MCP*, 13(9), pp. 2513–2526. Available at: https://doi.org/10.1074/MCP.M113.031591.

Cox, T.R. *et al.* (2013) 'LOX-mediated collagen crosslinking is responsible for fibrosis-enhanced metastasis', *Cancer Research* [Preprint]. Available at: https://doi.org/10.1158/0008-5472.CAN-12-2233.

D'Amici, S. *et al.* (2013) 'TNFα Modulates Fibroblast Growth Factor Receptor 2 Gene Expression through the pRB/E2F1 Pathway: Identification of a Non-Canonical E2F Binding Motif', *PLOS ONE*, 8(4), p. e61491. Available at: https://doi.org/10.1371/JOURNAL.PONE.0061491.

Dai, J. *et al.* (2005) 'Bone Morphogenetic Protein-6 Promotes Osteoblastic Prostate Cancer Bone Metastases through a Dual Mechanism', *Cancer Research*, 65(18), pp. 8274–8285. Available at: https://doi.org/10.1158/0008-5472.CAN-05-1891.

Dai, J. *et al.* (2021) 'DNA Damage Response and Repair Gene Alterations Increase Tumor Mutational Burden and Promote Poor Prognosis of Advanced Lung Cancer', *Frontiers in Oncology*, 11, p. 3324. Available at: https://doi.org/10.3389/FONC.2021.708294/BIBTEX.

Damstrup, L. *et al.* (1998) 'In vitro invasion of small-cell lung cancer cell lines correlates with expression of epidermal growth factor receptor', *British Journal of Cancer 1998 78:5*, 78(5), pp. 631–640. Available at: https://doi.org/10.1038/bjc.1998.553.

Danielpour, D. *et al.* (1989) 'Sandwich enzyme-linked immunosorbent assays (selisas) quantitate and distinguish two forms of transforming growth factor-beta (TGF-β1 and TGF-β2) in complex biological fluids', *Growth Factors* [Preprint]. Available at: https://doi.org/10.3109/08977198909069082.

Das, S. *et al.* (2012) 'ADAM17 Silencing in Mouse Colon Carcinoma Cells: The Effect on Tumoricidal Cytokines and Angiogenesis', *PLOS ONE*, 7(12), p. e50791. Available at: https://doi.org/10.1371/JOURNAL.PONE.0050791.

Davidson, S. *et al.* (2020) 'Single-Cell RNA Sequencing Reveals a Dynamic Stromal Niche That Supports Tumor Growth', *Cell Reports*, 31(7), p. 107628. Available at: https://doi.org/10.1016/J.CELREP.2020.107628.

Denais, C.M. *et al.* (2016) 'Nuclear envelope rupture and repair during cancer cell migration', *Science*, 352(6283), pp. 353–358. Available at: https://doi.org/10.1126/SCIENCE.AAD7297/SUPPL_FILE/PAPV2.PDF.

Derynck, R. and Weinberg, R.A. (2019) 'EMT and Cancer: More Than Meets the Eye', *Developmental Cell*, 49(3), pp. 313–316. Available at: https://doi.org/10.1016/J.DEVCEL.2019.04.026.

Dikic, I. and Elazar, Z. (2018) 'Mechanism and medical implications of mammalian autophagy', *Nature Reviews Molecular Cell Biology 2018 19:6*, 19(6), pp. 349–364. Available

at: https://doi.org/10.1038/s41580-018-0003-4.

Diop-Frimpong, B. *et al.* (2011) 'Losartan inhibits collagen I synthesis and improves the distribution and efficacy of nanotherapeutics in tumors', *Proceedings of the National Academy of Sciences of the United States of America*, 108(7), pp. 2909–2914. Available at: https://doi.org/10.1073/PNAS.1018892108/SUPPL_FILE/PNAS.201018892SI.PDF.

Doherty, M.R. *et al.* (2017) 'Interferon-beta represses cancer stem cell properties in triple-negative breast cancer', *Proceedings of the National Academy of Sciences of the United States of America*, 114(52), pp. 13792–13797. Available at: https://doi.org/10.1073/pnas.1713728114.

Dong, C. *et al.* (2013) 'Loss of FBP1 by Snail-Mediated Repression Provides Metabolic Advantages in Basal-like Breast Cancer', *Cancer Cell*, 23(3), pp. 316–331. Available at: https://doi.org/10.1016/J.CCR.2013.01.022.

Dong, F. *et al.* (2015) 'The metalloprotease-disintegrin ADAM8 contributes to temozolomide chemoresistance and enhanced invasiveness of human glioblastoma cells', *Neuro-Oncology* [Preprint]. Available at: https://doi.org/10.1093/neuonc/nov042.

Dongre, A. and Weinberg, R.A. (2018) 'New insights into the mechanisms of epithelial–mesenchymal transition and implications for cancer', *Nature Reviews Molecular Cell Biology 2018 20:2*, 20(2), pp. 69–84. Available at: https://doi.org/10.1038/s41580-018-0080-4.

Donners, M.M.P.C. *et al.* (2010) 'A Disintegrin and Metalloprotease 10 is a novel mediator of vascular endothelial growth factor-induced endothelial cell function in angiogenesis and is associated with atherosclerosis', *Arteriosclerosis, Thrombosis, and Vascular Biology*, 30(11), pp. 2188–2195. Available at: https://doi.org/10.1161/ATVBAHA.110.213124.

Du, Y.H. *et al.* (2021) 'The cancer-associated fibroblasts related gene CALD1 is a prognostic biomarker and correlated with immune infiltration in bladder cancer', *Cancer Cell International*, 21(1), pp. 1–15. Available at: https://doi.org/10.1186/S12935-021-01896-X/TABLES/2.

Duffy, M.J. *et al.* (2009) 'Role of ADAMs in cancer formation and progression', *Clinical Cancer Research* [Preprint]. Available at: https://doi.org/10.1158/1078-0432.CCR-08-1585.

Duffy, M.J. *et al.* (2011) 'The ADAMs family of proteases: New biomarkers and therapeutic targets for cancer?', *Clinical Proteomics* [Preprint]. Available at: https://doi.org/10.1186/1559-0275-8-9.

Düsterhöft, S. *et al.* (2013) 'Membrane-proximal domain of a disintegrin and metalloprotease-17 represents the putative molecular switch of its shedding activity operated by protein-disulfide isomerase', *Journal of the American Chemical Society* [Preprint]. Available at:

https://doi.org/10.1021/ja400340u.

Düsterhöft, S. *et al.* (2019) 'Status update on iRhom and ADAM17: It's still complicated', *Biochimica et Biophysica Acta (BBA) - Molecular Cell Research* [Preprint]. Available at: https://doi.org/10.1016/j.bbamcr.2019.06.017.

Düsterhöft, S., Lokau, J. and Garbers, C. (2019) 'The metalloprotease ADAM17 in inflammation and cancer', *Pathology - Research and Practice*, 215(6), p. 152410. Available at: https://doi.org/10.1016/J.PRP.2019.04.002.

Ebi, M. *et al.* (2010) 'TGFβ induces proHB-EGF shedding and EGFR transactivation through ADAM activation in gastric cancer cells', *Biochemical and Biophysical Research Communications*, 402(3), pp. 449–454. Available at: https://doi.org/10.1016/J.BBRC.2010.09.130.

Edward, M., Gold, J.A. and Mackie, R.M. (1992) 'Retinoic acid-induced inhibition of metastatic melanoma cell lung colonization and adhesion to endothelium and subendothelial extracellular matrix', *Clinical & Experimental Metastasis 1992 10:1*, 10(1), pp. 61–67. Available at: https://doi.org/10.1007/BF00163577.

Edwards, D.R., Handsley, M.M. and Pennington, C.J. (2009) 'The ADAM metalloproteinases', *Molecular Aspects of Medicine* [Preprint]. Available at: https://doi.org/10.1016/j.mam.2008.08.001.

Effenberger, T. *et al.* (2014) 'Senescence-associated release of transmembrane proteins involves proteolytic processing by ADAM17 and microvesicle shedding', *FASEB Journal* [Preprint]. Available at: https://doi.org/10.1096/fj.14-254565.

Elkabets, M. *et al.* (2011) 'Human tumors instigate granulin-expressing hematopoietic cells that promote malignancy by activating stromal fibroblasts in mice', *The Journal of Clinical Investigation*, 121(2), pp. 784–799. Available at: https://doi.org/10.1172/JCI43757.

Elmusrati, A.A. *et al.* (2017) 'Cancer-associated fibroblasts promote bone invasion in oral squamous cell carcinoma', *British Journal of Cancer* [Preprint]. Available at: https://doi.org/10.1038/bjc.2017.239.

Elyada, E. *et al.* (2019) 'Cross-species single-cell analysis of pancreatic ductal adenocarcinoma reveals antigen-presenting cancer-associated fibroblasts', *Cancer Discovery*, 9(8), pp. 1102–1123. Available at: https://doi.org/10.1158/2159-8290.CD-19-0094/333377/AM/CROSS-SPECIES-SINGLE-CELL-ANALYSIS-OF-PANCREATIC.

Erez, N. *et al.* (2004) 'Induction of apoptosis in cultured endothelial cells by a cadherin antagonist peptide: involvement of fibroblast growth factor receptor-mediated signalling', *Experimental Cell Research*, 294(2), pp. 366–378. Available at:

https://doi.org/10.1016/J.YEXCR.2003.11.033.

Erez, N. *et al.* (2010) 'Cancer-Associated Fibroblasts Are Activated in Incipient Neoplasia to Orchestrate Tumor-Promoting Inflammation in an NF-κB-Dependent Manner', *Cancer Cell* [Preprint]. Available at: https://doi.org/10.1016/j.ccr.2009.12.041.

Ershaid, N. *et al.* (2019) 'NLRP3 inflammasome in fibroblasts links tissue damage with inflammation in breast cancer progression and metastasis', *Nature Communications 2019 10:1*, 10(1), pp. 1–15. Available at: https://doi.org/10.1038/s41467-019-12370-8.

Esposito, M., Ganesan, S. and Kang, Y. (2021) 'Emerging strategies for treating metastasis', *Nature Cancer 2021 2:3*, 2(3), pp. 258–270. Available at: https://doi.org/10.1038/s43018-021-00181-0.

Evans, R.A. *et al.* (2003) 'TGF-β1-mediated fibroblast-myofibroblast terminal differentiation - The role of Smad proteins', *Experimental Cell Research* [Preprint]. Available at: https://doi.org/10.1016/S0014-4827(02)00015-0.

Fabre-Lafay, S. *et al.* (2005) 'Nectin-4, a New Serological Breast Cancer Marker, Is a Substrate for Tumor Necrosis Factor-α-converting Enzyme (TACE)/ADAM-17 *', *Journal of Biological Chemistry*, 280(20), pp. 19543–19550. Available at: https://doi.org/10.1074/JBC.M410943200.

Fan, D. *et al.* (2016) 'A Disintegrin and Metalloprotease-17 Regulates Pressure Overload-Induced Myocardial Hypertrophy and Dysfunction Through Proteolytic Processing of Integrin β1', *Hypertension*, 68(4), pp. 937–948. Available at: https://doi.org/10.1161/HYPERTENSIONAHA.116.07566.

Fang, T. *et al.* (2018) 'Tumor-derived exosomal miR-1247-3p induces cancer-associated fibroblast activation to foster lung metastasis of liver cancer', *Nature Communications 2018 9:1*, 9(1), pp. 1–13. Available at: https://doi.org/10.1038/s41467-017-02583-0.

Fang, W. *et al.* (2017) 'ADAM-17 expression is enhanced by FoxM1 and is a poor prognostic sign in gastric carcinoma', *Journal of Surgical Research*, 220, pp. 223–233. Available at: https://doi.org/10.1016/J.JSS.2017.06.032.

Farahani, R.M. and Xaymardan, M. (2015) 'Platelet-derived growth factor receptor alpha as a marker of mesenchymal stem cells in development and stem cell biology', *Stem Cells International*, 2015. Available at: https://doi.org/10.1155/2015/362753.

Feig, C. *et al.* (2013) 'Targeting CXCL12 from FAP-expressing carcinoma-associated fibroblasts synergizes with anti-PD-L1 immunotherapy in pancreatic cancer', *Proceedings of the National Academy of Sciences of the United States of America*, 110(50), pp. 20212–20217. Available at: https://doi.org/10.1073/PNAS.1320318110.

Fiaschi, T. *et al.* (2012) 'Reciprocal metabolic reprogramming through lactate shuttle coordinately influences tumor-stroma interplay', *Cancer Research* [Preprint]. Available at: https://doi.org/10.1158/0008-5472.CAN-12-1949.

Finnegan, E. *et al.* (1989) 'Allelotype of Colorectal Carcinomas', *Science*, 244(4901), pp. 207–211. Available at: https://doi.org/10.1126/SCIENCE.2565047.

Fischer, K.R. *et al.* (2015) 'Epithelial-to-mesenchymal transition is not required for lung metastasis but contributes to chemoresistance', *Nature 2015 527:7579*, 527(7579), pp. 472–476. Available at: https://doi.org/10.1038/nature15748.

Foers, A.D. *et al.* (2020) 'Proteomic analysis of extracellular vesicles reveals an immunogenic cargo in rheumatoid arthritis synovial fluid', *Clinical & Translational Immunology*, 9(11), p. e1185. Available at: https://doi.org/10.1002/CTI2.1185.

Frantz, C., Stewart, K.M. and Weaver, V.M. (2010) 'The extracellular matrix at a glance', *Journal of Cell Science* [Preprint]. Available at: https://doi.org/10.1242/jcs.023820.

Franzke, C.W. *et al.* (2012) 'Epidermal ADAM17 maintains the skin barrier by regulating EGFR ligand–dependent terminal keratinocyte differentiation', *Journal of Experimental Medicine*, 209(6), pp. 1105–1119. Available at: https://doi.org/10.1084/JEM.20112258.

Froeling, F.E.M. *et al.* (2011) 'Retinoic acid-induced pancreatic stellate cell quiescence reduces paracrine Wntβ-catenin signaling to slow tumor progression', *Gastroenterology* [Preprint]. Available at: https://doi.org/10.1053/j.gastro.2011.06.047.

Fröhlich, C. *et al.* (2006) 'Molecular profiling of ADAM12 in human bladder cancer', *Clinical Cancer Research* [Preprint]. Available at: https://doi.org/10.1158/1078-0432.CCR-06-1066.

Fukino, K. *et al.* (2004) 'Combined Total Genome Loss of Heterozygosity Scan of Breast Cancer Stroma and Epithelium Reveals Multiplicity of Stromal Targets', *Cancer Research*, 64(20), pp. 7231–7236. Available at: https://doi.org/10.1158/0008-5472.CAN-04-2866.

Gaggioli, C. *et al.* (2007) 'Fibroblast-led collective invasion of carcinoma cells with differing roles for RhoGTPases in leading and following cells', *Nature Cell Biology* [Preprint]. Available at: https://doi.org/10.1038/ncb1658.

Le Gall, S.M. *et al.* (2010) 'ADAM17 is regulated by a rapid and reversible mechanism that controls access to its catalytic site', *Journal of Cell Science* [Preprint]. Available at: https://doi.org/10.1242/jcs.069997.

Ganesh, K. and Massagué, J. (2021) 'Targeting metastatic cancer', *Nature Medicine 2021 27:1*, 27(1), pp. 34–44. Available at: https://doi.org/10.1038/s41591-020-01195-4.

Gao, M.Q. *et al.* (2013) 'Human breast cancer-associated fibroblasts enhance cancer cell proliferation through increased TGF-α cleavage by ADAM17', *Cancer Letters* [Preprint].

Available at: https://doi.org/10.1016/j.canlet.2013.05.011.

Garraway, L.A. and Lander, E.S. (2013) 'Lessons from the Cancer Genome', *Cell*, 153(1), pp. 17–37. Available at: https://doi.org/10.1016/J.CELL.2013.03.002.

Garton, K.J., Gough, P.J. and Raines, E.W. (2006) 'Emerging roles for ectodomain shedding in the regulation of inflammatory responses', *Journal of Leukocyte Biology*, 79(6), pp. 1105–1116. Available at: https://doi.org/10.1189/JLB.0106038.

Gascard, P. and Tlsty, T.D. (2016) 'Carcinoma-associated fibroblasts: Orchestrating the composition of malignancy', *Genes and Development*. Available at: https://doi.org/10.1101/gad.279737.116.

GCO (2021) *Cancer Tomorrow*, *World Health Organization (WHO)*. Available at: https://gco.iarc.fr/tomorrow/en/dataviz/isotype?types=1&sexes=0&mode=population&group_populations=1&multiple_populations=1&multiple_cancers=0&cancers=39&populations=903_904_905_908_909_935&single_unit=500000 (Accessed: 16 March 2022).

Ge, L. *et al.* (2009) 'Sheddase activity of tumor necrosis factor-α converting enzyme is increased and prognostically valuable in head and neck cancer', *Cancer Epidemiology Biomarkers and Prevention* [Preprint]. Available at: https://doi.org/10.1158/1055-9965.EPI-08-0898.

Gelling, R.W. *et al.* (2008) 'Deficiency of TNFα converting enzyme (TACE/ADAM17) causes a lean, hypermetabolic phenotype in mice', *Endocrinology* [Preprint]. Available at: https://doi.org/10.1210/en.2008-0775.

Ghesquière, B. *et al.* (2014) 'Metabolism of stromal and immune cells in health and disease', *Nature* [Preprint]. Available at: https://doi.org/10.1038/nature13312.

Giannoni, E. *et al.* (2010) 'Reciprocal activation of prostate cancer cells and cancer-associated fibroblasts stimulates epithelial-mesenchymal transition and cancer stemness', *Cancer Research*, 70(17), pp. 6945–6956. Available at: https://doi.org/10.1158/0008-5472.CAN-10-0785/656293/P/RECIPROCAL-ACTIVATION-OF-PROSTATE-CANCER-CELLS-AND.

Givel, A.M. *et al.* (2018) 'miR200-regulated CXCL12β promotes fibroblast heterogeneity and immunosuppression in ovarian cancers', *Nature Communications 2018 9:1*, 9(1), pp. 1–20. Available at: https://doi.org/10.1038/s41467-018-03348-z.

Goetz, J.G. *et al.* (2011) 'Biomechanical Remodeling of the Microenvironment by Stromal Caveolin-1 Favors Tumor Invasion and Metastasis', *Cell*, 146(1), pp. 148–163. Available at: https://doi.org/10.1016/J.CELL.2011.05.040.

Gooz, M. (2010) 'ADAM-17: The enzyme that does it all', *Critical Reviews in Biochemistry and Molecular Biology* [Preprint]. Available at: https://doi.org/10.3109/10409231003628015.

Goumas, F.A. *et al.* (2015) 'Inhibition of IL-6 signaling significantly reduces primary tumor growth and recurrencies in orthotopic xenograft models of pancreatic cancer', *International Journal of Cancer*, 137(5), pp. 1035–1046. Available at: https://doi.org/10.1002/IJC.29445.

Grugan, K.D. *et al.* (2010) 'Fibroblast-secreted hepatocyte growth factor plays a functional role in esophageal squamous cell carcinoma invasion', *Proceedings of the National Academy of Sciences of the United States of America* [Preprint]. Available at: https://doi.org/10.1073/pnas.0914295107.

Guaiquil, V. *et al.* (2009) 'ADAM9 Is Involved in Pathological Retinal Neovascularization', *Molecular and Cellular Biology*, 29(10), pp. 2694–2703. Available at: https://doi.org/10.1128/MCB.01460-08/ASSET/C6EC3A3C-BC22-4F55-B477-C2F37DBE015D/ASSETS/GRAPHIC/ZMB0100980690007.JPEG.

Guccini, I. *et al.* (2021) 'Senescence Reprogramming by TIMP1 Deficiency Promotes Prostate Cancer Metastasis', *Cancer Cell*, 39(1), pp. 68-82.e9. Available at: https://doi.org/10.1016/J.CCELL.2020.10.012/ATTACHMENT/898155E7-F6FD-4B11-B1F8-9CD9AC509877/MMC1.PDF.

Gui, P. and Bivona, T.G. (2022) 'Evolution of metastasis: new tools and insights', *Trends in Cancer*, 8(2), pp. 98–109. Available at: https://doi.org/10.1016/J.TRECAN.2021.11.002.

Guo, P. (2013) 'The emerging field of RNA nanotechnology', in *RNA Nanotechnology and Therapeutics*. Available at: https://doi.org/10.1201/b15152.

Guo, W. *et al.* (2012) 'Slug and Sox9 Cooperatively Determine the Mammary Stem Cell State', *Cell*, 148(5), pp. 1015–1028. Available at: https://doi.org/10.1016/J.CELL.2012.02.008.

Guo, X. *et al.* (2008) 'Stromal Fibroblasts Activated by Tumor Cells Promote Angiogenesis in Mouse Gastric Cancer', *Journal of Biological Chemistry*, 283(28), pp. 19864–19871. Available at: https://doi.org/10.1074/JBC.M800798200.

Hanahan, D. (2022) 'Hallmarks of Cancer: New DimensionsHallmarks of Cancer: New Dimensions', *Cancer Discovery*, 12(1), pp. 31–46. Available at: https://doi.org/10.1158/2159-8290.CD-21-1059.

Hanahan, D. and Coussens, L.M. (2012) 'Accessories to the Crime: Functions of Cells Recruited to the Tumor Microenvironment', *Cancer Cell*, 21(3), pp. 309–322. Available at: https://doi.org/10.1016/J.CCR.2012.02.022.

Hanahan, D. and Weinberg, R.A. (2011) 'Hallmarks of cancer: The next generation', *Cell* [Preprint]. Available at: https://doi.org/10.1016/j.cell.2011.02.013.

Hassan, G.S., Stagg, J. and Mourad, W. (2015) 'Role of CD154 in cancer pathogenesis and immunotherapy', *Cancer Treatment Reviews*, 41(5), pp. 431–440. Available at:

https://doi.org/10.1016/J.CTRV.2015.03.007.

Hazan, R.B. *et al.* (2000) 'Exogenous Expression of N-Cadherin in Breast Cancer Cells Induces Cell Migration, Invasion, and Metastasis', *Journal of Cell Biology*, 148(4), pp. 779–790. Available at: https://doi.org/10.1083/JCB.148.4.779.

Hazan, R.B. *et al.* (2004) 'Cadherin Switch in Tumor Progression', *Annals of the New York Academy of Sciences*, 1014(1), pp. 155–163. Available at: https://doi.org/10.1196/ANNALS.1294.016.

Hazlehurst, L.A. *et al.* (2000) 'Adhesion to fibronectin via β1 integrins regulates p27(kip1) levels and contributes to cell adhesion mediated drug resistance (CAM-DR)', *Oncogene* [Preprint]. Available at: https://doi.org/10.1038/sj.onc.1203782.

He, H. *et al.* (2001) 'Platelet-derived growth factor requires epidermal growth factor receptor to activate p21-activated kinase family kinases', *The Journal of biological chemistry*, 276(29), pp. 26741–26744. Available at: https://doi.org/10.1074/JBC.C100229200.

He, Y. *et al.* (2021) 'Targeting PI3K/Akt signal transduction for cancer therapy', *Signal Transduction and Targeted Therapy 2021 6:1*, 6(1), pp. 1–17. Available at: https://doi.org/10.1038/s41392-021-00828-5.

Hearnden, V. *et al.* (2009) 'Diffusion studies of nanometer polymersomes across tissue engineered human oral mucosa', *Pharmaceutical Research* [Preprint]. Available at: https://doi.org/10.1007/s11095-009-9882-6.

Heldin, C.H. *et al.* (2004) 'High interstitial fluid pressure - An obstacle in cancer therapy', *Nature Reviews Cancer* [Preprint]. Available at: https://doi.org/10.1038/nrc1456.

Henriksson, M.L. *et al.* (2011) 'Colorectal Cancer Cells Activate Adjacent Fibroblasts Resulting in FGF1/FGFR3 Signaling and Increased Invasion', *The American Journal of Pathology*, 178(3), p. 1387. Available at: https://doi.org/10.1016/J.AJPATH.2010.12.008.

Hong, S. *et al.* (2016) 'Role of ADAM17 in invasion and migration of CD133-expressing liver cancer stem cells after irradiation', *Oncotarget*, 7(17), pp. 23482–23497. Available at: https://doi.org/10.18632/ONCOTARGET.8112.

Hopfner, K.P. and Hornung, V. (2020) 'Molecular mechanisms and cellular functions of cGAS–STING signalling', *Nature Reviews Molecular Cell Biology 2020 21:9*, 21(9), pp. 501–521. Available at: https://doi.org/10.1038/s41580-020-0244-x.

Horiuchi, K. *et al.* (2003) 'Potential Role for ADAM15 in Pathological Neovascularization in Mice', *Molecular and Cellular Biology*, 23(16), pp. 5614–5624. Available at: https://doi.org/10.1128/MCB.23.16.5614-5624.2003/ASSET/2504E6A2-6761-42F7-AA83-6CA3CA6B25A8/ASSETS/GRAPHIC/MB1630338007.JPEG.

Horiuchi, K. *et al.* (2007) 'Cutting Edge: TNF-α-Converting Enzyme (TACE/ADAM17) Inactivation in Mouse Myeloid Cells Prevents Lethality from Endotoxin Shock', *The Journal of Immunology*, 179(5), pp. 2686–2689. Available at: https://doi.org/10.4049/JIMMUNOL.179.5.2686.

Horiuchi, K. *et al.* (2009) ' Conditional Inactivation of TACE by a Sox9 Promoter Leads to Osteoporosis and Increased Granulopoiesis via Dysregulation of IL-17 and G-CSF ', *The Journal of Immunology* [Preprint]. Available at: https://doi.org/10.4049/jimmunol.0802491.

Hosein, A.N. *et al.* (2019) 'Cellular heterogeneity during mouse pancreatic ductal adenocarcinoma progression at single-cell resolution', *JCI Insight*, 4(16). Available at: https://doi.org/10.1172/JCI.INSIGHT.129212.

Hu, B. *et al.* (2018) 'Short hairpin RNA-mediated gene silencing of ADAM17 inhibits the growth of breast cancer MCF-7 cells in vitro and in vivo and its mechanism of action', *Oncology Reports*, 39(4), p. 1640. Available at: https://doi.org/10.3892/OR.2018.6237.

Hu, C. *et al.* (2013) 'Effects of cancer-associated fibroblasts on the migration and invasion abilities of SGC-7901 gastric cancer cells', *Oncology Letters*, 5(2), p. 609. Available at: https://doi.org/10.3892/OL.2012.1023.

Huang, D.C. *et al.* (2014) 'Parathyroid Hormone-Related Protein: Potential Therapeutic Target for Melanoma Invasion and Metastasis', *Endocrinology*, 155(10), pp. 3739–3749. Available at: https://doi.org/10.1210/EN.2013-1803.

Huang, H. *et al.* (2019) 'Getting a grip on adhesion: Cadherin switching and collagen signaling', *Biochimica et Biophysica Acta (BBA) - Molecular Cell Research*, 1866(11), p. 118472. Available at: https://doi.org/10.1016/J.BBAMCR.2019.04.002.

Ino, Y. *et al.* (2013) 'Arginase II Expressed in Cancer-Associated Fibroblasts Indicates Tissue Hypoxia and Predicts Poor Outcome in Patients with Pancreatic Cancer', *PLoS ONE* [Preprint]. Available at: https://doi.org/10.1371/journal.pone.0055146.

Ishimoto, T. *et al.* (2017) 'Activation of Transforming Growth Factor Beta 1 Signaling in Gastric Cancer-associated Fibroblasts Increases Their Motility, via Expression of Rhomboid 5 Homolog 2, and Ability to Induce Invasiveness of Gastric Cancer Cells', *Gastroenterology*, 153(1), pp. 191-204.e16. Available at: https://doi.org/10.1053/J.GASTRO.2017.03.046.

Ivey, M.J. *et al.* (2019) 'Platelet-derived growth factor receptor-α is essential for cardiac fibroblast survival', *American Journal of Physiology - Heart and Circulatory Physiology*, 317(2), pp. H330–H344. Available at: https://doi.org/10.1152/AJPHEART.00054.2019/ASSET/IMAGES/LARGE/ZH400719286100 07.JPEG.

Jedeszko, C. *et al.* (2009) 'Fibroblast hepatocyte growth factor promotes invasion of human mammary ductal carcinoma in situ', *Cancer Research* [Preprint]. Available at: https://doi.org/10.1158/0008-5472.CAN-09-1043.

Jenkinson, S.E. *et al.* (2011) 'The αE(CD103)β7 integrin interacts with oral and skin keratinocytes in an E-cadherin-independent manner*', *Immunology*, 132(2), pp. 188–196. Available at: https://doi.org/10.1111/J.1365-2567.2010.03352.X.

Jiao, X. *et al.* (2018) 'ADAM-17 is a poor prognostic indicator for patients with hilar cholangiocarcinoma and is regulated by FoxM1', *BMC Cancer*, 18(1), pp. 1–11. Available at: https://doi.org/10.1186/S12885-018-4294-9/FIGURES/5.

Jin, M.Z. and Jin, W.L. (2020) 'The updated landscape of tumor microenvironment and drug repurposing', *Signal Transduction and Targeted Therapy* [Preprint]. Available at: https://doi.org/10.1038/s41392-020-00280-x.

Jin, Q. *et al.* (2020) 'A disintegrin and metalloproteinase 8 induced epithelial-mesenchymal transition to promote the invasion of colon cancer cells via TGF-β/Smad2/3 signalling pathway', *Journal of cellular and molecular medicine*, 24(22), pp. 13058–13069. Available at: https://doi.org/10.1111/JCMM.15907.

Jolly, M.K. *et al.* (2015) 'Implications of the hybrid epithelial/mesenchymal phenotype in metastasis', *Frontiers in Oncology*, 5(JUN), p. 155. Available at: https://doi.org/10.3389/FONC.2015.00155/BIBTEX.

Kabir, T.D. *et al.* (2016) 'A miR-335/COX-2/PTEN axis regulates the secretory phenotype of senescent cancer-associated fibroblasts', *Aging* [Preprint]. Available at: https://doi.org/10.18632/aging.100987.

Kalluri, R. (2016) 'The biology and function of fibroblasts in cancer', *Nature Reviews Cancer* [Preprint]. Available at: https://doi.org/10.1038/nrc.2016.73.

Kalluri, R. and Zeisberg, M. (2006) 'Fibroblasts in cancer', *Nature Reviews Cancer*, 6(5), pp. 392–401. Available at: https://doi.org/10.1038/nrc1877.

Kamarajan, P. *et al.* (2013) 'ADAM17-mediated CD44 cleavage promotes orasphere formation or stemness and tumorigenesis in HNSCC', *Cancer Medicine* [Preprint]. Available at: https://doi.org/10.1002/cam4.147.

Kanzaki, H. *et al.* (2016) 'A-Disintegrin and Metalloproteinase (ADAM) 17 Enzymatically Degrades Interferon-gamma', *Scientific Reports 2016 6:1*, 6(1), pp. 1–14. Available at: https://doi.org/10.1038/srep32259.

Kaplan, D.H. *et al.* (1998) 'Demonstration of an interferon γ-dependent tumor surveillance system in immunocompetent mice', *Proceedings of the National Academy of Sciences of the*

United States of America, 95(13), pp. 7556–7561. Available at: https://doi.org/10.1073/PNAS.95.13.7556.

Katlinski, K. V. *et al.* (2017) 'Inactivation of Interferon Receptor Promotes the Establishment of Immune Privileged Tumor Microenvironment', *Cancer Cell*, 31(2), pp. 194–207. Available at: https://doi.org/10.1016/J.CCELL.2017.01.004.

Kefaloyianni, E. *et al.* (2016) 'ADAM17 substrate release in proximal tubule drives kidney fibrosis', *JCI Insight*, 1(13), p. 87023. Available at: https://doi.org/10.1172/JCI.INSIGHT.87023.

Kenny, P.A. and Bissell, M.J. (2007) 'Targeting TACE-dependent EGFR ligand shedding in breast cancer', *The Journal of Clinical Investigation*, 117(2), pp. 337–345. Available at: https://doi.org/10.1172/JCI29518.

Kessenbrock, K., Plaks, V. and Werb, Z. (2010) 'Matrix Metalloproteinases: Regulators of the Tumor Microenvironment', *Cell* [Preprint]. Available at: https://doi.org/10.1016/j.cell.2010.03.015.

Kieffer, Y. *et al.* (2020) 'Single-cell analysis reveals fibroblast clusters linked to immunotherapy resistance in cancer', *Cancer Discovery*, 10(9), pp. 1330–1351. Available at: https://doi.org/10.1158/2159-8290.CD-19-1384/333435/AM/SINGLE-CELL-ANALYSIS-REVEALS-FIBROBLAST-CLUSTERS.

Kitamura, T. *et al.* (2010) 'Inactivation of chemokine (C-C motif) receptor 1 (CCR1) suppresses colon cancer liver metastasis by blocking accumulation of immature myeloid cells in amouse model', *Proceedings of the National Academy of Sciences of the United States of America*, 107(29), pp. 13063–13068. Available at: https://doi.org/10.1073/PNAS.1002372107.

Kobayashi, N. *et al.* (2010) 'Hyaluronan deficiency in tumor stroma impairs macrophage trafficking and tumor neovascularization', *Cancer Research* [Preprint]. Available at: https://doi.org/10.1158/0008-5472.CAN-09-4687.

Kornfeld, J.W. *et al.* (2011) 'Overexpression of TACE and TIMP3 mRNA in head and neck cancer: Association with tumour development and progression', *British Journal of Cancer* [Preprint]. Available at: https://doi.org/10.1038/sj.bjc.6606017.

Kramer, N. *et al.* (2013) 'In vitro cell migration and invasion assays', *Mutation Research/Reviews in Mutation Research*, 752(1), pp. 10–24. Available at: https://doi.org/10.1016/J.MRREV.2012.08.001.

Kuefer, R. *et al.* (2006) 'ADAM15 Disintegrin Is Associated with Aggressive Prostate and Breast Cancer Disease', *Neoplasia*, 8(4), pp. 319–329. Available at: https://doi.org/10.1593/NEO.05682.

Kuukasjärvi, T. *et al.* (1997) 'Genetic heterogeneity and clonal evolution underlying development of asynchronous metastasis in human breast cancer', *Cancer Research*, 57(8), pp. 1597–1604. Available at: https://aacrjournals.org/cancerres/article/57/8/1597/503984/Genetic-Heterogeneity-and-Clonal-Evolution (Accessed: 10 June 2022).

Kwon, Y.W. *et al.* (2021) 'Application of Proteomics in Cancer: Recent Trends and Approaches for Biomarkers Discovery', *Frontiers in Medicine*, 8, p. 1644. Available at: https://doi.org/10.3389/FMED.2021.747333/BIBTEX.

Kyula, J.N. *et al.* (2010) 'Chemotherapy-induced activation of ADAM-17: A novel mechanism of drug resistance in colorectal cancer', *Clinical Cancer Research* [Preprint]. Available at: https://doi.org/10.1158/1078-0432.CCR-10-0014.

Lambert, A.W., Pattabiraman, D.R. and Weinberg, R.A. (2017) 'Emerging Biological Principles of Metastasis', *Cell*, 168(4), pp. 670–691. Available at: https://doi.org/10.1016/J.CELL.2016.11.037.

Lambrecht, B.N., Vanderkerken, M. and Hammad, H. (2018) 'The emerging role of ADAM metalloproteinases in immunity', *Nature Reviews Immunology* [Preprint]. Available at: https://doi.org/10.1038/s41577-018-0068-5.

Lammens, T. *et al.* (2012) 'N-Cadherin in Neuroblastoma Disease: Expression and Clinical Significance', *PLOS ONE*, 7(2), p. e31206. Available at: https://doi.org/10.1371/JOURNAL.PONE.0031206.

Lamouille, S., Xu, J. and Derynck, R. (2014) 'Molecular mechanisms of epithelial–mesenchymal transition', *Nature Reviews Molecular Cell Biology 2014 15:3*, 15(3), pp. 178–196. Available at: https://doi.org/10.1038/nrm3758.

Laplane, L. *et al.* (2018) 'The Multiple Layers of the Tumor Environment', *Trends in Cancer*, 4(12), pp. 802–809. Available at: https://doi.org/10.1016/J.TRECAN.2018.10.002.

Laplane, L. *et al.* (2019a) 'Beyond the tumour microenvironment', *International Journal of Cancer*, 145(10), pp. 2611–2618. Available at: https://doi.org/10.1002/IJC.32343.

Laplane, L. *et al.* (2019b) 'Beyond the tumour microenvironment', *International Journal of Cancer*, 145(10), pp. 2611–2618. Available at: https://doi.org/10.1002/IJC.32343.

LeBleu, V.S. and Kalluri, R. (2018) 'A peek into cancer-associated fibroblasts: Origins, functions and translational impact', *DMM Disease Models and Mechanisms* [Preprint]. Available at: https://doi.org/10.1242/dmm.029447.

Lee, C.H. *et al.* (2006) 'Sensitization of B16 tumor cells with a CXCR4 antagonist increases the efficacy of immunotherapy for established lung metastases', *Molecular Cancer Therapeutics*, 5(10), pp. 2592–2599. Available at: https://doi.org/10.1158/1535-7163.MCT-

06-0310.

Lee, H.J. *et al.* (2014) 'Systematic family-wide analysis of sodium bicarbonate cotransporter NBCn1/SLC4A7 interactions with PDZ scaffold proteins', *Physiological Reports*, 2(5), p. e12016. Available at: https://doi.org/10.14814/PHY2.12016.

Lefèvre, G. *et al.* (2009) 'Activation of the FGF2/FGFR1 Autocrine Loop for Cell Proliferation and Survival in Uveal Melanoma Cells', *Investigative Ophthalmology & Visual Science*, 50(3), pp. 1047–1057. Available at: https://doi.org/10.1167/IOVS.08-2378.

Lever, J., Krzywinski, M. and Altman, N. (2017) 'Points of Significance: Principal component analysis', *Nature Methods*, 14(7), pp. 641–642. Available at: https://doi.org/10.1038/NMETH.4346.

Li, D. *et al.* (2014) 'The Notch ligand Jagged1 as a target for 1 anti-tumour therapy', *Frontiers in Oncology*, 4(SEP), p. 254. Available at: https://doi.org/10.3389/FONC.2014.00254/BIBTEX.

Li, H. *et al.* (2017) 'Reference component analysis of single-cell transcriptomes elucidates cellular heterogeneity in human colorectal tumors', *Nature Genetics 2017 49:5*, 49(5), pp. 708–718. Available at: https://doi.org/10.1038/ng.3818.

Li, T.M. *et al.* (2019) '17 Type I interferon modulates ADAM17 activity in photosensitive lupus mouse models', in *Lupus Science & Medicine*. Archives of Disease in childhood, p. A13.1-A13. Available at: https://doi.org/10.1136/lupus-2019-lsm.17.

Li, W. *et al.* (2019) 'ADAM17 promotes lymph node metastasis in gastric cancer via activation of the Notch and Wnt signaling pathways', *International Journal of Molecular Medicine*, 43(2), pp. 914–926. Available at: https://doi.org/10.3892/ijmm.2018.4028.

Li, Y. *et al.* (2018) 'ADAM17 promotes cell migration and invasion through the integrin β1 pathway in hepatocellular carcinoma', *Experimental Cell Research* [Preprint]. Available at: https://doi.org/10.1016/j.yexcr.2018.06.039.

Liang, W. *et al.* (2019) 'Vasorin stimulates malignant progression and angiogenesis in glioma', *Cancer Science*, 110(8), p. 2558. Available at: https://doi.org/10.1111/CAS.14103.

Lim, S. *et al.* (2013) 'SNAI1-Mediated Epithelial-Mesenchymal Transition Confers Chemoresistance and Cellular Plasticity by Regulating Genes Involved in Cell Death and Stem Cell Maintenance', *PLOS ONE*, 8(6), p. e66558. Available at: https://doi.org/10.1371/JOURNAL.PONE.0066558.

Lin, M.C. *et al.* (2017) 'Therapeutic vaccine targeting Epstein-Barr virus latent protein, LMP1, suppresses LMP1-expressing tumor growth and metastasis in vivo', *BMC Cancer*, 17(1), pp. 1–9. Available at: https://doi.org/10.1186/S12885-016-3027-1/FIGURES/6.

Liu, C. *et al.* (2009) 'TACE-Mediated Ectodomain Shedding of the Type I TGF-β Receptor Downregulates TGF-β Signaling', *Molecular Cell* [Preprint]. Available at: https://doi.org/10.1016/j.molcel.2009.06.018.

Liu, T. *et al.* (2019) 'Cancer-associated fibroblasts build and secure the tumor microenvironment', *Frontiers in Cell and Developmental Biology*, 7(APR), p. 60. Available at: https://doi.org/10.3389/FCELL.2019.00060/BIBTEX.

Liu, W. *et al.* (2009) 'Copy number analysis indicates monoclonal origin of lethal metastatic prostate cancer', *Nature Medicine 2009 15:5*, 15(5), pp. 559–565. Available at: https://doi.org/10.1038/nm.1944.

Liu, X., Luo, D. and Yang, N. (2015) 'Cytosolic Low Molecular Weight FGF2 Orchestrates RIG-I–Mediated Innate Immune Response', *The Journal of Immunology*, 195(10), pp. 4943–4952. Available at: https://doi.org/10.4049/JIMMUNOL.1501503/-/DCSUPPLEMENTAL.

Liu, Z. *et al.* (2017) 'Autophagy inhibitor facilitates gefitinib sensitivity in vitro and in vivo by activating mitochondrial apoptosis in triple negative breast cancer', *PLOS ONE*, 12(5), p. e0177694. Available at: https://doi.org/10.1371/JOURNAL.PONE.0177694.

Löhr, M. *et al.* (2001) 'Transforming growth factor-β1 induces desmoplasia in an experimental model of human pancreatic carcinoma', *Cancer Research*, 61(2), pp. 550–555. Available at: https://aacrjournals.org/cancerres/article/61/2/550/507865/Transforming-Growth-Factor-1-Induces-Desmoplasia (Accessed: 1 April 2022).

Lorenzen, I. *et al.* (2016) 'Control of ADAM17 activity by regulation of its cellular localisation', *Scientific Reports 2016 6:1*, 6(1), pp. 1–15. Available at: https://doi.org/10.1038/srep35067.

Luzzi, K.J. *et al.* (1998) 'Multistep Nature of Metastatic Inefficiency: Dormancy of Solitary Cells after Successful Extravasation and Limited Survival of Early Micrometastases', *The American Journal of Pathology*, 153(3), pp. 865–873. Available at: https://doi.org/10.1016/S0002-9440(10)65628-3.

Lv, X. *et al.* (2014) 'ADAM17 silencing suppresses the migration and invasion of non-small cell lung cancer', *Molecular Medicine Reports*, 9(5), pp. 1935–1940. Available at: https://doi.org/10.3892/MMR.2014.2029/HTML.

Maine, G.N. *et al.* (2007) 'COMMD1 promotes the ubiquitination of NF-κB subunits through a cullin-containing ubiquitin ligase', *The EMBO Journal*, 26(2), p. 436. Available at: https://doi.org/10.1038/SJ.EMBOJ.7601489.

Malapeira, J. *et al.* (2010) 'ADAM17 (TACE) regulates TGFβ signaling through the cleavage of vasorin', *Oncogene 2011 30:16*, 30(16), pp. 1912–1922. Available at:

https://doi.org/10.1038/onc.2010.565.

Maman, S. and Witz, I.P. (2018) 'A history of exploring cancer in context', *Nature Reviews Cancer*, 18(6), pp. 359–376. Available at: https://doi.org/10.1038/s41568-018-0006-7.

Manninen, O. *et al.* (2015) 'Impaired osteoclast homeostasis in the cystatin B-deficient mouse model of progressive myoclonus epilepsy', *Bone Reports*, 3, pp. 76–82. Available at: https://doi.org/10.1016/J.BONR.2015.10.002.

Martinez-Outschoorn, U.E. *et al.* (2011) 'Stromal-epithelial metabolic coupling in cancer: Integrating autophagy and metabolism in the tumor microenvironment', *International Journal of Biochemistry and Cell Biology* [Preprint]. Available at: https://doi.org/10.1016/j.biocel.2011.01.023.

Mauthe, M. *et al.* (2018) 'Chloroquine inhibits autophagic flux by decreasing autophagosome-lysosome fusion', *Autophagy*, 14(8), p. 1435. Available at: https://doi.org/10.1080/15548627.2018.1474314.

Mazzocca, A. *et al.* (2005) 'A secreted form of ADAM9 promotes carcinoma invasion through tumor-stromal interactions', *Cancer Research* [Preprint]. Available at: https://doi.org/10.1158/0008-5472.CAN-04-4449.

McAllister, S.S. and Weinberg, R.A. (2014) 'The tumour-induced systemic environment as a critical regulator of cancer progression and metastasis', *Nature Cell Biology 2014 16:8*, 16(8), pp. 717–727. Available at: https://doi.org/10.1038/ncb3015.

McGowan, P.M. *et al.* (2007) 'ADAM-17 Expression in Breast Cancer Correlates with Variables of Tumor Progression', *Clinical Cancer Research*, 13(8), pp. 2335–2343. Available at: https://doi.org/10.1158/1078-0432.CCR-06-2092.

McGowan, P.M. *et al.* (2008) 'ADAM-17 predicts adverse outcome in patients with breast cancer', *Annals of Oncology* [Preprint]. Available at: https://doi.org/10.1093/annonc/mdm609.

Meads, M.B., Gatenby, R.A. and Dalton, W.S. (2009) 'Environment-mediated drug resistance: A major contributor to minimal residual disease', *Nature Reviews Cancer* [Preprint]. Available at: https://doi.org/10.1038/nrc2714.

Mendelson, K. *et al.* (2010) 'Stimulation of Platelet-derived Growth Factor Receptor Î²2 (PDGFRÎ²2) Activates ADAM17 and Promotes Metalloproteinase-dependent Cross-talk between the PDGFRÎ²2 and Epidermal Growth Factor Receptor (EGFR) Signaling Pathways*'. Available at: https://doi.org/10.1074/jbc.M110.102566.

Mężyk-Kopeć, R. *et al.* (2015) 'ADAM17 Promotes Motility, Invasion, and Sprouting of Lymphatic Endothelial Cells', *PLOS ONE*, 10(7), p. e0132661. Available at: https://doi.org/10.1371/JOURNAL.PONE.0132661.

Miao, L. *et al.* (2017) 'Targeting tumor-associated fibroblasts for therapeutic delivery in desmoplastic tumors', *Cancer Research* [Preprint]. Available at: https://doi.org/10.1158/0008-5472.CAN-16-0866.

Micocci, K.C. *et al.* (2013) 'ADAM9 silencing inhibits breast tumor cell invasion in vitro', *Biochimie*, 95(7), pp. 1371–1378. Available at: https://doi.org/10.1016/J.BIOCHI.2013.03.001.

Midgley, A.C. *et al.* (2013) 'Transforming growth factor-β1 (TGF-β1)-stimulated fibroblast to myofibroblast differentiation is mediated by hyaluronan (HA)-facilitated epidermal growth factor receptor (EGFR) and CD44 co-localization in lipid rafts', *Journal of Biological Chemistry* [Preprint]. Available at: https://doi.org/10.1074/jbc.M113.451336.

Mink, S.R. *et al.* (2010) 'Cancer-associated fibroblasts derived from EGFR-TKI-resistant tumors reverse EGFR pathway inhibition by EGFR-TKIs', *Molecular Cancer Research* [Preprint]. Available at: https://doi.org/10.1158/1541-7786.MCR-09-0460.

Mishra, N., Chandrasekar, M. and Mishra, N. (2014) 'Hemocytometer', in *Practical Physiology Book*. Available at: https://doi.org/10.5005/jp/books/12105_3.

Mo, H.-N. and Liu, P. (2017) 'Targeting MET in cancer therapy', *Chronic Diseases and Translational Medicine*, 3(3), p. 148. Available at: https://doi.org/10.1016/J.CDTM.2017.06.002.

Mochizuki, S. *et al.* (2019) 'Expression and Function of a Disintegrin and Metalloproteinases in Cancer-Associated Fibroblasts of Colorectal Cancer', *Digestion* [Preprint].

Mohammad, K.S. *et al.* (2011) 'TGF-β-RI kinase inhibitor SD-208 reduces the development and progression of melanoma bone metastases', *Cancer Research*, 71(1), pp. 175–184. Available at: https://doi.org/10.1158/0008-5472.CAN-10-2651/649521/AM/THE-TRANSFORMING-GROWTH-FACTOR-RECEPTOR-I-KINASE.

Morancho, B. *et al.* (2015) 'Role of ADAM17 in the non-cell autonomous effects of oncogene-induced senescence', *Breast Cancer Research* [Preprint]. Available at: https://doi.org/10.1186/s13058-015-0619-7.

Moss, M.L. and Minond, D. (2017a) 'Recent Advances in ADAM17 Research: A Promising Target for Cancer and Inflammation', *Mediators of Inflammation* [Preprint]. Available at: https://doi.org/10.1155/2017/9673537.

Moss, M.L. and Minond, D. (2017b) 'Recent Advances in ADAM17 Research: A Promising Target for Cancer and Inflammation', *Mediators of Inflammation* [Preprint]. Available at: https://doi.org/10.1155/2017/9673537.

Motani, K. and Kosako, H. (2018) 'Activation of stimulator of interferon genes (sting) induces

adam17-mediated shedding of the immune semaphorin SEMA4D', *Journal of Biological Chemistry*, 293(20), pp. 7717–7726. Available at: https://doi.org/10.1074/JBC.RA118.002175/ATTACHMENT/F9703975-370E-4710-9F48-95D8193EF2C1/MMC1.ZIP.

Mueller, M.M. and Fusenig, N.E. (2004) 'Friends or foes - Bipolar effects of the tumour stroma in cancer', *Nature Reviews Cancer* [Preprint]. Available at: https://doi.org/10.1038/nrc1477.

Mullooly, M. *et al.* (2016) 'The ADAMs family of proteases as targets for the treatment of cancer', *http://dx.doi.org/10.1080/15384047.2016.1177684*, 17(8), pp. 870–880. Available at: https://doi.org/10.1080/15384047.2016.1177684.

Murphy, G. (2008) 'The ADAMs: Signalling scissors in the tumour microenvironment', *Nature Reviews Cancer* [Preprint]. Available at: https://doi.org/10.1038/nrc2459.

Najy, A.J., Day, K.C. and Day, M.L. (2008) 'The Ectodomain Shedding of E-cadherin by ADAM15 Supports ErbB Receptor Activation *', *Journal of Biological Chemistry*, 283(26), pp. 18393–18401. Available at: https://doi.org/10.1074/JBC.M801329200.

Ni, W.D. *et al.* (2017) 'Tenascin-C is a potential cancer-associated fibroblasts marker and predicts poor prognosis in prostate cancer', *Biochemical and Biophysical Research Communications* [Preprint]. Available at: https://doi.org/10.1016/j.bbrc.2017.03.021.

Nieman, M.T. *et al.* (1999) 'N-Cadherin Promotes Motility in Human Breast Cancer Cells Regardless of Their E-Cadherin Expression', *Journal of Cell Biology*, 147(3), pp. 631–644. Available at: https://doi.org/10.1083/JCB.147.3.631.

Nieto, M.A. *et al.* (2016) 'EMT: 2016', *Cell*, 166(1), pp. 21–45. Available at: https://doi.org/10.1016/J.CELL.2016.06.028.

Nilsson, G.M.A. *et al.* (2014) 'Loss of E-cadherin expression is not a prerequisite for c-erbB2-induced epithelial-mesenchymal transition', *International Journal of Oncology*, 45(1), pp. 82–94. Available at: https://doi.org/10.3892/IJO.2014.2424/HTML.

O'Connell, J.T. *et al.* (2011) 'VEGF-A and Tenascin-C produced by S100A4 + stromal cells are important for metastatic colonization', *Proceedings of the National Academy of Sciences of the United States of America*, 108(38), pp. 16002–16007. Available at: https://doi.org/10.1073/PNAS.1109493108.

Öhlund, D. *et al.* (2017) 'Distinct populations of inflammatory fibroblasts and myofibroblasts in pancreatic cancer', *The Journal of Experimental Medicine*, 214(3), p. 579. Available at: https://doi.org/10.1084/JEM.20162024.

Öhlund, D., Elyada, E. and Tuveson, D. (2014) 'Fibroblast heterogeneity in the cancer wound', *Journal of Experimental Medicine* [Preprint]. Available at:

https://doi.org/10.1084/jem.20140692.

Ohnishi, Y. *et al.* (2017) 'Regulation of cell migration via the EGFR signaling pathway in oral squamous cell carcinoma cells', *Oncology Letters*, 13(2), p. 930. Available at: https://doi.org/10.3892/OL.2016.5500.

Ohno, S. *et al.* (2002) 'Role of stromal collagen in immunomodulation and prognosis of advanced gastric carcinoma', *International Journal of Cancer* [Preprint]. Available at: https://doi.org/10.1002/ijc.10144.

Olumi, A.F. *et al.* (1999) 'Carcinoma-associated fibroblasts direct tumor progression of initiated human prostatic epithelium', *Cancer Research*, 59(19), pp. 5002–5011.

Orimo, A. *et al.* (2005) 'Stromal fibroblasts present in invasive human breast carcinomas promote tumor growth and angiogenesis through elevated SDF-1/CXCL12 secretion', *Cell*, 121(3), pp. 335–348. Available at: https://doi.org/10.1016/j.cell.2005.02.034.

Overdevest, J.B. *et al.* (2011) 'CD24 offers a therapeutic target for control of bladder cancer metastasis based on a requirement for lung colonization', *Cancer Research*, 71(11), pp. 3802–3811. Available at: https://doi.org/10.1158/0008-5472.CAN-11-0519/649896/AM/CD24-OFFERS-A-THERAPEUTIC-TARGET-FOR-CONTROL-OF.

Özdemir, B.C. *et al.* (2014) 'Depletion of carcinoma-associated fibroblasts and fibrosis induces immunosuppression and accelerates pancreas cancer with reduced survival', *Cancer Cell* [Preprint]. Available at: https://doi.org/10.1016/j.ccr.2014.04.005.

Palazuelos, J. *et al.* (2014) 'TACE/ADAM17 Is Essential for Oligodendrocyte Development and CNS Myelination', *Journal of Neuroscience*, 34(36), pp. 11884–11896. Available at: https://doi.org/10.1523/JNEUROSCI.1220-14.2014.

De Palma, M., Biziato, D. and Petrova, T. V. (2017) 'Microenvironmental regulation of tumour angiogenesis', *Nature Reviews Cancer*, 17(8), pp. 457–474. Available at: https://doi.org/10.1038/nrc.2017.51.

Park, C.S. *et al.* (2016) 'Therapeutic targeting of tetraspanin8 in epithelial ovarian cancer invasion and metastasis', *Oncogene 2016 35:34*, 35(34), pp. 4540–4548. Available at: https://doi.org/10.1038/onc.2015.520.

Parker, B.S., Rautela, J. and Hertzog, P.J. (2016) 'Antitumour actions of interferons: implications for cancer therapy', *Nature Reviews Cancer 2016 16:3*, 16(3), pp. 131–144. Available at: https://doi.org/10.1038/nrc.2016.14.

Pastushenko, I. and Blanpain, C. (2019) 'EMT Transition States during Tumor Progression and Metastasis', *Trends in Cell Biology*, 29(3), pp. 212–226. Available at: https://doi.org/10.1016/J.TCB.2018.12.001.

Paszek, M.J. *et al.* (2005) 'Tensional homeostasis and the malignant phenotype', *Cancer Cell*, 8(3), pp. 241–254. Available at: https://doi.org/10.1016/J.CCR.2005.08.010.

Paul, C.D., Mistriotis, P. and Konstantopoulos, K. (2016) 'Cancer cell motility: lessons from migration in confined spaces', *Nature Reviews Cancer 2016 17:2*, 17(2), pp. 131–140. Available at: https://doi.org/10.1038/nrc.2016.123.

Peduto, L. *et al.* (2006) 'ADAM12 is highly expressed in carcinoma-associated stroma and is required for mouse prostate tumor progression', *Oncogene* [Preprint]. Available at: https://doi.org/10.1038/sj.onc.1209536.

Peinado, H., Olmeda, D. and Cano, A. (2007) 'Snail, Zeb and bHLH factors in tumour progression: an alliance against the epithelial phenotype?', *Nature Reviews Cancer 2007 7:6*, 7(6), pp. 415–428. Available at: https://doi.org/10.1038/nrc2131.

Pelon, F. *et al.* (2020) 'Cancer-associated fibroblast heterogeneity in axillary lymph nodes drives metastases in breast cancer through complementary mechanisms', *Nature Communications 2020 11:1*, 11(1), pp. 1–20. Available at: https://doi.org/10.1038/s41467-019-14134-w.

Penn, J.W., Grobbelaar, A.O. and Rolfe, K.J. (2012) 'The role of the TGF-β family in wound healing, burns and scarring: a review', *International Journal of Burns and Trauma*, 2(1), p. 18. Available at: /pmc/articles/PMC3415964/ (Accessed: 12 April 2022).

Peschon, J.J. *et al.* (1998) 'An essential role for ectodomain shedding in mammalian development', *Science* [Preprint]. Available at: https://doi.org/10.1126/science.282.5392.1281.

Petersen, O.W. *et al.* (2001) 'The plasticity of human breast carcinoma cells is more than epithelial to mesenchymal conversion', *Breast Cancer Research 2001 3:4*, 3(4), pp. 1–5. Available at: https://doi.org/10.1186/BCR298.

Philippeos, C. *et al.* (2018) 'Spatial and Single-Cell Transcriptional Profiling Identifies Functionally Distinct Human Dermal Fibroblast Subpopulations', *Journal of Investigative Dermatology*, 138(4), pp. 811–825. Available at: https://doi.org/10.1016/J.JID.2018.01.016.

Pickup, M.W., Mouw, J.K. and Weaver, V.M. (2014) 'The extracellular matrix modulates the hallmarks of cancer', *EMBO reports* [Preprint]. Available at: https://doi.org/10.15252/embr.201439246.

Pietras, K. *et al.* (2008) 'Functions of paracrine PDGF signaling in the proangiogenic tumor stroma revealed by pharmacological targeting', *PLoS Medicine* [Preprint]. Available at: https://doi.org/10.1371/journal.pmed.0050019.

Pistore, C. *et al.* (2017) 'DNA methylation variations are required for epithelial-to-

mesenchymal transition induced by cancer-associated fibroblasts in prostate cancer cells', *Oncogene 2017 36:40*, 36(40), pp. 5551–5566. Available at: https://doi.org/10.1038/onc.2017.159.

Prime, S.S. *et al.* (1990) 'The behaviour of human oral squamous cell carcinoma in cell culture', *The Journal of Pathology* [Preprint]. Available at: https://doi.org/10.1002/path.1711600313.

Prime, S.S., Gamel, S.M., *et al.* (1994) 'Epidermal growth factor and transforming growth factor α characteristics of human oral carcinoma cell lines', *British Journal of Cancer 1994 69:1*, 69(1), pp. 8–15. Available at: https://doi.org/10.1038/bjc.1994.2.

Prime, S.S., Matthews, J.B., *et al.* (1994) 'TGF-β receptor regulation mediates the response to exogenous ligand but is independent of the degree of cellular differentiation in human oral keratinocytes', *International Journal of Cancer*, 56(3), pp. 406–412. Available at: https://doi.org/10.1002/IJC.2910560320.

Principe, S. *et al.* (2018) 'Proteomic Analysis of Cancer-Associated Fibroblasts Reveals a Paracrine Role for MFAP5 in Human Oral Tongue Squamous Cell Carcinoma', *Journal of Proteome Research*, 17(6), pp. 2045–2059. Available at: https://doi.org/10.1021/ACS.JPROTEOME.7B00925/SUPPL_FILE/PR7B00925_SI_003.XLSX.

Puram, S. V. *et al.* (2017) 'Single-Cell Transcriptomic Analysis of Primary and Metastatic Tumor Ecosystems in Head and Neck Cancer', *Cell*, 171(7), pp. 1611-1624.e24. Available at: https://doi.org/10.1016/J.CELL.2017.10.044.

Qian, B.J. *et al.* (2011) 'MTDH/AEG-1-based DNA vaccine suppresses lung metastasis and enhances chemosensitivity to doxorubicin in breast cancer', *Cancer Immunology, Immunotherapy*, 60(6), pp. 883–893. Available at: https://doi.org/10.1007/S00262-011-0997-3/FIGURES/7.

Qian, M., Shen, X. and Wang, H. (2016) 'The Distinct Role of ADAM17 in APP Proteolysis and Microglial Activation Related to Alzheimer's Disease', *Cellular and Molecular Neurobiology*, 36(4), pp. 471–482. Available at: https://doi.org/10.1007/S10571-015-0232-4.

Qian, X. *et al.* (2013) 'N-cadherin/FGFR promotes metastasis through epithelial-to-mesenchymal transition and stem/progenitor cell-like properties', *Oncogene 2014 33:26*, 33(26), pp. 3411–3421. Available at: https://doi.org/10.1038/onc.2013.310.

Qing, X. *et al.* (2016) 'iRhom2 regulates CSF1R cell surface expression and non-steady state myelopoiesis in mice', *European Journal of Immunology*, 46(12), pp. 2737–2748. Available at: https://doi.org/10.1002/EJI.201646482.

Quail, D.F. and Joyce, J.A. (2013) 'Microenvironmental regulation of tumor progression and metastasis', *Nature Medicine*, 19(11), pp. 1423–1437. Available at: https://doi.org/10.1038/nm.3394.

Quintero-Fabián, S. *et al.* (2019) 'Role of Matrix Metalloproteinases in Angiogenesis and Cancer', *Frontiers in Oncology*, 9, p. 1370. Available at: https://doi.org/10.3389/FONC.2019.01370/BIBTEX.

Rak, M. and Rustin, P. (2014) 'Supernumerary subunits NDUFA3, NDUFA5 and NDUFA12 are required for the formation of the extramembrane arm of human mitochondrial complex I'. Available at: https://doi.org/10.1016/j.febslet.2014.03.046.

Ramanathan, R.K. *et al.* (2019) 'Phase IB/II Randomized Study of FOLFIRINOX Plus Pegylated RecombinantHuman Hyaluronidase Versus FOLFIRINOX Alone in Patients With MetastaticPancreatic Adenocarcinoma: SWOG S1313', *Journal of Clinical Oncology*, 37(13), p. 1062. Available at: https://doi.org/10.1200/JCO.18.01295.

Ramdas, V. *et al.* (2013) 'GROWTH FACTORS, CYTOKINES, AND CELL CYCLE MOLECULES Canonical Transforming Growth Factor-b Signaling Regulates Disintegrin Metalloprotease Expression in Experimental Renal Fibrosis via miR-29', *The American Journal of Pathology*, 183, pp. 1885–1896. Available at: https://doi.org/10.1016/j.ajpath.2013.08.027.

Reiss, K., Ludwig, A. and Saftig, P. (2006) 'Breaking up the tie: Disintegrin-like metalloproteinases as regulators of cell migration in inflammation and invasion', *Pharmacology and Therapeutics* [Preprint]. Available at: https://doi.org/10.1016/j.pharmthera.2006.02.009.

Reiss, K. and Saftig, P. (2009) 'The "A Disintegrin And Metalloprotease" (ADAM) family of sheddases: Physiological and cellular functions', *Seminars in Cell and Developmental Biology* [Preprint]. Available at: https://doi.org/10.1016/j.semcdb.2008.11.002.

Ren, Y. *et al.* (2021) 'Autophagic secretion of HMGB1 from cancer-associated fibroblasts promotes metastatic potential of non-small cell lung cancer cells via NFκB signaling', *Cell Death & Disease 2021 12:10*, 12(10), pp. 1–13. Available at: https://doi.org/10.1038/s41419-021-04150-4.

Revandkar, A. *et al.* (2016) 'Inhibition of Notch pathway arrests PTEN-deficient advanced prostate cancer by triggering p27-driven cellular senescence', *Nature Communications* [Preprint]. Available at: https://doi.org/10.1038/ncomms13719.

Rios-Doria, J. *et al.* (2015) 'Amonoclonal antibody to ADAM17 inhibits tumor growth by inhibiting EGFR and non-EGFR-mediated pathways', *Molecular Cancer Therapeutics*, 14(7),

pp. 1637–1649. Available at: https://doi.org/10.1158/1535-7163.MCT-14-1040/86499/AM/A-MONOCLONAL-ANTIBODY-TO-ADAM17-INHIBITS-TUMOR.

Ritter, C.A. and Arteaga, C.L. (2003) 'The epidermal growth factor receptor–tyrosine kinase: A promising therapeutic target in solid tumors', *Seminars in Oncology*, 30(1), pp. 3–11. Available at: https://doi.org/10.1053/SONC.2003.50027.

Rocks, N. *et al.* (2008) 'Emerging roles of ADAM and ADAMTS metalloproteinases in cancer', *Biochimie* [Preprint]. Available at: https://doi.org/10.1016/j.biochi.2007.08.008.

Rogers, M.E., Krieger, J. and Vogt, R.G. (2001) 'Neuronal localization of the TNFalpha converting enzyme (TACE) in brain tissue and its correlation to amyloid plaques', *Journal of neurobiology*, 49(1), pp. 40–46. Available at: https://doi.org/10.1002/NEU.1064.

Romera, C. *et al.* (2004) 'In Vitro Ischemic Tolerance Involves Upregulation of Glutamate Transport Partly Mediated by the TACE/ADAM17-Tumor Necrosis Factor-α Pathway', *Journal of Neuroscience*, 24(6), pp. 1350–1357. Available at: https://doi.org/10.1523/JNEUROSCI.1596-03.2004.

Ronnov-Jessen, L. and Petersen, O.W. (1993) 'Induction of alpha-smooth muscle actin by transforming growth factor-beta 1 in quiescent human breast gland fibroblasts. Implications for myofibroblast generation in breast neoplasia.', *Laboratory Investigation; a Journal of Technical Methods and Pathology*, 68(6), pp. 696–707. Available at: https://europepmc.org/article/med/8515656 (Accessed: 12 April 2022).

Ruff, M. *et al.* (2015) 'The Disintegrin and Metalloprotease ADAM12 Is Associated with TGF-β-Induced Epithelial to Mesenchymal Transition', *PLOS ONE*, 10(9), p. e0139179. Available at: https://doi.org/10.1371/JOURNAL.PONE.0139179.

Saad, M.I. *et al.* (2019) 'ADAM17 selectively activates the IL-6 trans-signaling/ERK MAPK axis in KRAS-addicted lung cancer', *EMBO Molecular Medicine*, 11(4), p. e9976. Available at: https://doi.org/10.15252/EMMM.201809976.

Saad, M.I., Rose-John, S. and Jenkins, B.J. (2019) 'ADAM17: An emerging therapeutic target for lung cancer', *Cancers* [Preprint]. Available at: https://doi.org/10.3390/cancers11091218.

Saar-Kovrov, V., Donners, M.M.P.C. and van der Vorst, E.P.C. (2021) 'Shedding of Klotho: Functional Implications in Chronic Kidney Disease and Associated Vascular Disease', *Frontiers in Cardiovascular Medicine*, 0, p. 407. Available at: https://doi.org/10.3389/FCVM.2020.617842.

Sadok, A. *et al.* (2015) 'Rho kinase inhibitors block melanoma cell migration and inhibit metastasis', *Cancer Research*, 75(11), pp. 2272–2284. Available at: https://doi.org/10.1158/0008-5472.CAN-14-2156/651777/AM/RHO-KINASE-

INHIBITORS-BLOCK-MELANOMA-CELL.

Saha, N. *et al.* (2022) 'Inhibitory monoclonal antibody targeting ADAM17 expressed on cancer cells', *Translational Oncology*, 15(1), p. 101265. Available at: https://doi.org/10.1016/J.TRANON.2021.101265.

Sahai, E. *et al.* (2020) 'A framework for advancing our understanding of cancer-associated fibroblasts', *Nature Reviews Cancer* [Preprint]. Available at: https://doi.org/10.1038/s41568-019-0238-1.

Sahin, U. *et al.* (2004) 'Distinct roles for ADAM10 and ADAM17 in ectodomain shedding of six EGFR ligands', *The Journal of Cell Biology*, 164(5), pp. 769–779. Available at: https://doi.org/10.1083/jcb.200307137.

Sastre, M., Walter, J. and Gentleman, S.M. (2008) 'Interactions between APP secretases and inflammatory mediators', *Journal of Neuroinflammation*, 5(1), pp. 1–11. Available at: https://doi.org/10.1186/1742-2094-5-25/FIGURES/2.

Sato, M. *et al.* (2015) 'Differential Proteome Analysis Identifies TGF-β-Related Pro-Metastatic Proteins in a 4T1 Murine Breast Cancer Model', *PLOS ONE*, 10(5), p. e0126483. Available at: https://doi.org/10.1371/JOURNAL.PONE.0126483.

Sato, N. *et al.* (2016) 'Targeting hyaluronan for the treatment of pancreatic ductal adenocarcinoma', *Acta Pharmaceutica Sinica B* [Preprint]. Available at: https://doi.org/10.1016/j.apsb.2016.01.002.

Savinova, O. V., Hoffmann, A. and Ghosh, G. (2009) 'The Nfkb1 and Nfkb2 Proteins p105 and p100 Function as the Core of High-Molecular-Weight Heterogeneous Complexes', *Molecular Cell*, 34(5), pp. 591–602. Available at: https://doi.org/10.1016/J.MOLCEL.2009.04.033/ATTACHMENT/FACBBABA-24A7-48C3-956F-8C353E19F765/MMC1.PDF.

Scheller, J. *et al.* (2011) 'ADAM17: A molecular switch to control inflammation and tissue regeneration', *Trends in Immunology* [Preprint]. Available at: https://doi.org/10.1016/j.it.2011.05.005.

Schmidt, S. *et al.* (2018) 'ADAM17 is required for EGF-R–induced intestinal tumors via IL-6 trans-signaling', *Journal of Experimental Medicine*, 215(4), pp. 1205–1225. Available at: https://doi.org/10.1084/JEM.20171696.

Schmittgen, T.D. and Livak, K.J. (2008) 'Analyzing real-time PCR data by the comparative CT method', *Nature Protocols* [Preprint]. Available at: https://doi.org/10.1038/nprot.2008.73.

Scott, A.M. *et al.* (2003) 'A phase I dose-escalation study of sibrotuzumab in patients with advanced or metastatic fibroblast activation protein-positive cancer', *Clinical Cancer Research*

[Preprint].

Seals, D.F. and Courtneidge, S.A. (2003) 'The ADAMs family of metalloproteases: multidomain proteins with multiple functions', *Genes & Development*, 17(1), pp. 7–30. Available at: https://doi.org/10.1101/GAD.1039703.

Servais, C. and Erez, N. (2013) 'From sentinel cells to inflammatory culprits: cancer-associated fibroblasts in tumour-related inflammation', *The Journal of Pathology*, 229(2), pp. 198–207. Available at: https://doi.org/10.1002/PATH.4103.

Shah, A.D. *et al.* (2019) 'Lfq-Analyst: An easy-To-use interactive web platform to analyze and visualize label-free proteomics data preprocessed with maxquant', *Journal of Proteome Research*, pp. 204–211. Available at: https://doi.org/10.1021/ACS.JPROTEOME.9B00496/SUPPL_FILE/PR9B00496_SI_001.PDF.

Shen, H. *et al.* (2016) 'The role of ADAM17 in tumorigenesis and progression of breast cancer', *Tumor Biology*, 37(12), pp. 15359–15370. Available at: https://doi.org/10.1007/S13277-016-5418-Y/FIGURES/1.

Sherman, M.H. *et al.* (2014) 'Vitamin D Receptor-Mediated Stromal Reprogramming Suppresses Pancreatitis and Enhances Pancreatic Cancer Therapy', *Cell*, 159(1), pp. 80–93. Available at: https://doi.org/10.1016/J.CELL.2014.08.007.

Shi, W. *et al.* (2003) 'TACE is required for fetal murine cardiac development and modeling', *Developmental Biology*, 261(2), pp. 371–380. Available at: https://doi.org/10.1016/S0012-1606(03)00315-4.

Shieh, A.C. *et al.* (2011) 'Tumor cell invasion is promoted by interstitial flow-induced matrix priming by stromal fibroblasts', *Cancer Research* [Preprint]. Available at: https://doi.org/10.1158/0008-5472.CAN-10-1513.

Shiga, K. *et al.* (2015) 'Cancer-associated fibroblasts: Their characteristics and their roles in tumor growth', *Cancers* [Preprint]. Available at: https://doi.org/10.3390/cancers7040902.

Shimoda, M. *et al.* (2014) 'Loss of the Timp gene family is sufficient for the acquisition of the CAF-like cell state', *Nature Cell Biology* [Preprint]. Available at: https://doi.org/10.1038/ncb3021.

Shimojo, Y. *et al.* (2013) 'Attenuation of reactive oxygen species by antioxidants suppresses hypoxia-induced epithelial-mesenchymal transition and metastasis of pancreatic cancer cells', *Clinical and Experimental Metastasis*, 30(2), pp. 143–154. Available at: https://doi.org/10.1007/S10585-012-9519-8/FIGURES/4.

Shintani, Y. *et al.* (2008) 'ADH-1 suppresses N-cadherin-dependent pancreatic cancer

progression', *International Journal of Cancer*, 122(1), pp. 71–77. Available at: https://doi.org/10.1002/IJC.23027.

Shintani, Y. *et al.* (2016) 'IL-6 Secreted from Cancer-Associated Fibroblasts Mediates Chemoresistance in NSCLC by Increasing Epithelial-Mesenchymal Transition Signaling', *Journal of Thoracic Oncology*, 11(9), pp. 1482–1492. Available at: https://doi.org/10.1016/J.JTHO.2016.05.025.

Sieuwerts, A.M. *et al.* (2005) 'How ADAM-9 and ADAM-11 differentially from estrogen receptor predict response to tamoxifen treatment in patients with recurrent breast cancer: A retrospective study', *Clinical Cancer Research* [Preprint]. Available at: https://doi.org/10.1158/1078-0432.CCR-05-0560.

Simabuco, F.M. *et al.* (2014) 'ADAM17 mediates OSCC development in an orthotopic murine model', *Molecular Cancer* [Preprint]. Available at: https://doi.org/10.1186/1476-4598-13-24.

Sinnathamby, G. *et al.* (2011) 'ADAM metallopeptidase domain 17 (ADAM17) is naturally processed through major histocompatibility complex (MHC) class I molecules and is a potential immunotherapeutic target in breast, ovarian and prostate cancers', *Clinical and Experimental Immunology*, 163(3), pp. 324–332. Available at: https://doi.org/10.1111/J.1365-2249.2010.04298.X.

Son, D.S. *et al.* (2013) 'Characteristics of chemokine signatures elicited by EGF and TNF in ovarian cancer cells', *Journal of Inflammation (United Kingdom)*, 10(1), pp. 1–12. Available at: https://doi.org/10.1186/1476-9255-10-25/FIGURES/8.

Srour, N. *et al.* (2003) 'TACE/ADAM-17 maturation and activation of sheddase activity require proprotein convertase activity', *FEBS Letters* [Preprint]. Available at: https://doi.org/10.1016/S0014-5793(03)01159-1.

Steeg, P.S. (2016) 'Targeting metastasis', *Nature Reviews Cancer 2016 16:4*, 16(4), pp. 201–218. Available at: https://doi.org/10.1038/nrc.2016.25.

Stefan Düsterhöft, Juliane Lokau, C.G. (2019) 'The metalloprotease ADAM17 in inflammation and cancer.pdf'.

Steinbichler, T.B. *et al.* (2016) 'Tumor-associated fibroblast-conditioned medium induces CDDP resistance in HNSCC cells', *Oncotarget*, 7(3), p. 2508. Available at: https://doi.org/10.18632/ONCOTARGET.6210.

Stoecklein, N.H. and Klein, C.A. (2010) 'Genetic disparity between primary tumours, disseminated tumour cells, and manifest metastasis', *International Journal of Cancer*, 126(3), pp. 589–598. Available at: https://doi.org/10.1002/IJC.24916.

Strober, W. (2015) 'Trypan Blue Exclusion Test of Cell Viability', *Current protocols in*

immunology / edited by John E. Coligan ... [et al.] [Preprint]. Available at: https://doi.org/10.1002/0471142735.ima03bs111.

Stuelten, C.H., Parent, C.A. and Montell, D.J. (2018) 'Cell motility in cancer invasion and metastasis: Insights from simple model organisms', *Nature Reviews Cancer*. Nature Publishing Group, pp. 296–312. Available at: https://doi.org/10.1038/nrc.2018.15.

Su, H.T. *et al.* (2013) 'Stem cell marker nestin is critical for TGF-β1-mediated tumor progression in pancreatic cancer', *Molecular Cancer Research*, 11(7), pp. 768–779. Available at: https://doi.org/10.1158/1541-7786.MCR-12-0511/79498/AM/STEM-CELL-MARKER-NESTIN-IS-CRITICAL-FOR-TGF-BETA1.

Suh, J. *et al.* (2020) 'Fibroblast growth factor-2, derived from cancer-associated fibroblasts, stimulates growth and progression of human breast cancer cells via FGFR1 signaling', *Molecular Carcinogenesis*, 59(9), pp. 1028–1040. Available at: https://doi.org/10.1002/MC.23233.

Suh, J. *et al.* (2022) 'Nuclear Localization of Fibroblast Growth Factor Receptor 1 in Breast Cancer Cells Interacting with Cancer Associated Fibroblasts', *Journal of Cancer Prevention*, 27(1), pp. 68–76. Available at: https://doi.org/10.15430/JCP.2022.27.1.68.

Sun, C. *et al.* (2020) 'ADAM17-regulated CX3CL1 expression produced by bone marrow endothelial cells promotes spinal metastasis from hepatocellular carcinoma', *International Journal of Oncology*, 57(1), pp. 249–263. Available at: https://doi.org/10.3892/IJO.2020.5045/HTML.

Sun, J. *et al.* (2017) 'Therapeutic potential of ADAM17 modulation in gastric cancer through regulation of the EGFR and TNF-α signalling pathways', *Molecular and Cellular Biochemistry*, 426(1–2), pp. 17–26. Available at: https://doi.org/10.1007/S11010-016-2877-9/FIGURES/4.

Sun, L.P. *et al.* (2019) 'Cancer-associated fibroblast-derived exosomal miR-382-5p promotes the migration and invasion of oral squamous cell carcinoma', *Oncology Reports*, 42(4), pp. 1319–1328. Available at: https://doi.org/10.3892/OR.2019.7255/HTML.

Sun, Y. *et al.* (2017) 'Cancer-associated fibroblasts secrete FGF-1 to promote ovarian proliferation, migration, and invasion through the activation of FGF-1/FGFR4 signaling', *Tumour biology : the journal of the International Society for Oncodevelopmental Biology and Medicine*, 39(7), pp. 1–10. Available at: https://doi.org/10.1177/1010428317712592.

Suyama, K. *et al.* (2002) 'A signaling pathway leading to metastasis is controlled by N-cadherin and the FGF receptor', *Cancer Cell*, 2(4), pp. 301–314. Available at: https://doi.org/10.1016/S1535-6108(02)00150-2.

Swartz, M.A. and Lund, A.W. (2012) 'Lymphatic and interstitial flow in the tumour microenvironment: linking mechanobiology with immunity', *Nature Reviews Cancer 2012 12:3*, 12(3), pp. 210–219. Available at: https://doi.org/10.1038/nrc3186.

Taeger, J. *et al.* (2011) 'Targeting FGFR/PDGFR/VEGFR impairs tumor growth, angiogenesis, and metastasis by effects on tumor cells, endothelial cells, and pericytes in pancreatic cancer', *Molecular Cancer Therapeutics*, 10(11), pp. 2157–2167. Available at: https://doi.org/10.1158/1535-7163.MCT-11-0312/83295/AM/TARGETING-FGFR-PDGFR-VEGFR-IMPAIRS-TUMOR-GROWTH.

Takamune, Y. *et al.* (2008) 'Involvement of NF-κB-mediated maturation of ADAM-17 in the invasion of oral squamous cell carcinoma', *Biochemical and Biophysical Research Communications* [Preprint]. Available at: https://doi.org/10.1016/j.bbrc.2007.11.010.

Tanaka, H. *et al.* (no date) 'Monoclonal antibody targeting of N-cadherin inhibits prostate cancer growth, metastasis and castration resistance', *nature.com* [Preprint]. Available at: https://idp.nature.com/authorize/casa?redirect_uri=https://www.nature.com/articles/nm.2236&casa_token=9xdyzw4WtmwAAAAA:lZtzkjC6DEKQkjrjyqL7KWNgpLd0R7aMN1A0LOpTJt_ORwTC2krImL4vftHlUtdn4xDuceJhSRdCaBja (Accessed: 22 March 2022).

Tao, L. *et al.* (2017) 'Cancer associated fibroblasts: An essential role in the tumor microenvironment (review)', *Oncology Letters*. Available at: https://doi.org/10.3892/ol.2017.6497.

Thiery, J.P. *et al.* (2009) 'Epithelial-Mesenchymal Transitions in Development and Disease', *Cell*, 139(5), pp. 871–890. Available at: https://doi.org/10.1016/J.CELL.2009.11.007/ATTACHMENT/7E0CAE36-4693-4EE3-AF81-C2E478E595A2/MMC1.PDF.

Tholen, S. *et al.* (2016) 'Skin barrier defects caused by keratinocyte-specific deletion of ADAM17 or EGFR are based on highly similar proteome and degradome alterations', *Journal of Proteome Research*, 15(5), pp. 1402–1417. Available at: https://doi.org/10.1021/ACS.JPROTEOME.5B00691/SUPPL_FILE/PR5B00691_SI_002.PDF.

Toullec, A. *et al.* (2010) 'Oxidative stress promotes myofibroblast differentiation and tumour spreading', *EMBO Molecular Medicine* [Preprint]. Available at: https://doi.org/10.1002/emmm.201000073.

Trad, A. *et al.* (2013) 'ADAM17-overexpressing breast cancer cells selectively targeted by antibody-toxin conjugates', *Cancer Immunology, Immunotherapy*, 62(3), pp. 411–421. Available at: https://doi.org/10.1007/S00262-012-1346-X/FIGURES/6.

Turajlic, S. and Swanton, C. (2016) 'Metastasis as an evolutionary process', *Science*, 352(6282), pp. 169–175. Available at: https://doi.org/10.1126/SCIENCE.AAF2784/ASSET/4F0278D6-9EDC-4EE4-AFB5-6B2D48575F9D/ASSETS/GRAPHIC/352_169_F2.JPEG.

Ulrich, T.A., De Juan Pardo, E.M. and Kumar, S. (2009) 'The mechanical rigidity of the extracellular matrix regulates the structure, motility, and proliferation of glioma cells', *Cancer Research*, 69(10), pp. 4167–4174. Available at: https://doi.org/10.1158/0008-5472.CAN-08-4859/655093/P/THE-MECHANICAL-RIGIDITY-OF-THE-EXTRACELLULAR.

Valkenburg, K.C., De Groot, A.E. and Pienta, K.J. (2018) 'Targeting the tumour stroma to improve cancer therapy', *Nature Reviews Clinical Oncology* [Preprint]. Available at: https://doi.org/10.1038/s41571-018-0007-1.

VanSchaeybroeck, S. *et al.* (2014) 'ADAM17-Dependent c-MET-STAT3 Signaling Mediates Resistance to MEK Inhibitors in KRAS Mutant Colorectal Cancer', *Cell Reports* [Preprint]. Available at: https://doi.org/10.1016/j.celrep.2014.05.032.

Vega, S. *et al.* (2004) 'Snail blocks the cell cycle and confers resistance to cell death', *Genes & Development*, 18(10), pp. 1131–1143. Available at: https://doi.org/10.1101/GAD.294104.

Vilchez Mercedes, S.A. *et al.* (2021) 'Decoding leader cells in collective cancer invasion', *Nature Reviews Cancer 2021 21:9*, 21(9), pp. 592–604. Available at: https://doi.org/10.1038/s41568-021-00376-8.

Vogelstein, B. *et al.* (2013) 'Cancer genome landscapes', *Science*, 340(6127), pp. 1546–1558. Available at: https://doi.org/10.1126/SCIENCE.1235122/SUPPL_FILE/VOGELSTEIN.SM.COVER.PAGE.PDF.

Vosseler, S. *et al.* (2009) 'Distinct progression-associated expression of tumor and stromal MMPs in HaCaT skin SCCs correlates with onset of invasion', *International Journal of Cancer* [Preprint]. Available at: https://doi.org/10.1002/ijc.24589.

Walkiewicz, K. *et al.* (2016) 'Expression of Migration-Related Genes in Human Colorectal Cancer and Activity of a Disintegrin and Metalloproteinase 17', *BioMed research international*, 2016. Available at: https://doi.org/10.1155/2016/8208904.

Wan, L., Pantel, K. and Kang, Y. (2013) 'Tumor metastasis: moving new biological insights into the clinic', *Nature Medicine 2013 19:11*, 19(11), pp. 1450–1464. Available at: https://doi.org/10.1038/nm.3391.

Wang, E. *et al.* (2009) 'Transforming growth factor beta engages TACE/ADAM17 and ErbB3 to activate PI3K/Akt in HER2-overexpressing breast cancer and desensitizes cells to

trastuzumab.', *Cancer Research*, 69(2_Supplement), pp. 35–35. Available at: https://doi.org/10.1158/0008-5472.SABCS-35.

Wang, J. *et al.* (2015) 'Nestin regulates proliferation and invasion of gastrointestinal stromal tumor cells by altering mitochondrial dynamics', *Oncogene 2016 35:24*, 35(24), pp. 3139–3150. Available at: https://doi.org/10.1038/onc.2015.370.

Wang, N. *et al.* (2015) 'The IGF-trap: Novel inhibitor of carcinoma growth and metastasis', *Molecular Cancer Therapeutics*, 14(4), pp. 982–993. Available at: https://doi.org/10.1158/1535-7163.MCT-14-0751/85495/AM/THE-IGF-TRAP-NOVEL-INHIBITOR-OF-CARCINOMA-GROWTH.

Wang, S.E. *et al.* (2008) 'Transforming Growth Factor β Engages TACE and ErbB3 To Activate Phosphatidylinositol-3 Kinase/Akt in ErbB2-Overexpressing Breast Cancer and Desensitizes Cells to Trastuzumab', *Molecular and Cellular Biology*, 28(18), pp. 5605–5620. Available at: https://doi.org/10.1128/MCB.00787-08/SUPPL_FILE/SUPPL_TABLE_1.ZIP.

Wang, W.-B., Levy, D.E. and Lee, C.-K. (2011) 'STAT3 Negatively Regulates Type I IFN-Mediated Antiviral Response', *The Journal of Immunology*, 187(5), pp. 2578–2585. Available at: https://doi.org/10.4049/JIMMUNOL.1004128.

Wang, Y. *et al.* (2010) 'ADAM17 Activity and Other Mechanisms of Soluble L-selectin Production during Death Receptor-Induced Leukocyte Apoptosis', *The Journal of Immunology*, 184(8), pp. 4447–4454. Available at: https://doi.org/10.4049/JIMMUNOL.0902925.

Watson, H.A. *et al.* (2019) 'L-selectin enhanced T cells improve the efficacy of cancer immunotherapy', *Frontiers in Immunology*, 10(JUN), p. 1321. Available at: https://doi.org/10.3389/FIMMU.2019.01321/BIBTEX.

Weiss, F., Lauffenburger, D. and Friedl, P. (2022) 'Towards targeting of shared mechanisms of cancer metastasis and therapy resistance', *Nature Reviews Cancer 2022 22:3*, 22(3), pp. 157–173. Available at: https://doi.org/10.1038/s41568-021-00427-0.

Wen, S. *et al.* (2015) 'BM-MSCs promote prostate cancer progression via the conversion of normal fibroblasts to cancer-associated fibroblasts', *International Journal of Oncology*, 47(2), pp. 719–727. Available at: https://doi.org/10.3892/IJO.2015.3060/HTML.

White, D.E., Rayment, J.H. and Muller, W.J. (2006) 'Addressing the role of cell adhesion in tumor cell dormancy', *Cell Cycle* [Preprint]. Available at: https://doi.org/10.4161/cc.5.16.2993.

Whiteside, T.L. (2008) 'The tumor microenvironment and its role in promoting tumor growth', *Oncogene*, 27(45), pp. 5904–5912. Available at: https://doi.org/10.1038/onc.2008.271.

WHO (2020) *Cancer*. Available at: https://www.who.int/health-topics/cancer#tab=tab_1 (Accessed: 30 March 2022).

Williams, E. *et al.* (2000) 'A Novel Family of Cyclic Peptide Antagonists Suggests That N-cadherin Specificity Is Determined by Amino Acids That Flank the HAV Motif *', *Journal of Biological Chemistry*, 275(6), pp. 4007–4012. Available at: https://doi.org/10.1074/JBC.275.6.4007.

Withana, N.P. *et al.* (2012) 'Cathepsin B inhibition limits bone metastasis in breast cancer', *Cancer Research*, 72(5), pp. 1199–1209. Available at: https://doi.org/10.1158/0008-5472.CAN-11-2759/650139/AM/CATHEPSIN-B-INHIBITION-LIMITS-BONE-METASTASIS-IN.

Wolf, K. *et al.* (2003) 'Amoeboid shape change and contact guidance: T-lymphocyte crawling through fibrillar collagen is independent of matrix remodeling by MMPs and other proteases', *Blood*, 102(9), pp. 3262–3269. Available at: https://doi.org/10.1182/BLOOD-2002-12-3791.

World Health Organization (2020) *WHO - The top 10 causes of death*, *09 December*. Available at: https://www.who.int/news-room/fact-sheets/detail/the-top-10-causes-of-death (Accessed: 16 March 2022).

Wu, F. *et al.* (2021) 'Signaling pathways in cancer-associated fibroblasts and targeted therapy for cancer', *Signal Transduction and Targeted Therapy 2021 6:1*, 6(1), pp. 1–35. Available at: https://doi.org/10.1038/s41392-021-00641-0.

Wu, J. shun *et al.* (2021) 'Plasticity of cancer cell invasion: Patterns and mechanisms', *Translational Oncology*, 14(1), p. 100899. Available at: https://doi.org/10.1016/J.TRANON.2020.100899.

Wu, T. and Dai, Y. (2017) 'Tumor microenvironment and therapeutic response', *Cancer Letters*, 387, pp. 61–68. Available at: https://doi.org/10.1016/j.canlet.2016.01.043.

Wu, X. *et al.* (2012) 'Clonal selection drives genetic divergence of metastatic medulloblastoma', *Nature 2012 482:7386*, 482(7386), pp. 529–533. Available at: https://doi.org/10.1038/nature10825.

Xiang, Y. *et al.* (2020) 'ADAM17 promotes the invasion of hepatocellular carcinoma via upregulation MMP21', *Cancer Cell International*, 20(1), pp. 1–11. Available at: https://doi.org/10.1186/S12935-020-01556-6/FIGURES/6.

Xie, Y. *et al.* (2020) 'FGF/FGFR signaling in health and disease', *Signal Transduction and Targeted Therapy 2020 5:1*, 5(1), pp. 1–38. Available at: https://doi.org/10.1038/s41392-020-00222-7.

Xu, H. *et al.* (2015) 'Ubiquitin-mediated NFkB degradation pathway', *Cellular & Molecular*

Immunology, 12, pp. 653–655. Available at: https://doi.org/10.1038/cmi.2014.99.

Xu, M. *et al.* (2016) 'ADAM17 promotes epithelial-mesenchymal transition via TGF-α/Smad pathway in gastric carcinoma cells', *International Journal of Oncology*, 49(6), pp. 2520–2528. Available at: https://doi.org/10.3892/IJO.2016.3744/HTML.

Yachida, S. *et al.* (2010) 'Distant metastasis occurs late during the genetic evolution of pancreatic cancer', *Nature 2010 467:7319*, 467(7319), pp. 1114–1117. Available at: https://doi.org/10.1038/nature09515.

Yacoub, D. *et al.* (2013) 'CD154 Is Released from T-cells by a Disintegrin and Metalloproteinase Domain-containing Protein 10 (ADAM10) and ADAM17 in a CD40 Protein-dependent Manner *', *Journal of Biological Chemistry*, 288(50), pp. 36083–36093. Available at: https://doi.org/10.1074/JBC.M113.506220.

Yang, G. *et al.* (2021) 'Molecular switch in human diseases-disintegrin and metalloproteinases, ADAM17', *Aging*, 13(12), pp. 16859–16872. Available at: https://doi.org/10.18632/AGING.203200.

Yang, J. *et al.* (2020) 'Guidelines and definitions for research on epithelial–mesenchymal transition', *Nature Reviews Molecular Cell Biology 2020 21:6*, 21(6), pp. 341–352. Available at: https://doi.org/10.1038/s41580-020-0237-9.

Yang, J. and Weinberg, R.A. (2008) 'Epithelial-Mesenchymal Transition: At the Crossroads of Development and Tumor Metastasis', *Developmental Cell*, 14(6), pp. 818–829. Available at: https://doi.org/10.1016/J.DEVCEL.2008.05.009.

Yang, X. *et al.* (2016) 'FAP Promotes immunosuppression by cancer-associated fibroblasts in the tumor microenvironment via STAT3-CCL2 Signaling', *Cancer Research* [Preprint]. Available at: https://doi.org/10.1158/0008-5472.CAN-15-2973.

Yao, H., Veine, D.M. and Livant, D.L. (2016) 'Therapeutic inhibition of breast cancer bone metastasis progression and lung colonization: breaking the vicious cycle by targeting α5β1 integrin', *Breast Cancer Research and Treatment 2016 157:3*, 157(3), pp. 489–501. Available at: https://doi.org/10.1007/S10549-016-3844-6.

Yilmaz, M. and Christofori, G. (2009) 'EMT, the cytoskeleton, and cancer cell invasion', *Cancer and Metastasis Reviews*, 28(1–2), pp. 15–33. Available at: https://doi.org/10.1007/S10555-008-9169-0/FIGURES/3.

Yoon, H. *et al.* (2021) 'TGF-β1-mediated transition of resident fibroblasts to cancer-associated fibroblasts promotes cancer metastasis in gastrointestinal stromal tumor', *Oncogenesis 2021 10:2*, 10(2), pp. 1–12. Available at: https://doi.org/10.1038/s41389-021-00302-5.

Yousefi, H. *et al.* (2019) 'IL-6/IL-6R pathway is a therapeutic target in chemoresistant ovarian

cancer', *Tumori*, 105(1), pp. 84–91. Available at: https://doi.org/10.1177/0300891618784790.

Yu, C.C. *et al.* (2013) 'MiR145 targets the SOX9/ADAM17 axis to inhibit tumor-initiating cells and IL-6-mediated paracrine effects in head and neck cancer', *Cancer Research*, 73(11), pp. 3425–3440. Available at: https://doi.org/10.1158/0008-5472.CAN-12-3840/650851/AM/MIR145-TARGETS-THE-SOX9-ADAM17-AXIS-TO-INHIBIT.

Yu, S. *et al.* (2019) 'Conditioned medium from asbestos-exposed fibroblasts affects proliferation and invasion of lung cancer cell lines', *PLOS ONE*, 14(9), p. e0222160. Available at: https://doi.org/10.1371/JOURNAL.PONE.0222160.

Yu, W. *et al.* (2019) 'Cadherin Signaling in Cancer: Its Functions and Role as a Therapeutic Target', *Frontiers in Oncology*, 9, p. 989. Available at: https://doi.org/10.3389/FONC.2019.00989/BIBTEX.

Zaghdoudi, S. *et al.* (2020) 'FAK activity in cancer-associated fibroblasts is a prognostic marker and a druggable key metastatic player in pancreatic cancer', *EMBO Molecular Medicine*, 12(11), p. e12010. Available at: https://doi.org/10.15252/EMMM.202012010.

Zahalka, A.H. and Frenette, P.S. (2020) 'Nerves in cancer', *Nature Reviews Cancer 2020 20:3*, 20(3), pp. 143–157. Available at: https://doi.org/10.1038/s41568-019-0237-2.

Zeng, J. *et al.* (2017) 'Specific Inhibition of Acyl-CoA Oxidase-1 by an Acetylenic Acid Improves Hepatic Lipid and Reactive Oxygen Species (ROS) Metabolism in Rats Fed a High Fat Diet *', *Journal of Biological Chemistry*, 292(9), pp. 3800–3809. Available at: https://doi.org/10.1074/JBC.M116.763532.

Zhang, K. *et al.* (2021) 'Crosstalk Between Autophagy and the cGAS–STING Signaling Pathway in Type I Interferon Production', *Frontiers in Cell and Developmental Biology*, 9, p. 3294. Available at: https://doi.org/10.3389/FCELL.2021.748485/BIBTEX.

Zhang, L. *et al.* (2020) 'Single-Cell Analyses Inform Mechanisms of Myeloid-Targeted Therapies in Colon Cancer', *Cell*, 181(2), pp. 442-459.e29. Available at: https://doi.org/10.1016/J.CELL.2020.03.048.

Zhang, Z. *et al.* (2016) 'Hyaluronan synthase 2 expressed by cancer-associated fibroblasts promotes oral cancer invasion', *Journal of Experimental and Clinical Cancer Research* [Preprint]. Available at: https://doi.org/10.1186/s13046-016-0458-0.

Zhao, L. *et al.* (2013) 'Recruitment of a myeloid cell subset (CD11b/Gr1mid) via CCL2/CCR2 promotes the development of colorectal cancer liver metastasis*', *Hepatology*, 57(2), pp. 829–839. Available at: https://doi.org/10.1002/HEP.26094.

Zhen, Y., Guanghui, L. and Xiefu, Z. (2014) 'Knockdown of EGFR inhibits growth and invasion of gastric cancer cells', *Cancer Gene Therapy 2014 21:11*, 21(11), pp. 491–497.

Available at: https://doi.org/10.1038/cgt.2014.55.

Zheng, X. *et al.* (2009) 'ADAM17 promotes breast cancer cell malignant phenotype through EGFR-PI3K-AKT activation', *http://dx.doi.org/10.4161/cbt.8.11.8539*, 8(11), pp. 1045–1054. Available at: https://doi.org/10.4161/CBT.8.11.8539.

Zheng, X. *et al.* (2012) 'ADAM17 promotes glioma cell malignant phenotype', *Molecular Carcinogenesis*, 51(2), pp. 150–164. Available at: https://doi.org/10.1002/MC.20772.

Zheng, X. *et al.* (2015) 'Epithelial-to-mesenchymal transition is dispensable for metastasis but induces chemoresistance in pancreatic cancer', *Nature 2015 527:7579*, 527(7579), pp. 525–530. Available at: https://doi.org/10.1038/nature16064.

Zivotic, M. *et al.* (2018) 'Modulation of NCAM/FGFR1 signaling suppresses EMT program in human proximal tubular epithelial cells', *PLOS ONE*, 13(11), p. e0206786. Available at: https://doi.org/10.1371/JOURNAL.PONE.0206786.

Zunke, F. and Rose-John, S. (2017) 'The shedding protease ADAM17: Physiology and pathophysiology', *Biochimica et Biophysica Acta - Molecular Cell Research* [Preprint]. Available at: https://doi.org/10.1016/j.bbamcr.2017.07.001.